Chaotic Systems for Pattern Recognition and Brain Modelling

By

Dragos Calitoiu

A Thesis submitted to
the Faculty of Graduate Studies and Research
in partial fulfilment of
the requirements for the degree of
Doctor of Philosophy

Ottawa-Carleton Institute for Computer Science
School of Computer Science
Carleton University
Ottawa, Ontario

December 2006

Your file Votre référence
ISBN: 978-0-494-23288-0
Our file Notre référence
ISBN: 978-0-494-23288-0

Dedicated to my wife, Monica.

"*The great organizational richness of the dynamical brain provides a challenge to the application of chaotic dynamics. When inquiry proceeds at any one scale of organization - for example, do neurons fire chaotically? Does the EEG have fractal dimensions? - the attempted application seems straightforward enough, at least in principle. But when the various scales of complexity in the brain are considered, then the application become less clear.*"
(D.M. Alexander and G.G. Globus [4])

Abstract

The main aim of this thesis and our research endeavor is to propose methods and algorithms for controlling models related to the brain, in order for them to recognize and to modify their levels of chaos.

We investigated five problems:

1. We presented an original and novel strategy for Pattern Recognition (PR) using Chaotic Neural Networks. The algorithm is based on a formal hypothesis proposed by Freeman [56], who developed a model for an olfactory system. He conjectured that the brain is essentially a chaotic system in the absence of a stimulus (pattern) that it is supposed to recognize. During perception, when the attention is focussed on any sensory stimuli, the brain activity become periodic. We have designed a PR system, namely a Chaotic Neural Network, which demonstrates such a phenomenon.

2. We proposed a new approach for modelling a PR system which loses its ability to recognize, even though the *quality* of the stimulus is "perfect". By using a Chaotic Neural Network, we have provided a chaotic rationale for both perception and the lack thereof, even in cases when the stimulus is "error-free".

3. We investigated in the piriform cortex (modelled as a large scale network), the dependence of the level of chaos as a function of a few variables (or parameters). Our aim was to discover methods by which we could increase the level of chaos in *almost* synchronized large scale networks, as in the epileptic brain.

4. We studied a classical model of the Hodgkin-Huxley (HH) neuron, and analytically proved its stability properties and the existence of a brief current pulse, which, when delivered to the HH neuron during its repetitively firing state, annihilates its spikes. The experimental properties of this phenomenon have also been investigated.

5. We presented a stability analysis for small scale networks consisting of Bursting neurons. We proved that if the coupling between the neurons is arbitrarily small, the network exhibits chaos and that the network rapidly converges to a synchronized behavior, implying

that increasing the number of neurons does not contribute significantly to the synchronization of the individual bursting neurons. The consequences of this *behavioral synchronization*, and its implications to a new hypothesis for the genesis of epileptic seizures have also been analyzed. Finally, we have developed methods for controlling the behavioral synchronization of the network.

The thesis also lists various open problems and avenues for future research.

Acknowledgements

First, I wish to express my sincere gratitude to my supervisors, Prof. B. John Oommen and Prof. Doron Nussbaum. I am indebted to Prof. Oommen who has taught me what it means to be a researcher, and has provided encouragement and valuable criticism through all these years. He has never failed in supporting me as a Professor, "Father", "Brother" and "Friend". Thank you for the time and effort you have invested in me, for your generosity, dependability and clear concern for my research and career.

I am also indebted to Prof. Nussbaum for his continued guidance, by keeping things in perspective, and for his fruitful good counsel. He has assisted me in the development of the ideas and the evolution of the thesis.

I thank Prof. Witold Kinsner for graciously being the External Examiner for my thesis. I also express my gratitude for his constructive comments. Undoubtedly, in my opinion, the quality of the final version of the thesis has increased significantly.

My indebtedness to Prof. J. P. Corriveau, Graduate Director in the School of Computer Science, Carleton University. Thank you, Sir, for looking after the issues concerning my financial support.

Next, I thank Prof. Dan McIntyre for accepting me, even as early as September 2003, to be involved in the laboratory research using rats, and for teaching me about kindling and epilepsy. In addition, Prof. McIntyre gave me the honor of meeting Prof. Bruce Hutcheon. My very special thanks to Dr. Hutcheon for introducing me to the exciting area of dynamic neuroscience, for generously sharing his knowledge and expertise in this area, and for giving me professional advice. He was, informally, my third "supervisor".

I would like to thank Prof. Stan Matwin from the University of Ottawa for all the challenging discussions about brain modeling and machine learning.

Thanks to Prof. Tony White for his encouragement and many discussions about complex networks, synchronization, and collective behavior, to Prof. Andre Longtin (University of Ottawa) for clarifying questions related to computational neuroscience, and to Prof. Victor LeBlanc (University of Ottawa) for his thoughtful comments in the field of controlling nonlinear dynamics.

My very special thanks go to Professors Petre Pidlepa, Aurora Costeschi, Nicolae Pintilie, and Mihai Teodor, all of whom are Romanian professors who contributed to my education. Also, I also had the privilege of working together with Prof. Victor Neagoe and Prof. Edmond Nicolau, from the Polytechnic University of Bucharest, Romania, who taught me about neural networks, and with Dr. Alistair Sutherland (Dublin City University, Ireland), who opened for me the door of Chaotic Neural Networks.

Last, but not least, I am very grateful to my family (my wife, Monica, my parents Sabina and Valentin, and my children Marta and Mihail) who has always believed in me and encouraged me through this uphill road. My wife was a great source of support during those times when I was again student. It has been a long road, and her patience and endurance have made a difference in completing this thesis. This work is dedicated to her. In addition, Monica and her sister, Oana, did a lot of work in "proofreading" all my papers, presentations and projects during my Doctoral studies. I am also very grateful to my wife's parents, for their encouragements.

The financial support during the course of my Doctoral studies was provided by the Natural Sciences and Engineering Research Council of Canada (NSERC), the Government of Ontario (OGS), Carleton University, and Nortel Networks Corporation. This financial assistance was crucial to the success of my research, and, I gratefully acknowledge it.

Contents

List of Figures

Chapter 1

Introduction

The first computer was designed as a machine intended for mathematical calculations. Recognizing its limitations, scientists started the process of optimizing it, gradually augmenting it with the key features of modern computers. Of all the sources of inspiration that computer scientists have used to improve the capability of computers, none can be compared with the brain. One of the goals of both computer engineers and scientists is to build a machine with attributes resembling human intelligence. This process could also involve mimicking the architecture of the brain, and in particular, its massive parallelism. Research in the area of understanding the brain, so as to improve the computational power of computers, in turn, led to the study of the "inverse" problem, namely that of using the obtained computational power for a better understanding of the brain itself. To be more specific, the symbiosis between biology, physics, chemistry, psychology, and computer science led to a better understanding of the human brain's remarkable capabilities. This remarkable organ comprises of trillions of cells, constituting almost one hundred billion neurons, the latter figure rivaling the number of stars in our galaxy.

Scientists have devised various plausible models for certain aspects of the functioning of the brain. On one hand, some of these models have been used in practical applications to mimic brain activities such as memory, recognition, and cognition. On the other hand, other models have been used in achieving investigations of the brain to treat diseases such as epilepsy, schizophrenia, and Parkinson's disease. This thesis considers both of these approaches. First of all, the recognition in the olfactory system is used as an inspiration for a model for recognition

using chaotic neural networks. Additionally, in the case of the inverse problem, a model for the piriform cortex and models of small realistic neural networks are explored for understanding the mechanism of diseases such as those mentioned above. In our study, both of these approaches revolve around the concept of chaos. Indeed, chaos can be found in the brain and also simulated in its models. Alternatively, models of the brain can be used to investigate its phenomena.

The primary goal of this thesis is to propose methods and algorithms for controlling these models in order to modify their levels of chaos. We hope that this process of controlling chaos will be a step forward in the area of medical research, for example, for desynchronizing an epileptic brain.

This chapter provides an introduction to the thesis, and illustrates its main objectives and contributions. The chapter is organized as follows: Section 1.1 submits the main motivations and the objectives of the work. Section 1.2 describes the problems to be studied, and Section 1.3 presents the organization of the Thesis and the main contributions of each Chapter.

1.1 Motivations and Objectives

1.1.1 Motivations

The motivations of the thesis are three-fold:

1. We would like to investigate if the brain's characteristics of recognition and blurring can be based on a chaotic model of learning and if such a model can be artificially designed and implemented.
2. We would like to understand how chaos in large scale network models of the brain can be simulated and controlled. This, hopefully, will lead to a better understanding of certain brain disorders such as epilepsy, schizophrenia or Parkinson's disease.
3. We would like to comprehend how chaos in small scale network models of the brain can be simulated and controlled. This, on the other hand, could lead to a better understanding of diseases such as epilepsy.

1.1.2 Objectives

There are numerous models of the brain which consider it as a deterministic, stochastic, or fuzzy system. In this thesis, we advocate an alternate model, namely that of a *chaotic system*. It is our belief that, we, as human beings, do not do matrix inversions, grammatical syntax analysis or probability density computations in accomplishing mundane tasks such as recognition and cognition. We advocate that the brain is essentially a chaotic system, and that this chaos is observable in measurements such as those obtained from EEGs. Such a hypothesis has also been suggested by Freeman through his clinical experiments [56, 153]. Therefore, the objectives for this thesis can be listed as follows:

1. To demonstrate that Chaotic Neural Networks (CNNs) can achieve Pattern Recognition. This hopefully leads to a completely new branch of the latter field.
2. To demonstrate that CNNs can adequately hypothesize the theory of blurring or inaccurate perception.
3. To demonstrate that if the brain is modelled as a large scale network of neurons, where each neuron has a fairly elementary model, the resulting network can demonstrate chaotic phenomena. In this regard, we worked with a primitive model of the pyramidal neuron of the piriform cortex.
4. To demonstrate that if portions of the brain are modelled as small scale networks, the latter again demonstrates chaotic behavior. In this regard, we utilized the Hodgkin-Huxley neuron and a Bursting neuron to demonstrate that the chaos in the networks of such neurons can be controlled.

1.2 Problems Studied and Resulted Obtained

The Problems studied in this thesis are listed below. In each case we mention and briefly describe the problem, and summarize the results obtained.

1.2.1 Chaotic Pattern Recognition

We propose a new field of research, one that involves *Pattern Recognition using Chaotic Neural Networks*. Pattern Recognition (PR) is the study of how a system observes the environment, learns to distinguish patterns of interest from its background, and makes decisions about their classification or categorization. The four best approaches for PR are: template matching, statistical classification, syntactic or structural recognition, and Artificial Neural Networks (ANNs). The first contribution of this thesis is the introduction of a PR system which is founded on the theory of chaotic networks.

The biological evidence that inspired our work was the clinical research of Freeman [153]. He observed that the olfactory cortex has a strange attractor, with a large number of "wings". He then stated the possibility of each "wing" corresponding to a certain recognized smell. When the system is presented with something new to smell, it wanders "randomly" around the strange attractor, until it settles down and restricts its fluctuations to one wing of the attractor, which is intended to represent the smell that it has inferred. The states within the strange attractor represent recognized patterns, and the patterns of the strange attractor represent patterns of transition.

We believe that this behavior can be suitably modelled using CNNs. Each wing of Freeman's attractor represents a certain recognized pattern. The network has to possess a chaotic movement within the attractor, and thus, from each part of the attractor, the system is capable of rapidly moving to other parts of the attractor. However, when a pattern to be recognized is presented to the system, it leads to a strong periodic component which we refer to as "sympathetic resonance". To be more specific, during perception, when the attention is focused on any sensory stimuli, the brain activity becomes periodic. Our aim is to design a PR system, namely a *Chaotic* Neural Network, which demonstrates such phenomena.

To achieve this, we present a CNN model which is a modified version of the one proposed by Adachi [2]. To investigate the stability of the system, we apply two criteria, namely the Routh-Hurwitz Criterion and the Lyapunov Exponents Criterion. Using these, we are able to arrive at constraints which can lead the model to a chaotic behavior. The utility of this model for PR is then validated by testing it on two data sets, namely (i) the one developed by Adachi, and (ii) a new set developed by us, involving numerals. Using these two data sets we compute

the periodicities of the output when the patterns are recognized. The PR results were good even when the patterns have a large level of noise, the noise to signal ratio being as high as 15 %.

1.2.2 Modelling Inaccurate Perception

The next problem which we studied is related to the "inverse" problem, which consists of understanding why a PR system loses its recognition capabilities. To motivate this problem we first presented some concepts concerning the task of perception, i.e., a description of the processes by which the brain organizes and interprets sensations, which are simple experiences caused by physical stimuli. What we know about the world (e.g. objects) depends on the information obtained by our senses and which are channelled into our brain. The brain organizes sensations in such a way that it can later recognize objects and events in the environment, and, if applicable, detect actions or movements of these objects. Understanding perceptual organization is a matter of understanding how one perceives form, depth, and the motion of objects.

To demonstrate inaccurate perception in a neural world, we present an architecture of a CNN that *loses* (!!) its PR capabilities even though the *quality* of the stimulus is "noiseless". With this new approach, we believe that we can provide a chaotic rationale for both perception and the lack thereof (i.e., "blurring"), even in cases when the stimulus is "noise free".

In this context, the traditional goal of modelling natural and artificial perception involves determining how a system can extract an object that it perceives from an image which is noisy. In contrast, we consider in this thesis the "inverse" of this problem and study how even a clear image can be perceived to be blurred in some contexts (and, thus, mis-recognized), without involving the simple model where the true image is garbled with noise.

Even without the inclusion of additional noise, the perception can be *inaccurate* if the dynamics of the chaotic PR system are modified. In this thesis, we present a model for inaccurate perception and use the theories of Routh-Hurwitz criteria and Lyapunov exponents to analyze it. We also investigate experimentally the validity of the model by using the dataset of Adachi and the numeral dataset (referred to earlier). A byproduct of this model is the theoretical possibility of desynchronization of the periodic behavior of the brain (as a chaotic system), which could

render us the possibility of predicting, controlling, and annulling epileptic behavior. We consider, in this thesis, only simulations related to the modelling of the piriform cortex. In addition to this, we also believe that our approach to control the piriform cortex can be extrapolated to other parts of the brain, such as the hypocampus, the visual cortex, etc.

1.2.3 Controlling Chaotic Behavior Using Large Scale Models

After discussing the first main contributions of the thesis, namely those which deal with chaotic PR models inspired from the brain, we explore the second directions of our research, namely those involving the chaotic *models* of the brain that are hopefully suitable for modelling (and possibly, treating) diseases such as epilepsy and schizophrenia. Additionally, we present the open problem of finding the "suitable" scale for such a modelling of the brain.

The problem is described as follows: What is the suitable scale to describe the behavior of the 100 billions neurons in the brain, each of which may have anywhere from a few 1,000's up to 100,000 synapses impinging on them. Through these synapses, neurons can receive information from hundreds or thousands of other neurons, and thus the total number of synapses in the entire brain is as large as 100 trillion. To the best of our knowledge, the problem of determining a suitable scale for modelling the brain is unsolved.

Neuromodelling is usually motivated by a desire to better understand specific neural circuits, particularly those whose failure triggers human illnesses. In our thesis, we concentrate on a few such models, with the additional hope that they can be used to suggest their respective methods of treatment.

In this context, we explore the concept of desynchronizing the epileptic brain by using two types of scales: large scale models (mentioned in this subsection) and small scale models (mentioned in next subsection).

To explore large scale network models, we investigate one such model suitable for the piriform cortex. Well known from clinical experiments for its chaotic behavior, the piriform cortex is easy to model because it appears to be almost independent of other portions of the brain.

In this thesis, we describe the behavior of the system by moving the analysis from the time

space into the phase space of the EEG signals. Although the model of the piriform cortex contains hundreds of variables, useful information can be extracted from a single EEG signal which can be perceived as a time series computed from the artificial electrodes. This transformation, from the time space of a time series to the phase space, is considered mandatory to extract the nonlinear characteristics related with chaos. In the phase space, we analyze the attractor built from the EEG by computing the Largest Lyapunov Exponent (LLE) (which describes the total predictability of the dynamic due to the sensitive dependence on initial condition), and the correlation dimension (which describes the dimensionality of the space occupied by the attractor). In addition, the analysis in the phase space opens the problem of measuring the synchronization between two coupled subsystems from the model of the piriform cortex. One of the observations of the thesis is the necessity of redefining the concept of synchronization when the computation is generated in the phase space. We mention that the nonlinear interdependence used to measure the synchronization between two systems in the phase space tends to better describe the interaction between the systems than the classical synchronization between them. To be more specific, the interdependence describes whether or not two systems mutually affect one another, or, in mathematical terms, whether or not the output of two systems are functions of one another when viewed as a two-body model. The uniqueness of our research is the fact that we study communication as being between two components of the same system, namely as pairs of signals being compared, belonging to the same system. In contrast to other models which evaluate relationships between two different systems, (or rather between two partially coupled systems), we investigate a new approach for such a model of communication, where the investigation is made using two subsystems which are embedded in a larger system, namely between two coupled sub-systems of the same system.

The goal of studying the piriform cortex model is to see if we can generate certain desirable phenomena by modifying various control parameters. The extremely large number of control parameters raises an important question that we answer: Which control parameters can be modified, and what are the consequent implications. The solutions to these issues are not intuitive.

Concerning the issue of determining the importance of the control parameters, we investigate the piriform cortex from the perspective of three problems as initiated from clinical motivations. The first one is the *Problem of Density and Strength*, which is clinically motivated by the

density of neurons as observed in the slides of the human brain which has diseases related to network disorders, and also by the increase in the inhibition level which can generate an epileptic behavior. The second problem is the *Problem of Connectivity*, which is motivated by two hypotheses related to the schizophrenic brain. The last problem is the *Problem of Stimulus Frequency*, which is motivated by studies of the frequency of the olfactory stimuli as recognized by the piriform cortex via its bulb.

1.2.4 Controlling Chaotic Behavior Using Small Scale Models

The underlying motivation for investigating the small scale network model of the brain is to consider the simplest neural modules capable of displaying chaotic behavior, and to use the knowledge gained from studying these systems to obtain a broader understanding of the possible relevance of chaotic dynamics to brain functioning.

Two models of neurons are investigated in this study, namely, a classical Hodgkin-Huxley neuron, and a Bursting neuron. The results of the explorations of these models, and the control methods proposed can be applied to networks of neurons. The goal of this phase of the research is to develop methods for controlling the level of chaos, with the particular cases of desynchronizing the networks, and also of increasing the chaos. In this thesis, the informal expression "level of chaos" should be read so as quantify the total predictability of the dynamic due to the sensitive dependence on the initial condition. This is measured, for example, in terms of the spectrum of Lyapunov exponents. As opposed to the work done which relate to large scale networks, small scale models lend themselves to a more mathematical analysis, inasmuch as the small size of the networks permits us to apply the mathematical tools related to computing steady states and Jacobian matrices.

1.3 Thesis Organization and Main Contributions

In this section, we present the overall organization of the thesis, and the contributions made in each chapter.

- **Chapter 2: Chaos in Dynamical Systems and Brain Modelling**
  This chapter serves to present the background material needed for the thesis. We first introduce some theoretical properties concerning the concept of chaos. We then present a few models for systems which exhibit chaotic behavior, and give a general overview of chaotic neural networks. Next, we describe various metrics used for analyzing and quantifying chaos, and in particular, specify how they can be computed. We continue the chapter with a survey about how the brain is modelled as a chaotic system, and about methods for controlling and "anti-controlling" chaos. We conclude the chapter with a discussion about the limitations of the models that have been used to analyze the brain, and in particular the epileptic brain.

- **Chapter 3: Chaotic Pattern Recognition**
  This chapter presents an original and novel algorithm for Pattern Recognition (PR) using Chaotic Neural Networks. The algorithm is based on a formal hypothesis proposed by Freeman [56] who developed a model for an olfactory system. He conjectured that the brain is essentially a chaotic system in the absence of a stimulus (pattern) that it is supposed to recognize. During perception, when the attention is focussed on any sensory stimuli, the brain activity become periodic. In this chapter, we design a PR system, namely a Chaotic Neural Network, which demonstrate such a phenomenon. The research presented here has been published in [32] and [33].

- **Chapter 4: Modelling Inaccurate Perception**
  In this chapter, we propose a new approach for modelling a PR system which loses its ability to recognize, even though the the *quality* of the stimulus is "noiseless". By using a Chaotic Neural Network, we have provided a chaotic rationale for both perception and the lack thereof, even in cases when the stimulus is "error-free". The research presented here has been published in [31].

- **Chapter 5: Controlling Chaotic Behavior Using Large Scale Models**
  In this chapter, our aim is to discover methods by which we can increase the level of chaos in *almost* synchronized large scale networks, as in the epileptic brain. We investigate, in the piriform cortex (modelled as a large scale network), the dependence of the level of chaos as a function of a few variables (or parameters). The level of chaos can be quantified by two components: a global measure expressed by the Largest Lyapunov Exponent (LLE)

(as explained in Section 2.6) and a geometrical measure expressed by the Correlation Dimension (D_2) (as explained in Section 2.5). Both of these are used in our evaluations.

To be more specific, we examine the following problems:

- **Problem of Density and Strength**: We investigate the dependence of the level of chaos as a function of the density of the neurons in the network, and the strength of the connections between then.
- **Problem of Connectivity**: In this case we analyze the dependence of the level of chaos as a function of the density of the connectivity of the synapses (i.e, the number of synapses generated between the neurons). In addition, we investigate the variation of the maximum nonlinear interdependence of two subsystems embedded in a larger system. Thus, we consider how the coupling of two interconnected subsystems of the same underlying system would change as a function of the connectivity of the synapses. We show that the levels of local connections between the neurons can be used as a hypothesis to explain the mechanism underlying illnesses such as schizophrenia. Some preliminary results concerning our hypotheis have been published in [28].
- **Problem of Stimulus Frequency**: In this case we study the dependence of the level of chaos as a function of the frequency of a stimulus that is globally applied within the network. In addition, we study the maximum nonlinear interdependence of two subsystems which are embedded in a larger system as a function of the frequency of the stimulus that is globally applied in the network.

- **Chapter 6: Controlling Chaotic Behavior Using Small Scale Models: Spike Annihilation in a Hodgkin-Huxley Neuron**
  This chapter presents methods by which the behavior of *small* scale networks can be investigated. A classical model of Hodgkin-Huxley neuron is studied here. We analytically prove its stability properties, and the existence of a brief current pulse, which, when delivered to the HH neuron during its repetitively firing state, annihilates its spikes. We also formally derive the characteristics of this brief current pulse. We then proceed to explore experimentally, by numerical simulations, the properties of this pulse, namely the range of time when it can be inserted, its magnitude, and its duration. In addition, we study the solution of annihilating the spikes by using two successive stimuli, when the

first is, of its own, unable to annihilate the neuron. Finally, we investigate the inverse problem of annihilation, namely the spike generation problem, when the neuron switches from resting to firing.

The results of the explorations of this model can be used to develop control methods for a networks of neurons. The "ultimate" goal of this phase of the research is to develop methods for controlling the level of chaos, with the particular cases of desynchronizing the networks and of increasing the chaos. The paper containing the salient results of this work have been submitted for publication.

- **Chapter 7: Controlling Chaotic Behavior Using Small Scale Models: Behavioral Synchronization in a Network of Bursting Neurons**
  In this chapter, we present a stability analysis for small scale networks consisting of bursting neurons. We prove that if the coupling between neurons is arbitrarily small, the network exhibits chaos. We then show that the network rapidly converges to a synchronized behavior implying that increasing the number of neurons does not contribute significantly to the synchronization of the individual bursting neurons. The consequences of such a conclusion lead to a phenomenon that we call *behavioral synchronization*, and we examine the implications of this phenomenon by presenting a new hypothesis for the genesis of epileptic seizures. Finally, we develop methods for controlling the behavioral synchronization of the network. The paper containing the salient results of this work have been submitted for publication.

- **Chapter 8: Summary, Conclusions and Future Research**
  This chapter summarizes the work done in the thesis, gives the final conclusions and presents the future research that is yet to be pursued in the area of *large* scale chaotic neural networks. In particular, we believe that the antiepileptic effect of new "patterned stimuli", (determined by our results presented in Chapters 6 and 7), versus low frequency brain stimulation against kindled seizures in rats, deserves future investigation.

Chapter 2

Chaos in Dynamical Systems and Brain Modelling

The definition and the utilization of the concept of chaos are arguably two of the most amazing scientific achievements of the last century. They have inspired interest in complex systems by radically changing many fundamental beliefs that scientists have had about "chaos". In this chapter we introduce some theoretical properties concerning the concept of chaos. We present a few models of systems which exhibit chaotic behavior, and give a general overview of chaotic neural networks. Next, we describe various metrics used for analyzing and quantifying chaos. We continue the chapter with a survey about chaotic brain modelling and methods of controlling the chaos in these models of the brain. We conclude the chapter with a discussion about the limitations of a model used to analyze the brain (focussing on the epileptic brain).

2.1 Chaos Theory: What is Chaos ?

We first introduce the concept of a trajectory as proposed by Falconer [51]. Let B be a domain in R^n, and $F : B \rightarrow R^n$ be a function with continuous derivatives up to a pre-specified order. The differential equation

$$\dot{X} = F(X) \tag{2.1}$$

has a family of solutions which are *curves* or *trajectories* in B. If $X(0)$ is an initial point, then the solution $X(t)$ remains on the unique trajectory with the following properties: (i) it satisfies Equation (2.1), and (ii) it simultaneously passes through $X(0)$ whenever $t = 0$. If F satisfies some specific conditions, none of the underlying trajectories intersect, because if that were not the case, Equation (2.1) would not be able to determine the motion of X. In addition, the trajectories vary across B except at points where $\dot{X} = F(X) = 0$, implying that the trajectories are singular points.

In both the discrete and continuous cases, a dynamical system can generate so-called attractors and/or repellers [51]. A closed subset A of B can be denoted as an attractor with a basin of attraction V containing A if for all initial points $X(0)$ in the open set V, the trajectory $X(t)$ through $X(0)$ approaches A as t tends to infinity. It turns out that A is an invariant of the system, and so if $X(0)$ is a point of A, then $X(t)$ is in A for $-\infty < t < \infty$, implying that A can be found in a union of trajectories. We also require A to be minimal, implying that there is some point $X(0)$ such that the trajectories generated are dense in F. The terms "invariant", "attractor" and "dense" will be formally described, in detail, later in this Section.

Chaos is a type of unpredictable behavior of a dynamical system governed by deterministic nonlinear equations, which are typically differential or difference equations [87]. The space used to describe the chaotic system is called the phase space. Two trajectories in this phase space, which are infinitesimally-separated separated and generated with two different initial conditions, will separate exponentially in time. The degree with which two infinitesimally-separated trajectories move away from or approach each other is measured by a coefficient termed the Lyapunov exponent (See Section 2.6). Chaos is often characterized by a system having at least one positive Lyapunov exponent. If the initial value is changed infinitesimally, the final state may become quite different, and thus the system has "a sensitive dependence" on the initial condition.

In the case of chaos, by decomposing the output of the system into its Fourier modes, we can encounter an uncountably infinite number of modes in the form of its "continuous spectra". In other words, chaos contains infinitely many periodic solutions, and these periods are characterized by the set of natural numbers.

Fourier analysis provides a frequency-content analysis of a signal. If the signal is periodic

(or quasi-periodic), the Fourier power spectrum will consist of a sequence of "spikes" at the fundamental frequencies, their harmonics, and the frequencies that are the sums and differences of these previous frequencies. Thus, the spectrum will consist of a discrete set of frequencies. In the case of a chaotic signal, the Fourier power spectrum will be continuous. The appearance of a continuous power spectrum from a discrete spectrum when a control parameter of the system is changed is considered to be an indicator of the onset of chaotic behavior [78]. However, a continuous Fourier power spectrum can also appear if external noise is present. In order to discriminate between chaos and white noise, an investigator typically resorts to computing the generalized dimensions. A chaotic signal will have noninteger generalized dimensions, as opposed to white noise which possesses no such correlation.

In [39], Devaney proposed a definition of a chaotic system that contains three principal characteristics:

Definition 2.1.

A dynamical system F is ***chaotic*** *if:*

1. *The Periodic points for F are dense.*
2. *F is transitive.*
3. *F depends sensitively on the initial conditions.*

We now introduce the definition of a dense set. A set A is said to be *dense* in X if for any point x in X, any neighborhood of x contains at least a point from A. The density property is presented below, (effectively taken from [39]).

The Density Proposition: Suppose $F : X \rightarrow Y$ is a continuous map that is onto, and suppose also that $B \subset X$ is a dense subset. Then $F(B)$ is dense in Y.

The most popular equation used to illustrate chaos is the so-called "Logistic equation". The term "Logistic" has a mathematical meaning, and refers to a particular type of so-called growth curve. This expression specifies how the size of a population varies with time. It is a one-dimensional feedback system designed to model the long-term population of a species [111]. The population x_t is assumed to change at discrete time intervals (rather than continuously) as per the following equation:

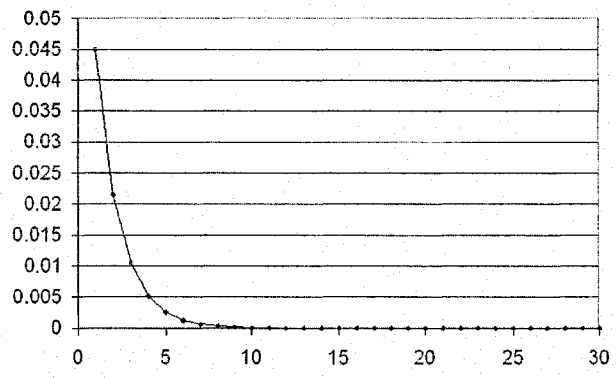

Figure 2.1: Approaching the Fix Point $x^* = 0$ in the *Logistic Map* for A=0.5; the First 30 Iterations.

$$x_{t+1} = Ax_t(1 - x_t). \tag{2.2}$$

This equation is an ideal example of chaos because it is simple, it has only one variable and one constant.

Chaos can be illustrated by examining the bifurcations of the Logistic map for positive values of A and x [155] as below. The converging solutions, 'x^*', of the equation $x_{t+1} = x_t$ (or $x_{t+1} = Ax_t(1 - x_t)$) are called the "Fixed Points", and are studied below.

The following cases are encountered:

Case 1: $0 \leq A < 1$

All the initial conditions in the range $0 < x_0 < 1$ are attracted to the single fixed-point solution $x^* = 0$, as seen in Figure 2.1. These points lie within the basin of attraction of $x^* = 0$, and this fixed point is stable. Values of x_0 outside the basin of attraction (0,1) are unbounded.

Case 2: $1 \leq A < 3$

For $A = 1$, a bifurcation occurs and the fixed point $x^* = 0$ becomes unstable, the attractor turning into a repellor. If x_0 is exactly zero, x_t remains at that value. If it is slightly positive, it grows initially at an exponential rate. In this case, (when $A = 1$), the Logistic map develops a new fixed point, at $x^* = 1 - 1/A$. When $A > 1$, this point moves away from zero. This new fixed point is an attractor because all initial values in the range $0 < x_0 < 1$ will converge to it.

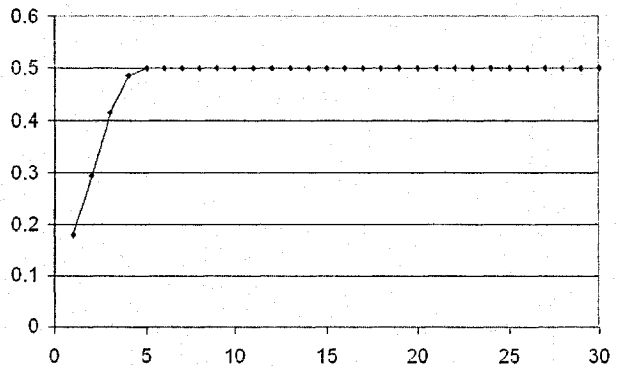

Figure 2.2: Approaching the Fixed Point $x^* = 0.5$ in the *Logistic Map* for A=2; the First 30 Iterations.

The final state is a *period-1 cycle* because each iterate is the same as the one before it. This behavior can be seen in Figure 2.2.

Case 3: $3 \leq A < 3.44948$

When $A = 3$, the fixed point at $x^* = 1 - \frac{1}{A}$ still exists but changes from being stable to unstable, becoming a repellor. For $A > 3$, the system begins to oscillate (see Figure 2.3) to a condition in which every alternate iterate is the same, and thus $x_n = x_{n+2} = x_{n+4}$ etc. In other words, there are two real values between which x oscillates on successive iterations in the steady state. This is an example of a *period-2 cycle*. It is a periodic attractor since any initial condition in the unit interval approaches it.

Case 4: $3.44948 \leq A < 3.56994$

The period-2 cycle exists for all $A > 3$, but it becomes unstable when A reaches a particular value $A = 1 + 6^{1/2} = 3.449490..$ At this bifurcation, the period-2 cycle becomes unstable and a stable *period-4 cycle* is generated, as seen in Figure 2.4. The process continues with successive period doublings, with a new period appearing just as the previous one becomes unstable. From [155] we report that the next few values are listed as:

1. $A_3 = 3.544090...$(leading to a *period-8 cycle*);
2. $A_4 = 3.564407...$(leading to a *period-16 cycle*);
3. $A_5 = 3.568759...$(leading to a *period-32 cycle*);

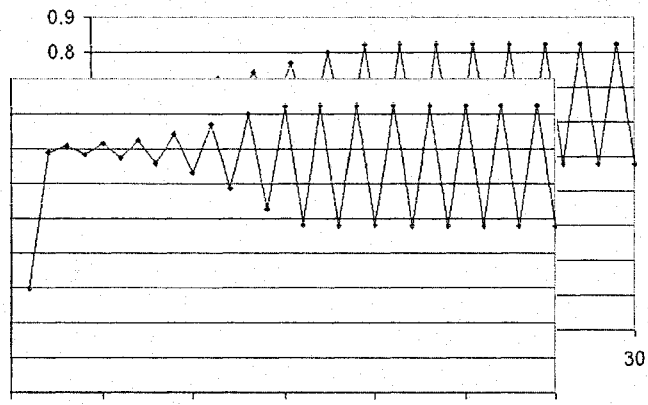

Figure 2.3: A Period-2 Cycle in the *Logistic Map* for A=3.3; the First 30 Iterations.

4. $A_6 = 3.569692...$(leading to a *period-64 cycle*);
5. $A_7 = 3.569891...$(leading to a *period-128 cycle*);
6. $A_8 = 3.569934...$(leading to a *period-256 cycle*);
7. $A_9 = 3.569943...$(leading to a *period-512 cycle*);
8. $A_{10} = 3.569945...$(leading to a *period-1024 cycle*);
9. .....
10. $A_\infty = 3.5699456718...$(leading to an *accumulation point*).

The period doublings become successively closer, eventually accumulating at the point $A_\infty = 3.5699456718...$, known as the *accumulation point.* At this point, the period becomes infinite. The cycle never repeats, and the trajectory visits many x values infinitely.

Case 5: $A_\infty \leq A < 4$

When A increased beyond the accumulation point, chaos appears. The period is infinitely long, and finite regions of the unit interval are visited by the trajectory.

Case 6: $A = 4$

In this case, the system maps the unit interval back onto itself. A map with such a property is called an *endomorphism.*

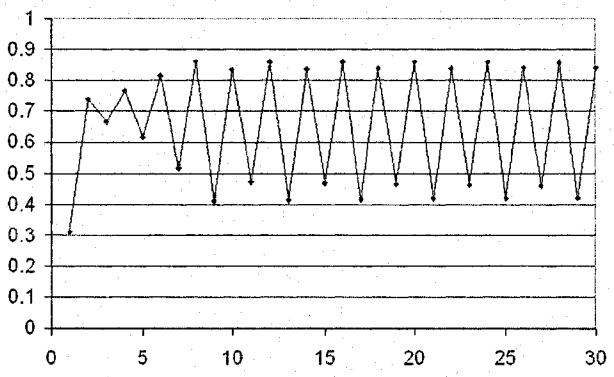

Figure 2.4: A Period-4 Cycle in the *Logistic Map* for A=3.45; the First 30 Iterations.

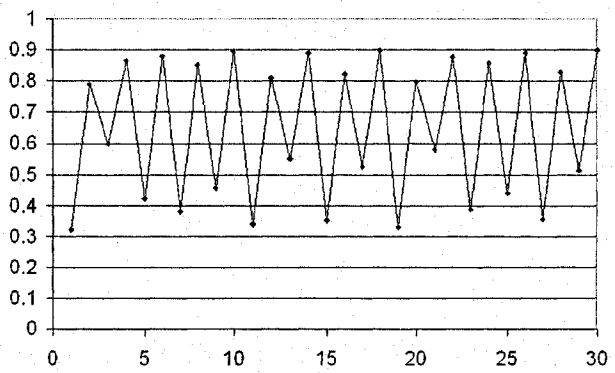

Figure 2.5: The Chaotic Behavior of the *Logistic Map* for A=3.6; the First 30 Iterations.

Case 7: $A > 4$

When $A > 4$, most initial conditions have iterates that eventually reach $x_n > 1$. When that occurs, the next iterate is negative, and the repellor at $x = 0$ pushes the trajectory to $-\infty$ rapidly. Most trajectories are unbounded for $A > 4$.

2.1.1 Models of Chaotic Systems

The reader will observe that the above Logistic Map is rather simplistic. It is appropriate to mention a few more involved scenarios. There are two categories of dynamical systems which exhibit chaos: those involving iterated maps, and those with continuous flows. Maps[1] are easier to analyze numerically and have a rich variety of dynamical behavior, even in a single dimension. By contrast, in general, flows[2] require approximate numerical methods. In a single dimension, the most complicated behavior is a growth or a decay to an equilibrium point. As opposed to this, in two dimensions, the most complicated behavior is a growth or a decay to a periodic limit cycle. Starting with three dimensions, flows can exhibit chaos.

The literature has many examples of maps and flows, the most "popular" ones are listed below. They are classified as being either maps or flows, depending on whether the phase space is 2-dimensional or multi-dimensional. In each case, some parameters and salient characteristics are mentioned.

Others Maps

The following are some examples of maps that appear in the chaos literature[3].

1. The *Henon Map* was invented by Henon in 1976 [75].

   (a) The updating equations, for the variables X_n and Y_n are:

[1]Maps are described with difference equations, with time assuming discrete values. The general updating equations obey: $X_{n+1} = f(X_n)$.

[2]Flows are described with differential equations, with time assuming continuous values. The general updating equations obey: $dx/dt = f(x)$.

[3]The examples are taken from Sprott's book [155]. As per [155], we mention that all the Lyaponov exponents are reported to the base logarithm of e. They were calculated using the algorithm of Benettin *et al.*

$$X_{n+1} = 1 - aX_n^2 + bY_n,$$
$$Y_{n+1} = X_n.$$

(b) The usually chosen parameters are: $a = 1.4$, $b = 0.3$. The initial conditions are: $X_0 = 0$, $Y_0 = 0.9$. The Lyapunov exponents are: $\lambda \simeq 0.41922, -1.62319$.

2. The *Ikeda Map* was discovered by Ikeda in 1979 [83].

(a) The updating equations, for the variables X_n and Y_n are:

$$X_{n+1} = \gamma + \mu(X_n cos\phi - Y_n sin\phi),$$
$$Y_{n+1} = \mu(X_n sin\phi - Y_n cos\phi),$$
$$\text{where } \phi = \beta - \alpha/(1 + X_n^2 + Y_n^2).$$

(b) The usually chosen parameters are: $\alpha = 6$, $\beta = 0.4$, $\gamma = 1$, $\mu = 0.9$. The initial conditions are: $X_0 = 0$, $Y_0 = 0$. The Lyapunov exponents are: $\lambda \simeq 0.50760, -0.71832$.

3. The *Lorenz 3-D Chaotic Map* was presented by Lorentz in [101].

(a) The updating equations, for the variables X_n, Y_n, and Z_n, are:

$$X_{n+1} = X_n Y_n - Z_n,$$
$$Y_{n+1} = X_n,$$
$$Z_{n+1} = Y_n.$$

(b) The initial conditions are: $X_0 = 0$, $Y_0 = 0$, $Z_0 = -1$. The Lyapunov exponents are: $\lambda \simeq 0.07456, 0, -0.07456$.

2.1.2 Others Flows

The following are two examples of 3-dimensional flows that appear in the chaos literature.

1. The *Lorenz Attractor* was presented by Lorentz in 1963 [100].

(a) The dynamical equations, for the variables $x(t)$, $y(t)$, and $z(t)$, are:

$$\begin{aligned} \frac{dx}{dt} &= \sigma(y-x), \\ \frac{dy}{dt} &= -xz + rx - y, \\ \frac{dz}{dt} &= xy - bz. \end{aligned}$$

(b) The usually chosen parameters are $\sigma = 10$, $r = 28$, and $b = 8/3$. The initial conditions are: $x_0 = 0$, $y_0 = -0.01$, $z_0 = 9$. The Lyapunov exponents are: $\lambda \simeq 0.9056$, 0, -14.5723.

2. The *Rossler Attractor* was discovered by Rossler in 1976 [142].

(a) The dynamical equations, for the variables $x(t)$, $y(t)$, and $z(t)$ are:

$$\begin{aligned} \frac{dx}{dt} &= -y - x, \\ \frac{dy}{dt} &= x + ay, \\ \frac{dz}{dt} &= b + z(x-c). \end{aligned}$$

(b) The usually chosen parameters are $a = b = 0.2$, $c = 5.7$. The initial conditions are: $x_0 = -9$, $y_0 = 0$, $z_0 = 0$. The Lyapunov exponents are: $\lambda \simeq 0.0714$, 0 , -5.3943.

2.1.3 Chaotic Neural Networks

A particular case of maps, which we intend to investigate in our research involves the family of chaotic neural networks (CNN).

The CNNs consist of many primary or foundational units called "neurons" which are connected with each other via synaptic connections. One of the aims of studying CNNs networks is to understand and to model the information processing achieved in the brain.

We mention that there are two levels of chaotic behavior which concern CNNs. The first level of chaos is generated by the neuron *itself* [86]. The second level is generated by the network, viewed as a globally or partially coupled map of nonlinear oscillators [2],[120]. These aspects will be clarified later.

In particular, we concentrate on a few maps including Adachi's model [2] which will be explained in greater details in a later chapter.

2.2 Properties of Brain-related Chaotic Models

Chaotic models have been (and can be) used to advantageously model the brain. The most important properties of brain-related modelling dynamical systems using chaos are:

1. *Chaos is a novelty detector*: Chaotic activity can occur when a new stimulus is presented as the input.

2. *Chaos supports explorative behavior*: The presence of chaos in the system enables it to "visit" large regions of the state space.

3. *Chaos permits multiple patterns*: The models of classical NN have stationary attractors which are limited to one "winning" pattern at a time. In chaotic dynamical neural networks, the oscillatory properties of the system permit it to process multiple patterns simultaneously.

4. *Chaos explains rapid learning*: Chaotic models can be used for learning a simple Hebbian procedure for resynchronization [57].

5. *Chaos accounts for forgetting*: In classical NNs, the weights have a linear decay term which is included to simulate the exponential forgetting. In the chaotic model, the concept of "forgetting" can be simulated by changing the weights while the system oscillates in the phase space around a new state. The dynamics lead to a spontaneous unlearning phenomenon.

2.3 Phase Space Reconstruction

One of the best ways to understand a dynamical system is to render the corresponding dynamics visual, namely, by representing the system graphically. Usually, this involves an n-dimensional plot of $n-1$ variables, *versus* time. There is also another type of graph, referred to as *the state space graph* which does not involve time. Apart from the variable associated with time, this graph also involves all the other $n-1$ variables. A point plotted on this graph reflects the *state* or *phase* of the system at a particular time.

The space on the state space graph is typically referred to as the *phase space* or *state space*[4]. More formally, the phase space is an abstract mathematical space in which the *coordinates* represent variables required to specify the phase (or state) of the underlying dynamical system, and it includes all the instantaneous states that the system can be in. As opposed to the more traditional time-series plots, a phase space plot provides a different view of the evolution. It is also pertinent to mention that whereas some time series are not easily displayed graphically on a single graph, a phase space plot compactly condenses all the data graphically.

In a phase space plot, the succession of the plotted points in their chronological order creates a curve displaying the temporal evolution. This curve is termed *trajectory*. Each point plotted along a trajectory has, typically, evolved directly from the precedent point, and reflects the evolution of the dynamical system. Thus, such a representation yields a concise geometric "picture" that attempts to fully describe the history of the system.

Consider Figure 2.6 which represents a phase space for a system which can be described with the equation:

$$w(t) = f(x, y, z, t), \tag{2.3}$$

where f is a nonlinear function and x, y, and z are variables. The phase space for this system has three coordinates x, y, and z. The four points from the phase space correspond to four states:

[4]For the rest of this document, we will use the terms "phase space" and "state space" synonymously.

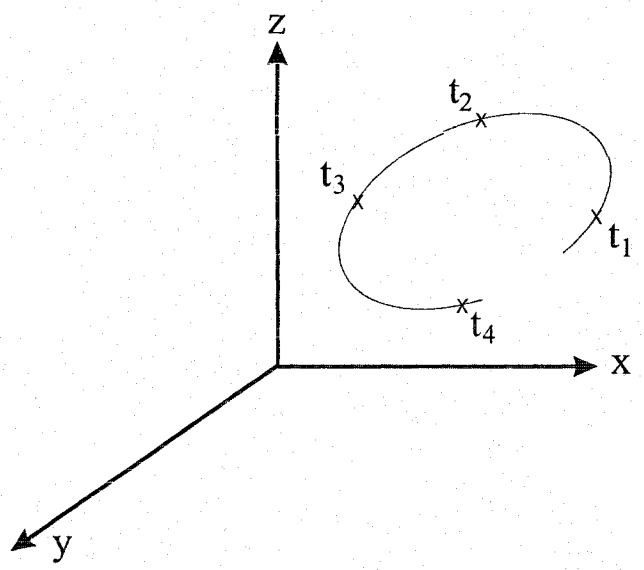

Figure 2.6: Phase Space for the System Described with Equation $w(t) = f(x, y, z, t)$.

1. t_1 with values $x(t_1)$, $y(t_1)$, $z(t_1)$,
2. t_2 with values $x(t_2)$, $y(t_2)$, $z(t_2)$,
3. t_3 with values $x(t_3)$, $y(t_3)$, $z(t_3)$, and
4. t_4 with values $x(t_4)$, $y(t_4)$, $z(t_4)$.

Consider a dynamical system treated as a black box, that generates a time series, $w(t)$, which, for example, can be an EEG. Typically, we are not informed about the process "inside" the black box, for example, about the number of variables that constitute the state dynamical equation, or what the relation between $w(t)$ and the variables is. We would like to devise a method that could extrapolate the significance of the information found in the raw data, without knowing the complete details of what the constituent functions and variables are. This is achieved by utilizing a so-called "delay and embedding" method, used to reconstruct the phase space [155]. This new and reconstructed phase space, often called the *pseudo phase space*, is a graphical setting by which one is able to compare a time series to other measurements within the same data, namely, a subseries. An example will help clarify this.

Consider the case when a plot of $w(t+1)$ *versus* $w(t)$ shows how each observation $w(t)$, compares to the next one, $w(t+1)$. In this comparison, we refer to the sequence $w(t)$, as the basic series, and to the sequence $w(t+1)$ as the subseries. By extending this concept, we can also compare each observation with the one made two time-instants later, (i.e. $w(t+2)$ versus $w(t)$), three time-instants later (i.e. $w(t+3)$ versus $w(t)$), and so on. The displacement, quantified in terms of the number of time-instants, is called the *delay* or *lag*, which is a selected, constant time interval (or, from another perspective, the number of iterations) between the basic time series and any subseries we are comparing it to. This lag also specifies the rule or basis for defining the subseries. For instance, the subseries $w(t+1)$ is based on a single time lag, $w(t+2)$ is based on a lag of length two, and so on. Each such subseries can be processed as follows.

By plotting the lagged values of a given feature one can achieve a so-called "*embedding*" of the feature in the phase space. The total number of separate time series (i.e. the original series, plus the shorter ones obtained by lagging the original one) included in the analysis, is called the *embedding dimension* (see Section 2.4).

From a graphical perspective, the embedding dimension is the number of axes (coordinates) within a reconstructed phase space graph. Analytically, it is the number of variables ($w(t_1)$, $w(t_2)$, etc.) to be used in the analysis.

Embedding a time series is one of the most important tools in chaos theory. The major application of creating an embedding is the reconstruction of an "attractor", which is an object, confined over time, to a sub-region of the phase space. The geometrical properties of these attractors provide crucial information about the global state of the system.

In principle, through the method of delays described by Packard *et al.* [124] and Takens [159], the sampling of a single variable of a system over time can reproduce the related attractors of the system in the phase space. As we shall see, this technique for the reconstruction of the phase space from an observable perspective, can be used for processing chaotic waveforms, such as those encountered in EEGs.

The geometrical properties of the phase portrait of a system can be expressed quantitatively using measures that ultimately reflect the dynamics of the system. For example, the complexity

of an attractor is reflected by its geometrical dimension[5] [159]. The larger the dimension of an attractor, the more complicated it appears in the phase space. It is important to distinguish between the dimension of the phase space (the embedding dimension) and the dimension of the attractor. The embedding dimension, m, is the dimension of the phase space that contains the attractor and is always a positive integer. On the other hand, the attractor dimension, D, which may be a non-integer, is directly related to the number of variables of the system, and inversely related to the existing coupling between them. According to Takens [159], in order to correctly embed an attractor in the phase space, the embedding dimension, m, should be at least equal to $(2 * D + 1)$.

2.4 The False Nearest Neighbour (FNN) Statistics

In order to view the dynamics of a time series from the perspective of nonlinear systems, we have to make a time-delay reconstruction of the phase space. To do this, we use the time-delayed versions of an observed scalar quantity: $x(t_0 + nT) = x(n)$ as the coordinates of the phase space [91]. From the set of observations we can thus obtain vectors in an m-dimensional space which are used to trace out the trajectory of the system:

$$\mathbf{Y}(n) = (x(n), x(n+T), ..., x(n+(m-1)T)), \tag{2.4}$$

where T is the time delay (or lag), and the time evolution of the $\mathbf{Y}$'s is given by $\mathbf{Y}(n) \longrightarrow \mathbf{Y}(n+1)$.

In this phase space, our task is to discover an attractor. One of the important features of an attractor is that it is often a compact object in the phase space. Consequently, points of a trajectory which lie on the attractor acquire neighbors within this phase space. The utility of these neighbors is that they provide the information on how phase-space neighbors evolve, which information can be used to generate equations for the prediction of the time evolution of the new points on or near the attractor [1].

If the embedding dimension is too small to unfold the attractor, not all points that lie close

[5] To be more specific, in Section 2.5.2 we use the spectrum of generalized dimensions to describe an attractor.

to one another will be neighbors. This is a result of the dynamics of the system. Indeed, some of them which are distant from each other will, quite simply, appear as neighbors, because the geometric structure of the attractor has been projected onto a subspace of smaller dimension.

A familiar question thus arises: What time delay, T, and what embedding dimension, m, can be used to effectively achieve the time-delay reconstruction. Typically, the lag should be as small as possible to capture the shortest change present in the data. On the other hand, it should be large enough to generate (with the method of delays) the maximum possible independence between the components of the vectors in the phase space. In the literature [76], these two conditions are usually addressed by selecting the lag to be the first minimum of the mutual information between the components of the vectors in the phase space, or at the first zero of the time domain autocorrelation function of the data [1].

The embedding dimension, m, is determined by the so-called False Nearest Neighbors procedure (FNN) explained below.

2.4.1 Computing the Embedding Dimension using FNN Procedure

The False Nearest Neighbors (FNN) procedure is a method used to obtain the optimum embedding dimension for the phase space reconstruction [91]. While moving ones consideration from dimension m to dimension $m+1$, the analysis can differentiate between points on the trajectory that are "true" neighbors and points on the trajectory which are "false" neighbors. A false neighbor is a point in the data set that is considered as a neighbor solely because we are viewing the trajectory $\mathbf{Y}(n), n = 1, 2, ...N$, in a highly-projected embedding space. The result of this trajectory will be the attractor. When we achieve a large-enough embedding space, all neighbors of every point on the trajectory in the multivariate phase space become true neighbors.

When the number of false nearest neighbors drops to zero, the attractor becomes embedded or unfolded in R^m, an m-dimensional Euclidian space. Working in any dimension larger than the minimum required by the data, obviously leads to excessive computation. We then encounter the problem of contamination by round-off or instrumental error, since this "noise" will populate and dominate the additional dimensions (greater than m) of the embedding space, when, in fact, no such operating dynamics exist.

By checking the neighborhood of points embedded in projection manifolds of increasing dimension, the algorithm eliminates these so-called "false neighbors". Thus, the points that apparently lie close together due to projection are separated in the higher embedding dimensions.

If there are m dimensions, then the square of the Euclidian distance between the point $\mathbf{Y}(n)$ and this neighbor is:

$$R_m^2(n,r) = \sum_{k=0}^{m-1} [x(n+kT) - x^{(r)}(n+kT)]^2, \tag{2.5}$$

where$\mathbf{Y}^r(n)$ is the r^{th} nearest neighbor of $\mathbf{Y}(n)$.

The reader should observe that the $\{\mathbf{Y}(i)\}$ is obtained from the $\{x(i)\}$'s as per (2.4).

When we increase the dimension from m to $m+1$ by increasing a time-delay term, we are actually adding a $(m+1)^{th}$ coordinate onto each of the vectors $\mathbf{Y}(n)$, which is $x(n+mT)$. We compute the Euclidian distance, as measured in dimension $m+1$, between $\mathbf{Y}(n)$ and the same r^{th} neighbor, as determined in dimension m. After the addition of the new $(m+1)^{th}$ coordinate, the distance between $\mathbf{Y}(n)$ and the same r^{th} nearest neighbor in m dimensions is:

$$R_{m+1}^2(n,r) = R_m^2(n,r) + [x(n+mT) - x^{(r)}(n+mT)]^2. \tag{2.6}$$

A natural criterion for detecting embedding errors is that the increase in distance between two neighbors, $\mathbf{Y}(n)$ and $\mathbf{Y}^{(r)}(n)$, is large when we are going from dimension m to $m+1$. We state this criterion by designating any neighbor to be a FNN whenever the following is satisfied:

$$\left[\frac{R_{m+1}^2(n,r) - R_m^2(n,r)}{R_m^2(n,r)}\right]^{1/2} > R_{tol} \Rightarrow \frac{|x(n+mT) - x^{(r)}(n+mT)|}{R_m(n,r)} > R_{tol}, \tag{2.7}$$

where R_{tol} is a user-defined tolerance threshold.

In general, this criterion, by itself, is insufficient for determining a proper embedding dimension. A problem occurs if a point is the nearest neighbor of another, without necessarily

being close to it. Therefore, the number of FNNs increases as the dimension increases. To adequately handle this situation, we introduce a second criterion, the so-called *loneliness* criterion, represented by the "loneliness tolerance" threshold explained below.

First of all, as a measure of the size of the attractor, Kennel *et al.* [91] chose the value R_A^2 to be:

$$R_A^2 = \frac{1}{N}\sum_{i=1}^{N}[x(n) - E(x)]^2, \tag{2.8}$$

where

$$E(x) = \frac{1}{N}\sum_{n=1}^{N}x(n). \tag{2.9}$$

Using these terms, if the nearest neighbor to $\mathbf{Y}(n)$ satisfies $R_m(n) \approx R_A$, and it is a FNN, then the distance $R_{m+1}(n)$ resulting from adding an additional $(m+1)^{th}$ component to the data vectors, will be $R_{m+1}(n) \approx 2R_A$. The FNNs are stretched to the extremities of the attractor when they are unfolded from each other. Thus, the second criterion can thus be written as:

$$\frac{R_{m+1}(n)}{R_A} > A_{tol}, \tag{2.10}$$

where A_{tol} is a user defined threshold.

Informally, the second criterion states that if the distance to the nearest neighbor becomes smaller than the standard deviation of the data divided by the threshold, the point is omitted.

Combining both these thresholds, the output produced by the method is the percentage amount of FNNs *versus* the increase in the magnitude of the dimension, and this yields a monotonically decreasing graph.

In conclusion, the parameters required for computing the FNNs are:

1. The delay of coordinates, T, needed for the space reconstruction;

2. The maximum embedding dimension, m_{max}. The percentage of FNNs will be computed from the embedding dimension by increasing it from unity up to this maximum embedding dimension.

3. The distance tolerance, R_{tol}, which is the first threshold for the embedding criterion. Very high values of R_{tol} result in an underestimation of the number of FNNs, and very low values for R_{tol} identify too many FNNs, which is true when the points on the attractor became sparse. The choice of $R_{tol} = 10$ usually identifies the FNN clearly [91].

4. The loneliness tolerance, A_{tol}, which is the threshold for the second criterion given by Equation (2.10). Unusually high or low values of A_{tol} have the same effects as described above for R_{tol}. A choice of $A_{tol} = 2$ is good in most cases [91].

It is worth mentioning that there are also alternative methods to compute the optimum number of embedding dimensions [154]. It suffices to mention two such schemes:

i) *False strands*: Whereas the method of FNN consists of measuring the divergence of nearby points after a short time, the method of false strands measures whether trajectories which cross continue to stay relatively close to each other over their entire "lifespan".

ii) *The "doctrine" of ever increasing embedding dimension*: In this case, the method recommends that we choose increasing embedding dimensions, and in each case that we measure the correlation integral. When no change in the behavior of the correlation integral with increasing dimension is observed, the method determines that a sufficiently large embedding dimension has been obtained.

2.5 Concepts Concerning Dimensionality

2.5.1 Rationale and Definitions

The evolution of the system from an initial state corresponds to a trajectory in its state space. If the trajectory approaches a subset of the state space, this set is called an attractor. One of the key concepts used in analyzing chaos involves measuring the "dimensionality" of the objects concerned. In this context, the Correlation Dimension is *one* of the measures used to describe the attractors discovered in the phase space. However, to place this discussion in the right perspective, we provide here a brief introduction to the concepts involving dimensionality. More details can be found in Appendix E and in Falconer [51].

Definition 2.2.

Let E be a closed subset of R^n. A Mapping $S : E \rightarrow E$ is called a ***contraction*** *on E if $\exists t : 0 < t < 1 : |S(x) - S(y)| \leq t|x - y|, \forall x, y \in E$.*

Definition 2.3.

Let E be a closed subset of R^n. A Mapping $S : E \rightarrow E$ is called a ***similarity*** *on E if $\exists t : 0 < t < 1 : |S(x) - S(y)| = t|x - y|, \forall x, y \in E$.*

In the case of Definition 2.3, S transforms sets to geometrically similar ones.

Definition 2.4.

Let $S_1, ..., S_m$ be a finite family of contractions, called an ***iterated function systems (IFS)****. A non-empty compact subset F of E is called an* ***attractor*** *(or* ***invariant set****) for the transformations $\{S_i\}$ if*

$$F = \bigcup_{i=1}^{m} S_i(F) \tag{2.11}$$

Definition 2.5.

A set that is invariant under a collection of similarities is called a ***self-similar*** *set, implying that it is the union of a number of smaller copies of itself.*

The fundamental property of an IFS is that it determine a unique attractor, which is usually a fractal. The word *fractal* was used by Mandelbrot [106], and it is derived from the Latin *fractus*, meaning "broken", to describe objects that are too irregular to fit into traditional geometrical settings. Falconer [51] described a fractal F as follows:

(i) F has a fine structure, i.e detail on arbitrarily small scales.

(ii) F is too irregular to be described in traditional geometrical language, both locally and globally.

(iii) Often F has some form of self-similarity, perhaps approximate or statistical.

(iv) Usually, the "fractal dimension" of F, defined suitably, is greater than the topological dimension.

(v) In most cases of interest, F is defined recursively.

The following theorem (stated without proof) describes the "uniqueness" characteristic of an attractor that corresponds to a set of contraction transformations.

Theorem 2.1

Let $S_1, ..., S_m$ be contractions on a subset E of R^n such that

$$|S(x) - S(y)| \leq t_i|x - y|, (x, y) \in E, \tag{2.12}$$

with $t_i < 1$ for each i. Then, there exists a unique attractor F, i.e. non-empty compact set F such that

$$F = \bigcup_{i=1}^{m} S_i(F) \tag{2.13}$$

Observe that since $F \subseteq R^n$ and is compact, it must be closed.

Self-affine sets constitute an important class of sets, for which self-similar sets occur as a particular case.

Definition 2.6.

*An **affine** transformation $S : R^n \to R^n$ is a transformation of the form*

$$S(x) = T(x) + b \tag{2.14}$$

where T is a non-singular linear transformation on R^n (represented by an $n \times n$ matrix) and b is a vector in R^n.

Thus, an *affine transformation* S is a combination of translation, rotation, and dilatation. The particular cases are the transformation from a sphere to an ellipsoid, from a square to a parallelograms, etc. Contrasting with the particular case of similarities, affine transformations contract with differing ratios in different directions.

Definition 2.7.

Let $A_1, ..., A_m$ be affine contractions on R^n. The set F which satisfies

$$F = \bigcup_{i=1}^{m} S_i(F) \tag{2.15}$$

*is called **self-affine**.*

Definition 2.8.

Let U be a non-empty subset of R^n. The diameter of U is defined as

$$|U| = \sup |x - y| : x, y \in U. \tag{2.16}$$

If $F \subset \bigcup_{i=1}^{\infty} U_i$ with $0 < |U_i| \leq \delta$ for each i, U_i is called a *δ-cover* of F.

The following definition introduces the oldest "fractal dimension", namely the Hausdorff dimension. This dimension has the advantage of being defined for any set but it has a major disadvantage: in many cases it is hard to calculate or to estimate by computational methods [51]. The Hausdorff dimension, introduced in 1918 by the mathematician Felix Hausdorff, gives an accurate way to measure the dimension of an arbitrary metric space; this includes complicated sets such as fractals. Suppose (X,d) is a metric space. Haussdorf was interested in counting the number of balls of some radius necessary to cover a given set. It is possible solve it directly for many sets (leading to the so-called box-counting dimension), but Hausdorff's insight was to approach the problem indirectly using the theory of measure developed earlier in the century by Henri Lebesgue and Constantin Caratheodory. In order to deal with the technical details of this approach, Hausdorff defined an entire family of measures on subsets of X. Many of the technical developments used to compute the Hausdorff dimension for highly irregular sets were obtained by Abram Besicovitch. For this reason, the Hausdorff dimension is sometimes referred to as the Hausdorff-Besicovitch dimension [43].

Definition 2.9. (Hausdorff Measure)

Suppose that F is a subset of R^n and that s is a non-integer number. For any $\delta > 0$, define $H^s_\delta(F)$ as:

$$H^s_\delta(F) = \inf \left\{ \sum_{i=1}^{\infty} |U_i|^s : U_i \text{ is a } \delta\text{-cover of } F \right\}$$

*where the infimum is over all countable δ-covers $\{U_i\}$ of F. The **s-dimensional Hausdorff measure** of F is defined as:*

$$H^s(F) = \lim_{\delta \to 0} H^s_\delta(F). \tag{2.17}$$

The limit, $H^s(F)$, exists for any $F \in R^n$, though the limiting value can often be zero or infinity. Formally,

$$dim_H F = inf\{s \geq 0 : H^s(F) = 0\} = sup\{s : H^s(F) = \infty\}. \tag{2.18}$$

The next definition represents one of the most widely used dimension, due its relative easy of calculation and estimation, namely the box-counting dimension[8].

Definition 2.10.

Let F be an non-empty bounded subset of R^n and let $N_\delta(F)$ be the smallest number of sets of diameter of F respectively are defined as

$$\underline{dim}_B F = \underline{\lim}_{\delta \to 0} \frac{\log N_\delta(F)}{-\log \delta} \tag{2.19}$$

$$\overline{dim}_B F = \overline{\lim}_{\delta \to 0} \frac{\log N_\delta(F)}{-\log \delta} \tag{2.20}$$

*If there are equal, we refer to a common value as the **box-counting dimension** of F:*

$$dim_B F = \lim_{\delta \to 0} \frac{\log N_\delta(F)}{-\log \delta}. \tag{2.21}$$

[8]This dimension is also termed Kolgomorov entropy, entropy dimension, capacity dimension or information dimension.

Definition 2.11.

The contractions S_i are said to satisfy the **open set conditions** *if there exists a non-empty open bounded set V such that*

$$V \supseteq \bigcup_{i=1}^{m} S_i(V) \tag{2.22}$$

with the union being disjoint.

The following theorem (stated without proof) specifies the relation between the dimensions of an attractor.

Theorem 2.2

Suppose that the open set conditions hold for similarities $\{S_i\}$ on R^n with ratios t_i $(i = 1, ..., m)$. If F is the invariant satisfying

$$F = \bigcup_{i=1}^{m} S_i(F) \tag{2.23}$$

then $dim_H F = dim_B F = s$, where s is given by

$$\sum_{i=1}^{m} t_i^s = 1. \tag{2.24}$$

Further, for this value of s, $0 < H^s(F) < \infty$.

2.5.2 Fractal Dimensions

An object can be fully represented by a set of points is a Euclidian space R^m provided that m is sufficiently large to be able to uniquely locate the position of each point in the object. For each set in R^m, it is possible to assign a topological dimension d that is an integer in the range $[0, m]$. If the set contains all of R^m, then $d = m$. In Euclidian geometry, points have dimension $d = 0$, lines have dimension $d = 1$, plane surfaces have dimension $d = 2$, solids have dimension $d = 3$, etc [76].

A *fractal dimension* D is any dimension measurement that allows non-integer values [106]. The reader can observe that such a generalization permits the use of many measures for the quantity D. A fractal, defined in the previous Subsection, has a non-integer fractal dimension. The importance of fractals in dynamical systems consists of the fact that their fractal dimension D is simply related to the minimum number of dynamical variables required to model the dynamics of the fractal.

Conceptually, the simplest way to measure the dimension of a set is to measure the Kolmogorov capacity (or box-counting dimension). In this measurement, a set is covered with small squares of size ϵ for sets embedded in two dimensions or small cubes of size ϵ for sets embedded in three dimensions. By denoting with $M(\epsilon)$ the number of such elements that contain parts of the set, the dimension D is defined as :

$$D = \lim_{\epsilon \to 0} \frac{log(M(\epsilon))}{log(\frac{1}{\epsilon})}. \tag{2.25}$$

For the case of n isolated points, $m(\epsilon) = m$ and $D = 0$. Similarly, for a straight line of length L, $M(\epsilon) = L/\epsilon$ and $D = 1$ and for a 2-dimensional a region of area A, $M(\epsilon) = A/\epsilon^2$ and $D = 2$. In practical applications, the computation cannot attain the limit ϵ. The number $M(\epsilon)$ is derived for a range of small values of ϵ and the dimension D is estimated as the slope of the straight line portion of the plot of $log(M(\epsilon))$ versus $log(1/\epsilon)$. More details of such computations can be found in [76].

In the process of computing the box-counting dimension, a box is counted whenever it contains parts of the set, without differentiating between whether a box contains many points of the set or not. There are more elaborate dimension measurements that take into considerations inhomogeneities or correlations in the set. The *dimension spectrum* defined by Hentschel and Procaccia [77] provides a set of generalized or Rényi dimensions that take into account higher order correlations as q is increased, where q is the index specified in the following relation:

$$D_q = \lim_{r \to 0} \frac{1}{q-1} \frac{log \sum_{i=1}^{M(r)} p_i^q}{log\ r}, \quad q = 0, 1, 2, ... \tag{2.26}$$

In the dimension spectrum, $M(r)$ is the number of m-dimensional elements of size r, namely hypercubes of side r, needed to cover the set and $p_i = N_i/N$ is the probability of finding a point

in the set in hypercube i. Similarly, N is the total number of points in the set, and N_i is the number of points of the set in hypercube i. The reader can easily observe that the box-counting dimension is equivalent to D_0.

In addition to D_0, the literature also contains definitions corresponding to D_1 and D_2. Dimension D_1 is called the *information dimension*, defined as:

$$D_1 = \lim_{q \to 1} D_q = \lim_{r \to 0} \frac{\sum_{i=1}^{M(r)} p_i \; log \; p_i}{log \; r}. \tag{2.27}$$

Kaplan and Yorke [89] conjectured the relationship between the information dimension[9] and the Lyapunov exponents as:

$$D_1 = j + \frac{\sum_{i=1}^{j} \lambda_j}{|\lambda_{j+1}|}, \tag{2.28}$$

where λ_i are the Lyapunov exponents of the attractor ordered from the largest to the smallest, and where $\sum_{i=1}^{j} \lambda_i \geq 0$; $\sum_{i=1}^{j+1} \lambda_i < 0$.

For the case when $q = 2$, the dimension D_2 is called the *correlation dimension* and it can be written as:

$$D_2 = \lim_{r \to 0} \frac{log \; C(r)}{log \; r}, \tag{2.29}$$

where

$$C(r) = \sum_{i=1}^{M(r)} p_i^2 \tag{2.30}$$

is the correlation sum, which is the probability that two points of the set are in the same element, which leads to an exact result in the limit as $N \to \infty$.

A characteristic of the generalized dimensions is that they generally decrease with increasing q so that $D_{q_1} \geq D_{q_2}$ if $q_2 > q_1$. More generally $D_E \geq D_0 \geq D_H \geq D_1 \geq D_2 \geq ... \geq D_T$ where D_E is the Euclidian dimension (the integer of the space in which the set is embedded), D_H is the Hausdorff dimension, and D_T is the topological dimension (the largest integer dimension of the pieces that compose the set) [155]. The Renyi dimension with $q = 0$ treats all parts of the support of the attractor equally. However, larger values of q imply that none a increasing weight is assigned in the calculation to the parts of the attractor which are visited more frequently.

[9]Such a dimension has also been called the Kaplan-Yorke dimension (DK-Y) or Lyapunov dimension.

An attractor for which the Renyi dimensions are not all equal is said to be a multifractal, or to exhibit multifractal structure. This is a signature that signifies that a varying scaling behavior occurs at different parts of the attractor.

In addition to the multifractal (or *inhomogeneous fractal*) model, which has D_q dependent on q, it is also possible to define a monofractal (or *homogenous fractal*) model that has D_q independent of q. In our thesis, we assume that the system under consideration can be adequately modelled using a monofractal system. This is, in our opinion, a valid assumption as long as we are dealing with realistic neural network models. We observe, though, that this is only an approximation when we encounter real-life *brain* signals.

2.5.3 Computing the Correlation Dimension

Two data points that fall in the proximity of each other in phase space are highly spatially correlated, and thus the coordinates of one value leads to a close estimate of the second. The Correlation Dimension (D_2) attempts to achieve this by merely testing points for their *spatial* interrelations; while simultaneously ignoring time and thus their temporal relationship.

The D_2 is one of the most widely used metrics of fractal dimension, measuring the complexity of the system related to its number of degrees of freedom, or in a more intuitive way, with its topological dimension. Since, in principle, the D_2 converges to finite values for deterministic systems and does not converge in the case of a random signal, it can be used as a good parameter for evaluating the inherent deterministic or noisy nature of a system. In the context of this research, the question of evaluating the deterministic or noisy nature signals (such as EEG waveforms) has recently captivated the attention of many research groups.

This dimension, although mathematically defined, is determined by examining experimental data, and is therefore very useful to the understanding of the system. This is particularly true for deciding if the system is periodic, chaotic, or noisy. The D_2 can be used to approximate the dimension of all these types of graphs, and is traditionally computed from the underlying time series diagram which is a simplified phase space diagram constructed from a single data vector.

In our research we have opted to use the algorithm proposed by Grassberger and Procaccia [64, 65] to compute the D_2. The principal idea is to construct the so-called correlation function,

$C(r)$, which evaluates the probability that two arbitrary points on the trajectory are closer than a parameter r. This is achieved by calculating the separation between every pair of N data points and sorting them into bins of width Δr proportionate to r. The D_2 can then be calculated using the distances between each pair of points in the set.

To compute the latter, as mentioned, we use the quantity $C(r)$, which measures the number of points X_j that are correlated with each other in a sphere of radius r around the reference point, X_i. It has the form:

$$C(r) = \frac{2}{N(N-1)} \sum_{i=1}^{N-1} \sum_{j=i+1}^{N} \Theta(r - ||X_i - X_j||), \tag{2.31}$$

where:

1. X_i , X_j are points of the trajectory in the phase space, which are $||X_i - X_j||$ units apart,
2. N is the number of data points in phase space,
3. r is the radial distance around each reference point X_i, and
4. Θ is the Heaviside function.

Using the function $C(r)$, the D_2 can be calculated in term of its fundamental definition:

$$D_2 = \lim_{r \to 0} \frac{\log C(r)}{\log(r)}. \tag{2.32}$$

2.5.4 Finding the Time Lag and the Embedding Dimension

In order to achieve the phase space reconstruction described in Equation (2.4), we have to use an appropriate time lag, T, and an appropriate embedding dimension, m.

If the time lag, T, is too small, the components in Equation (2.4) will all have approximately the same value, and they will not properly span the phase space. This condition is called *redundancy*. In the extreme case, the attractor will be constricted to a diagonal line, and its

topology will be lost. On the other hand, if the time lag, T, is very large, the components of each embedding vector will become totaly unrelated to each other, thus rendering it meaningless, which is called *irrelevance*. Several methods have been developed for estimating the optimal time lag, and among them, the most popular one utilizes the first zero of the autocorrelation function. Another approach, given by Rosenstein *et al.* [141], proposed a geometrical-based method. In this case, the main idea is to search for a time lag that gives an optimal expansion of the embedding vectors with respect to the diagonal in the phase space.

The accuracy of the nonlinear time series analysis also lies in the selection of the optimum embedding dimension, m. If m is too small, the attractor will not be completely unfolded, and on the other hand, if m is to large, the computations will be dominated by noise. Embedding theorems, specified and proven by Takens [159], state that for a strange attractor, the embedding using time delay coordinates becomes one-to-one if $m \geq 2D_2 + 1$, where m is the embedding dimension. But the limitation on the applicability of the theorems is that, in general, the measure D_2 is not known. For practical applications, it is wise to first apply the Grassberger and Procaccia algorithm [64],[65], and to then calculate the D_2 for various embedding dimensions. Subsequently, the minimum embedding dimension of the attractor for one-to-one embeddings is assigned the value $m + 1$, where m is the embedding dimension above which the D_2 saturates.

In this context, we mention that the software that we have used to compute the D_2 is the so-called *Dataplore*, created by Ixellence GmbH.

With regard to implementation of these methods, the data points used in calculating the autocorrelation come from a time series, whose time resolution can be either too small or too large, and which may introduce spurious effects. Here, if the time resolution is too small, the data may contain multiple copies of essentially the same measurements, which leads to multiple-counting. In such a case, the D_2 is artificially low because all the points are temporally close to each other. This effect occurs when the time resolution Δt of the analyzed data is much smaller than the autocorrelation time τ_{ac} (or any characteristic time scale), implying that $\Delta t \ll \tau_{ac}$.

The correction proposed by Theiler [162] can be described as follows. For each reference point X_i, we consider measurements X_j, which are at least $w = \tau_{ac}$ steps away from X_i. Using this correction, the correlation function is computed using the vectors which are distanced at least w data points ($|i - j| > w$) away.

2.6 Lyapunov Exponent (LE)

2.6.1 The Individual Lyapunov Exponent and the Spectrum of Lyapunov Exponents

The Lyapunov Exponent (LE) is a quantitative measure of the dependence of the sensitivity of the dynamical system on the initial conditions. It defines the average rate of divergence of two neighboring trajectories. An exponential divergence of initially nearby trajectories in the phase space, coupled with the folding of trajectories, (to ensure that the solutions will remain finite), is the general mechanism for generating deterministic randomness and unpredictability. Therefore, the existence of a positive LE for almost all initial conditions in a bounded dynamical system is a widely-used definition of deterministic chaos, and it helps to discriminate between chaotic and periodic signals.

By way of explanation, the LE is a measure of the rate at which two trajectories separate from each other. The trajectories of chaotic signals in phase space follow typical patterns, and so closely spaced trajectories converge and diverge exponentially, relative to each other. The sensitivity to these initial conditions is quantified by the LE, which characterizes the average rate of divergence of these neighboring trajectories [155]. Indeed:

a) A negative exponent implies that the trajectories approach a common fixed point.

b) A zero exponent means that the orbits maintain their relative positions; they are on a stable attractor.

c) A positive exponent implies that the trajectories are on a chaotic attractor.

Let $X_0(t)$ denote a reference trajectory passing through $X_0(0)$ at time $t = 0$ and let $X_1(t)$ denote a reference trajectory passing through $X_1(0)$ at $t = 0$. The Lyapunov exponent $\lambda(X_0)$ is defined with respect to the reference trajectory X_0 by

$$\lambda(X_0) = \lim_{t\to\infty} \lim_{||\Delta||\to 0} \frac{1}{t} log \frac{||\Delta X(t)||}{||\Delta X(0)||}, \tag{2.33}$$

where $||\Delta X(0)||$ is the Euclidian distance between the trajectories $X_0(t)$ and $X_1(t)$ at the initial time $t = 0$, and $||\Delta X(t)||$ is the Euclidian distance between the trajectories $X_0(t)$ and $X_1(t)$

at the subsequent time, t. In this definition, $X_1(t)$ can be any trajectory that is initially infinitesimally close to $X_0(0)$ at time $t = 0$. The correspondence between the system's sensitivity to initial conditions and a positive Lyapunov exponent is obvious in the expression:

$$||\Delta X(t)|| \sim ||\Delta X(0)||e^{\lambda t} \tag{2.34}$$

To define the full set of Lyapunov exponents, one for each embedding dimension, we consider an infinitesimal m-dimensional sphere of initial conditions that is anchored to a reference trajectory. As the sphere evolves, it becomes deformed into an ellipsoid. Let $p_i(t)$ denote the length of the i^{th} principal axis, ordered from most rapidly growing one to the least rapidly growing one. The following expression:

$$\lambda_i = \lim_{t\to\infty} \frac{1}{t} log\left(\frac{p_i(t)}{p_i(0)}\right), \quad i = 1, 2, ..., m, \tag{2.35}$$

defines the set of Lyapunov exponents [155] ordered in their decreasing order. The evolution in the phase space of the volume elements will be as:

$$V(t) \sim V(0)exp\left(\sum_{i=1}^{m} \lambda_i t\right). \tag{2.36}$$

Since the Lyapunov exponent and the spectrum of the Lyapunov exponents have been defined, it is now appropriate to discuss possible algorithms for numerically computing them.

For any flow in an m dimensional phase space described by the set of first-order differential equations:

$$\dot{X} = G(X), \tag{2.37}$$

$$X = \{x_i\}, \quad i = 1, 2, ..., m \tag{2.38}$$

it is clear that there are m Lyapunov exponents. There are three main algorithms reported for the computation of the complete spectrum of Lyapunov exponents [13, 14, 48, 130, 149, 177]. In all the algorithms, m subsequent trajectories are computed in addition to the reference trajectory. The subsequent trajectories are differentially separated from the reference trajectory

and obey the linearized equations obtained by differentiating Equation (2.37) as:

$$\frac{d}{dt}(\delta X)_l \equiv \dot{\delta}_l = \frac{\partial G(X)}{\partial X}\delta_l, \quad l = 1, 2, ..., m. \tag{2.39}$$

An arbitrarily oriented set of orthonormal vectors are chosen as initial condition for the set of m different vectors δ_l. In the case of analyzing a chaotic system, these vectors do not stay orthogonal to each other. They will start to rotate into the direction of maximum phase-space growth, when $t > 0$. In the converse case, it is also possible that they will diverge. To avoid this computational problem, a Gram-Schmidt re-orthonormalization (GSR) procedure must be applied to the vector δ_l after every few times steps [20] (the details of which can be found in Section D). In this case, after some transient time, δ_1 tends to point into the direction (in the phase space) which grows most rapidly, in a manner proportional to $exp(\lambda_1 t)$. Similarly, the pair δ_1, δ_2 spans a subspace whose area grows most rapidly proportional to $exp(\lambda_1 + \lambda_2)t$. In general, $\delta_1, \delta_2, ..., \delta_n$ span a subspace with a maximum volume growth proportional to $exp(\lambda_1 + \lambda_2 + ... + \lambda_l)t$. By observing this sequence, $\lambda_1 + \lambda_2 + ... + \lambda_l$ can be computed. More details of this algorithm can be found in *Wolf et al.* [177].

Eckmann et al. [48] proposed a matrix orthogonalization algorithm as an alternative to GSR. Posch and Hoover [130] introduced the third algorithm (suggested also by Goldhirch *et al.* [62]), utilizing ideas from control theory and constraint dynamics. Instead of allowing the linearized trajectories computed in Equation (2.39) to evolve freely and computing the Lyapunov exponents by periodically rescaling the differential offset vectors δ_l in the tangent space, as in the GSR algorithm, these vectors may be constrained to stay normalized and orthogonal to each other at all times. The details of this third algorithm can be found in [130]. In our research, we have utilized the first algorithm, proposed by Wolf *et al.* [177] to compute the LE from a data signal, such as an simulated EEG waveform.

According to Das *et al.* [37], an embedding dimension between 5 to 20 and a delay of unity should be chosen when calculating the LE for chaotic data signals such as EEG signals, and we have found that these are valid parameters.

2.7 Synchronicity Between Two Coupled Nonlinear Systems

In order to describe the synchronization between two coupled nonlinear systems, we introduce two measures, namely the Cross Correlation (CC) and the nonlinear interdependence, typically referred to by the symbol S.

2.7.1 Cross Correlation Coefficient (CC)

The Cross Correlation Coefficient is a standard metric for estimating the degree to which two series are correlated. Consider two series $X = \{x_i\}$ and $Y = \{y_i\}$ where $i = 1..N$. The CC at delay d is defined as:

$$CC(d) = \frac{\sum_{i=1}^{N}[(x_i - m_x) \times (y_{(i+d)} - m_y)]}{\sqrt{\sum_{i=1}^{N}(x_i - m_x)^2 \times \sum_{i=1}^{N}(y_{i+d} - m_y)^2}}, \tag{2.40}$$

where m_x and m_y are the means of the corresponding series. If the above is computed for all possible delays $d = 0..N-1$, we obtain a cross correlation series.

The range of delays d, and thus the length of the cross correlation series, can be less than N, if, for example, the aim is to test the correlation at short delays only. The denominator in the above expression serves to normalize the CCs in a such manner that $-1 \leq CC(d) \leq 1$, where these extreme bounds indicate the maximum correlation, and 0 indicates no correlation. A large negative CC indicates a large inter-relationship between the two series, when one is the "inverse" of the other.

2.7.2 Nonlinear interdependence (S)

As the theory of nonlinear dynamics clearly shows [79], a state space is the natural framework in which the properties of nonlinear dynamical systems can be described and quantified. These

properties may be undetectable in the time domain of the system output, e.g., in the EEG tracing. Nonlinear interdependence is said to occur when the phase-space reconstructed trajectories of one time series experimentally predicts the evolution of the phase space trajectories of the other time series [147]. A phase space representation may reveal the salient features of the nonlinear structure which are hidden or occluded to standard linear approaches [156]. This measure of predictability has the advantage over linear measures of being sensitive to interdependence between dissimilar types of activity [26].

Let $\mathcal{X}$ and $\mathcal{Y}$ be two systems and let us associate with them their respective time series $X = \{x_i\}$ and $Y = \{y_i\}$. Consider now how we can reconstruct the so-called delay vectors $x'_n = [x_n, ..., x_{n-(m-1)T}]$ and $x'_n = [y_n, ..., y_{n-(m-1)T}]$, where $n = 1..N$, m is the embedding dimension, and T denotes the time lag. We denote the series of the new reconstructed vectors as $X'=\{x'_i\}$ and $Y'=\{y'_i\}$.

Let $p_{n,j}$ and $s_{n,j}$, $j = 1..k$, denote the time indices of the k nearest neighbors of x'_n and y'_n, respectively. For each x'_n, the mean-squared Euclidean distance to its k neighbors is defined as:

$$R_n^{(k)}(X') = \frac{1}{k}\sum_{j=1}^{k}(x'_n - x'_{p_{n,j}})^2. \tag{2.41}$$

Similarly, the Y'-conditioned[10] mean-squared Euclidean distance is defined by replacing the nearest neighbors by the equal time partners of the closest neighbors of y'_n. Let the nearest neighbors in X' to a particular y'_n be the sample $\{x'_{s_{n,j}}\}$. Then, this Y'-conditioned quantity is:

$$R_n^{(k)}(X'|Y') = \frac{1}{k}\sum_{j=1}^{k}(x'_n - x'_{s_{n,j}})^2. \tag{2.42}$$

If the point cloud x'_n has an average squared radius R(X') given by:

$R(X') = (1/N)\sum_{n=1}^{N} R_n^{(N-1)}(X')$,

then:

a) $R_n^{(k)}(X'|Y') \approx R_n^{(k)}(X') \ll R(X')$ if the systems are strongly correlated, while

[10]The conditional/conditioned quantities are achieved by treating them as "given" variables as in any probability/stochastic context.

b) $R_n^{(k)}(X'|Y') \approx R(X') \ll R^{(k)}(X')$ if they are independent.

Accordingly, we can define an interdependence measure $S^{(k)}(X'|Y')$ [5] as:

$$S^{(k)}(X'|Y') = \frac{1}{N}\sum_{n=1}^{N}\frac{R_n^{(k)}(X')}{R_n^{(k)}(X'|Y')}. \tag{2.43}$$

Since the indices of the conditioned random variable X' which are closest cannot be any closer then the corresponding elements in X for the unconditioned random variable, we know that $R_n^{(k)}(X'|Y') \geq R_n^{(k)}(X')$, and thus,

$$0 < S^{(k)}(X'|Y') \leq 1. \tag{2.44}$$

Low values of $S^{(k)}(X'|Y')$ indicate relative independence between X' and Y', while higher values of $S^{(k)}(X'|Y')$ indicate a higher degree of synchronization, which attains its maximum when $S^{(k)}(X'|Y') \longrightarrow 1$.

The opposite interdependence $S(Y'|X')$ is defined in an analogous manner, and in general, not equal to $S(X'|Y')$. The asymmetry of S is the main advantage of using these quantifiers over other nonlinear measures such as the mutual information and the phase synchronization while this asymmetry provides information about driver response relationships [5],[131]. Besides, it can also reflect the different dynamical properties of the data set [5],[131].

To address this point we can compare results with synchronization values obtained from time-shifted signals used as surrogates[11], but for the present, we refer the reader to an excellent

[11]The purpose of surrogate data is to test for any nonlinearity in a data set, where strong and consistent nonlinear deterministic signatures are expected. To be more specific, the method of surrogate data is a statistical approach that was developed to test hypotheses about whether the observations in a given time series are independent and identically distributed (IID), linear and/or nonlinear in nature. This is accomplished through studying surrogates that are generated by resampling the original time series without replacement such that the surrogate time series is consistent with either the null hypothesis that the data is IID or the hypothesis that the data is linear. Many such surrogates are generated and the time series statistic being considered is calculated from each. This yields a distribution of the time series statistic under the IID or linear null hypothesis. If the time series statistic from the original time series is large or small when compared with the distribution of the

work of Quiroga *et al.* which presents a detailed study of inter-systems synchronization [131]. Given a cloud of points characterizing a neighborhood of one point in one of the attractors, say X', we see how this maps into the other system Y'. For synchronized systems, the point cloud in Y' will still be in a small neighborhood. On the other hand, for independent systems, the points in Y' will most likely be spread over the entire attractor. Thus, in effect, the measure described above, S, is just a different way of normalizing these ratio of distances.

2.8 Chaotic Brain Modelling

In this Section we present a survey concerning chaotic brain modelling and methods related to controlling the chaos in models of the brain. We undertake this survey because one ultimate goal of our research is to use chaotic modelling to anticipate and/or prevent epileptic seizures.

2.8.1 Aspects of Nonlinear Behavior in Brain Modelling

The first step in analyzing nonlinear system is usually, when possible, to linearize it around a nominal (quiescent) operating point. The reason is that linear systems are mathematically easier to handle. Assuming that deviations from the linearized model are not too large, such an approximation may well be adequate as a basis for design and analysis over a limited range of operations. In fact, control systems are initially normally designed in this way, and the effect of departures from linearity are then investigated by simulation methods.

The stability properties of a nonlinear system are essentially more complicated than those of the linear case, and in particular, one has to distinguish between local and global aspects. For a linear system there is no such distinction, but when nonlinearities are present, several new features can appear. First of all, the stability of a nonlinear system in the neighborhood of an equilibrium point does not necessarily imply a global phenomenon. Indeed, in such systems,

statistic under the null hypothesis, one can conclude that there is evidence in favor of the alternate hypothesis. The surrogate signal can be produced by phase randomizing the given data [163]. To be more specific, the complex phase values of the Fourier-transformed input signal are chosen randomly. This surrogate signal has similar spectral properties as the given data, namely, it possesses the same mean, the same variance, the same autocorrelation function etc., and consequently, the same power spectrum as the original sequence. The only difference between the two is that the nonlinear phase relations are destroyed in the surrogate data.

there may be many point of equilibria, some of which could be stable. In the case of unstable equilibria, there could only be a limited region of convergence (i.e., the domain of attraction) around any given equilibrium point which can also be locally asymptotically stable. Furthermore, there can be other, essentially nonlinear modes of behavior, such as persistent oscillations known as limit cycles, which constitute a kind of dynamic, rather than static, equilibrium. Such equilibrium phenomena have no true counterpart in linear systems. In fact, there are possibilities which are much more complicated than the periodic behavior associated with simple limit cycles, including those which reach to the extent of a quasi-stochastic situation arising, despite the deterministic nature of the system's equations. This phenomenon is, indeed, *chaos*, which can be generated in both discrete-time or continuous-time systems, and can occur even relatively simple, low-order models. In any case, the type of behavior actually manifested by a nonlinear system, whether stable, unstable, oscillatory or chaotic, may depend critically on the input applied to it. In contrast, in the linear case, all the dynamical properties can be described, for example by a transfer function, independent of the input.

This research intends to investigate the generation of chaos in the models of neurons of the brain, of small-scale networks of neurons, and ultimately of large-scale networks of neurons. These investigations can lead to interesting results, because during the last years, the mathematical analysis of nonlinear systems related with neural models has been enriched with new concepts such as the families of Unstable Periodic Orbits[12] (UPO) and Milnor attractors[13].

2.8.2 The Models of the Epileptic Brain

The brain can be described using two approaches:

1. The *traditional neuroscience* focuses on the details of the brain involving neurotransmitters, receptors and neurons, where the latter entities are considered alone or in small

[12]Consider D a domain in R^n and $F[n] : D \to R^n$ be a smooth function, definite in a discrete time. For any point X in the phase space let $W^u(X)$ denote the *unstable periodic orbit*, that is the set of points Z such that the $||F[-n](X) - F[-n](Z)|| \to 0$ as $n \to \infty$. This definition is taken from [67].

[13]The Milnor attractors [114] are described as follows: An arbitrary small perturbation to an orbit at a Milnor attractor can force the orbit away from it to a different one, even though a finite measure of initial conditions is attracted to the attractor by temporal evolution. An orbit is often attracted to the Milnor attractor, but can be forced away from it by an infinitesimal perturbation. In other words, the basin of the attractor touches the attractor itself, somewhere.

groups.

2. The *nonlinear dynamic* analysis is a mathematical approach which attempts to identify large-scale patterns that emerge when neurons interact *en masse*, leading to "small" scale networks or to "large" scale networks.

Research is this area is dominated by studies of epilepsy. This is partially due to the fact that the widespread and convulsive firing of neurons in epileptic seizures offer an interesting case by which the underlying collective dynamics can be studied.

While the medical challenge is to prevent seizures from occurring and to, thus, restore the patient to a "normal" life, the mathematical challenge is to understand the way qualitative changes occur in the dynamics of the brain, and the way by which these are reflected by changes in the corresponding waveforms, for example, as displayed in the EEGs. Finally, the scientific goal is to translate the mechanism of generating qualitative changes in the brain into effective therapeutic strategies. This leads to the practical goal, namely that of finding a way to control seizures without major surgery or drugs.

One solution can be the development of a computer chip[14] that can receive EEGs from the brain, detect the approach of a seizure, and apply spurts of current or electric fields to specific regions of the brain, using electrodes inside the skull. This objective is to "nudge" the dynamical system away from its tendency to attain a catastrophic firing state.

Two groups of researchers have proposed families of models which describe the fundamental dynamical structure of the brain. We mention them below and describe the details subsequently.

- **Bistability Model:** An analysis of brain recordings by physicists Manuca *et al.* [107] suggests that in spite of all its complexity, the epileptic brain might actually behave as a "bistable" entity, analogous to the behavior of a ball that is being "knocked" into one of two cups. Controlling this system could involve preventing it from jumping wildly between the two states.

[14] An external responsive neurostimulator (eRNS) and a programmer system (PS) were developed by NeuroPace to suppress seizures in patients with refractory epilepsy. They have been under clinical trials in the latter part of 2002. The eRNS is programmed to deliver responsive electrical stimulation to the patient when the onset of a seizure is detected with the goal of desynchronizing the epileptiform activity.

• **Multistability Model:** Schiff *et al.* [146] portray the brain's electrical state as wandering over a subtler dynamical "landscape" of peaks and valleys. Controlling this system might involve nudging the state up some of the peaks and balancing it there. This phenomenon is analogous to that of a beach ball on a walrus's nose.

Given these two approaches the question arises: Which model of the dynamical brain is the best? To address this, we shall consider both of these models in greater depth below.

2.9.2.1 Bistability Hypothesis

The bistability hypothesis dates experimentally to the 1980's, when Rinzel and Guttman [68] showed that the firing of *a single neuron* can jump between two different states. The researchers stimulated a squid giant axon with an electrical current, and noticed that the axon fired repetitively at high values of the current and shut off at low values. At some values in between, though, slight perturbations in the current made the axon jump between the firing and quiet states. In other words, they pushed the axon between two bistable states. The drastic jump meant that the system's response was not "linear".

When such neurons are linked in a network, they can behave (as the saying goes) "like dogs in the backyards of a neighborhood". If one dog barks, all the rest may start up, but once they fall silent, most of them may sleep through the afternoon [68]. The network itself would be bistable.

Milton *et al.* [117] suggested that "waves" of excitation could spread through such a bistable network, just as the dogs on one block may already have grown tired while those two blocks away have only started barking. Such waves haven't been observed directly in human brains during seizures, but measurements made by Milton's group through grids of electrodes reveal correlations in the firing of distant neurons, which could result from these excitation waves.

Another evidence of the bistability hypothesis emerges from studies that apply complex mathematical tools to searching for coherence in data recorded by electrodes implanted deep in epileptic brains. Linear measures of synchronization can determine whether two waves are locked in phase. Nonlinear measures can elaborate on more general relationships of arbitrary wave trains. Manuca *et al.* [107] identified a particular kind of nonlinear synchronization in

epileptic brains. Each location can switch between one of two different states: spiky firing patterns or smooth wave forms, depending on the position of each probe in the brain.

2.9.2.2 Multistability Hypothesis

Multistability refers to the coexistence of multiple attractors. This phenomenon arises because of a certain bifurcation (i.e. subcritical Hopf bifurcation) where more then one dynamical behavior is possible. The experimental and theoretical work indicate that the onset of oscillations in neurons [16, 22, 34, 35, 54, 68, 82, 98] and in neuronal populations [10, 38, 80, 81, 90, 116, 170, 171, 180] is characterized by multistability.

Multistable dynamical systems can be envisioned as a landscape with multiple valleys corresponding to the basins of attractions for each attractor separated by ridges of varying heights, which correspond to the *separatix*, or energy barrier, between the basins of attraction.

2.8.3 Controlling Dynamic Collective Behavior in Epilepsy

A *dynamic* disease is characterized by a sudden change in the qualitative dynamics of a patient when he is affected by a stimulus. It can arise, for example, because of alterations in the underlying physiological control mechanisms [12, 61, 103, 104, 115]. Analogous to mathematical models, changes of certain physiologically important parameters into critical ranges determine the sudden appearance of qualitatively different dynamical behaviors. In mathematical models, these changes in qualitative dynamics correspond to *bifurcations.*

There are over 30 diseases of the nervous system in which the recurrence of symptoms or the appearance of oscillatory signs are defining characterizing features [115]. The significance of identifying which of these disorders is a dynamic disease lies in the fact that it raises the possibility of treating the specific disease based on the manipulation of the underlying control mechanisms. The precise nature of the control strategies that are possible depends on the type of bifurcation that has occurred, and the nature of the abnormal dynamics that arose from the bifurcations. The simplest therapeutic strategy is to manipulate the altered control parameter back into a range associated with the "system's" healthy dynamics. In most cases this is not

possible, since the identity of the altered parameter is not known. However, it may be possible to devise control strategies that exploit the properties of the abnormal dynamics that arise. Thus, for example, chaotic dynamics can be controlled using control-of-chaos techniques [146], and similarly, multistable dynamics can be controlled using brief perturbations [68].

2.8.4 Techniques to Control Chaos

The general problem that has been tackled in the literature involves one of "destroying" (or rather, annihilating) chaos and generating synchronization. Chaos is generally considered to be an undesirable phenomenon. A few theoretical methods capable of controlling chaotic systems were earlier presented in the literature to solve the above problem. Since our work attempts to use these techniques in realistic neural models, and to take "advantage" of chaos, we believe that it is beneficial to review these techniques.

2.9.4.1 The Ott-Grebogy-Yorke (OGY) Control Method

Ott *et al.* [122] proved that one can convert a chaotic attractor to any one of a large number of possible attracting time-periodic motions. This is achieved by making *small* time-dependent perturbations on an available system parameter. The chaos can always be suppressed by shadowing one of the infinitely unstable periodic orbits (or perhaps, steady states) embedded in the chaotic attractor. The method utilizes delay coordinate embedding, and it is applicable to experimental situations in which *a priori* analytical knowledge of the system dynamics is not available.

The basic assumptions of the method are:

1. The dynamics of the system can be described by an N-dimensional map[15].

   To control chaotic dynamics, one only needs to learn the *local* dynamics around the desired periodic orbit by observing iterates of the map near the desired orbit and fitting them to

[15]Note that while the dynamics is assumed to arise from a map, one does not need a model for the global dynamics. This assumption allows for the control of any chaotic system for which a Poincare section can be constructed. The details of the construction of a map form and the determination of the location of a periodic orbit in the experimental data can be found in [97].

a local linear approximation of the map f [48]. From this, one can find the stable and unstable eigenvalues, as well as the local stable and unstable manifolds represented by the eigenvectors. Next, by changing p slightly and observing how the desired orbit changes its position, one can estimate the partial derivatives of the local orbit with respect to p to yield a function of the form[16], $\xi_{n+1} = f(\xi_n, p)$.

2. p is an accessible system parameter which can be changed in some small neighborhood of its nominal value, p^*.

3. For this value, p^*, there is a periodic orbit within the attractor around which we would like to stabilize the system.

4. The position of this orbit changes smoothly with regard to changes in p, and there are small changes in the local system behavior for small variations of p.

Let ξ_F be a chosen fixed point of the map, f, of the system, specified in terms of the parameter value p^*. In the close vicinity of this fixed point we can assume that the dynamics are linear, and that they can be expressed approximately by:

$$\xi_{n+1} - \xi_F = M(\xi_{n+1} - \xi_F). \tag{2.45}$$

The elements of the matrix M can be calculated by using the measured chaotic time series and by analyzing its behavior in the neighborhood of the fixed point. Further, the eigenvalues λ_s, λ_u and eigenvectors e_s, e_u of this matrix determine the stable and unstable directions in the small neighborhood of the fixed point.

Let us denote by f_s and f_u the contravariant eigenvectors, i.e. the vectors which satisfy:

$$f_s e_s = f_u e_u = 1, f_s e_u = f_u e_s = 0. \tag{2.46}$$

We can find the linear approximation that is valid for small $|p_n - p*|$ as:

$$\xi_{n+1} = p_n g + (\lambda_n e_n f_n + \lambda_s e_s f_s)(\xi_n - p_n g), \tag{2.47}$$

[16]The map for such continuous-time systems can be constructed by introducing a transversal surface of a section of the system's trajectories. Such a map is called the Poincare map.

where $g = \frac{\partial \xi_F(p)}{\partial p}$ when $p = p^*$.

Because ξ_{n+1} should fall on the stable manifold of ξ_F, p_n has to be chosen such that $f_u \xi_{n+1} = 0$, and thus:

$$p_n = \frac{\lambda_n \xi_n f_u}{(\lambda_u - 1) g f_u}. \tag{2.48}$$

The main properties [88] of the OGY algorithm are:

1. The algorithm requires no formal model for the system's dynamics. One can utilize either full information from the process or a delay coordinate embedding technique using single variable experimental time series. An extremely interesting development in this direction has been described by Dressler and Nitsche [45].
2. Any accessible (controllable) variable, which serves as a system parameter, can be used as the control parameter.
3. In the absence of noise and error, the amplitude of the applied control signal must be large enough to achieve control.
4. Inevitable noise can destabilize the controlled orbit, resulting in occasional chaotic bursts.
5. Before settling into the desired periodic mode, the trajectory exhibits chaotic transients, whose lengths depend on the actual starting point.

Chaotic attractors, typically, have embedded within them a dense set of unstable periodic orbits. The case studied in [122] is one in which only small changes of the parameter are permitted. These small changes cannot create new orbits with properties that are vastly different from the un-perturbed scenario.

The OGY method consists of three steps.

- The first step involves the identification of low-period unstable periodic orbits.
- The second step requires choosing an unstable periodic orbit which yields improved system performance.

- The last step computes small-parameter adjustments that need to be done to stabilize the unstable periodic orbit.

The OGY Method algorithm for a two-dimensional map

We now describe the OGY method for two-dimensional maps as explained in [122].

Consider the case of a two-dimensional map $M(x,p)$ where p is such a system parameter. At p=$\bar{p}$ the map M has a chaotic attractor which has, embedded within it, an unstable fixed point[17] $x_F(\bar{p})$. Our intention is to convert the chaotic motion to a stable orbit $x = x_F(\bar{p})$ by performing small variations on the parameter p (see Figure 2.7 and 2.8). Since we vary p at each step, we replace p by $p_n = \bar{p}+q_n$, where we restrict the perturbation q_n to satisfy $|q_n|<q*$, and $q*$ (a small quantities) is the maximum allowed perturbation of p. Linearizing the map $x_{n+1} = M(x_n, p)$ about $x = x_F(\bar{p})$ and p=$\bar{p}$, we have:

$$x_{n+1} \simeq q_n g + [\lambda_u e_u f_u + \lambda_s e_s f_s] * [x_n - q_n g], \tag{2.49}$$

where we have chosen the coordinate system so that $x_F(\bar{p})$=0, and the quantities appearing in Equation (2.49) are as follows:

- g=$\frac{\partial x_F}{\partial p}$ when p=$\bar{p}$,
- λ_s and λ_u are stable and unstable eigenvalues,
- e_s and e_u are contravariant basis vectors satisfying $f_s e_s = f_u e_u = 1$, $f_s e_u = f_u e_s = 0$.

Now assume that x_n falls near the fixed point so that Equation (2.49) applies. If we now attempt to pick q_n so that x_{n+1} falls approximately on the stable manifold of $x_F(\bar{p})$=0, we see that we have to choose q_n so that $f_u x_{n+1} = 0$. If x_{n+1} falls on the stable manifold of $x = 0$, we can then set $q_n = 0$, and the orbit will approach the fixed point at the geometrical rate of λ_s. Multiplying Equation (2.49) with f_u, one obtains the equation for q_n as:

$$q_n = q(x_n) = \frac{\lambda_u x_n f_u}{(\lambda_u - 1) g f_u}, \tag{2.50}$$

[17]The extension to the case of a higher period is straightforward.

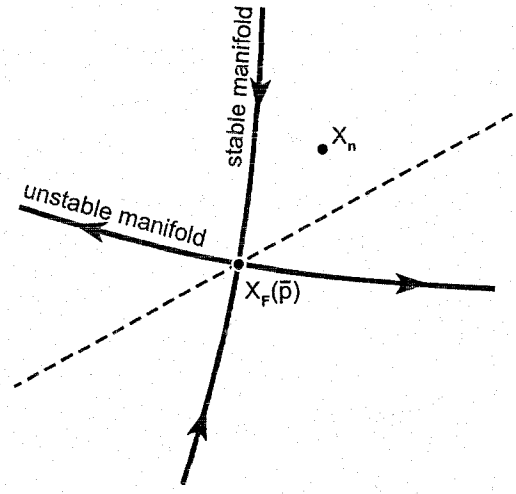

Figure 2.7: The period-1 point, $X_F(\overline{p})$, the stable and unstable manifolds (given by the solid lines), and the trajectory (the dashed line) along which $X_F(\overline{p})$ can be shifted by perturbing the parameter $\overline{p}$.

which is the pertinent form whenever $|q(x_n)| < q*$. When $|q(x_n)| > q*$, one has to set $q_n = 0$.

Summarizing what we have said, for small values of $q*$, a typical initial condition will generate a chaotic orbit which is exactly the same as what we would obtain for the uncontrolled case until x_n falls within a narrow slab $|x_n^u| < x*$, where $x_n^u = f_u x_n$ and $x* = q * |(1 - \lambda^{-1})g f_u|$, at which time the control given by the Equation (2.50) will be activated. Even when that occurs, the orbit may not be brought to the fixed point because of nonlinearities not included in Equation (2.50). In such a scenario, the orbit will leave the slab and continue to move chaotically as if there was no control. Eventually, due to the ergodicity of the uncontrolled attractor, the orbit will fall near enough to the desired fixed point, thus forcing its attraction to this point.

The reader will observe that we have obtained a stable orbit that is preceded by a chaotic transient. The duration of such a chaotic transient depends sensitively on the initial conditions, and for randomly chosen initial conditions, it has an average value, τ, which scales as $\tau \sim q*^{-\gamma}$, where the exponent γ is given by:

$$\gamma = 1 + \frac{1}{2}\frac{ln(\lambda_u)}{ln(\lambda_s{}^{-1})}.$$

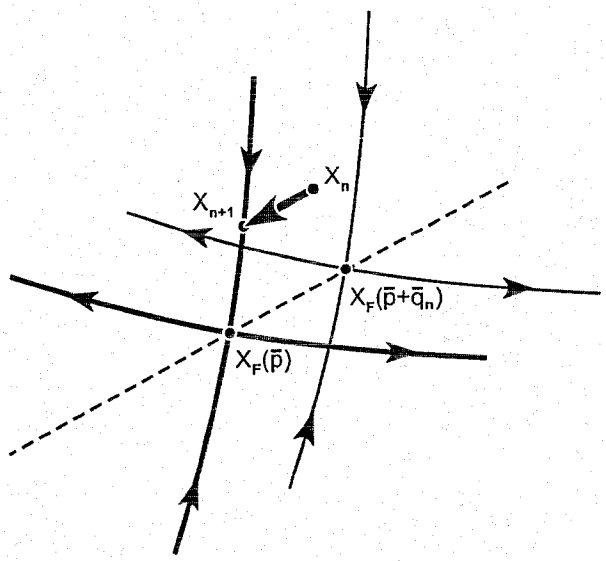

Figure 2.8: Result of perturbing $\overline{p}$ to $\overline{p} + g_n$. In this case the stable and unstable manifolds of $X_F(\overline{p} + g_n)$ are shown as thin solid lines through $X_F(\overline{p} + g_n)$.

The OGY (Pole replacement) Method for a N-Dimensional Map.

The above procedure of specifying the control, q_n, is a special case of the general "pole placement" technique well known in the theory of control systems [121]. For an N-dimensional map $\mathbf{M}(x, P)$, linearization around a fixed point $x_F(\bar{P})$ and the nominal parameter value $\bar{P}$ yields

$$\delta_{n+1} = \mathbf{A}\delta_n + \mathbf{B}q_n,$$

where $\delta = x(\bar{P})$-$x_F(\bar{P})$, $\mathbf{A}$ is the NXN Jacobian matrix of partial derivatives of $\mathbf{M}$ with respect to x, and $\mathbf{B}$ is the N-vector derivative of $\mathbf{M}$ with respect to P, and $q_n = \mathbf{K}\delta_n$ is the linear control with $\mathbf{K}$ being an N-dimensional row vector. Thus, $\delta_{n+1} = (\mathbf{A} + \mathbf{BK})\delta_n$, where $\mathbf{K}$ has to be chosen so that the new control matrix $\mathbf{A}'= (\mathbf{A} + \mathbf{BK})$ is stable (i.e., has eigenvalues of magnitude less than unity). If $\mathbf{A}$ and $\mathbf{B}$ satisfy the so-called "controllability" condition (which is typically satisfied), the pole placement technique[18] allows the analyst to choose the matrix

[18]For more details we refer the reader to Appendix B.

$\mathbf{A}'$, which can be *exactly* determined. Equation (2.50) corresponds to the choice wherein the unstable eigenvalue of $\mathbf{A}$ is made zero, while the stable eigenvalue is unaltered by the control.

By choosing one of the unstable fixed points in the control process, q_n can be set equal to $K\delta_n$ whenever $|K\delta_n|<q*$, and to $q_n = 0$ otherwise[19].

2.9.4.3 Romeiras Method

Romeiras *et al.* [138] described a method that converts the motion on a chaotic attractor to a desired attracting time periodic motion by making only small time dependent perturbations of a control parameter. The time periodic motion results from the stabilization of one of the infinite number of previously unstable periodic orbits embedded in the attractor. This method extends the one proposed by of Ott *et al* [122], allowing for a more general choice of the feedback matrix and for the extension of the implementation to higher-dimensional systems.

Since we are not utilizing this method in our Thesis, we omit further details here. They can be found in [138].

2.9.4.4 Dressler and Nitsche Method

The OGY control method [122] was further analyzed by Dressler and Nitsche [45] for the case that the attractor is reconstructed from a time series using time-delay coordinates. In this case, the experimental surface of the section map depends not only on the actual parameter, but also on the preceding one.

Rationale for the method: Dressler and Nitsche considered the case that the only perceivable information about the system is obtained from a measurement process which is mathematically realized by a *scalar* function Z on the state space, M. If $Y(t) \in M$ is the state of the system at time t, we can obtain the experimental times series $z(t) = Z(Y(t))$. Using the delay

[19]Using the OGY method, Ditto *et al.* [42] succeeded in developing a technique which requires only small time-dependent perturbations of a single-system parameter which did not need the knowledge of the model equations for the dynamics. The authors of [42] demonstrated the power of the method by controlling a particular chaotic system, namely that of a magnetoelastic ribbon around its unstable periodic orbits of orders 1 and 2, which allowed a switching between them, at will.

coordinates with delay τ and the embedding dimension, m, a m-dimensional delay coordinate vector can be constructed as:

$$X(t) = (z(t), z(t-\tau), ..., z(t-(m-1)\tau)) \in R^d.$$

The experimental surface of the section is obtained by the convention that one component of $X(t)$ equals a constant. Typically, this is the first component $x_1(t_i)$ of the vector $X(t_i)$, which is set equal to $z(t_i) = c$. This procedure leads to the computation of the the successive points $\xi_i \in R^{m-1}$ in the surface of the section, and the surface of the section map $\xi_{i+1} = P(\xi_i)$. Since we shall be explicitly utilizing this method, we shall briefly present the analysis of the obtained experimental surface of section map P.

Let us assume that one wants to stabilize an unstable fixed point ξ_F of P which has been localized by the technique of recurrent points as specified in [45]. The OGY control algorithm implies the instantaneous change of the parameter p at the times t, from p_{i-1} to an appropriately chosen parameter, p_i. Let assume that the time between successive piercings of the surface of the section is bigger than the lag window, i.e., $t_{i+1} - t_i > (m-1)\tau$. The reason why one hopes to be able to control the original system $Y(t)$ by observing $X(t)$ is that for appropriately chosen embedding parameters d and τ there is a bijective relation Φ between the states $X(t)$ and $Y(t)$, i.e., $X(t) = \Phi(Y(t))$. The mapping Φ is, however, closely related to the dynamical equations of the system, and thus, in general, dependent on the actual value of the control parameter, p_i. This will be taken into account by specifying Φ as Φ_p.

The point ξ_i on the surface of the section at time t_i is related to the original state by the relationship:

$$Y(t_i) = \Phi^{-1}_{p_{i-1}}(c, z(t_i - \tau), ..., z(t_i - (m-1)\tau)).$$

The assumption used here is that $(d-1)\tau < t_i - t_{i-1}$, which assures that p_{i-1} is the actual value of p during the whole time interval $[t_{i-1}, t_i]$. The time development of the original system from time t_i to the time t_{i+1} is given, in the case of activated control, by $\Phi^{t_{i+1}-t_i}_{p_i}$. We denote by Φ^t_p the flow map of the dynamical system depending of p. Thus the state of the system at time t_{i+1} is obtained by:

$$Y(t_{i+1}) = \Phi_{p_i}^{t_{i+1}-t_i}(Y(t_i)),$$

and the corresponding state in the embedding space is given by:

$$X(t_{i+1}) = \Phi_{p_i}(Y(t+i+1).$$

This results in the formalism of $X(t_{i+1})$ as:

$$X(t_{i+1}) = (\Phi_{p_i} \circ \Phi_{p_i}^{t_{i+1}-t_i} \circ \Phi_{p_i}^{t_{i+1}-t_i})(X(t_i)).$$

The ultimate conclusion of this argument is the following: In the case of an activated control system (i.e., when we switch the parameter from p_{i-1} to p_i at time t_i) the experimental surface of the section map P depends not only on the new actual value p_i, but also on the preceding value p_{i-1}, as:

$$\xi_{i+1} = P(\xi_i, p_{i-1}, p_i).$$

Taking this as the starting point, the Dressler and Nitsche method modifies the OGY algorithm as follows:

- The first step involves the identification, *in the phase space*, of low-period unstable periodic orbits.
- The second step requires choosing, *in the phase space*, an unstable periodic orbit which yields improved system performance.
- The last step computes small-parameter adjustments that need to be done to stabilize *in the phase space* the unstable periodic orbit.

In order to solve the first step we have to linearize that system as follows:

$$\delta\xi_{i+1} \cong A\delta\xi_i + v\delta p_{i-1} + u\delta p_i,$$

where:

- A is the Jacobian of the system,
- $v = \frac{\partial P}{\partial p_{i-1}(\xi_F, p_0, p_0)}$, and
- $u = \frac{\partial P}{\partial p_i(\xi_F, p_0, p_0)}$.

Enforcing $f_u \delta\xi_{i+1} = 0$, one obtains a new control law

$$\delta p_i = -\frac{\lambda_u}{f_u u} f_u \delta\xi_i - \frac{f_u v}{f_u u} \delta p_{i-1}. \tag{2.51}$$

When P is not influenced by the preceding perturbation δp_{i-1}, i.e., $v = 0$, the above control formula reduces to the original OGY relationship.

The new control formula contains one possible avenue of instability. When $|\frac{f_u v}{f_u u}| \geq 1$, the required perturbations δp_i, will grow until they exceed the maximum allowed value δp_{max}, with the possibility of going outside of the control region. To avoid this instability (i.e., the unbounded growth of δp_i) the literature reports an alternative approach, namely one which specifies a control law for δp_i such that δp_{i+1} automatically tends towards zero. This is achieved by demanding that the system stabilizes at the step after the next one, i.e. at $i+2$, and that $\delta p_{i+1} = 0$ by the requirement forced by the constraint $f_u \delta\xi_{i+2} = 0$.

By applying the linearization operation twice, these requirements yield the second modification of the control formula, namely:

$$\delta p_i = -\frac{\lambda_u^2}{\lambda_u f_u u + f_u v} f_u \delta\xi_i - \frac{\lambda_u f_u v}{\lambda_u f_u u + f_u v} \delta p_{i-1}. \tag{2.52}$$

We believe that this level of detail of the Dressler and Nitsche Method is sufficient for the purpose of this Thesis.

2.9.4.6 The Pinning Control Method: He *et al.* *[73]*

In this method, a chaotic neural network model is constructed with chaotic neurons by considering the spatio-temporal summation of external inputs from the other chaotic neurons. Each neuron is coupled with others. The main idea of the pinning control [73] is that if *a subset* of

the neurons in the network are controlled, the controlling effect can be forced to permeate to the entire neural network as time elapses as a consequence of the systems's coupling and delay feedback.

2.8.5 Control vs. Anti-Control

The inverse operation of a control mechanism is what we call an "anti-control" scheme. In practical applications, for example, in the study of controlling the characteristics of the brain, anti-control can be used to increase the complexity of the behavior of the brain by decreasing the periodicity of the EEGs.

We present here two approaches: The first approach is advocated by the clinical work of Schiff *et al.* [146]. The second one is proposed by the methods suggested by Yang *et al.* [179] and In *et al.*[84, 85], regarding the multistability hypothesis. These approaches have not been applied until now to realistic models, and one of the aims of this Thesis is to create models with which we can test anti-control methods.

2.9.5.1 Anti-Control Method of Schiff

The Experimental work done by Schiff *et al.* [146] demonstrated an *ad hoc* method for increasing the complexity (decreasing the periodicity) of the slice preparation in the *in vitro* hippocampal rat brain. With the use of small, correctly timed electrical perturbations, the authors of [146] transformed the dynamics of a synchronously firing hippocampal[20] slice (that simulated a epileptic seizure[21]) into a more normal chaotic regime.

By creating a first-return map of the interspike interval measured in the hippocampal slice,

[20]The hippocampus, a part of the medial temporal lobe, is well known for its capability to generate focal seizures in the human brain. As a first approximation, its circuitry is organized in a "lamellar" pattern orthogonal to the long axis of the temporal lobe. Thus, thin slices in planes that are parallel to these lamellae preserve most of the important intercellular connections and can be used in the laboratory as an important experimental system.

[21]Several types of *in vitro* brain slice preparations, usually after exposure to convulsant drugs that reduce neuronal inhibition, exhibit population burst-firing activity similar to the interictal spike. One of these preparations is the high potassium (K^+) model, where slices from the hippocampus of the temporal lobe of the rat brain are exposed to artificial cerebrospinal fluid containing a high (K^+) concentration that causes spontaneous bursts of synchronized neuronal activity.

these investigators demonstrated that the dynamics can be controlled with small electrical perturbations, which maintain the trajectory to be near an unstable period-1 limit cycle. They were also able to steer the brain slice into a more normal, chaotic regime. This technique, called *anti-control*, may have possible clinical applications for controlling seizures in human patients in the future, since typically, a seizure is associated with the the onset of periodic dynamics.

If one observes the timing of these bursts, he discovers clear evidence for UFPs (Unstable Fixed Points) as displayed in the return map. Schiff *et al.* [146] regularized the timing of such bursts through intervention with stimuli delivered by a micropipette with a timing as dictated by the chaos control algorithm so as to force the system onto the stable direction. They regularized the interval between the spikes, but they were also able to make the intervals more chaotic through a chaos "anti-control" strategy. It is the latter that might serve a useful purpose in breaking up seizure activity through the prevention or eradication of pathological order in the timing of the spikes. This original anti-control or chaos maintenance strategy of Schiff *et al.* has been further elaborated and generalized for higher dimensions by the work of In and Yang [42].

2.9.5.2 Anti-Control Methods based on Multi-stability Hypothesis

In a multistable dynamical system, perturbations cause sudden changes in the dynamics because it involves a switch between basins of attraction. The hypothesis is that it might be possible to treat epilepsy by using carefully honed perturbations designed to confine the dynamics within the nonepileptic basins of attractions. Thus, in the spirit of modern implantable cardiac defibrilators, it might prove possible to develop brain defibrillators for the treatment of patients with medically intractable epilepsy [60].

History of the Theoretical Analysis

In [143], Ruelle and Takens considered four-frequency quasiperiodic[22] flows on the torus T^4. They showed that it was possible to make arbitrarily small (but very carefully chosen) smooth perturbations to the flow, in such a way that the quasiperiodic flow is converted into a chaotic

[22]Quasiperiodic motion can be thought of as a mixture of periodic motions of several different fundamental frequencies. The N-frequency quasiperiodicity is the general case when the number of fundamental frequencies that are "mixed" is N.

flow on a strange attractor lying in the torus T^4. Furthermore, these chaotic attractors, once created, cannot be destroyed by arbitrarily small perturbation of the flow.

Newhouse, Ruelle, and Takens [119] later showed that the same could be said for a three-frequency quasiperiodic flow on the torus T^3 (see also D'Humieres *et al.* [41]). This led to the conjecture that three and four-frequency quasiperiodicities are unlikely to occur because they are "easily" destroyed and supplanted by chaos. Furthermore, it was also conjectured that, in the case of the two-frequency periodicity, (where the third-frequency periodicity was destabilized by increasing a stress parameter of the system), the flow can immediately become chaotic.

A question arises naturally: What causes the transition from three-frequency quasiperiodicity to chaos. We first observe that only one parameter can be modified in this transition. The transition can be explained by two alternative processes, namely, the embedding of the invariant three-dimensional toroidal surface in the phase space or the destruction of a T^3 surface. Both of these phenomena are possible depending on the specific system considered. Indeed, what truly happens in the brain is actually unknown.

As an example, Battelino *et al.* [11] formulated a numerical technique for testing whether a chaotic attractor lies on a three torus[23]. For two coupled Van der Pool oscillators, they discovered that the destruction of the three torus apparently preceded the occurrence of a chaotic attractor.

Anti-Control by Avoiding "Loss Regions"

Consider a nonlinear system that behaves chaotically when a system parameter p is below a critical value, $p < p_c$. As the value of p is increased past p_c, there is a bifurcation in which the chaotic motion is replaced by periodic motion. The problem we consider is whether it is possible to maintain the motion to be chaotic when $p > p_c$, by using small controls.

[23]Two coupled driven Van der Pol oscillators can have three-frequency quasiperiodic attractors, which lie on a 3-torus. The evidence presented in the Battelino *et al.*'s paper indicates that the torus is destroyed when the stable and unstable manifolds of an unstable orbit become tangential. Furthermore, no chaotic orbits lying on a torus were observed, suggesting that, in most cases, (or at least in the case of this system), orbits do not become chaotic before their tori are destroyed. To expedite the calculations, the authors of [11] developed a method which can be used to determine if an orbit is on a torus without actually displaying that orbit. The method, also described in their paper, was designed specifically for their particular system. The basic idea, however, can be used for studying attractors of other systems. Very few modifications of the method would be necessary when studying systems in which the number of degrees of freedom equals that of a Van der Pol system.

As an example, consider the case of a d-dimensional map,

$$x_{n+1} = F(x_n, p, c_n), \tag{2.53}$$

where x_n is the d-dimensional state of the system at time n, and c_n denotes the control variable. We can perceive the control aspect as that which involves changing c_n.

For $c_n = 0$, the map F bifurcates from chaos to periodicity as p increases through p_c. The question now is the following : How does one program the time dependence of c_n so as to ensure chaotic dynamics when $p > p_c$. The additional imposed condition is that $|c_n|$ must be small, and that the control has to be applied infrequently (i.e., $c_n = 0$ most the time).

There are two solutions for this anti-control problem, the first proposed by Yang *et al.* [179] and the second proposed by In *et al.* [84, 85].

Anti-Control by Avoiding "Loss Regions": Method by Yang

Yang *et al.* [179] indicated that intermittent chaotic systems can be made to exhibit continuous chaotic behavior (i.e., with no intermittent periodic episodes). As opposed to the *ad hoc* method for increasing the complexity implemented by Schiff *et al* [146], the method of chaos anti-control proposed by Yang *et al.* is based on the observation that a map-based system in a regime of transient chaos, i.e., in the vicinity where periodicity could have a transition into chaos, has special regions in its phase space. These regions are called "loss regions". If the system enters such a region it immediately ceases its chaotic motion. Yang *et al.* [179] identified these regions along with n preiterates of each loss region. If the system enters a preiterate, the authors applied a small perturbation to an accessible system parameter, in order to interrupt the progression of the system toward a loss region. The perturbation places the system in the region of a phase space that is neither a loss region nor a preiterate one. This requires explicit knowledge of the map of the system and is consequently difficult to accomplish.

The three most common bifurcations that can lead from chaotic motion directly to a low period attracting periodic orbit are (i) Crises, (ii) Type I intermittency, and (iii) Type III intermittency[24]. In all of the above three cases, for $p > p_c$, one can identify a loss region L, such

[24]The reader is referred to Appendix C for more details on these issues.

that, after the orbit falls onto L, it is rapidly drawn to the periodic orbit. Before falling into L, the orbit motion can exhibit chaos-like behavior, typically termed as its "chaotic transient".

One strategy to ensure chaos for $p > p_c$ is to consider successive preiterates of L as:

$$\begin{aligned}
&L_1 = F^{-1}(L, p, 0),\\
&L_2 = F^{-1}(L_1, p, 0) = F^{-2}(L, p, 0),\\
&L_3 = F^{-1}(L_2, p, 0) = F^{-3}(L, p, 0),\\
&\vdots\\
&L_m = F^{-1}(L_{m-1}, p, 0) = F^{-m}(L, p, 0).
\end{aligned}$$

Thus L_m is a set of points that map to the loss region L in m iterates. Note that as m increases, the width of L_m in the unstable direction[25] (or directions) has a general tendency to shrink exponentially. This suggests the following approach.

- We first pick some suitable value of m, denoted here as M. Assume that the orbit initially starts outside the regions $L_{M+1} \cup L_M \cup \ldots \cup L_1 \cup L$.
- If the orbit lands in L_{M+1} we apply our control c_n on iterates n so as to force the orbit out of L_M on the next iterate. Because L_M is thin, the required c_n can be small. By making M larger, one can control the size of the parameter to be smaller. Thus, there is a trade-off involving the control size and the number of preiterates, M. Consideration of this trade-off becomes particularly important if noise is present, or if the dynamical system F is not known with absolute precision.
- After the orbit is force out of L_M, it is expected that it will execute a chaotic orbit, until it falls again on L_{M+1}, at which time the small control is again activated, and the process continues. Thus, the desired result can be achieved and the control is set to zero most of the time.

Analogous algorithms, which are less general and depend on the type of bifurcation involved (Crisis, Type I intermittency, or Type III intermittency) have been formulated in the literature. As our research does not involve them, we omit any further details concerning them.

[25]Observe that there is always at least one unstable direction due to the existence of chaos.

Control by avoiding "loss regions": Method by In

The lack of generality of the Schiff method and the difficulty of the experimental implementation of the Yang *et al.* method were the primary motivation for the work of In *et al.* [84, 85]. The authors of [84, 85] proposed a general anti-control method that is more readily applicable to experimentation and relies, for its implementations, only on experimentally measured quantities.

The work of [84, 85] assumes the following about the system under consideration:

1. The dynamic of the system can be represented as an n-dimensional nonlinear map (e.g. a surface of a section or a return map) in such a way that points or iterates on the map are given by $\xi_n = f(\xi_{n-1}, p)$, where ξ_n is a vector, f is a vector function, and p is an accessible system parameter.

2. There is at least one specific region of the map (the so-called "a loss region") that lies on the attractor onto which the iterates will fall when making the transition from chaos to periodicity.

3. The structure of the map does not change significantly when small changes[26] $\delta p = p - p_0$ occur.

The locations of the loss regions on the return map derived from the system are determined by observing immediate preiterates of undesired points which correspond to periodic orbits. Clusters of these preiterates are identified as the loss regions. The extent of each loss region is determined by the distribution of points in that region. The time evolution of each region may be traced back through m preiterates, as desired.

In a manner similar to the OGY chaos control method, In *et al.* changed p slightly, observed the resulting change in each loss region's location, and estimated the local shift of the attractor g for each loss region with respect to a change in p as follows:

$$g = \frac{\partial f(\xi_n, p)}{\partial p} \approx \frac{\triangle f(\xi_n, p)}{\triangle p}. \tag{2.54}$$

[26] $\delta p = p - p_0$ where p_0 is the initial value of the control parameter p.

As an approximation, In *et al.* [85] took g to be the same[27] for all loss regions on the attractor for sufficiently small parameter changes, δp.

Anti-control can be applied once the system has entered the m^{th} preiterate of the loss region. Since the map is constructed as a return map (or as a delay coordinate embedding with ξ_n vs ξ_{n-1}), the y coordinate of the n^{th} point becomes the x coordinates of the $(n+1)^{st}$ point. We know the x coordinate of the next point and the size of the region that the $(n+1)^{st}$ point will fall into. Thus, a minimum distance can be calculated using which we can move the attractor in such a way that this next point falls outside of that region. The distance d is translated into the appropriate parameter change δp by $\delta p_n = d_{n+1}/|g|$, where the direction of the motion is along g.

If each of the m preiterates of the loss region is circumscribed by a circle of radius t_m (which is the worst scenario), we have $\delta p_n = 2r_m/|g|$, where the $(n+1)^{st}$ point falls into the m^{th} preiterate region. This is the maximum perturbation needed to achieve anti-control, and it guarantees that the next point falls outside the m^{th} preiterate region by moving the point by an amount equivalent to the full diameter of the circle surrounding the loss region. This worst case can be improved as follows.

In a return map, we know the x coordinate of the next point. Since there is a choice of applying the perturbation in either the positive or negative g direction, one can select the sign of the perturbation to move the next point to the left if this x coordinate is in the left half of the preiterate region, and vice versa. Thus, the minimum distance to be moved is reduced to r_m, and consequently, $\delta p = r_m/|g|$, which is a significant reduction in the strength of the perturbation.

Additionally, if the shape of the preiterate region of interest is approximately linear and its slope is perpendicular to g, then d is at most r_m and may approach the thickness of this linear segment ($\delta p_n \ll r_m|g|$). Thus, (although this is not mandatory to achieve anti-control), detailed knowledge of the shape of the loss region and its preiterates can further reduce the size of the perturbation required to achieve it.

[27] Without such an assumption, the user would have to calculate g for each loss region. This assumption is strictly not necessary in order to implement the method. It is merely a convenience that is approximately true for many systems and for small δp's.

In *et al.* constructed a return map by measuring the position ξ_n, once during every driving period, and by plotting the current position ξ_n as a function of ξ_{n-1}. Then, on the return map, they identified the loss region (R_L) and its preiterates ($R_{L-1}..R_{L-m}$), and the points that entered the preiterate regions mediated the intermittent transition form chaos to periodicity. During anti-control, they proposed the application of a perturbation when the orbit entered the region R_{L-1} so that the next orbit fell out of R_L.

The extent of the m^{th} preierate region is determined by observing the set of points that fall into the loss region after m-iterations, as well as by studying the neighboring points that do not fall into the loss region after m iterations. The boundary of the loss region lies between these points.

During anti-control, the orbit is sometimes (although this occurs rarely) forced into the Period-1 region, of the succeeding iteration. This requires the user to apply anti-control for this periodic region to ensure that the system does not remain there. Whenever this occurs, a slightly larger perturbation will be required to move the system away from this periodic orbit.

A more elegant, but computationally difficult solution, would be to choose the original perturbations so that they avoid all of the loss regions and the preiterates. Although In *et al.* [85] mention this option, it has not been investigated in the literature.

2.9 Modelling the epileptogenesis

There are three families of possible neural models, used to understand the processes of the brain:

- cellular level;
- small scale neural networks;
- large scale neural networks.

The study of brain disorders has lead to a better understanding of brain functions. Epilepsy is the most studied brain disorder and it has been the topic of a long debate whether congenital epilepsy is a **cellular disorder**, rooted in the malfunctioning of biophysical mechanisms in the neuron, or a **network disorder**, derived from an aberrant synaptic network.

2.9.1 Cellular Disorders

Until 1991, when Segal recorded signals from single-cell microcultures of hippocampal pyramidal neurons [99], epileptiform activity in single cells had been recorded only from neurons in large cultures and *in vivo*. With Segal's observations, however, it became possible to model a a simplified epileptiform activity generator, identifying the dominant physiological and morphological properties of a single epileptiform neuron. Later, slice studies have isolated the intrinsic dynamics of epileptic hippocampal pyramidal cells by utilizing synaptic blockers [145], and some models have been capable of generalizing, predicting and explaining their properties. These models identified the major features of their intrinsic dynamics and extrapolated them to larger networks. The results of Heilman *et al.* [74] indicate that a cellular basis of epilepsy is arguable, and provide a hypothesis for its mechanism.

2.9.2 Network Disorders

The large scale network models have been successful *only* from a mathematical perspective. It is very difficult to predict if the models are capable to describe reality accurately. The experiments are also difficult because they require measurements at the level of individual cells (e.g., their frequency and their response to stimuli of varying strength and timing) *and* at the level of the entire network (e.g. measurements to quantify the interactions between oscillators and the resulting collective behavior [158]). It is particularly difficult to measure interactions between pairs of oscillators. Thus, if they are left included in the network, the measurements may be strongly influenced (and even over-shadowed) by other oscillators. As opposed to this, if they are removed from the network, surgically or otherwise, the surrounding oscillators and connections among them may be damaged in the process. Furthermore, the connectivity of networks is typically unknown, except for a few small systems of neurons. Without knowing "who" is interacting with "whom", it is impossible to test the models quantitatively. In addition, in the clinical verifications of the large scale models, it is also difficult to study and analyze the case of uncoupled cells. Drugs can be used to uncouple the cells progressively, but, usually it is hard to demonstrate that the incorporation of these drugs does not change any other properties of the cells besides their mutual coupling.

2.9.3 Our Models

In a later Chapter, we intend to achieve an analysis of a few models of biologically realistic neurons. One contribution of our research is to select control parameters and anti-control algorithms for different types of models. In some models, the system equations can be inferred. In the case of other models, we know only the output, and we will create the reconstruction space for controlling the system. For each control parameter we propose a "regions of parameter space" as proposed by Bhalla and Bower [17]. It will be a future work for clinicians to verify if the variation of our control parameter in a specific region of the parameter space can have a "positive" effect in a large scale network, like the brain. It will also be a future work for clinicians to identify the physiological equivalent of the control parameter with which we propose to achieve modification. This is, indeed, because the mathematical model may give solutions that are not too closely related to the biological variables of the real neural networks.

2.10 Conclusions

This Chapter has served to present the background material needed for the Thesis. We first introduced some theoretical properties concerning the concept of chaos. We then presented a few models for systems which exhibit chaotic behavior, and gave a general overview of chaotic neural networks. Next, we described various metrics used for analyzing and quantifying chaos and specified how they could be computed. We continued the Chapter with a survey about modelling the brain as a chaotic system, and about methods of controlling and anti-controlling chaos. We concluded the Chapter with a discussion about the limitations of models that have been used to analyze the brain, and in particular the epileptic brain.

Chapter 3

Chaotic Pattern Recognition

3.1 Introduction

This Chapter[1] constitutes the first novel contribution of the Thesis, and it pertains to a, hopefully, new field of research, one that involves *Pattern Recognition using Chaotic Neural Networks.* The neurological foundation for this strategy is based on a formal theory proposed by Freeman [56] who developed a model for an olfactory system detailed herein. He conjectured that the brain is essentially a chaotic system in the absence of a stimulus (pattern) to be recognized. During perception, when the attention is focussed on any sensory stimuli, the brain activity becomes periodic. Our aim is to design a PR system, namely a *Chaotic* Neural Network, which demonstrate such phenomena.

Pattern Recognition is the study of how a system can observe the environment, learn to distinguish patterns of interest from their background, and make decisions about their classification or categorization. In general, a pattern can be any entity described with features, where the dimensionality of the feature space can range from being few to thousands. The four best approaches for PR are: template matching, statistical classification, syntactic or structural

[1]Some preliminary results from this Chapter were published in the *Proceedings of PRIP'2005, the 2005 Conference on Pattern Recognition and Information Processing*, Minsk, Belarus, pp.252-259, *(This talk was a Plenary talk of the Conference)*, and in the *Proceedings of CORES'2005, the 2005 Conference on Computer Recognition Systems*, Wroclaw, Poland, pp.3-16, *(This talk was also a Plenary talk of the Conference)*.

recognition, and Artificial Neural Networks (ANNs) [58, 59, 137, 165]. The latter approach attempts to use some organizational principles such as learning, generalization, adaptivity, fault tolerance and distributed representation, and computation in order to achieve the recognition. The main characteristics of ANNs are that they have the ability to learn complex nonlinear input-output relationships, use sequential training procedures, and adapt themselves to data. Some popular models of ANNs have been shown to be capable of associative memory and learning [52, 92, 148]. The learning process involves updating the network architecture and modifying the weights between the neurons so that the network can efficiently perform a specific classification/clustering task.

An associative memory permits its user to specify part of a pattern or key, and to thus retrieve the values associated with that pattern. One limitation of the associative memory model is its dependency on an external input. As opposed to biological NNs, once an output pattern has been identified, the ANN remains in that state until the arrival of an external input. To be more specific, once a pattern is recalled from a memory location, the brain is capable of recalling other associated memory patterns without being prompted by any additional external stimulus. This ability to "jump" from one memory state to another *in the absence of a stimulus* is one of the hallmarks of the brain, and this is one phenomenon that we want to emulate.

The evidence that indicates the possible relevance of chaos to brain functions was first obtained by Freeman [56] through his clinical work on the large-scale collective behavior of neurons in the perception of olfactory stimuli. Freeman developed a model for an olfactory system having cells in a network connected by both excitatory and inhibitory synapses. He described how a chaotic system state in the neighborhood of a desired attractor can fall on a stable direction when a perturbation is applied to a system parameter. From this model, he conjectured that the quiescent state of the brain is *chaos*, while during perception, when attention is focused on any sensory stimulus, the brain activity becomes more *periodic*, where the periodic orbits can be interpreted as specific memories. If the patterns stored in memory are identified with an infinite number of unstable periodic attractors which are embedded in an attractor, then the transition from the quiescent state onto an "attention" state can be interpreted as the controlling of chaos. The controlling of chaos gives rise to periodic behavior, culminating in the identification of the sensory stimulus that has been received. Thus, mimicking this identification on a neural network

can lead to a new model of pattern recognition[2].

The NN model we propose is not altogether unique - it is a "distant cousin" of the family of Hopfield-like chaotic NNs which have been proposed in the literature [3, 105, 150, 151]. However, its use in generating periodic responses to achieve PR is, to our knowledge, new.

A Chaotic NN (CNN) with non-fixed weights of the connections between neurons can reside in one of the infinite number of possible states that are allowed by the functions of the network. In the general case, the dimensionality of the possible state space is finite, although the number of states is infinite. When the weights of the CNN are specified, the volume of the state space decreases, but the number of possible states continues to be infinite. During its evolution, a CNN with fixed weights can be in one of the infinite states. In the case when one inserts one of the memorized patterns as an input to the network, we want the network to resonate with that pattern, generating that pattern with, hopefully, small periodicity, where the actual period of resonance is not of critical importance. Between two consecutive appearances of the memorized pattern, we would like the network to be in one of the non-memorized infinite number of states, and in the memorized states with an arbitrary small probability.

The *resonance* with the memorized pattern given as input, and the *transition* through several states from the infinite set of possible states (even when the memorized pattern is inserted as the input) represent the difference between this kind of PR and the classical type which correspond to the strategies associated with syntactical or statistical pattern recognition.

The dynamic neural networks proposed by Adachi [2], referred to here as AdNN, can store a large number of dynamic spatio-temporal patterns and spontaneously recall these associated patterns on the arrival of specific external stimulus. In the AdNN, the learning process is solved in a *single* step by the computation of the weights, and this is analogous to how the training is achieved in Hopfield-like NNs [3, 105]. Observe that the testing process, however, is a dynamical one. How to "juggle" between chaos and periodicity is, indeed, an art, and this is what we attempt to control by design.

[2]Unfortunately, if the external excitation forces the brain out of chaos completely, it can lead to an epileptic seizure, and a future goal of this research is to see how these episodes can be anticipated, remedied and or prevented. Some initial results of how this can be achieved are currently available.

3.1.1 Our Contributions

The primary contribution of this Chapter is the introduction of a PR system which is founded on the theory of chaotic networks. However, rather than relying only on the chaos of the system, we have shown that chaos and periodicity are, informally, "negotiable" quantities. In particular, by modifying Adachi's model, we analyze the dynamics of a new model of chaotic neural networks, the Modified AdNN (M-AdNN) which demonstrates PR behavior. We especially focus on the stability of the network and its transient and dynamic retrieval characteristics. Adachi [2] explained that when the duration of the transient phase is long, the attracting state may not be useful for information processing. We have shown that by increasing the multiplicity of the eigenvalues of the AdNN, the PR property of the network can be enhanced, leading to the system resonating "sympathetically" whenever a reasonable version of a stored pattern is presented. The M-AdNN has a very short transient phase, and a higher retrieval frequency. The analysis is achieved using eigenvalue considerations, the Lyapunov exponent and the Routh-Hurwitz criterion. Explicit experimental results justifying the claims are also provided.

3.2 Adachi's Model of Neural Networks: AdNN

The AdNN, which actually is a Hopfield-like model, is composed of N neurons, topologically arranged as a completely connected graph. It is modelled as a dynamical associative memory, by means of the following equations relating internal states $\eta_i(t)$ and $\xi_i(y)$, $i = 1..N$, and the output $x_i(t)$ as:

$$\begin{aligned}
&\eta_i(t+1) = k_f\eta_i(t) + \textstyle\sum_{j=1}^{N} w_{ij}x_j(t), \\
&\xi_i(t+1) = k_r\xi_i(t) - \alpha x_i(t) + a_i, \\
&x_i(t+1) = f(\eta_i(t+1) + \xi_i(t+1)).
\end{aligned} \tag{3.1}$$

In the above, $x_i(t)$ is the output of the neuron i which has an analog value in [0,1] at the discrete time "t", and f is the logistic function with the steepness parameter ε satisfying $f(y) = 1/(1 + exp(-y/\varepsilon))$. Additionally, k_f and k_r are the decay parameters for the feedback inputs

and the refractoriness respectively, w_{ij} are the synaptic weights to the i^{th} constituent neuron from the j^{th} constituent neuron, and a_i denotes the temporally constant external inputs to the i^{th} neuron. Finally, the feedback interconnections are determined according to the following symmetric auto-associative matrix of the p stored patterns as:

$$w_{ij} = \frac{1}{p}\sum_{s=1}^{p}(2x_i^s - 1)(2x_j^s - 1), \tag{3.2}$$

where x_i^s is the i^{th} component of the s^{th} stored pattern.

In his instantiation, Adachi set $N = 100$, $p = 4$, $k_f = 0.2$ and $k_r = 0.9$.

Adachi *et al.* [2] also investigated the dynamics of the associative network with external stimulations corresponding to one of the stored patterns when the external inputs are applied, and they did this by increasing their bias terms[3], a_i, as: $a_i = 2 + 6x_i^s$.

3.3 A New Model of Chaotic Neural Networks: M-AdNN

We propose a model of CNNs which modify the AdNN to support pattern recognition. The Modified AdNN (M-AdNN), which actually is also a Hopfield-like model, is composed of N neurons, topologically arranged as a completely connected graph. Each neuron i, $i = 1..N$, has internal states $\eta_i(t)$ and $\xi_i(y)$ and output $x_i(t)$. We give a brief rationale for each modification.

1. The M-AdNN has two global states used for all neurons, which are $\eta(t)$ and $\xi(t)$ obeying:

$$\begin{aligned}
&\eta_i(t+1) = k_f\eta(t) + \textstyle\sum_{j=1}^{N} w_{ij}x_j(t),\\
&\xi_i(t+1) = k_r\xi(t) - \alpha x_i(t) + a_i,\\
&x_i(t+1) = f(\eta_i(t+1) + \xi_i(t+1)).
\end{aligned} \tag{3.3}$$

[3]They did this in an input specific manner as follows. Let suppose that x_i^s is the value of i^{th} feature (i.e., the pixel, in the domain example) of the s^{th} pattern. Rather than feeding x_i^s directly to the network, they added a bias of '2' if the pixel value was '0', and a bias of '8' if the pixel value was '1', and fed the resulting value to be the input a_i to the network. The intention was to artificially create a greater (scaled) disparity between the values of '0' and '1'. Adachi *et al.* also tried to explain the significance of these biases.

After time $t+1$, the global states are updated with the values of only *one*[4] neuron, $\eta_N(t+1)$ and $\xi_N(t+1)$, as: $\eta(t+1) = \eta_N(t+1)$ and $\xi(t+1) = \xi_N(t+1)$.

Rationale: At every time instant, when we compute a new internal state, we only use the contents of the memory from the internal state[5] *for neuron N*. This is in contrast to the AdNN in which the updating at time *t+1* uses the internal state values of *all* the neurons at time t.

2. The weight assignment rule for the M-AdNN is the classical variant:

$$w_{ij} = \frac{1}{p}\sum_{s=1}^{p} x_i^s x_j^s. \tag{3.4}$$

This again, is in contrast to the AdNN which uses $w_{ij} = \frac{1}{p}\sum_{s=1}^{p}(2x_i^s - 1)(2x_j^s - 1)$.

Rationale: We believe that the duration of the transitory process will be short if the coupling betweens the neurons is small. Shuai [150] explained the role of coupling construction of chaotic neural networks.

3. The external inputs are applied, in the M-AdNN, by increasing the biases, a_i, from 0 to unity whenever $x_i^s = 1$, keeping the other biases to be 0 whenever $x_i^s = 0$.

Rationale: In our case $a_i = x_i^s$, as opposed to the AdNN in which $a_i = 2 + 6x_i^s$. In the case of the latter, the range of inputs is $[2, 8]$ unlike the M-AdCNN for which the range is $[0, 1]$. Thus, the M-AdNN will be, hopefully, more "receptive" to external inputs, leading to, hopefully, a superior PR system.

We conclude this section by briefly mentioning that the main difference between the M-AdNN and the reported auto-associative memory model is that unlike the latter, the M-AdNN

[4]It is well know that the Adachi model (see in Kawakami, Ed., Bifurcation phenomena in nonlinear systems and theory of dynamical systems, World Scientific, Singapore, pp. 143-161, 1990.) has a biology background. In the latter paper, the authors showed that the output of each neuron has a relation with *its own* history, through the information in the states. But in our model, the output of each neuron has a relation with historical status of a special neuron, and the historical status with its own "past" is achieved by an *interaction between the states*. Such a modification leads to the possibility of switching from chaos to periodicity although the biological rationale is not fully yet understood. However, its role in controlling epilepsy seems to have been resolved [31].

[5]It is also possible to relate $\eta(t+1)$ and $\zeta(t+1)$ to $\eta_K(t+1)$ and $\zeta_K(t+1)$ for any fixed K. However, we would like to highlight that the uniqueness of our model consists of "binding" these global state values to the specific values of any *one* state variable (as opposed to binding each $\zeta_i(t+1)$ to $\zeta_i(t)$ itself, as the AdNN does. Theoretically, it seems to be clear that the specific value of K, which identifies this "binding" neuron, is of no significance. However, the question of whether it will give us any added PR capability remains open.

is chaotic, and this chaotic behavior is a consequence of the dynamics of the underlying system. Indeed, in the classical auto-associative memory, the output, which is a consequence of a static system, is directly related to the input, and is not necessarily related to the *dynamics*. Thus, in this case, unlike the M-AdNN, the output, which reproduces the stored input, is not obtained as a result of a sympathetic resonance[6] in the midst of a chaotic behavior. We believe that (as supported by Freeman), the M-AdNN is more representative of the way by which the brain achieves pattern recognition.

3.4 The M-AdNN Orbital Instability

In this section we analyze the stability issues concerning the M-AdNN. We do this by first using Lyapunov Exponents, and then by using the Routh-Hurwitz Criterion.

3.4.1 Analysis Using Lyapunov Exponents

For a dynamical system, sensitivity to initial conditions is quantified by the Lyapunov exponents[7]. For example, consider two trajectories with initial conditions near to an attracting manifold. When an attractor is chaotic, the related trajectories, on average, diverge at an exponential rate characterized by the largest Lyapunov exponent. This concept is also generalized for the spectrum of Lyapunov exponents, λ_i $(i = 1..2r)$, by considering a small r-dimensional sphere of initial conditions, where r is the number of equations (or, equivalently, the number of state variables) used to describe the system. As time progresses, the sphere evolves into an ellipsoid whose principal axes expand (or contract) at rates given by the Lyapunov exponents. The presence of positive exponents is sufficient for diagnosing chaos, and represents local instability

[6]The term "sympathetic resonance" is used for lack of a better one. Quite simply, all we require is that the trained pattern periodically surfaces as the output of the CNN.

[7]We submit here (as a footnote) a few introductory sentences regarding such an analysis. The analysis of a general nonlinear system has two steps: The first consists of computing the steady states points as determined by the testing pattern. The second consists of the analysis of the stability of each steady states. The stability consideration generally involves approximating the dynamics of the "nonlinear system" (for example, by computing the Jacobian) in terms of the approximated linear system. This phenomenon is a consequence of the operating characteristics in a neighborhood of the quiescent steady states (or attracting manifold), and the decomposition of the system using a Taylor series, thus neglecting the higher-order terms.

in particular directions [140].

We consider a discrete time ($t \in Z^+$) dynamical system $A \longmapsto F(A)$ and its Jacobian matrix of partial derivatives $J(A) = D_A F(A)$. Consider also the sequence $\{A_0, A_1, ..., A_{k-1}\}$ generated by successive iterations of the initial condition, A_0. For this sequence, we introduce the matrix

$$J_k(A) = J(Y_{k-1}(A))J(Y_{k-2}(A))...J(Y_1(A))J(Y_0(A)).$$

The Lyapunov exponents are given by the logarithms of the eigenvalues of $\Lambda := [J^T(A)J(A)]^{1/2}$, where $J^T(A)$ denotes the transpose of $J(A) = \lim_{k\to\infty} J_k(A)$.

Theorem 3.1.

Under a Lyapunov exponents analysis, the M-AdNN, described by the set of Equations (3.3), is locally unstable.

Proof: Consider the dynamical system for the M-AdNN, whose asymptotic dynamical matrix J is given as:

$$J(A)=\begin{pmatrix} [J_{ij}^1] & [J_{ij}^2] \\ [J_{ij}^3] & [J_{ij}^4] \end{pmatrix}, \tag{3.5}$$

where each $[J_{ij}^k]$ is an $N \times N$ sub-matrix of J(A), for $1 \leq k \leq 4$ and $1 \leq i \leq N$ and $1 \leq j \leq N$. Each $[J_{ij}^k]$ is a result of the partial derivatives of $\eta_i(t+1)$ and $\xi_i(t+1)$ with respect to $\eta_j(t)$ and $\xi_j(t)$ respectively. This will be clarified presently.

The term $J_{ij}^k(t)$, for $1 \leq k \leq 4$, is the arbitrary element at time "t", and each J_{ij}^k in Equation (3.5) is obtained by taking the limit as $t \longrightarrow \infty$. Therefore $J_{ij}^k(t)$ takes on four distinct forms as follows:

1. $J_{ij}^1(t)=\frac{\partial \eta_i(t+1)}{\partial \eta_j(t)}$ when $1 \leq i \leq N$ and $1 \leq j \leq N$,
2. $J_{ij}^2(t)=\frac{\partial \eta_i(t+1)}{\partial \xi_j(t)}$ when $1 \leq i \leq N$ and $1 \leq j \leq N$,

3. $J^3_{ij}(t)=\frac{\partial \xi_i(t+1)}{\partial \eta_j(t)}$ when $1 \leq i \leq N$ and $1 \leq j \leq N$,

4. $J^4_{ij}(t)=\frac{\partial \xi_i(t+1)}{\partial \xi_j(t)}$ when $1 \leq i \leq N$ and $1 \leq j \leq N$.

Because $x_i(t+1) = f(\eta_i(t+1)+\xi_i(t+1))$, where f is the logistic function with the steepness parameter ε satisfying $f(y) = 1/(1+exp(-y/\varepsilon))$, and $\frac{df(y)}{dy} = \frac{d}{dy}\frac{1}{1+exp(-y/\varepsilon)}$ (or $\frac{df(y)}{dy} = \frac{1}{\varepsilon}x(1-x)$ where $x \equiv f(y)$), the following explicit forms of $J_{ij}(t)$ result:

(a) $J^1_{ij}(t) = \frac{w_{ij}}{\varepsilon}x_j(t)(1-x_j(t))$ when $1 \leq i \leq N-1$ and $1 \leq j \leq N$,

(b) $J^1_{ij}(t) = k_f + \frac{w_{ij}}{\varepsilon}x_j(t)(1-x_j(t))$ when $i = N$ and $1 \leq j \leq N$,

(c) $J^2_{ij}(t) = \frac{w_{ij}}{\varepsilon}x_j(t)(1-x_j(t))$ when $1 \leq i \leq N$ and $1 \leq j \leq N$,

(d) $J^3_{ij}(t) = -\frac{\alpha}{\varepsilon}x_j(t)(1-x_j(t))$ when $1 \leq i \leq N$ and $1 \leq j \leq N$ and $i = j$,

(e) $J^3_{ij}(t) = 0$ when[8] $1 \leq i \leq N$ and $1 \leq j \leq N$ and $i \neq j$,

(f) $J^4_{ij}(t) = -\frac{\alpha}{\varepsilon}x_j(t)(1-x_j(t))$ when $1 \leq i \leq N$ and $1 \leq j \leq N-1$ and $i = j$,

(g) $J^4_{ij}(t) = 0$ when $1 \leq i \leq N$ and $1 \leq j \leq N-1$ and $i \neq j$,

(h) $J^4_{ij}(t) = k_r - \frac{\alpha}{\varepsilon}x_j(t)(1-x_j(t))$ for $i = N$ and $1 \leq j \leq N$.

Since we seek the asymptotic value J(A), we observe that the derivative (i.e., $x_i(t)(1-x_i(t))$) is always positive and attains the value zero only when $x(t) = 0$ or 1. Thus, the outputs of the neurons converge to the values zero or unity, and the term $x_i(t)(1-x_i(t))$ has an asymptotic value of zero for all $1 \leq i \leq N$. Thus, to obtain $J(A)$ we enforce the limiting argument to get

[8]Observe that $J^3_{ij}(t)$ has the value zero; this result is obtained as follows : $\frac{\partial \xi_i(t+1)}{\partial \eta_j(t)} = \frac{\partial(k_r\xi_i(t)-\alpha x_i(t)+a_i)}{\partial \eta_j(t)} = 0$.

$$J(A) = \begin{pmatrix} 0 & \dots & k_f & 0 & \dots & 0 \\ \vdots & \vdots & \ddots & & & \\ 0 & \dots & k_f & 0 & \dots & 0 \\ 0 & \dots & 0 & 0 & \dots & k_r \\ \vdots & \vdots & \ddots & & & \\ 0 & \dots & 0 & 0 & \dots & k_r \end{pmatrix}.$$

Since Λ_A=$[J(A)^T J(A)]^{1/2}$ we have:

$$\Lambda_A = \begin{pmatrix} 0 & \dots & 0 & 0 & \dots & 0 & \\ \vdots & \vdots & \ddots & & & & \\ 0 & \dots & 0 & N^{1/2}k_f & 0 & \dots & 0 \\ 0 & \dots & 0 & 0 & 0 & \dots & 0 \\ \vdots & \vdots & \ddots & & & & \\ 0 & \dots & 0 & 0 & \dots & 0 & N^{1/2}k_r \end{pmatrix}.$$

Observe that this matrix has $2N$ eigenvalues. One eigenvalue with multiplicity 2N-2 is 0, and the others are $N^{1/2}k_f$ and $N^{1/2}k_r$. Thus, $\mu_1 = \cdots = \mu_{2N-2} = 0$; $\mu_{2N-1} = N^{1/2}k_f$; $\mu_{2N} = N^{1/2}k_r$.

Since the Lyapunov exponents are given by the logarithms of the eigenvalues: $\lambda_1 = \cdots = \lambda_{2N-2} = -\infty$; $\lambda_{2N-1} = \frac{1}{2}lnN + ln(k_f)$; $\lambda_{2N} = \frac{1}{2}lnN + ln(k_r)$.

We know [140] that the Lyapunov exponent of a super-stable point (or super-stable orbit) is $-\infty$, and that the Lyapunov exponent of a bifurcation point is 0. Every value between $-\infty$ and 0 implies a stable solution. The M-AdNN has *one* positive Lyapunov exponent with the value $\frac{1}{2}lnN + ln(k_f)$ and another *one* positive exponent with the value $\frac{1}{2}lnN + ln(k_r)$. The presence of the positive exponents proves the theorem. □

3.4.1.1 Remarks on the Lyapunov Analysis:

1. Adachi *et al.* [2] have set $k_f = 0.2$, $k_r = 0.9$ and $N = 100$ i.e., the AdNN involves a $200X200$ matrix. Thus, the AdNN[9] has 100 Lyapunov exponents with the value -1.609437,

[9]It turns out that the AdNN is actually not operating as a chaotic NN, and this further strengthens the claim

and 100 Lyapunov exponents with the value -0.105360.

2. Using the same coefficients[10] and parameters, the M-AdNN has *one* Lyapunov exponent with the value 2.197225, *one* with the value 0.693148, and 198 Lyapunov exponents with the value $-\infty$.

3. Although fascinating, the reason why the system switches from chaos to periodicity is not too mysterious. A single analogy could help. Consider the system of two differential equations:

$$\frac{dx}{dt} = (I+2)x^2 + 2y + 3,$$

$$\frac{dy}{dt} = x + y,$$

where I is the input to the system.

This system has two isoclines: $(I+2)x^2 + 2y + 3 = 0$ and $x + y = 0$. From these isoclines, we can compute the equilibrium points, which are the roots of the equation $(I+2)x^2 + 2(-x) + 3 = 0$. These roots, say θ_1 and θ_2, are clearly function of I whose stability can be verified. To achieve this, we compute the Jacobian in the neighborhood of the roots as:

$$J(A) = \begin{pmatrix} 2(I+2)\theta & 2 \\ 1 & 1 \end{pmatrix},$$

where θ is either θ_1 or θ_2.

Observe that the Jacobian has a characteristic equation $(2(I+2)\theta - \lambda)(1-\lambda) - 2 = 0$.

presented here. On the other hand, it slowly converges towards the stable but periodic orbits. Adachi, actually, indirectly mentions it in his paper when he states that the "chaos" of his model is dependent on the parameters of the network.

[10] As opposed to the AdNN, the M-AdNN has an *additive* positive term in the computation of the Lyapunov exponents as: $\lambda_{2N-1} = 1/2 \ln N + \ln(k_f)$ and $\lambda_{2N} = 1/2 \ln N + \ln(k_r)$ granting us the flexibility of *forcing* the system to be chaotic. Notice that since all but two of the eigenvalues are zero, it implies a rapid convergence to a fixed value for all directions corresponding to the eigenvalues whose value is zero. For the other eigenvalues the convergence is chaotic.

The solutions of this equation are λ_1 and λ_2. If one of them is greater than unity, the Lyapunov exponent, the logarithm of this solution will be positive, whence we can conclude that the corresponding root is unstable.

Thus it is clear that the stability of a system can depend of the value of the input, I, and this is exactly what we have succeeded in doing, namely forcing the system from chaos to periodicity. The question of how this actually transpires in the M-AdNN is yet unresolved.

4. A comparison of the AdNN and M-AdNN with respect to their pattern recognition capabilities can be briefly summarized as follows:

   a) The transitory phase for the AdNN is a few orders of magnitude larger than that of the M-AdNN;

   b) When it concerns the pattern recognition capabilities of the AdNN, we observe that the system is periodic, although the output pattern doesn't always mimic the input. Furthermore, the periodicity of the AdNN is again a few orders of magnitude larger than that of the M-AdNN.

3.4.2 Discussion About the Stability Analysis Using the Routh-Hurwitz Criterion for the Continuous Systems

Consider a nonlinear system described by the equation $\frac{d\vec{X}}{dt} = \vec{F}(\vec{X})$. An equilibrium $\overrightarrow{X_{eq}}$ is a solution to $\vec{F}(\overrightarrow{X_{eq}}) = \vec{0}$. We can calculate the Jacobian of the system to produce an associated linear equation: $\frac{d\vec{x}}{dt} = A\vec{x}$ where

$$A = \begin{pmatrix} \frac{\partial F_1}{\partial x_1} & \frac{\partial F_1}{\partial x_2} & \cdots \\ \frac{\partial F_2}{\partial x_1} & \frac{\partial F_2}{\partial x_2} & \cdots \\ \vdots & \vdots & \frac{\partial F_r}{\partial x_r} \end{pmatrix},$$

and all partial derivatives are evaluated at $\overrightarrow{X_{eq}}$.

Using the A matrix, we can compute the characteristic equation $|A - \lambda I| = 0$, where I is the identity matrix. When expanded, this r^{th}-order determinant leads to an equation of the form:

$c_0\lambda^r + c_1\lambda^{r-1} + \ldots + c_{r-1}\lambda + c_r = 0.$

Given the coefficients c_k of the characteristic equation, we get the following series of determinants:

$$\Delta_1 = det(c_1),\ \Delta_2 = det\begin{pmatrix} c_1 & c_0 \\ c_3 & c_2 \end{pmatrix}, \cdots, \Delta_r = det\begin{pmatrix} c_1 & c_0 & 0 & 0 & \ldots & \ldots \\ c_3 & c_2 & c_1 & c_0 & \ldots & \ldots \\ c_5 & c_4 & c_3 & c_2 & \ldots & \ldots \\ \ldots & \ldots & \ldots & \ldots & \ldots & \ldots \\ 0 & 0 & 0 & 0 & \ldots & c_r \end{pmatrix}.$$

It is well known that the equilibrium state is stable if and only if $\Delta_k > 0$ for $1 \leq k \leq r$.

The RH criterion states that the real part of the roots $\{\lambda\}$ are negative provided that all the coefficients $\{c_0, c_1, \ldots c_r\}$ and that all the determinants $\{\Delta_1, \Delta_2, \ldots \Delta_r\}$ are positive. Since the bottom row of the determinant Δ_r is composed entirely of zeros, except for the last element c_r, it follows that $\Delta_r = c_r\Delta_{r-1}$. Thus, for stability, it is required that both $c_r > 0$ and $\Delta_{r-1} > 0$, implying that Δ_r need not be actually evaluated.

3.4.2.1 Formal Results: The Continuous Case

We now briefly prove some chaos-related properties of the M-AdNN using the RH criterion.

Theorem 3.2.

Under a Routh-Hurwitz analysis, the M-AdNN described by Equations (3.3) is locally unstable.

Proof: In the case of the M-AdNN, the Jacobian matrix for the system is given by:

$$\begin{pmatrix} 0 & \ldots & k_f & 0 & \ldots & 0 \\ \vdots & \vdots & \ddots & & & \\ 0 & \ldots & k_f & 0 & \ldots & 0 \\ 0 & \ldots & 0 & 0 & \ldots & k_r \\ \vdots & \vdots & \ddots & & & \\ 0 & \ldots & 0 & 0 & \ldots & k_r \end{pmatrix}.$$

Thus, the characteristic equation is $\lambda^{2N} - (k_f + k_r)\lambda^{2N-1} + k_f k_r \lambda^{2N-2} = 0$, and thus, $\Delta_1 = det(c_1) = -(k_f + k_r)$. Clearly the sign of the Δ_1 depends on the magnitude of the coefficients k_f and k_r. The theorem follows since $k_f > 0$ and $k_r > 0$. □

3.4.2.2 Conjecture - the Discrete Case

We presented here the analysis for the M-AdNN using a continuous-space Routh-Hurwitz analysis. Strictly speaking the analysis should be done for the discrete-time case, which unfortunately is not so straightforward. Indeed, to the best of our knowledge, we are not aware of any existing analysis for the Routh-Hurwitz stability for *discrete* CNNs. The analysis for the continuous case becomes feasible because we are essentially dealing with continuous derivatives (as opposed to the Z-transforms) that lead to examining the Jacobian. Although we are, at present, considering the stability analysis for the discrete case, we feel that the present work would be incomplete without at least, stating briefly the analysis for the continuous case. From an informal perspective, we believe, that this approximates the discrete-time case if Δt is made correspondingly small.

3.4.2.3 Remarks:

1. The computation of Δ_1 is non-trivial for the AdNN. The first two terms of the characteristic equation are : λ^{2N} and $(k_f + k_r)N(-1)^{N-1}\lambda^{2N-1}$ respectively. In this case, Δ_1, which is equal to $(k_f + k_r)N(-1)^{N-1}$, depends on the magnitude of the coefficients k_f and k_r, and the value of N. It appears as if Adachi *et al.* [2] proved the instability of the AdNN *empirically* and not *analytically.*

2. We admit that there is a certain level of imprecision in our formalism. Just saying that for "any Δt" the continuous-time system appropriately approximates the corresponding discrete-time system is not really accurate. Indeed, we mean that Δt, the size of the step, should be so small that the first order Taylor approximation is valid. Otherwise, we cannot expect that the discrete-time system and its continuous-time "cousin" will have similar behaviors. A number of discrete time systems demonstrate bifurcation and chaos only for ranges for which the Δt parameter is far from being small. Therefore, the behavior of the discrete and continuous time "cousins" can, in fact, be very distinct. The logistic map, for example, is a very simple and well-known discrete time system for which we have bifurcation and chaos, but for which the continuous-time version is a stable system

with not even periodic attractors (only fixed point attractors). We believe our conjecture, however, based on our experimental evidence.

We conclude this section by mentioning again that the continuous results are included just to serve as a pointer as to what the corresponding discrete results *could be* when the discretizing time steps are correspondingly small.

3.5 Designing Chaotic PR Systems

To attempt to design PR systems based on the brain model suggested by Freeman [56] is no easy task. Typically, PR systems work with the following model: given a set of training patterns, the PR system learns the characteristics of the class of the patterns, and this information is retained either parametrically or non-parametrically. When a testing sample is presented to the system, a decision of the *identity* of the class of the sample is made using the corresponding "discriminant" function, and this class is "proclaimed" by the system as the identity of the pattern. The same philosophy is also essentially true for syntactic/structural PR systems.

As opposed to this, we do not foresee chaotic PR systems to report the identity of testing pattern with such a "proclamation". Rather what we are attempting to achieve is to have the chaotic PR system continuously demonstrate chaos as long as there is no pattern to be recognized or whenever a pattern that is not to be recognized is presented. But, when a pattern which is to be recognized is presented to the system, we would like the proclamation of the identity to be made by requiring that the chaos level decreases significantly, and that the system simultaneously possesses a strong periodic component, which we refer to as "sympathetically resonance".

To be more specific, let us suppose that we want the chaotic PR system to recognize patterns P_i and P_j. To accomplish this, we shall train the system (in this case, the M-AdNN) using these patterns. It is interesting to observe what this training accomplishes. By a mere straightforward computation (as opposed to an *iterative* computation) this training phase assigns the weights between the neurons of the CNN. These weights effectively memorize the training patterns so that the network, in turn, effectively behaves as an "Associative Memory" system. The reader will observe that such a "one shot" training scheme is analogous to the phenomenon of the

Hopfield-like networks. Subsequently, on testing, if any pattern *other than* P_i or P_j is presented, the CNN must continue to be chaotic, since it is *not trained* to recognize such a pattern. However, if P_i or P_j, (or a pattern resembling either of them) is presented, the CNN must switch from being chaotic to being periodic. Note that as opposed to traditional PR systems, the output is not a single value. It is a *sequence* of values, which is chaotic (i.e., displays no periodicity) unless one of the trained patterns is presented. In the latter case, the system switches to being periodic, and by examining the output which occur periodically, the user will be able to infer that one of the stored patterns has been encountered, and then continue to decide on the identity of the pattern.

There is yet one issue in this whole decision process, which deserves more attention, namely that of determining if the CNN's output is *periodic*. This can be achieved by, for example, examining the Fourier spectrum of the CNN's output. This spectrum would be effectively representing white noise if the system is chaotic, but would contain a "spike" when the system switches to become periodic. When the user is alerted that the system is periodic, he then determines the identity of the actual test pattern using a sequential (or hierarchical) test, for example, by a "template match"-like comparison.

What then is the advantage of such a chaotic PR system? Quite simply, apart from the new model of PR, it also prevents the user from having to invoke such a comparison strategy unless a periodic behavior is observed.

We would have liked a chaotic PR system to resonate with a different frequency for each pattern class[11] - unfortunately, the M-AdNN does not. Our only comfort is that it appears (as suggested by Freeman) as if the brain too works with such a chaotic PR model. It has the amazing capability of picking out patterns it knows (or is trained with) right in the middle of the most chaotic environment.

We conclude this section by observing that Adachi *et al.*[2] had suggested, rather informally, that such a chaotic PR system could be developed. However, the mechanics of the system were not fully explained, and unfortunately, his AdNN was not chaotic. By decreasing the

[11]The periodicity of the M-AdNN has nothing to do with the identity of the classes. We believe that the brain possesses this same property (for otherwise, it would resonate differently for every single pattern that it is trained with, and the set of patterns which we can recognize is truly "infinitely large"). But we are currently investigating how we can set the parameters of the M-AdNN (k_r and k_f) to be class-dependent.

number of k_r and k_f terms along the principal diagonal, we have been able to obtain such a chaotic/periodic system, which can be trained in a "one shot" manner, and tested by recognizing periodic behavior.

In practice, on testing, only one pattern is repeated. If the testing pattern is close enough to more than a single "training" pattern, both may be periodically repeated. This is the rationale for the array count which records the periodicity of all the trained patterns in the output.

The formal procedure[12] to be for the PR system follows is as below. We remark that the periodicity can be observed using a frequency domain analysis. However, for the sake of simulation (to prove that the concepts are valid) in this pseudo-code we assume that we are dealing with serial machines, and that the periodicity is marked by a "compare against all" strategy. We are open to any superior schemes to achieve this task.

Input: A pattern Y. k_r, k_f, N, *Threshold* and *Iter*, the maximum number of iterations, are parameters.
Output: A periodic sequence of one (or more) of the memorized patterns X^f if $Y = [y_1 \cdots y_N]^T$ is close X^f. The sequence must not contain any memorized pattern if Y is "far away" from any $\{X^s\}$, for $s = 1..p$. The output of the M-AdNN is given by $U = [u_1 \cdots u_N]$ obeying (1).
Criterion: Y is considered "close" to any X^s if the noise level is less than a predefined value, *Threshold*.
Method:
/*Read input pattern $Y = [y_1 \cdots y_N]$ */
for i=1 to N **do**
  $a_i = y_i$
end for
/*Compute the output using the dynamical equations (1) */
$\eta(0) = 0$; $\xi(0) = 0$; $c_f = 0$;
/* initialize the periodicity counter for the training set */
for $f = 1$ to p **do**
  $count(f, c_f) = 0$

[12]The training, which is a "one-shot" assignment, initializes each w_{ij} to be zero and than sums this, for all the training patterns, $\{X^S = [x_1^s \cdots x_N^s]\}$, to be $w_{ij} = w_{ij} + x_i^s x_j^s$.

end for
for $t = 0$ to $Iter$ **do**
  for $i = 1$ to N **do**
    $\eta_i(t+1) = k_f\eta(t) + \sum_{j=1}^{100} w_{ij}u_j(t)$;
    $\xi_i(t+1) = k_r\xi(t) - \alpha u_i(t) + a_i$;
    $u_i(t+1) = f(\eta_i(t+1) + \xi_i(t+1))$;
  end for
  $\eta(t+1) = \eta_N(t+1)$
  $\xi(t+1) = \xi_N(t+1)$
  /* Compute the distance between the output U and each pattern X^s */
  for $s = 1$ to p **do**
    $d_s(t) = 0$;
  end for
  for $s = 1$ to p **do**
    for i=1 to N **do**
      $d_s(t) = d_s(t) + |(u_i(t) - x_i{}^s)|$
    end for
    /* we accept a level of noise for Y, equal with $(Threshold/N)\%$ */
    if $d_s(t) \leq Threshold$ **then**
      $f = s$ /*index of recognized pattern X^f, close to Y */
      $count(f, c_f) = t$; $c_f = c_f + 1$;
    end if
  end for
end for
/* Test the periodicity for only 2 cycles */
$periodicity[f] = count(f, 2) - count(f, 1)$
Report index f and $periodicity[f]$.
End_Module_Testing
End_Algorithm PR_using_M-AdNN

Rather than involve a Fourier analysis of the output spectrum, we maintained an array of output signals and have tested for periodicity in the time domain. This is, of course, laborious, but was done just because our system was intended to be of a prototype "proof of concept"

nature.

3.6 Experimental Results

As the reader can observe, a chaotic PR system would be distinct, in operation and characteristics, from the more traditional systems. In the training phase, we would present the system with a set of patterns, and thus by a sequence of simple assignments (as opposed to a sequence of iterative computations), it "learns" the weights of the CNN. The testing involves detecting a periodicity in the system, signaling the user that a learned pattern has occurred, and then inferring what the periodic pattern is. We shall now demonstrate how the latter task is achieved in a *simulation.*

In a simulation setting, we are not dealing with a real-life chaotic system (as the brain[13]). Indeed, in this case, the output of the CNN is continuously monitored, and a periodic behavior can be observed by studying the frequency spectrum, or by processing, in the time domain, the outputs as they came. Notice that the latter is an infeasible task, as the number of distinct outputs could be countably infinite. This is a task which the brain, (or, in general, a chaotic system), seems to be able to do, quite easily, and in multiple ways. However, since we have to work with serial machines, to demonstrate the periodicity, we have opted to compare the output patterns with the various trained patterns. Whenever the distance between the output pattern and *any* trained pattern is less than a threshold, we mark that time instant with a distinct marker characterized by the class of that particular pattern. The question of determining the periodicity of a pattern is now merely one of determining the periodicity of *these markers*[14].

To present our results in the right perspective, we have tested the schemes for a sets of data which involves the recognition of numerals.

[13]How the brain is be able to record and recognize such a periodic behavior amidst chaos is yet unexplained [56].

[14]The unique characteristic of such a PR system is that each trained pattern has a unique attractor. When the testing pattern is fed into the system, the system converges to the attractor that characterizes it best. The difficult question, for which we welcome suggestions, is one of knowing which attractor it falls on. As it stands now, we have used a simplistic "compare against all" strategy, but even here, we believe that hierarchical strategies where use syntactic clustering could enhance the search. Beside, such a comparison needs to be invoked only if a periodicity is observed by, for example, a frequency domain analysis. This is an extremely interesting area of research which we are currently pursuing.

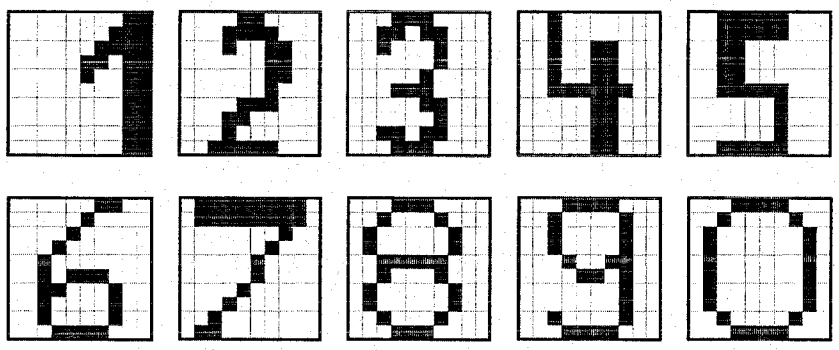

Figure 3.1: The set of patterns used in the PR experiments. These were the 10×10 bitmaps of the numerals $0 \cdots 9$. The initial state used was randomly chosen.

3.6.1 PR with a Numeral Data Set

We conducted numerous experiments on the Adachi dataset [2] and other datasets. However, in the interest of space, we report the results of training/testing on a numeral dataset described below. The training set had 10 patterns, given in Figure 3.1, and consisted of 10×10 bitmaps of the numerals $0 \cdots 9$. The parameters used for Equations (3.3) were $N = 100$ neurons, $\varepsilon = 0.00015$, $k_f = 0.2$ and $k_r = 0.9$.

Periodicity-based Accuracy for the Non-noisy and Noisy Numeral Dataset

The trained M-AdNN, demonstrated a periodic response when the non-noisy external stimuli were applied, after an initial non-periodic transient phase. The transient phase was *very* short - its mean length was 23.1 time units, and most of the transitory phases were of length 24 units. The actual length of the transient phase in each case is given in Table 3.1. The system resonated sympathetically with the input pattern, with a fairly small periodicity. The periodicity of the response is also tabulated in Table 3.1, where the initial starting input pattern was randomly chosen. Note that the periodicity was fairly "small" (26 in most cases - the first pattern has a

Pattern	No of steps in transitory process	Periodicity
1	15	7,15
2	24	26
3	24	26
4	24	26
5	24	26
6	24	27
7	24	26
8	24	26
9	24	26
10	24	26

Table 3.1: The transitory phase and the periodicity for M-AdNN, for the non-noisy versions of the training set, namely, the numerals. The first pattern has a limit cycle with double periods, the first with 7 units and the second with 15.

limit cycle with double periods, the first with 7 units and the second with 15). The accuracy[15] of recognition was 100%.

To investigate the power of the M-AdNN for noisy samples, we also tested the system with "noisy" testing samples, where the noise was included in a bit-wise manner[16]. The noise in each case was measured by the percentage of pixels which were modified from 0 to 1 and vice versa. Thus, if the noise was 10%, 10 (out of the 100) randomly chosen pixel values (say, x_i^p) of X^p were modified and were rendered different from those in the original pattern, X^p.

For each class (i.e, each trained prototype), we computed the distances $d_p(t)$ between it and the network's output pattern, where the distance was a Hamming-type measure defined by $d_p(t) = \sum_{i=1}^{N} |(u_i(t) - x_i^p)|$ for the p^{th} stored pattern. For a pattern to be recognized, the value of the threshold specified in the algorithm, was set to be the same as the level of the noise.

[15]It would have been good if the periodicity was uniquely linked to the pattern classes, but, unfortunately, this is not the case. Rather, the system possesses the characteristic that it switches from being chaotic to periodic whenever a noisy version of one of the trained patterns is received. So, it would be more appropriate to say that this switching phenomenon occurs with 100% accuracy. We have taken the liberty to refer to this as "100% PR" accuracy.

[16]We would like to emphasize that the pattern, from a PR perspective, is not a "shape". Rather, it is a 100-dimensional vector. Every component of this vector can be modified. Thus, since the noise is bit-wise, the current PR exercise may not work if the "images" are subject to translation/rotation operations. For solving translations, we propose to preprocess the patterns by extracting the features that one will save in the vector latter

Pattern	Transient(10%)	Periodicity (10%)	Transient(15%)	Periodicity (15%)
1	8	7, 7, 8	24	25
2	24	26	8	7,7,8
3	24	26	8	7,7,8
4	24	26	8	7,7,8
5	24	26	8	7,7,8
6	24	27	8	7,7,8
7	24	26	8	7,7,8
8	24	26	8	7,7,8
9	24	26	8	2,5,7,8
10	7	22	7	22

Table 3.2: The transitory phase and the periodicity for M-AdNN, when the testing is done with patterns from the numeral training set containing 10% noise and also patterns containing 15% noise. The first pattern with 10% noise has a limit cycle with triple periods, the first two with a period of 7, and the last with a period of 8. Similar scenarios are observed in the 15% noise case.

Numerous tests were done, but in the interest of simplicity, we merely mention two cases, namely, the case when the noise was 10% (see Figure 3.2) and the case when the noise was 15% (see Figure 3.3). In both cases, after an initial non-periodic transient phase, the trained M-AdNN demonstrated a periodic response when it was presented with the noisy numerals. As before, the transient phase (see Table 3.2) was rather insignificant when we consider that *Iter* is 20,000 (it had an average value of 20.7 when the noise was 10%), but the periodic resonance was significant. The resonance periodicity[17] was consistently "small" (also tabulated in Table 3.2).

The salient characteristics of the PR can be summarized as:

1. The system is almost insensitive to the *initial* pattern, but rather, very sensitive only to the input pattern. Indeed, even if the initial state was any of the *other* stored patterns, the transient and periodicity are essentially unaffected.

2. The identity does not depend on the specific period - many trained patterns can lead to the

[17]The periodicity (7,15) means that we encounter a "double cycle". Thus after the transient phase, the training pattern occurs at times 7, 22, 29, 44 etc. This is actually because we have a 8-shaped limit cycle with the smaller loop of the '8' having a periodicity of '7', and the larger loop having a periodicity of '15'.

same periodicity. Such a unique mapping between the trained pattern and the periodicity, unfortunately, does not exist.

3. Numerous additional simulations for the case when the testing patterns are not training patterns were also done. It turns out that no output with a distance smaller than the chosen threshold was obtained.

4. The threshold was not too crucial. We opted to use a threshold that is directly related to the acceptable level of noise found in the testing pattern. In our experiments, we used noise levels from 0 to 15%. The question of how this "acceptable threshold" varies with the noise is open. If the threshold is too small, a "non-periodic" signal could possibly be inferred. But as mentioned above, we increased the threshold as the permitted noise level was increased.

5. The recognition accuracy was 100%, even though the images were quite degraded. This "accuracy" must be reckoned as described in Footnote 13.

6. The question of why the M-AdNN yield cycles of finite periodicity remains open. However, we should point out that since the number of neurons is so high, there is a possibility that there are other attractors, which we did not locate, whose periodicities are many orders of magnitude larger (for example, of order of 10,000) than the periodicities that we otherwise observed for the trained patterns. But even if that were the case, the large differences in these periodicities would help us in discriminating between these two "classes" of attractors: the "useful" ones which achieve PR, and the "non -useful" one. But the existence of the latter still seems to be a conjecture.

In our opinion, the results are remarkable, especially when we observe the extremely poor quality of the testing samples.

3.7 Conclusion

In this Chapter, we have proposed a new model for PR, namely one that involves Chaotic Neural Networks (CNNs). To achieve this, we have enhanced the basic model proposed by Adachi [2],

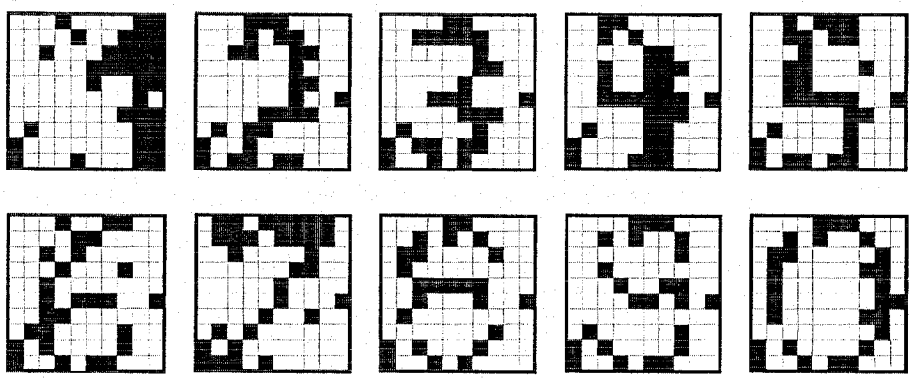

Figure 3.2: The second set of patterns with 10% noise.

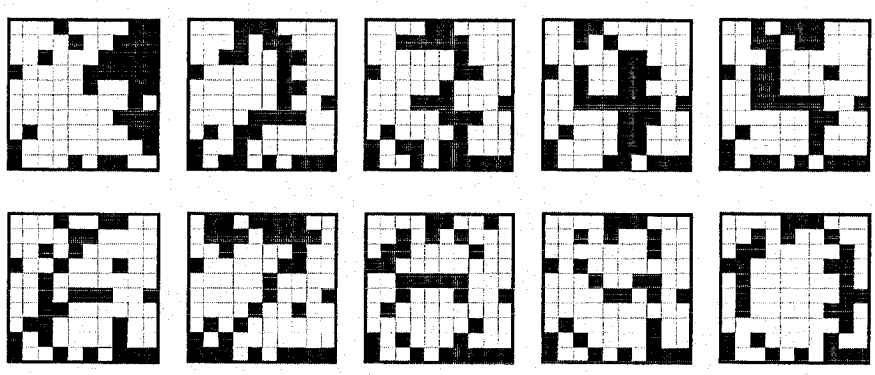

Figure 3.3: The second set of patterns with 15% noise.

referred to as *Adachi's Neural Network* (AdNN), which though dynamic, is not chaotic. We have shown (by both Lyapunov and a Routh-Hurwitz analysis) that by decreasing the multiplicity of the eigenvalues of the AdNN's control system, we can effectively drive the system into chaos, and also increase the possibility of periodic behavior. With this premise, we then demonstrated that such a Modified AdNN (M-AdNN) has the desirable property that it can recognize various input patterns by the system essentially *sympathetically* "resonating" with a finite periodicity whenever *these* samples (or their reasonable resemblances) are presented. The M-AdNN has been tested for a real-life PR problem involving numerals, yielding a perfect 100% accuracy. We believe that this research also opens a host of new research avenues, some of which have been mentioned.

In the next Chapter we propose to investigate the architecture of a neural network which generalizes the M-AdNN model, thus demonstrating that the modification of the system can actually change its PR capabilities.

Chapter 4

Modelling Inaccurate Perception

4.1 Introduction

In the last Chapter, we had proposed a new model for PR, namely one that involves Chaotic Neural Networks (CNNs). We had enhanced the basic model proposed by Adachi the (AdNN), and showed (by both a Lyapunov and a Routh-Hurwitz analysis) that by decreasing the multiplicity of the eigenvalues of the AdNN's control system, we can effectively drive the system into chaos, and also increase the possibility of periodic behavior. With this premise, we then demonstrated that the M-AdNN has the desirable property that it can recognize various input patterns by the system essentially *sympathetically* "resonating" with a finite periodicity whenever *these* samples (or their reasonable resemblances) are presented.

In this Chapter[1] we propose to solve the "inverse" problem, which consists of understanding why a PR system loses its recognition capabilities. In our opinion, this problem has not been solved in any PR model. To demonstrate this in a neural world, we intend to investigate the architecture of a CNN that loses its PR capabilities even though the *quality* of the stimulus is "perfect". With this new approach, we believe that we can provide a chaotic rationale for both perception and the lack thereof, even in cases when the stimulus is "noise free".

[1]Some preliminary results from this Chapter were published in the *Proceedings of the 14th Scandinavian Conference in Image Analysis*, Joensuu, Finland, 2005, pp: 821-830.

4.1.1 The Perception

Sensations can be viewed as simple experiences that are caused by physical stimuli. Perceptions are the processes by which the brain organizes and interprets sensations [27]. What we know about the world (e.g. objects) depends on the information gathered by our senses and channelled into our brain. The brain organizes sensations in such a way that it can later recognize objects and events in the environment, and, if applicable, detect actions or movements of these objects. Understanding perceptual organization is a matter of understanding how one perceives form, depth, and motion of objects.

After the turn of the last century, a number of German scientists, known as Gestalt psychologists, argued that the key to understanding perception was to identify *the relations* between various parts of a stimulus. In other words, one does not simply perceive a triangle, for example, as consisting of three separate lines; rather, one perceives *the relation* between these three lines.

Perception, in itself, is not just a reception of what is received. It involves a processing of what is received, and an activity of analysis, synthesis, and generalization. The essence of perception is the continuous exploration of the objects. This exploration can become, under certain conditions, disorganized and incoherent, and can lead to a high level of perturbation of the operations involved in perception. *This Chapter intends to model the perturbation of perception from a neural and an image analysis point of view.*

Perception is a conscious process, oriented and organized, which implies that many actions with objects are involved, such as measuring, decomposing, recomposing, grouping, classifying, transforming, and modelling. As an active mechanism, perception is created, corrected, and verified by action. When the action involving the objects is limited, perception is poor, incomplete, or erroneous.

4.1.2 Modelling Inaccurate Perception

Since we are interested in modelling an extremely complex system, namely the brain, it is clear that it is difficult, if not impossible, to model all the functionalities using a simple architecture. Often, when modelling such a complex system, the optimization of one function will have an

effect on other phenomena related to the system and, thus, could lead to the decline in the performance of other functions performed by the model. In our research, we intend to study the concept of perception and its "inverse", which we refer to here as "blurring" or inaccurate perception[2]. We would like to understand the function of such an *artificial* recognition system by modelling inaccurate perception. To do this, in Chapter 3 we explored a model, used for PR, with the hope that we could demonstrate that this model can also be used to analyze the effects of anomalies to the process of perception.

We illustrate this concept using the visual system of humans. In visual recognition, there are two classes of problems which affect the process of perception:

(i) Issues regarding the stimulus, which, in this case, involve the resolution of the image, and,

(ii) Issues regarding the recognition system itself. In this context, we envisage three reasons why vision can be blurred:

1. The eye itself has a disease (e.g. myopia, hyperopia, astigmatism) which affects the *reception* of stimuli, by decreasing the visual acuity.
2. The optical nerve is unhealthy, thus affecting the *transmission* of stimuli.
3. The visual cortex is unhealthy, thus affecting the *processing* of the stimuli.

The second class, which includes problems as the blurring problem, related to the quality of the recognition system, have not been studied extensively in the modelling of artificial perception systems. This lead us, quite naturally, to the "inverse" problem, which consists of why people see inaccurately. Unlike previous studies, which primarily address the degradation of the quality of the stimulus (e.g. adding noise, decreasing the resolution, decreasing the number of bits per pixel) we provide a model and the analysis for the case when the image and sensor units are "perfect".

In this Chapter, we propose a new approach for modelling, and demonstrating the modification of the quality of a system, one which does not modify the *quality* of the stimulus. We attempt to provide a chaotic rationale for both perception and the lack thereof, even in cases when a stimulus is "perfect".

[2]This is done, not only to model the brain as a chaotic system, but also to see how such a model can be used in artificial neural systems, capable of achieving perception.

4.1.3 Biological Motivation of the Problem

The term "perception" can philosophically be related to the phenomenon of discovery [176]. During perception, an individual directs his attention to the object under observation, and attempts to understand the characteristics of the physical world by utilizing the input received from his/her senses. In this regard, philosophers have been concerned with the *analysis* of perception, and with the query of whether or not it, in itself, can be regarded as a source of knowledge. From the biological and psychological point of view, the concept of perception depends on the accuracy with which an object being observed, is correctly interpreted. If an entity (a system in our approach) observes the object inaccurately, or interprets the information poorly, it becomes susceptible to mistakes that can change its perception. The important idea, which is the kernel of our research hypothesis, consists of the consideration that *the quality of the perception depends of the system and can be independent of the object.* This would be the scenario when the latter is perfect - void of distortion or deformation in the biological field, or noise in the technical field. Indeed, this is also the problem we study.

We present here a few scientific and published reflections that sustain the above consideration.

Piaget [127] categorized classified perception-related schemes into four algorithms that transform an object into its perceived image by "invoking" empirical and geometric functions on one hand, and deforming or compensatory ones on the other. All of these schemes, in themselves, may contain deforming aspects because, as Piaget states, "all perceptual activities, whether they give rise to stable schematization or not, can also have secondary illusory consequences". Piaget's classification was a pioneering work which inspired us to propose a possible algorithm (*chaotic* or otherwise) to explain why perception, or the lack thereof, can be dependent on the *model* of the perceptive system, and not merely on the object being observed.

To further strengthen this research, Forgus and Melamed [55] advanced and developed the concept of inaccurate perception. Their contribution was that they proposed an explanation for the generative causes for this type of perception, and succeeded in developing a classification mechanism for the same. In their research [55], they described "illusions" as being determined by multiple variables including perspective corrections, contrast, orientation, and "probably certain other kinds of hypotheses" peculiar to the individual. They also stated that the technique by which perceptual constancies are related to illusions, like most other issues that relate to

perception, depends on the *kinds* of models, sets, and coding devices that the individual brings to the perceptual scene. While the result of Forgus and Melamed was "daring", and possibly pioneering from a systems point of view, the question of how the user could switch his model from being perceptive to non-perceptive was unvisited. We highlight that such a formal explanation is yet unavailable for the traditional theories of PR. Our aim here is to put "meat and skin" to the skeletal hypothesis proposed by Forgus and Melamed, and in particular in a *chaotic* realm.

From the cognitive point of view, Matlin [110] took the latter hypothesis one step further. She speculated that a phenomenon that rendered perceptions to be incorrect was also related to the cause of illusionary mechanisms. She stated that, in an illusion, what we see does not correspond to the true qualities of the object being observed or perceived. Thus, her psychological conjecture was that such inaccurate perception is important in our daily lives. Although this is not our primary area of research, our study has lead us to a vast body of literature involving such phenomena, which we are now try to model using a chaotic background.

Finally, the process of modelling inaccurate perception in vision was recorded to be an open problem by Marr [108]. He mentioned that the critical issues in vision revolve around the nature of the representations used for describing the object perceived. These issues include the particular characteristics of the world that are made explicit during vision, and the nature of the processes that recover these characteristics, create and maintain the representations, and eventually inspect them. He stated that there is no real recipe for this type of research, any more than there is a straightforward procedure for discovering things in any branch of science other than biology and psychology.

As far as we know, from the view point of Marr's assertion, our research is of a pioneering sort, when it concerns tackling this open problem. We do not claim that we have solved it. Rather, we modestly state that we have made a few steps in the direction of solving this dilemma, and even then, only for the *Chaotic* PR domain.

We emphasize that to design a system that does not achieve PR by virtue of *changing the parameters* (for example, by changing the coefficients of the discriminant function) is easy. But to design a chaotic NN, which switches *abruptly* from demonstrating a small, finite periodicity to a chaotic behavior is not trivial - which is the phenomenon that we have demonstrated. We investigated, furthermore, the chaotic NN, by proposing a modification for maintaining the

chaotic behavior but altering the PR capabilities. Beside this, to further demonstrate that this phenomenon (i.e. of altering the PR capabilities of the network), is not a function of the parameters, but of the connectivity (i.e. the "change" in connectivity which results in moving the diagonal terms to an off-diagonal column) is far from obvious.

4.1.4 Perception and the M-AdNN Model

Many models have been proposed in the literature to account for the individual aspects of perception. However, there has been little insight into generalizing these models to account for other aspects of perception. Many of these models involve neural modelling. Examples are: (a) The *recognition by components* (RBC) models of Biederman [19], (b) the *feature analysis* models [126] (using Principal Component Analysis (PCA), the Independent Component Analysis (ICA) and Fisher Linear Discriminant Analysis[3]), and (c) the *template matching*[4] [6] models. The failure of conventional approaches to model all aspects of perception suggests that the current concepts of classical neural computation are inadequate, and we submit that many novel principles and mechanisms of perceptual computation remain to be discovered. We attempt to make a few modest steps in this direction.

Classical neural computation does not include Chaotic Neural Networks. By using a Modified AdNN, denoted as M-AdNN and proposed in Chapter 3 (and published in [30, 32, 33]) we formulate a model for the foundation of inaccurate perception, caused by the properties of the system and *not by the quality of the stimulus*. To our knowledge, such a phenomenon has not been proposed in previous models. The reason for excluding such a phenomenon in the modelling is not due to the lack of evidence of this property in human perception; rather it is due to the lack of a mechanism that can "implement" it.

[3]These three methods find a mapping between the original feature space and a lower dimensional feature space.

[4]Template matching and its variants [46] is commonly used in many computer vision applications such as feature-based tracking, object recognition and stereo-matching. In general, it requires similarity measures between the features of a template and the query image.

4.1.5 Our Contributions

The first step of our research endeavor was to find a relationship between the NN model proposed by Adachi and the clinical results obtained by Freeman. This was far from obvious, because it turns out that Adachi's NN is not chaotic. We wanted to propose a new method of achieving PR, and we were further confronted with the challenge to achieve the recognition involving a dynamical process. In this respect, the only available approach was the following: By increasing the level of chaos in a model similar to the Adachi network, and by setting the weights corresponding to certain "patterns", we were able to confirm that the proposed architecture possessed PR capabilities. Chapter 3 presented, in more detail, the algorithms and the stability analysis.

The second step of our research was to understand the difference between our model and that of Adachi. Given the differences associated with the stability issues, we investigated which of our modifications affected this stability. It turns out that of the three major modifications introduced to the AdNN, only one was related to stability, namely the modification of m, the number of non-zero eigenvalues. The parameter m behaves exactly as a stability-control parameter. If $m = N$, we obtain an extreme case, the Adachi's NN, where none of the eigenvalues are zero. The opposite extreme case is our previous model, which has only a single non-zero eigenvalue. Thus, the tacit unanswered question was: What occurs between these two extremes? This is investigated in this present Chapter.

As mentioned before, the goal of modelling natural and artificial perception involves determining how a system can extract an object that it perceives from an image which is noisy. In contrast, we consider the "inverse" of this problem, and study how even a clear image can be perceived to be blurred (and, thus, mis-recognized) in some contexts. Here, we do not consider the simple model where the true image is garbled with noise. Our model involves a chaotic model of PR. Unlike in Chapter 3 where the chaotic PR system extracts the pattern from the input, in this Chapter we show that, even without the inclusion of additional noise, the perception can be *inaccurate* if the dynamics of the chaotic system are modified. Here we propose a model for inaccurate perception and present a formal analysis using the Routh-Hurwitz criterion and Lyapunov exponents. We also demonstrate experimentally the validity of the proposed model by using the benchmark dataset of Adachi [2] and the numeral dataset described in the Section 3.7. A byproduct of this model is the theoretical possibility of desynchronization of periodic

behavior of the brain (as a chaotic system), which could render us the possibility of predicting, controlling, and annulling epileptic behavior.

4.2 A Chaotic NN for Inaccurate Perception: The Mb-AdNN

The rationale for transforming the AdNN into the M-AdNN was essentially one of forcing the former system into chaos, and at the same time attempting to demonstrate a periodic behaviour if required[5]. When it concerns inaccurate perception, it appears as if we have to strike a proper medium between the AdNN and the M-AdNN. For the first part, unlike the AdNN, we would like the new system to demonstrate chaos. But, on the other hand, unlike the M-AdNN, we don't want the system to be "all too periodic" (i.e., stable) if the trained non-noisy patterns are presented, because we are, indeed, attempting to model the *lack of perception* or "blurring".

We shall show how this can be achieved by modifying the dynamics of the control system so as to force the number of non-zero eigenvalues to be $2m$, where m is a "parameter" of the model. We named this new network Mb-AdNN (Modified for Blurring AdNN). In each case, we show how we modify the AdNN (or the M-AdNN) and present the rationale[6] for the modification.

1. The Mb-AdNN has two global states used ONLY for the first m neurons, which are $\eta(t)$ and $\xi(t)$ obeying:

   $x_i(t+1) = f(\eta_i(t+1) + \xi_i(t+1))$,

   $\eta_i(t+1) = k_f\eta(t) + \sum_{j=1}^{N} w_{ij}x_j(t)$, for $i \leq m$,

   $\eta_i(t+1) = k_f\eta_i(t) + \sum_{j=1}^{N} w_{ij}x_j(t)$, for $i > m$,

[5]It is true that our model is far from a large scale network built with realistic neurons such as the Hodgkin-Huxley neurons, Rinzel neurons, Traub Neurons or Bursting Neurons. Our aim was to find a simplistic NN model which is phenomenologically close to Freeman's hypothesis of recognition in the olfactory system. We investigated many architectures and we found that the Adachi's NN, a Hopfield-like network, is sufficiently simplistic to switch from chaos to periodicity and to simultaneously possess PR capabilities. We do mention, however, that the arena for research here is vast. The question of designing Chaotic PR systems with other NN models is open. Furthermore, the question of whether these NNs will lose their periodicity abruptly is also open.

[6]We request the reader to kindly refer to the rationale for the AdNN and M-AdNN (see Section 3.2 and 3.3) to get a better perspective of how the Mb-AdNN differs from them.

$$\xi_i(t+1) = k_r\xi(t) - \alpha x_i(t) + a_i, \text{ for } i \leq m,$$
$$\xi_i(t+1) = k_r\xi_i(t) - \alpha x_i(t) + a_i, \text{ for } i > m. \tag{4.1}$$

After time $t+1$, the global states are updated with the values of $\eta_m(t+1)$ and $\xi_m(t+1)$ as: $\eta(t+1) = \eta_m(t+1)$ and $\xi(t+1) = \xi_m(t+1)$.

Rationale: Unlike in the AdNN, which at every time instant computes a new internal state vector, the Mb-AdNN uses the contents of the memory from m *other* internal states. In the case of the M-AdNN, this value of m was set to be exactly unity, and we observed that it was possible to relate $\eta(t+1)$ and $\xi(t+1)$ to $\eta_K(t+1)$ and $\xi_K(t+1)$ for any[7] fixed K. Our current model lies in between the two extremes, namely (a) The AdNN model, where the updating at time *t+1* uses the internal state values of *all* the neurons at time t, and (b) The M-AdNN model (which demonstrates PR capability), where the updating at time *t+1* uses the internal state values of any *one* of the neurons at time t.

2. The weight assignment rule for the Mb-AdNN is the same as in M-AdNN.

3. The external inputs are applied in the Mb-AdNN, as in M-AdNN.

   Rationale: The rationales for the last two rules follow the same reasoning as the M-AdNN and are omitted here (See Section 3.3).

4.3 The Mb-AdNN Orbital Stability Properties

In this Section we analyze the stability issues concerning the Mb-AdNN. We do this first using Lyapunov Exponents, and then using the Routh-Hurwitz Criterion.

4.3.1 Analysis Using Lyapunov Exponents

The theoretical concepts regarding the Lyapunov analysis were presented in Section 3.2.1. For the sake of completeness, a few aspects of this technique are briefly repeated here.

[7] K is the index of first neurons which used the two global states.

We consider a discrete time ($t \in Z$) dynamical system $A \longmapsto F(A)$ and we compute its Jacobian matrix of partial derivatives $J(A) = D_A F(A)$, by using the approximation of the dynamics of the system near the steady states. Consider also the sequence $\{A_0, A_1, ..., A_{k-1}\}$ generated by successive iterations of the initial condition, A_0. For this sequence, we introduce the matrix

$$J_k(A) = J(Y_{k-1}(A))J(Y_{k-2}(A))...J(Y_1(A))J(Y_0(A)).$$

The Lyapunov exponents, which quantify the sensitivity to initial conditions, are given by the logarithms of the eigenvalues of $\Lambda := [J^T(A)J(A)]^{1/2}$, where $J^T(A)$ denotes the transpose of $J(A) = \lim_{k\to\infty} J_k(A)$.

Theorem 4.1.

Under a Lyapunov exponent analysis, the Mb-AdNN described by Equations (4.1) is locally unstable.

Proof: Consider the dynamical system for the Mb-AdNN, whose asymptotic dynamical matrix J is given as:

$$J(A)=\begin{pmatrix} [J_{ij}^1] & [J_{ij}^2] \\ [J_{ij}^3] & [J_{ij}^4] \end{pmatrix}, \tag{4.2}$$

where each $[J_{ij}^k]$ is an $N \times N$ sub-matrix of J(A), for $1 \leq k \leq 4$, $1 \leq i \leq N$ and $1 \leq j \leq N$. Each $[J_{ij}^k]$ is a result of the partial derivatives of $\eta_i(t+1)$ and $\xi_i(t+1)$ with regard to $\eta_j(t)$ and $\xi_j(t)$ respectively. This will be clarified presently.

The term $J_{ij}^k(t)$, for $1 \leq k \leq 4$, is the arbitrary element at time "t", and each J_{ij}^k in Equation (7.17) is obtained by taking the limit as $t \longrightarrow \infty$. Therefore, $J_{ij}^k(t)$ takes on four distinct forms as follows:

1. $J_{ij}^1(t)=\frac{\partial \eta_i(t+1)}{\partial \eta_j(t)}$ when $1 \leq i \leq N$ and $1 \leq j \leq N$,

2. $J^2_{ij}(t)=\frac{\partial \eta_i(t+1)}{\partial \xi_j(t)}$ when $1 \leq i \leq N$ and $1 \leq j \leq N$,

3. $J^3_{ij}(t)=\frac{\partial \xi_i(t+1)}{\partial \eta_j(t)}$ when $1 \leq i \leq N$ and $1 \leq j \leq N$,

4. $J^4_{ij}(t)=\frac{\partial \xi_i(t+1)}{\partial \xi_j(t)}$ when $1 \leq i \leq N$ and $1 \leq j \leq N$.

Because $x_i(t+1) = f(\eta_i(t+1)+\xi_i(t+1))$, where f is the logistic function with the steepness parameter ε satisfying $f(y) = 1/(1+exp(-y/\varepsilon))$, and $\frac{df(y)}{dy} = \frac{d}{dy}\frac{1}{1+exp(-y/\varepsilon)}$ (or $\frac{df(y)}{dy} = \frac{1}{\varepsilon}x(1-x)$ where $x \equiv f(y)$), the following explicit forms of $J_{ij}(t)$ result:

(a) $J^1_{ij}(t) = \frac{w_{ij}}{\varepsilon}x_j(t)(1-x_j(t))$ when $1 \leq i \leq N-m-1$ and $1 \leq j \leq N-m$,

(b) $J^1_{ij}(t) = k_f + \frac{w_{ij}}{\varepsilon}x_j(t)(1-x_j(t))$ when $i = N-m$ and $1 \leq j \leq N-m$,

(c) $J^1_{ij}(t) = \frac{w_{ij}}{\varepsilon}x_j(t)(1-x_j(t))$ when $N-m+1 \leq i \leq N$ and $N-m+1 \leq j \leq N$ and $i \neq j$,

(d) $J^1_{ij}(t) = k_f + \frac{w_{jj}}{\varepsilon}x_j(t)(1-x_j(t))$ when $N-m+1 \leq i = j \leq N$,

(e) $J^2_{ij}(t) = \frac{w_{ij}}{\varepsilon}x_j(t)(1-x_j(t))$ when $1 \leq i \leq N$ and $1 \leq j \leq N$,

(f) $J^3_{ij}(t) = -\frac{\alpha}{\varepsilon}x_j(t)(1-x_j(t))$ when $1 \leq i \leq N$ and $1 \leq j \leq N$ and $i = j$,

(g) $J^3_{ij}(t) = 0$ when[8] $1 \leq i \leq N$ and $1 \leq j \leq N$ and $i \neq j$,

(h) $J^4_{ij}(t) = -\frac{\alpha}{\varepsilon}x_j(t)(1-x_j(t))$ when $1 \leq i \leq N-m-1$ and $1 \leq j \leq N-m$ and $i = j$,

(i) $J^4_{ij}(t) = 0$ when $1 \leq i \leq N-m-1$ and $1 \leq j \leq N-m$ and $i \neq j$,

(j) $J^4_{ij}(t) = k_r - \frac{\alpha}{\varepsilon}x_j(t)(1-x_j(t))$ for $i = N-m$ and $1 \leq j \leq N-m$,

(l) $J^4_{ij}(t) = 0$ when $N-m+1 \leq i \leq N$ and $N-m+1 \leq j \leq N$ and $i \neq j$,

(m) $J^4_{ij}(t) = k_r - \frac{\alpha}{\varepsilon}x_j(t)(1-x_j(t))$ when $N-m+1 \leq i \leq N$ and $N-m+1 \leq j \leq N$ and $i = j$.

Since we seek the asymptotic value J(A), we observe that the derivative (i.e., $x_i(t)(1-x_i(t))$) is always positive and attains the value zero only when $x(t) = 0$ or 1. Thus, the outputs of the neurons converge to the values zero or unity, and the term $x_i(t)(1-x_i(t))$ has an asymptotic

[8] Observe that $J^3_{ij}(t)$ has the value zero; this result is obtained as follows : $\frac{\partial \xi_i(t+1)}{\partial \eta_j(t)} = \frac{\partial(k_r\xi_i(t)-\alpha x_i(t)+a_i)}{\partial \eta_j(t)} = 0$.

value of *zero* for all $1 \leq i \leq N$. Thus, to obtain $J(A)$ we enforce the limiting argument to get the dynamical matrix[9]:

$$Y(A) = \begin{pmatrix}
0 & \dots & 0 & k_f & 0 & 0 & 0 & 0 & \dots & 0 & 0 & 0 & 0 & 0 \\
\vdots & \ddots & \vdots & \vdots & \vdots & \vdots & \vdots & \vdots & \ddots & \vdots & \vdots & \vdots & \vdots & \vdots \\
0 & \dots & 0 & k_f & 0 & 0 & 0 & 0 & \dots & 0 & 0 & 0 & 0 & 0 \\
0 & \dots & 0 & 0 & k_f^{(2)} & 0 & 0 & 0 & \dots & 0 & 0 & 0 & 0 & 0 \\
0 & \dots & 0 & 0 & 0 & \ddots & 0 & 0 & \dots & 0 & 0 & 0 & 0 & 0 \\
0 & \dots & 0 & 0 & 0 & 0 & k_f^{(m)} & 0 & \dots & 0 & 0 & 0 & 0 & 0 \\
0 & \dots & 0 & 0 & 0 & 0 & 0 & 0 & \dots & 0 & k_r & 0 & 0 & 0 \\
\vdots & \ddots & \vdots & \vdots & \vdots & \vdots & \vdots & \vdots & \ddots & \vdots & \vdots & \vdots & \vdots & \vdots \\
0 & \dots & 0 & 0 & 0 & 0 & 0 & 0 & \dots & 0 & k_r & 0 & 0 & 0 \\
0 & \dots & 0 & 0 & 0 & 0 & 0 & 0 & \dots & 0 & 0 & k_r^{(2)} & 0 & 0 \\
0 & \dots & 0 & 0 & 0 & 0 & 0 & 0 & \dots & 0 & 0 & 0 & \ddots & 0 \\
0 & \dots & 0 & 0 & 0 & 0 & 0 & 0 & \dots & 0 & 0 & 0 & 0 & k_r^{(m)}
\end{pmatrix}.$$

Since Λ_A=$[Y^*(A)^T Y^*(A)]^{1/2}$, a simple computation shows that:

[9]As seen from the dynamical equations, the elements denoted by $k_f^{(i)}$, for $1 < i < m$, represent the i^{th} occurrence of k_f along the diagonal. The other entries corresponding to k_f lie on the respective *column*, and do not lie on the diagonal. The same comment can be made about the elements denoted by $k_r^{(i)}$.

$$\Lambda_A = \begin{pmatrix}
0 & \dots & 0 & 0 & 0 & 0 & 0 & 0 & \dots & 0 & 0 & 0 & 0 & 0 \\
\vdots & \ddots & \vdots & \vdots & \vdots & \vdots & \vdots & \vdots & \ddots & \vdots & \vdots & \vdots & \vdots & \vdots \\
0 & \dots & 0 & 0 & 0 & 0 & 0 & 0 & \dots & 0 & 0 & 0 & 0 & 0 \\
0 & \dots & 0 & (N-m+1)^{1/2}k_f & 0 & 0 & 0 & 0 & \dots & 0 & 0 & 0 & 0 & 0 \\
0 & \dots & 0 & 0 & k_f^{(2)} & 0 & 0 & 0 & \dots & 0 & 0 & 0 & 0 & 0 \\
0 & \dots & 0 & 0 & 0 & \ddots & 0 & 0 & \dots & 0 & 0 & 0 & 0 & 0 \\
0 & \dots & 0 & 0 & 0 & 0 & k_f^{(m)} & 0 & \dots & 0 & 0 & 0 & 0 & 0 \\
0 & \dots & 0 & 0 & 0 & 0 & 0 & 0 & \dots & 0 & 0 & 0 & 0 & 0 \\
\vdots & \ddots & \vdots & \vdots & \vdots & \vdots & \vdots & \vdots & \ddots & \vdots & \vdots & \vdots & \vdots & \vdots \\
0 & \dots & 0 & 0 & 0 & 0 & 0 & 0 & \dots & 0 & 0 & 0 & 0 & 0 \\
0 & \dots & 0 & 0 & 0 & 0 & 0 & 0 & \dots & 0 & (N-m+1)^{1/2}k_r & 0 & 0 & 0 \\
0 & \dots & 0 & 0 & 0 & 0 & 0 & 0 & \dots & 0 & 0 & k_r^{(2)} & 0 & 0 \\
0 & \dots & 0 & 0 & 0 & 0 & 0 & 0 & \dots & 0 & 0 & 0 & \ddots & 0 \\
0 & \dots & 0 & 0 & 0 & 0 & 0 & 0 & \dots & 0 & 0 & 0 & 0 & k_r^{(m)}
\end{pmatrix}.$$

From the above, it is easy to see that the system has $2m$ eigenvalues distinct than 0, and a single eigenvalue with multiplicity $2N-2m$ of magnitude 0. With regard to the non-zero eigenvalues, to be more specific, we see that we have one eigenvalue of magnitude k_f with multiplicity $m-1$, another eigenvalue of magnitude k_r with multiplicity $m-1$, and two eigenvalues of multiplicity unity which have the magnitudes $(N-m+1)^{1/2}k_f$ and $(N-m+1)^{1/2}k_r$. Thus,

$\mu_1 = \cdots = \mu_{2N-2m} = 0,$

$\mu_{2N-2m+1} = \mu_{2N-m} = k_f,$

$\mu_{2N-m+1} = \mu_{2N-2} = k_r,$

$\mu_{2N-1} = (N-m+1)^{1/2}k_f,$

$\mu_{2N} = (N-m+1)^{1/2}k_r.$

The Lyapunov exponents are thus obtained by computing the logarithms of the eigenvalues as :

$\lambda_1 = \cdots = \lambda_{2N-2m} = -\infty,$

$\lambda_{2N-2m+1} = \lambda_{2N-m} = ln(k_f)$,

$\lambda_{2N-m+1} = \lambda_{2N-2} = ln(k_r)$,

$\lambda_{2N-1} = 1/2ln(N-m+1) + ln(k_f)$,

$\lambda_{2N} = 1/2ln(N-m+1) + ln(k_r)$.

For any fixed value of N, we can choose an appropriate m so as to yield positive Lyapunov exponents values for λ_{2N-1} and λ_{2N}. Hence the theorem. □

4.3.1.1 Remark: The reader should observe that there is a value of m for which the maximum between $1/2ln(N-m+1) + ln(k_f)$ and $1/2ln(N-m+1) + ln(k_f)$ is smaller than 0. For this value of m, the system will lean more towards behaving like the AdNN, i.e., possessing no chaos, because of the absence of positive Lyapunov exponents. For values of m smaller than this critical value, the system is will lean towards behaving like the M-AdNN, because it will exhibit chaos by virtue of the corresponding positive Lyapunov exponents. How m relates to the desynchronization issue is yet unsolved.

4.3.2 Discussion About the Stability Analysis Using the Routh-Hurwitz Criterion for Continuous System

The theoretical concepts regarding the R-H analysis were presented earlier in Section 3.4.2. In the interest of continuity, a few aspects of this technique are briefly repeated here.

Consider a continuous nonlinear system described by the equation $\frac{d\vec{X}}{dt} = \vec{F}(\vec{X})$ having an equilibrium point $\vec{X_{eq}}$ as a solution to $\vec{F}(\vec{X_{eq}}) = \vec{0}$. We can calculate the Jacobian of the system to produce an associated linear equation: $\frac{d\vec{x}}{dt} = A\vec{x}$.

Using the A matrix, we can compute the characteristic equation $|A - \lambda I| = 0$, where I is the identity matrix. Given the coefficients c_k of the characteristic equation, we get the following series of determinants:

$$\Delta_1 = det(c_1),\ \Delta_2 = det\begin{pmatrix} c_1 & c_0 \\ c_3 & c_2 \end{pmatrix}, \cdots, \Delta_r = det\begin{pmatrix} c_1 & c_0 & 0 & 0 & \dots & \dots \\ c_3 & c_2 & c_1 & c_0 & \dots & \dots \\ c_5 & c_4 & c_3 & c_2 & \dots & \dots \\ \dots & \dots & \dots & \dots & \dots & \dots \\ 0 & 0 & 0 & 0 & \dots & c_r \end{pmatrix}.$$

It is well known that the equilibrium state is stable if and only if $\Delta_k > 0$ for $1 \leq k \leq r$.

As mentioned in Section 3.4.2, the RH criterion states that the real part of the roots $\{\lambda\}$ are negative provided that all the coefficients $\{c_0, c_1, \dots c_r\}$ and all the determinants $\{\Delta_1, \Delta_2, \dots \Delta_r\}$ are positive. Since the bottom row of the determinant Δ_r is composed entirely of zeros, except for the last element c_r, it follows that $\Delta_r = c_r\Delta_{r-1}$. Thus, for stability, it is required that both $c_r > 0$ and $\Delta_{r-1} > 0$, implying that Δ_r doesn't need to be evaluated.

Consider now the Mb-AdNN in which the size of the discrete time step, Δt, is made arbitrarily small. This would lead us to a continuous version of the Mb-AdNN. The latter has the following stability property when analyzed by the R-H criterion.

Theorem 4.2.

Consider the continuous-time Mb-AdNN, described by the set of Equations (4.1) obtained when Δt is made arbitrarily small. Under a Routh-Hurwitz analysis, the set of constraints $k_r > 0$ and $k_f > 0$ is a necessary *condition for the continuous-time Mb-AdNN to be locally unstable.*

Proof: For the general case of the system possessing $2m$ eigenvalues different than 0, it can be seen (in the interest of brevity, we omit the straightforward algebraic steps) that the characteristic equation for this system is

$\lambda^{2N} - (k_f + k_r)((N-(m-1))^{1/2} + (m-1))\lambda^{2N-1} + \dots = 0$, with

$\Delta_1 = det(c_1) = -(k_f + k_r)((N-(m-1))^{1/2} + (m-1))$.

Clearly, the sign of the Δ_1 depends on the magnitude of the coefficients k_f and k_r, because $((N-(m-1))^{1/2} + (m-1))$ is larger than zero, for all $m \leq N$. Thus, the system is unstable according to R-H criterion, since $k_f > 0$ and $k_r > 0$. □

4.3.2.1 Conjecture: the Discrete Case

We presented above the analysis for the Mb-AdNN using a continuous-space Routh-Hurwitz analysis. Although the analysis should be done for the discrete-time case, we believe, as in Section 3.4.2.1, that the continuous-space approximates the discrete-time case, if Δt is made correspondingly small. The corresponding result for the discrete time Mb-AdNN is conjectured below.

Conjecture 4.1.

Consider the discrete-time Mb-AdNN, described by the set of Equations (4.1) in which Δt can be made arbitrarily small although it does not tend to zero. Under a Routh-Hurwitz analysis, the set of constraints $k_r > 0$ and $k_f > 0$ is a necessary *condition for the discrete-time Mb-AdNN to be locally unstable.*

4.3.2.1.1 Remark: The Remark 3.4.2.1.1 is also valid here. We admit again that there is a certain level of imprecision in our formalism. Just saying that for "any Δt" the continuous-time system appropriately approximates the corresponding discrete-time system is not really accurate. Indeed, the size of the step Δt, should be so small to satisfy the validation of the first order Taylor approximation. However, as in Section 3.4.2.1, we believe our conjecture based on our experimental evidence.

4.4 Modelling Inaccurate Perception in Mb-AdNN

As we have seen, the AdNN and the M-AdNN lie on the two extremes of the neural spectrum. The AdNN is "quite simply" not chaotic. As opposed to this, the M-AdNN can be driven into chaos by forcing the minimum number of the eigenvalues to lie on the diagonal. As we move along the spectrum, we forfeit some of the chaos and consequently some of the chaotic PR capabilities. It is also clear from the Lyapunov analysis that chaos can exist for many values of m which are astonishingly, quite large (i.e., for $1 < m < max\{N+1-\frac{1}{k_f}, N+1-\frac{1}{k_r}\}$). However,

it turns out, for reasons which are yet unexplained, that the PR capabilities do not extend for such large values of m.

When $m = 1$, the Mb-AdNN degenerates to the M-AdNN, leading to a system that exhibits PR, as shown in Section 3.7. Thereafter, as m increases, this PR capabilities decrease in a "smooth" or "gradual" manner when it concerns the number of patterns recognized. But, for the other patterns, it turns out that the degeneration of the PR capabilities is *abrupt* - the system "suddenly" changes from being able to recognize it to not recognize it.

For $m = 2$ (with four eigenvalues different from zero) the Mb-AdNN continues to demonstrate PR capabilities. As soon as m is increased to 3 (with six eigenvalues different from zero) the system has and continues to have chaos, whether the input samples are the trained samples or not. The categoric periodic behavior, however, abruptly disappears for the input patterns as m is increased from 3 - even though the system still continues to be "partially periodic". By the latter expression we mean that the number of patterns for which such a periodic behavior is displayed, systematically decreases as m is increased, indicating the phenomenon of increased inaccurate perception or "blurring", even though the input is exact (i.e., non-noisy). There is *no* observed periodicity for all values of $m > 8$. The theoretical reasoning for this phenomenon is still unavailable, but we shall demonstrate it experimentally in the next section.

4.5 Experimental Results

In a simulation setting, we are not dealing with a real-life chaotic system (as the brain). Indeed, in this case, the output of the CNN is continuously monitored, and a periodic behavior can be observed by studying the frequency spectrum, or by processing, in the time domain, the outputs as they came. Notice that the latter is an infeasible task, as the number of distinct outputs could be countably infinite. This is a task which the brain (in general, a chaotic system) seems to be able to do, quite easily, and in multiple ways. However, since we have to work with serial machines, to demonstrate the periodicity we have opted to compare the output patterns with the various trained patterns. Whenever the distance between the output pattern and *any* trained pattern is less than a threshold, we mark that time instant with a distinct marker characterized by the class of that particular pattern. The question of determining the periodicity of a pattern

is now merely one of determining the periodicity of *these markers*.

To present our results in the right perspective, we have tested the schemes for a set of data which involves the recognition of numerals.

4.5.1 PR with a Numeral Data Set

We conducted numerous experiments on the Adachi dataset [2] and other datasets. Any data set that can be vectorially treated as the input to the NN is adequate. The only available benchmark in this context is the Adachi's and, to be consistent with his results, we initially used it. We found that our theory works well on that data set. However, to render the testing more completely, we opted to work with hundred-bit vectors which were the 10 X 10 pixels representing the numerals[10]. We report in this Chapter the results of training/testing on a numeral dataset described below. The training set had 10 patterns, given in Figure 3.1, and consisted of 10×10 bit-maps of the numerals $0 \cdots 9$. The parameters used for Equations (4.1) were $N = 100$ neurons, $k_f = 0.2$ and $k_r = 0.9$.

Periodicity-based Accuracy for the Non-noisy Numeral Dataset

The trained Mb-AdNN with $m = 1$ demonstrated a periodic response when the non-noisy external stimuli were applied, after an initial non-periodic transient phase. The transient phase was *very* short - its mean length was 23.1 time units, and most of the transitory phases were of length 24 units. The actual length of the transient phase in each case is given in Table 4.1. The system resonated sympathetically with the input pattern, with a fairly small periodicity. The periodicity of the response is also tabulated in Table 4.1, where the initial starting input pattern was randomly chosen. Note that the periodicity was fairly "small" (26 in most cases - the first pattern has a limit cycle with double periods[11], the first with 7 and the second with

[10] A more interesting avenue involves the investigation of whether such chaotic models can be applied to "non-visual" data - which is what we are currently researching. Our intention is to see if sound/speech data can be vectorized and recognized using a Chaotic PR system, and if this recognition fails under conditions analogous to those presented here.

[11] The periodicity (7,15) means that we encounter a "double cycle". Thus after the transient phase, the training pattern occurs at times 7, 22, 29, 44 etc. This is actually because we have a 8-shaped limit cycle with the smaller loop of the '8' having a periodicity of 7, and the larger loop having a periodicity of '15'.

Pattern		m=1	m=2	m=3	m=4	m=5	m=6	m=7	m=8
0	Transient	24	24	24	11	∞	∞	∞	∞
	Periodicity	26	26	26	12	∞	∞	∞	∞
1	Transient	15	15	∞	∞	∞	∞	∞	∞
	Periodicity	7,15	7,15	∞	∞	∞	∞	∞	∞
2	Transient	24	24	24	11	∞	∞	∞	∞
	Periodicity	26	26	25	12	∞	∞	∞	∞
3	Transient	24	24	24	29	16	∞	∞	∞
	Periodicity	26	26	25	25	12	∞	∞	∞
4	Transient	24	24	24	11	∞	∞	∞	∞
	Periodicity	26	26	25	12	∞	∞	∞	∞
5	Transient	24	24	15	107	∞	∞	∞	∞
	Periodicity	26	26	7,15	120	∞	∞	∞	∞
6	Transient	24	24	24	11	∞	∞	∞	∞
	Periodicity	27	27	25	12	∞	∞	∞	∞
7	Transient	24	24	24	29	31	31	31	42
	Periodicity	26	26	25	25	32	32	32	7,15
8	Transient	24	24	24	29	16	16	16	∞
	Periodicity	26	26	25	25	12	12	12	∞
9	Transient	24	24	24	11	∞	∞	∞	∞
	Periodicity	26	26	26	12	∞	∞	∞	∞

Table 4.1: The transitory phase (named "Transient") and the periodicity for Mb-AdNN as the value of m is increased from 1. The testing samples were the *exact* non-noisy versions of the original "numerals" training set. The first pattern has a limit cycle with double periods, the first with 7 and the second with 15. Notice that the chaotic PR phenomenon decreases as m increases. After $m = 8$, the system fails to recognize any pattern even if it is an exact version of a trained pattern.

15). The accuracy[12] of recognition was 100%.

We now examine the "blurring" phenomenon demonstrated by the Mb-AdNN. When $m = 1$ the Mb-AdNN degenerates to the M-AdNN. Clearly, as shown in Section 3.7, the system exhibits PR. Thereafter, as m increases, this PR capabilities decreases in a "smooth" or "gradual" manner when it concerns the number of patterns recognized. But, for the other patterns, it turns out

[12]It would have been good if the periodicity was uniquely linked the pattern classes, but, unfortunately, this is not the case. Rather, the system possesses the characteristic that it switches from being chaotic to periodic whenever a noisy version of one of the trained patterns is received. So, it would be more appropriate to say that this switching phenomenon occurs with 100% accuracy. We have taken the liberty to refer to this as "100% PR" accuracy.

that the degeneration of the PR capabilities is *abrupt* - the system "suddenly" changes from being able to recognize it to not recognize it.

For $m = 2$ (with four eigenvalues different from zero), the Mb-AdNN continues to demonstrate PR capabilities for all the ten patterns. The mean length of the transient phase is 24 time units, and the average periodicity is 23.1 time units. As soon as m is increased to 3 (with six eigenvalues different from zero), the system displays chaos, but fails to be periodic when the numeral '1' is presented. The number of classes for which the periodic behavior is demonstrated decreases to 3, for $m = 5$, and keeps falling to unity, when $m = 8$. For example, when $m = 5$, the system recognized only the patterns corresponding to the numerals '3', '7' and '8', and then, when $m = 7$, the system recognized only the patterns corresponding to the numerals '7' and '8'. We also emphasize that this periodicity for the same pattern class sometimes changed as the value of m changed. Thus, the periodicity (for $m = 7$) for the numeral '7' was 32 time units, and for the numeral '8' was 12 time units. On the other hand, the periodicity (for $m = 8$) for '7' was a double cycle of periodicities 7 and 15. Observe that the number of patterns for which such a periodic behavior is displayed, systematically decreases as m is increased, indicating the phenomenon of increased inaccurate perception or "blurring", even though the input is exact (i.e., non-noisy). A graph displaying the number of patterns recognized as m increases is given in Figure 4.1. There is *no* observed periodicity for all values of $m > 8$. This confirms our hypothesis.

4.6 Conclusion

In this Chapter, we have studied the problem which is the "inverse" problem of Pattern Recognition (PR), namely that of modelling how even a *clear* image can be perceived to be blurred in certain contexts. To our knowledge, there is no solution to this in the literature, other than for the oversimplified model in which the true image is garbled with *noise* by the perceiver himself. In this Chapter, we have proposed a chaotic model of PR for the theory of "blurring" and we have shown how we can model blurring from the view point of a chaotic PR system. Unlike the Chapter 3, in which the chaotic PR system extracted the pattern from the input, in this case we showed that *even without the inclusion of additional noise* the perception can be "blurred" if the dynamics of the chaotic system are modified. We thus proposed a formal model for chaotic

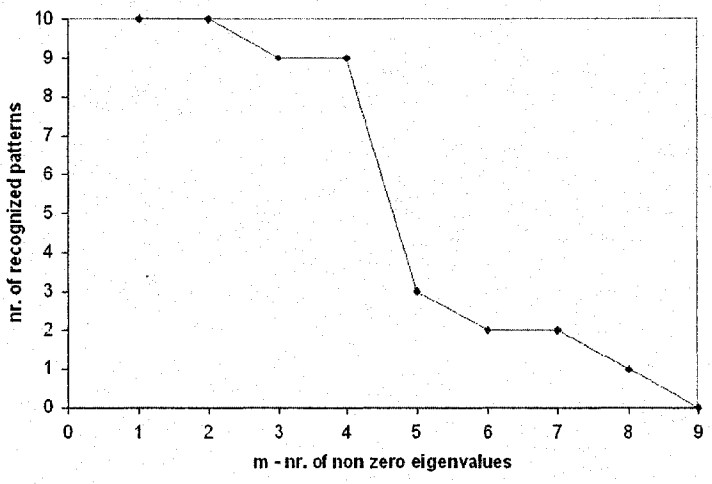

Figure 4.1: The number of patterns recognized as m increases.

"blurring", and presented a rigorous analysis using the Routh-Hurwitz criterion and Lyapunov exponents. We also experimentally demonstrated the validity of our model by using a numeral dataset. We believe that a potential byproduct of this model is the theoretical possibility of desynchronization of the periodic behavior of the brain (as a chaotic system), rendering us the potential of predicting, controlling, and annulling epileptic behavior.

Chapter 5

Controlling Chaotic Behavior Using Large Scale Models

5.1 Introduction

Neuromodelling is usually motivated by a desire to better understand specific neural circuits, particularly those whose failure triggers human illnesses. Depression, anxiety, schizophrenia, Alzheimer's disease, memory impairment, paralysis, epilepsy, multiple sclerosis, Parkinson's disease, etc. are areas in which intense research efforts are being made so as to better understand and treat these conditions. In this respect, from a modelling perspective, one hypothesis is that the analysis of the *connections* between the neurons is fundamental. Apart from providing a better understanding of the conditions and symptoms of a disease, such an analysis also leads to a better understanding of the development and function of the normal brain.

The brain is virtually unique in its exquisitely complex three dimensional structure[1]. Although the structure and the functionality of other types of tissues can be explained without a precise knowledge of their shape and the specific connections of each cell, this is not easily

[1]Each of the 100 billions neurons in the brain may have anywhere from a few 1,000s up to 100,000 synapses impinging on it, and through these synapses they can receive information from hundreds or thousands of other neurons. This means that the brain contains as many as 100 trillion synapses, rendering the entire "neural network" vast and hugely complex [139].

achieved for the brain. The tools used today to analyze the shape and structure at the brain's cellular level are scarcely capable of describing the precise performance of systems consisting of more than a handful of neurons. One must analyze the shape and connections of probably millions and perhaps billions of nerve cells before claiming to *fully* understand the structures that determine the behavior of flies, worms, mice, and humans. To the best of our knowledge, the problem of defining the minimum scale for modelling the brain (or large sections of the brain) remain unsolved.

In this context, research involving brain modelling has followed two distinct approaches, namely (a) those which involve a large scale network of neurons, and (b) those which incorporate a small scale network of neurons. Each of these models has advantages and disadvantages briefly listed below.

1. Large scale models may generate functions that can be observed only when a minimum of thousands of neurons are connected into topographic maps containing millions of connections. Many important phenomena cannot be studied without such large networks, including the two-dimensional organization of visual orientation, motion direction maps, and those involving the processes of object segmentation and grouping. When such a model is utilized, the objective must not merely be to determine the structure of the network, but also to correlate the *modifications* in the structure with the detailed (electrical) behavior of the neurons. In general, large scale models are avoided because they are difficult to build, which is augmented by the fact that it is hard to assign "realistic" parameters for their implementations. Finally, the corresponding computations are also very time consuming.

2. In many examples, small scale networks are preferred because they provide easy access to the parameters of the network. These are later replicated in order to approximate the behavior of large portions of the brain. The disadvantage of using such small scale networks is that in the final analysis, it appears as if we are dealing with "toy" problems.

In our research, we consider both levels of modelling. The large scale models are presented in this Chapter, and the small scale models are examined in Chapters 6 and 7.

5.1.1 Large Scale NNs problems

In this Chapter, we consider the problem of controlling the level of chaos in large scale NNs. This research is inspired by the biological problem of modifying the levels of chaos in the brain. For example, during an epileptic seizure, the phenomenon of chaos disappears and the neural network becomes synchronized, generating a periodic behavior with the frequency between 3-5 Hz. Any method to re-enforce the state of chaos would thus be useful for the health of the brain. Thus, in this setting, it would be beneficial if we could drive the system from periodicity to chaos. This goal, at present, is a little overambitious, and so, to initiate research in this field, we consider how we can manipulate the system from one *level* of chaos to another. In other words, the periodic behavior of the model is an *extreme* scenario, and it seems to be a very difficult task to return the system to chaos if we start from a periodic behavior. Thus, our initial research investigates only the scenario when we have chaotic behavior and we intend to modify the level of chaos. Furthermore, we propose to model only the piriform cortex, which is well known for its chaotic behavior.

Our aim is to discover methods by which we can increase the level of chaos in *almost* synchronized networks, as in the epileptic brain. We intend to investigate the dependence of the level of chaos as a function of a few variables (or parameters). The level of chaos can be quantified by two components: a global measure expressed by the Largest Lyapunov Exponent (LLE) (see Section 2.6) and a geometrical measure expressed by the Correlation Dimension (CD) (see Section 2.5). Both of these will be used in our evaluations.

The experiments were done using GENESIS (GEneral NEural SImulation System)[2] proposed by Bower *et al.*. This simulation software was initially developed in CALTECH (California Institute of Technology) laboratory by Matthew Wilson as an extension of efforts to model the olfactory cortex. It was designed to allow the multi-scale modelling within a single simulation system and, until now, it is the only simulator with this capacity. GENESIS was developed for constructing biologically realistic neuronal simulations with three basic objectives [24]:

(i) The simulator is capable of addressing problem with many levels of detail, namely from parts of neurons to large neural systems,

[2]The GENESIS simulation software is free and can be downloaded from http://www.genesis-sim.org/GENESIS/.

(ii) The system is open-ended, placing few limits on the kinds of problems that can be addressed, and

(iii) The system is user-extensible to allow the incorporation of new modelling efforts.

When one chose a neural simulator, its reliability, accuracy and speed are important characteristics. In order to quantify the speed and the accuracy of both GENESIS and other simulators, Bower *et al.* [24] developed a set of benchmarks containing:

1. A linear passive cable with many compartments,
2. A highly branched cable, and
3. A linear axon containing Hodgkin-Huxley channels.

Bower mentioned that in the first two cases, the results from GENESIS can be compared to exact analytic solutions. In the third case, which is an example in which the complexity of the problems cannot generate analytic solutions, the results compared with those obtained from other simulators demonstrated that GENESIS is as fast and accurate as any other existing simulation system. From our point of view, in addition to GENESIS, the research community uses also NEURON. However, the latter can be applied only to investigate the behavior of a single neuron, without the inclusion of tools to explore networks of neurons.

Using this simulation software, we examine in this Chapter the following problems:

- **Problem of Density and Strength**: We propose to investigate the dependence of the level of chaos as a function of the density of the neurons in the network, and the strength of the connections between then. In this regard, there are two types of connections, namely the inhibitory and the excitatory ones. We know, from the biological experiments, that the inhibitory connections have a more significant effect than the excitatory one. Thus, we propose to analyze the influence of the modification of the strength of the inhibitory connections on the level of chaos. This will be discussed in greater detail in Section 5.3.

- **Problem of Connectivity**[3]: In this case we propose to analyze the dependence of the level of chaos as a function of the density of connectivity of the synapses (i.e, the number of synapses generated between the neurons). In addition, we propose to investigate the variation of the maximum nonlinear interdependence (see Section 2.8) of two subsystems embedded in a larger system. Thus, we plan to consider how the coupling of two interconnected subsystems of the same underlying system would change as a function of the connectivity of the synapses. We believe that the levels of local connections between the neurons can be used as a hypothesis to explain the mechanism underlying illnesses such as schizophrenia.

- **Problem of Stimulus Frequency**: In this case we propose to study the dependence of the level of chaos as a function of the frequency of a stimulus that is globally applied within the network. In addition, we plan to study the maximum nonlinear interdependence of two subsystems which are embedded in a larger system as a function of the frequency of the stimulus globally applied in the network.

5.1.2 Organization of this Chapter

After the presentation of the problems which we intend to investigate, Section 5.2 contains a brief description of the biological model of the the piriform cortex. In the same Section we also describe the importance of a nonlinear parametrization of the artificial EEGs generated with the model. We conclude this Section with a detailed description of the computation model. In Section 5.3 we present the details of the problems explored. Section 5.4 concludes the Chapter.

[3]Some preliminary results from this Problem were published in the *Proceedings of CCECE05, The 18th Annual Canadian Conference on Electrical and Computer Engineering*, May 1-4, 2005, Saskatoon, Canada, pp. 1652-1656.

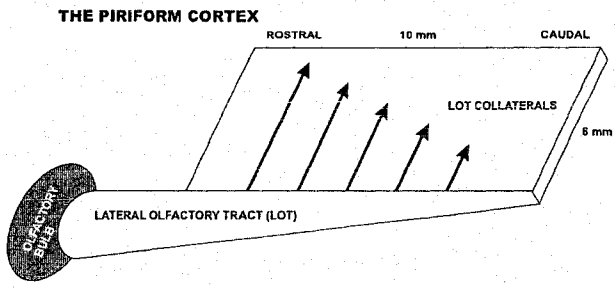

Figure 5.1: The Model of the Piriform Cortex (Adapted from [24]).

5.2 The Biological Model: the Piriform Cortex

The investigations presented in this Chapter use a *computational* model[4] based, in turn, on a *biological* model. The chosen biological model for the "large scale" brain, concerns the piriform cortex (also known as the primary olfactory cortex), well known for its chaotic behavior. Although interest in olfactory neuroscience has seen a great increase in the past decade, the nature of the computations performed by the olfactory regions of the brain remain obscure. We believe that the combination of electro-physiological experimental techniques and computer modelling would help to elucidate the function of the olfactory system [9, 17, 18].

The evidence that indicates the possible relevance of chaos to brain functions was obtained first by Freeman [56] through his clinical work on the large-scale collective behavior of neurons, in the perception of olfactory stimuli. Freeman developed a model for an olfactory system having cells in a network connected by both excitatory and inhibitory synapses. He described how a chaotic system state in the neighborhood of a desired attractor, can fall on a stable direction when a perturbation is applied to a system parameter.

The piriform cortex is a three layered cortical area which receives its input from the olfactory bulb via a lateral olfactory tract (see Figure 5.1). Neurons in the olfactory bulb receive inputs from receptors in the nasal epithelium. The principal neuron of the piriform cortex is the pyramidal[5] cell which receives afferent input from the bulb. There are also inhibitory interneurons

[4]The field of computational neuroscience focusses on how the nervous system *computes*. Instead of obtaining experimental information about the structure of the neural system, a computational approach involves collecting and processing information that is most relevant for its functional understanding.

[5]The pyramidal neuron consists of a cell body or soma, a long apical dendrite or dendrites extending to the surface of the cortex, and a number of basal dendrites that receive local excitatory inputs. Each neuron makes

which mediate feedforward and feedback inhibition.

In addition to the excitatory input from the lateral part of the olfactory tract, pyramidal cells make local excitatory connections on basal dendrites, and distant connections on apical dendrites of other pyramidal cells. Intrinsic excitatory connections attenuate exponentially as the distance from the originating cell increases.

5.2.1 Chaos Analysis in a Computer Simulation of the Piriform Cortex

The electrical activity of the brain measured by EEGs exhibits a complex behavior with nonlinear dynamic properties. This behavior assumes the form of various EEG patterns with different complexities. Considering this, we believe that the theory of nonlinear dynamics may be a superior approach (than the traditional linear methods) for characterizing the intrinsic nature of EEGs. The literature shows that efforts have been made to determine nonlinear parameters for pathological signals, and it has been demonstrated that they are useful indicators of pathologies [118]. Many investigators, for example, Duke *et al.* [47], have proved that complex dynamical evolutions lead to chaotic regimes.

In the theoretical modelling of neural systems, extensive work (involving multiple perspective of mathematics, physics, engineering, chemistry, and physiology, [8, 15]) has been done to lead to an understanding of complexities associated with the brain. Indeed, there has been a sustained interest to describe neural processes and brain signals, especially those represented by the EEG, within the context of nonlinear dynamics and the theory of deterministic chaos [132, 133]. The former theory opens a new perspective for the understanding of the EEG (see the models proposed by Freeman *et al.* [56] for neocortical dynamics, and by Wright *et al.* [178] for chaotic dynamics in neurobiology). Also, in the analysis of real or "synthetic" EEG data, different chaotic measures such as the correlation dimension, the Lyapunov exponent, and entropy have been used in recent literature [25, 96, 164].

As mentioned earlier, in our research, we analyze the systems under consideration using two measures, namely the LLE and CD described earlier. The signals analyzed are the artificial EEGs obtained from a *model* of the piriform cortex. In the specialized literature, these two

connections with other pyramidal cells within the piriform cortex, both locally and globally.

measures are presented together only in the cases obtained from two categories of sources:

1. The first consists of very simple mathematical models, which do not possess any clear biological applicability.

2. The second consists of signals obtained from the brain, such as the EEG, that do not require a knowledge of any equations that describe the system producing them. In this case, the system is treated as a black box, where the coupling between the elements of the system, namely the neurons, is only assumed. It is not possible to modify the value of the coupling due to the fact that its quantitative description is not available.

Before we proceed, we present a *computational* model which is distinct from the above-mentioned categories, namely one which is a "realistic" simulation of the piriform cortex. This model exceeds in complexity a mathematical model (for example, the Bondarenko model [21]), but it is simpler than the structure of the brain.

5.2.2 The Computational Model

The computational model which we present can be viewed as a nonlinear system. Simulation of the piriform cortex requires the numerical solution of systems of differential equations that describe the state of neurons as a function of time and space. These numerical techniques describe how the system advances the state variables of the simulation (e.g., the potential of the membrane) from time i to time $i+1$, through numerical integration of the differential equations that describe the system.

The computational model of the piriform cortex is treated as a loosely-coupled system of ordinary differential equations. The evaluation of a state of any neuron in the system requires only the past state information from other neurons, and it can be solved (hopefully independently) for each neuron at every time step. These types of equations can typically be solved using numerical integration techniques.

The GEneral NEural SImulation System [24] provides an excellent model for the piriform cortex. The model used in this Ph.D. Thesis was created by Wilson [172], and it served as the

initial basis for the construction of GENESIS itself. The goal of the model was to generate patterns that are similar to EEGs, and to explore their possible physiological basis. The EEG has a long history in neurophysiology, the origins of which are still debated.

Numerous models of brain circuitry have focused on simulating the macroscopic functionality of systems containing simplified neuronal units. The increase in computational power in the last decade allowed simulations to include models with considerable complexity, namely *realistic* large scale neural networks. In this context, the Wilson model of the piriform cortex is generally accepted as a realistic model since it is based on the anatomical structure, and it contains physiological characteristics of actual biological networks.

One of the ultimate objectives of the Wilson's model was to understand the role of the piriform cortex in olfactory object recognition [23, 72]. One motivation of Wilson's and Bower's research was the assumption that this cortex computationally represents a kind of associative memory [69, 70]. The model has been used to explore a wide range of cortical behavior [172, 174], including associative memory functions [173]. It has been cited in more that 100 refereed papers.

The initial architecture consists of three 15 $\times$ 9 arrays of 135 nodes. Each array has only one type of neurons, being either of the pyramidal cells, the feedforward inhibitory cells (K^+ mediated inhibition), or the feedback inhibitory cells (Cl^- mediated inhibition). The array is proposed to represent the whole piriform cortex, which falls within an area of approximately 10 mm $\times$ 6 mm.

The pyramidal cells consist of five compartments, each compartment receiving a distinct kind of synaptic input. The inhibitory cells are modelled using the differences between the exponential functions. The interactions between the excitatory and inhibitory neurons are as depicted in Figure 5.2. The model also contains 10 cells representing the excitatory input to the cortex from the olfactory bulb.

5.2.2.2 The Cell-based Equations

In order to model individual cells, the analyst has to consider several structural details, adapted from [172], listed below:

1. The spatial/cellular structure, including the characteristics of the cell such as its dimension,

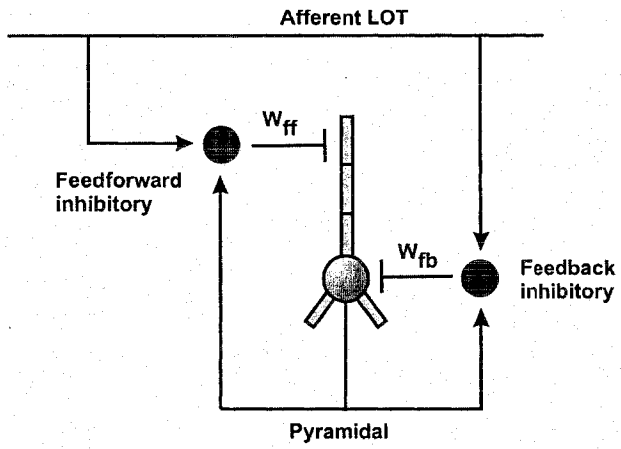

Figure 5.2: The Interactions Between the Excitatory and Inhibitory Neurons (Adapted form [24]).

location of cell bodies, dendrites, and axons must be taken into consideration.

2. The biophysical/subcellular structure with membranes, channels, receptors, and their voltage- and time-dependent characteristics (including the channel conductances, membrane resistance and capacitance, the nature of receptor binding, and the ionic diffusion) must be accounted for.

3. The network modeler must determine the relative benefit of including as much detail as is necessary given the computational overhead incurred.

In the multi-compartment implementation of pyramidal cells, (adapted form [24]), each compartment consists of one or more synaptic input channels, a membrane resistance r_m, and a membrane capacitance c_m obeying:

$$r_m = \frac{R_m}{\pi l d}, \tag{5.1}$$

$$c_m = C_m \pi l d, \tag{5.2}$$

where l is the length of the dendritic segment, d is its diameter, R_m is the membrane resistivity and C_m is the capacitance per unit area.

Each compartment is coupled to its adjacent compartment(s) with an axial resistance r_a as:

$$r_a = \frac{1}{2}\frac{4R_a L}{\pi d^2}, \tag{5.3}$$

where R_a is the axial resistivity.

If we select a compartment and designate its two axial ends with + and -, then the total axial current into the compartment is given by:

$$I_a = I_a^- + I_a^+, \tag{5.4}$$

where the individual axis components from the two adjoining compartments are calculated by:

$$I_a^- = \frac{V^- - V}{r_a^- + r_a}, I_a^+ = \frac{V^+ - V}{r_a^+ + r_a}. \tag{5.5}$$

In Equation (5.5), V is the membrane potential of the compartment, $V^{+/-}$ is the membrane potential of the compartment on the + and - sides of the compartment respectively, and $r_a^{+/-}$ is the axial resistance of that compartment. $I_a^{+/-}$ is the current entering the compartment from the +/- sides, respectively. To simplify notation the time-dependent variables $V(t)$ and $I(t)$ are written as V and I, respectively.

The boundary conditions assume sealed ends with $I_a^{+/-} = 0$. This can be extended to a branching structure using

$$I_a^{+/-} = \sum_{j=1}^{N^{+/-}} \frac{V^{j+/-} - V}{r_a^{j+/-}} \left(1 + r_a \sum_{j=1}^{N^{+/-}} \frac{1}{r_a^{j+/-}}\right)^{-1}, \tag{5.6}$$

where $N^{+/-}$ is the number of compartments adjoining the + and - sides of the present compartment under consideration.

The ohmic portion of the transmembrane current is given by :

$$I_m = \frac{E_{rest} - V}{r_m} + \sum_{k=0}^{n_{channels}} (E_k - V) g_k(t), \tag{5.7}$$

where $g_k(t)$ is the time-varying conductance of the channel k.

The first term represents the passive leakage component with the resting potential E_{rest}, and leakage resistance, r_m. The summation terms give the input through synaptically activated conductances, $g_k(t)$. These conductances are activated by the arrival of presynaptic signals.

Finally, the membrane potential, V, of each compartment is calculated by integrating the current across the membrane capacitance. The differential change in the membrane potential

with time is given by:

$$\frac{dV}{dt} = \frac{1}{c_m}(I_a + I_m). \tag{5.8}$$

This quantity $V(t)$ is interpreted as the state variable $X(t)$ if the cell is considered as a dynamical system.

5.2.2.3 The Multi-Cellular Network Equations

In the previous subsection, we had explained the dynamics of a *single* cell. We now consider the properties of the network of interconnected cells. Since, in our research, we explore the properties of the large scale model, we are more concerned with the equations of the system at large. Because the control parameters are effective only at this level, the behavior at the individual cell level are not so crucial. Rather, the cell characteristics are considered as an individual variable in the picture.

The general dynamical equation for the state variable x^p of the p^{th} neuron, obtained from the dynamics of the entire system is

$$X^p(t+1) = \mathcal{Z}(Z_{1p}(t), Z_{2p}(t), Z_{3p}(t), Z_{4p}(t)), \tag{5.9}$$

with $Z_{1p}(\cdot)$, $Z_{2p}(\cdot)$, $Z_{3p}(\cdot)$, and $Z_{4p}(\cdot)$ being nonlinear functions relating the individual state variables, their feedback/feedforward coefficients, and the frequency of the signal inserted in the bulb. Thus,

$$\begin{aligned}
Z_{1p}(t) &= Z_{1p}(w_{p1}X^1(t), \cdots, w_{pN-1}X^{N-1}(t), w_{pN}X^N(t)),\\
Z_{2p}(t) &= Z_{2p}(w_{ff_p1}Y_{ff}^1(t), \cdots, w_{ff_pN_1-1}Y_{ff}^{N_1-1}(t), w_{ff_pN_1}Y_{ff}^{N_1}(t)),\\
Z_{3p}(t) &= Z_{3p}(w_{fb_p1}Y_{fb}^1(t), \cdots, w_{fb_pN_2-1}Y_{fb}^{N_2-1}(t), w_{fb_pN_2}Y_{fb}^{N_2}(t)),\\
Z_{4p}(t) &= Z_{4p}(w_{bb_p3}F^1(\omega,t), \cdots, w_{bb_pN_3-1}F^{N_3-1}(\omega,t), w_{bb_pN_3}F^{N_3}(\omega,t)),
\end{aligned} \tag{5.10}$$

where:

1. $X^p(t)$ is the output of the p^{th} pyramidal neuron at time t.
2. $Y_{fb}^j(t)$ is the output from the j^{th} feedback inhibitory neuron at time t.

3. $Y_{ff}^{j}(t)$ is the output from the j^{th} feedforward inhibitory neuron at time t.
4. $F^{j}(\omega, t)$ is the input in the j^{th} neuron from the bulb with the frequency ω.
5. N is the total number of pyramidal neurons.
6. N_1 is the total number of feedback inhibitory neurons.
7. N_2 is the total number of feedforward inhibitory neurons.
8. N_3 is the total number of neuron in the bulb.
9. w_{pj} is the coupling between the j^{th} pyramidal neuron and the p^{th} pyramidal neuron.
10. w_{ff_pj} is the coupling between the j^{th} feedforward inhibitory neuron and the p^{th} pyramidal neuron.
11. w_{fb_pj} is the coupling between the j^{th} feedback inhibitory neuron and the p^{th} pyramidal neuron.
12. w_{bb_pj} is the coupling between the j^{th} neuron from the bulb and the p^{th} pyramidal neuron.
13. Finally, $\mathcal{Z}$ in Equation (5.9) represent a general nonlinear function whose *explicit* form is not directly used in this research.

The time series used for determining the chaos in the overall system will be the EEG. As is well known, EEGs are calculated using an array of evenly spaced electrodes on the surface of the simulated cortex. Recordings from the array are averaged to produce the EEGs as below:

$$EEG(t+1) = \frac{1}{m}\sum_{i=1}^{m}[\Phi_i(t)], \tag{5.11}$$

where m is the number of electrodes and $\Phi_i(t)$ is the field potential depending of the output of the pyramidal neurons, $X^p(t)$ for $p = 1 \cdots N$. We assume that the influence of the inhibitory neurons is marginal in the process of the EEG computation, and can thus be omitted.

The relation between the field potential $\Phi_i(t)$ recorded from the electrode i and the output of the pyramidal neurons $X^p(t)$ is:

$$\Phi_i(t) = \frac{1}{4\Pi} \sum_{p=1}^{N} \frac{X^p(t)}{d_{pi}}, \tag{5.12}$$

where N is number of pyramidal neurons, and d_{pi} is the distance of the p^{th} pyramidal neuron from the recording site (the electrodes i).

Having this description of the model at the cellular level and the network level, we conclude that in order to investigate the nonlinear properties of the overall system (namely the LLE or CD) it is enough to use the equations only at the network level. Using these equations, we can now start to solve the problems proposed in Subsection 5.1.1.

5.3 The Problems Investigated

The piriform cortex is a network with a large number of neurons which manifests, as explained earlier, chaotic behavior. One of our goals is to explore what is the cause of nonlinearity (and consequently, chaos) in the EEG computed from this part of the brain.

From the clinical point of view, the clinician can explore the "output" of the system, namely the EEG, by using three modifications, namely by treating with drugs (medication), adding electrical stimuli, and doing surgery.

The option of using medication is a global approach, and has an important limitation. Drugs affect the brain only at the *chemical* level, in synapses, and it is very difficult to correlate the quantitative analysis at this level with the *electrical* level of the EEGs.

Applying electrical stimuli is a local approach, but it also has an important limitation. The number of the neurons at which one can insert the electrical stimuli using electrodes is limited due to the size of the devices used, the size of the electrodes, and the the precision of the implantation.

Finally, the last approach, namely surgery, is very difficult as is to be considered as a "final solution". Indeed, no surgeon knows precisely how deep the invasion must be, and how many connections must be severed during an intervention [102].

The reader should observe that in these modifications, the clinician has no access to the control parameters. There is a possibility that the effectiveness of the controlling process can be enhanced by exploring only small local networks, used in *in vitro* experiments, but the relevance of the results to entire network is questionable.

From the mathematical point of view, a nonlinear analysis of the system is not feasible due to the large scale nature of the network. The computations of the steady state and the Jacobian matrix for a network with 500 (let alone 500 million) neurons is an unrealistic goal.

With this as a background, we believe that the only meaningful way to explore the piriform cortex (without dealing explicitly with a human brain) is by making simulations using realistic models. The output for the system will be the EEG computed with the simulated "electrodes", and the intention will be to analyze the correlation between the nonlinear properties of the EEGs and the control parameters of the system. From our point of view, as being an integral part of the modeller, the method of processing the artificially generated EEG consists of a sequence of computational steps which will be listed at the appropriate juncture.

The intention of this study is to see if we can generate certain desirable phenomena by modifying various control parameters. The question which contributes the uncertainty associated with this research is that of determining which control parameters can be modified, and what the consequent modifications are. Neither of these issues is intuitive. Indeed, as researchers who have to be content with working with simulation models, we will be pleased if we can obtain a marked resemblance between the results of the simulations and the phenomena observed by clinicians.

In this respect, the problems to be studied in this phase of the research (and described in this Section) are defined from clinical considerations as below:

1. The **Problem of Density and Strength**, which is motivated from:
   (a) The density of the neurons as observed in the slides of the human brain which have diseases related to network disorders.
   (b) The increase in inhibition level which can generate an epileptic behavior.
2. The **Problem of Connectivity**, which is motivated by two hypotheses related to the

schizophrenic brain.

3. The **Problem of Stimulus Frequency**, which is motivated by studies of the frequency of the olfactory stimuli as recognized by the piriform cortex via its bulb.

To our knowledge, such an analysis of the nonlinear chaotic exploration of these portions of the brain using only simulations has not been studied or reported in the literature.

With the computational model presented in Subsection 5.2.2, we consider the whole piriform cortex as a dynamical system. Thereafter, choosing a few accessible control parameters, we will attempt to modify their values so as to explore, by simulation, the level of chaos in the network.

5.3.1 Problem of Density and Strength

The problem of density and strength involves investigating the modification of structure and inhibition within the piriform cortex. More specifically, we propose to investigate the dependence of the level of chaos as a function of the density of the neurons in the network, namely, studying the number of neurons which can be included in the whole piriform cortex, and the strength of the connections between them. The latter involves the strength of the feedforward and the feedback connectivity coefficients between the inhibitory neurons and the pyramidal neurons.

The **Problem of Density and Strength** is motivated from two clinical considerations:

1. Consider the density of the neurons from slides of the human brain which have diseases related with network disorders. We intend to explore if the density of the neurons in the network is related to the capacity of leading to epileptic seizures. If the network has a level of chaos as described with an LLE, the problem we consider is that of determining how large this value is in comparison with its corresponding value for the epileptic scenario in which the brain is synchronized and the LLE is negative. We believe that the modification of the density of the pyramidal neurons, namely, N, will lead to different values for the LLE. Our initial results seen to demonstrate that if the LLE is greater, the system will be far from an epileptic crisis, because the initial state of the system is more chaotic. Consequently, a system with a lower LLE, will be closer to an epileptic crisis.

2. It seems to be an accepted "fact" that a decrease in the inhibition level can generate an epileptic behavior. We know from clinical experiments and also from small mathematical models, that if the inhibitory coupling between neurons is decreased, the neurons will lead to a more independent behavior. We believe that this neural "freedom" will be more conducive to a frequent spiking process which can be synchronized. With our simulations, we hope to explore the importance of the feedback and feedforward inhibitory synapses by modifying the values of w_{fb_pj} and w_{ff_pj}.

As mentioned before, these results are not intuitive and, to our knowledge, such simulations have not been studied or reported in the literature.

5.3.1.1 The Research Plan

1. First of all, we consider N, the number of the pyramidal neurons, as a control parameter and we explore the effect of modifying the initial value suggested by Wilson [174]. We investigated:
   (a) The computation[6] of the EEGs as a function of the number of electrodes.
   (b) The determination of the optimum value for the embedding dimension for the phase space reconstruction using the FNN method *for the number of neurons, N.*
   (c) The computation of the LLE and CD.
2. We also consider w_{ff_pj} and w_{fb_pj} , the feedforward/feedback coupling between the pyramidal neurons and feedforward/feedback inhibitory neurons, as control parameters and explore the effect of modifying the initial value of the Wilson model [174]. Again, this involves:
   (a) The computation of the EEGs as a function of the number of electrodes.
   (b) The determination of the optimum value for the embedding dimension for the phase space reconstruction using the FNN method *for the range of coupling coefficients.*
   (c) The computation of the relevant LLE and CD.

[6]The EEGs will be computed at 5000 samples/sec, for a duration of half a second.

5.3.1.2 Results

We show experimentally that by modifying the structure of the model, namely by increasing the density of the neurons, level of chaos decreases. We also present the evolution of the geometry of the attractor (the correlation dimension) as a function of the level of inhibition.

Using the model of piriform cortex, we analyze the behavior in time function of structural changes or synaptic changes. We present in detail these modifications. The aim of our research is to analyze LLE and CD, function of the changes which we make.

1. **Changing the structure:** The initial architecture created by Wilson and Bower [174] consisted of three 15 X 9 arrays of 135 nodes. We increased the density of the neurons in the same simulated area of approximately 10 mm X 6 mm. We then analyzed two other models:
   (a) Three 15 X 50 arrays of 750 nodes, where the network was covered by 50 electrodes. The details of the resulting EEG are given in the file ini_15_50 of Table 5.1.
   (b) Three 30 X 50 arrays of 1500 nodes, where the network is covered by 50 electrodes. The details of the resulting EEG are given in the file ini_30_50 of Table 5.1.
2. **Changing the inhibition**:
   (a) Only the feedforward inhibition w_{ff_pj} is decreased from 1 to 0.1. The details of the resulting EEG are given in the file ff_0 of Table 5.1.
   (b) Only the feedback inhibition w_{fb_pj} is decreased from 1 to 0.1. The details of the resulting EEG are given in the file fb_0 of Table 5.1 ;
   (c) Both the feedback w_{fb_pj} and feedforward w_{ff_pj} inhibition are decreased from 1 to 0.1. Here, the EEG is stored in the file syn[7].
   (d) The inhibition is increased. We modified the feedforward w_{ff_pj} and feedback w_{fb_pj} inhibition simultaneously from 1 to 1.5 and also from 1.5 to 2. The details of the EEGs for these cases are given in the files $inhib\_15\_15$ and $inhib\_20\_20$ of Table 5.1.

[7]We chose this name because with these settings, all the piriform cortex is now synchronized.

Table 5.1: The characteristics of each setting and the LLE computed for each of these settings.

Name	w_{ff}	w_{fb}	No.cells	No.electrodes	LLE
ini	1	1	9X15	40	1.734e-1
*ini*_15_50	1	1	15X50	50	1.833e-2
*ini*_30_50	1	1	30X50	50	1.325e-2
ff_0	0.1	1	9X15	40	1.716e-1
fb_0	1	0.1	9X15	40	1.241e-2
syn	0.1	0.1	9X15	40	-7.462e-2
*inhib*_15_15	1.5	1.5	9X15	40	1.92e-1
*inhib*_20_20	2	2	9X15	40	0.873e-1

Table 5.2: The correlation dimension function of embedding dimension (range from 2 to 15)

name of file	**2**	**3**	4	**5**	**6**	**7**	**8**
	9	**10**	**11**	**12**	**13**	**14**	**15**
ini	1.6	1.68	1.9	2.22	2.27	2.43	2.71
	2.71	2.83	3.3	3.35	3.43	3.59	3.57
ff_0	1.83	1.92	2.10	2.4	2.71	2.52	2.58
	1.95	2.66	2.74	2.77	2.8	2.85	1.87
fb_0	1.29	0.53	0.58	0.73	0.7	0.82	0.71
	0.78	1.05	1.07	1.17	1.22	1.31	1.37
syn	0.93	0.99	1.01	1.2	0.93	0	0
	0	0	0	0	0	0	0
*inhib*_15_15	1.91	2.52	2.03	3.39	2.83	2.89	2.99
	2.5	3.89	4.48	4.3	4.95	4.98	4.97
*inhib*_20_20	0.95	1.59	1.9	2.14	2.30	2.27	2.46
	2.45	2.49	2.53	2.68	2.64	2.82	2.93

The aim of our research was to analyze the level of chaos and the fractal dimension as a function of changes which we make. The first experimental step was to compute the optimum embedding dimension for each case, using statistics of the FNN. Next, we estimated the LLE. We did 20 experiments with the same model and the averages are shown in Table 5.1. To evaluate the D_2, we computed it for a range of embedding dimensions, starting from 2 to 15. We report, in the Table 5.2, the averages for 20 experiments made with the same model.

5.3.1.3 Conclusions for this problem

The following are the conclusions of the above study:

1. The architecture proposed by Wilson has the largest LLE. By increasing the density of the neurons, we indirectly increased the coupling between them. The neurons lose the independence because of the increase in this coupling, and the level of chaos decreases. This result is not intuitive.

2. We showed experimentally that modifying the structure of the model by increasing the density of the neurons, will lead to a decrease in the level of chaos. This can be interpreted as a *chaos-destroying synchronization* process in the entire piriform cortex model.

3. The feedforward inhibition has a small contribution to the level of chaos and also to the correlation dimension. In the initial case, the maximum of the correlation dimension (see Table 5.2) is 3.59. In the case of decreasing the feedforward inhibition from 1, in the initial case, to 0.1, the maximum of the correlation dimension becomes 2.85. The efficiency of this modification is low if we compare it with the maximum of the D_2, 1.37, obtained in the case of decreasing the feedback inhibition from 1, in the initial case, to 0.1.

4. By increasing the inhibitions from 1 to 1.5, the system increases the LLE (from 0.174 to 0.192) and the maximum D_2 (from 3.59 to 4.98). Thus it appears as if the neurons can "chat" more. The increasing behavior for these two measures does not occur when we continue to modify the inhibitions from 1.5 to 2. In this last case, the LLE becomes 0.0873 and the maximum D_2 becomes 2.93.

5.3.2 Problem of Connectivity

The problem of connectivity involves investigating the modification of local connectivity within the piriform cortex. More specifically, we analyze the dependence of the level of chaos as a function of the density of the synapses (i.e, the number of synapses generated between the neurons). In addition, we investigate the variation of the maximum nonlinear interdependence (see Section 2.8) of two subsystems embedded in a larger system. Thus, we consider how the coupling of two interconnected subsystems of the same underlying system would change as a function of connectivity of the synapses. We believe that the levels of local connections between the neurons can be used as a hypothesis to explain the mechanism underlying illnesses such as schizophrenia.

The **Problem of Connectivity** is motivated from the following clinical considerations. In spite of intensive research over the last decades and the discovery of effective medication, the cause and the mechanisms leading to schizophrenia are still unclear. It is widely agreed that schizophrenia is most likely based on fundamental neuronal changes of the brain. Unfortunately, physiological methodologies have not been able to contrive reliable tests beside the current assessments. Perhaps the high complexity of the human brain is what renders it vulnerable to diseases such as schizophrenia because animals do not develop the same types of diseases [53].

The mechanisms underlying schizophrenia can be explained using two antagonist hypotheses:

1. **Low level of local connections between neurons (excessive synaptic pruning).** During adolescence, the number of synaptic connections is reduced. This is actually very beneficial because it helps humans to focus on specifics. If we didn't have such a pruning mechanism, we would be attending to hundreds of different items, thus "diluting" our attention. Consequently, because we have fewer connections, we can only focus on a limited number of stimuli. This theory originated from two inter-related empirical findings [53] in schizophrenia-related brain research:
   (a) The age of the onset of schizophrenia (late adolescence) correlates heavily with the decline in the density of synapses in the frontal cortex by 50%.
   (b) Schizophrenic patients show abnormally low connectivity in the frontal cortex, which is responsible for higher cognitive processes that are impaired in schizophrenia.

2. **High level of connectivity between neurons (insufficient pruning).** This theory asserts that in schizophrenia, the normal synaptic pruning doesn't happen, causing schizophrenics to have difficulty in focusing attention or filtering stimuli. This causes them to pay attention to hundreds of issues simultaneously. Over 250,000 brain cells are created every minute in a two-month-old fetus. These cells slither across the brain seeking out their proper destination, and send out billions of axons, analogous to new branches of huge trees in a forest. The axons make connections with other brain cells, and a single neuron may have 100,000 connections with other neurons. This connection building phase is followed by a pruning phase. Many of these synapses will die, inasmuch as only half of the 200 billions created neurons will survive to adulthood. Neurotransmitters like glutamate and GABA play a key role in making this pruning step an efficient process [53]. If the pruning of the synapses is not efficient, the aberrant connectivity can lead to diseases like schizophrenia.

In our research we have performed modifications to the number of connections between the pyramidal neurons. By changing the connectivity, we proposed to simulate the level of pruning to be excessive or insufficient.

We chose to describe the effect of pruning on the level of chaos and the degree of synchronization between the two subsystems embedded in the piriform cortex model, using three measures: the LLE, S, and CC. These three measures were chosen based on two hypotheses. First, schizophrenia symptoms, like thought disorder, hallucinations and delusions, are assumed to be dependent on the level of chaos in the brain. Second, the symptoms are triggered by the existence of false attractors near "good" attractors, which suggests that areas from the brain could be highly correlated in an unhealthy manner. To our knowledge, the investigation of the two theories, namely excessive and insufficient pruning, based on these three measures, is new.

The uniqueness of our research is strengthened by the fact that the pairs of signals being compared belong to the same system. Other authors [125, 131, 147], consider two initially independent systems and partially couple them; subsequently, they analyze the synchronization of the signals obtained from the two systems. In contrast to previous models that evaluate relationships between two different systems (or rather, two partially coupled systems), we propose a new approach where the investigation is made using two subsystems which are embedded in a larger system, namely, two coupled sub-systems of the same system.

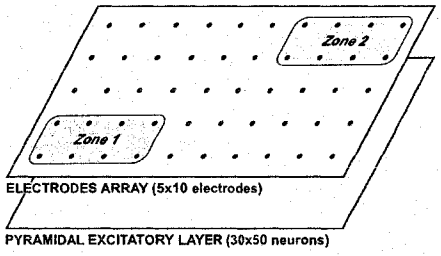

Figure 5.3: The Distribution of the Electrodes in Zone1 and Zone2.

5.3.2.1 The Research Plan

In our research, we considered two zones of the piriform cortex (Figure 5.3). For each zone treated as a subsystem we analyzed the artificially generated EEGs, each of them being computed with a fixed number of electrodes, and computed at a suitable frequency.

We considered the density of the synapses corresponding to the pyramidal neurons as a control parameter, and explored the effect of modifying the initial values suggested by Wilson model [174]. Again, this involved:

1. The computation of the EEGs as function of the number of electrodes for each subsystem.
2. The determination of the optimum value for the embedding dimension for the phase space reconstruction using the FNN method *for the density of the synapses.*
3. The computation of the LLE for EEGs generated by the subsystems, and the CC and S measures *between* the EEGs.

5.3.2.2 Results

The time series used to describe the systems are the EEGs. They were calculated using an array of n evenly spaced electrodes on the surface of the simulated cortex. Recordings from the array were averaged to produce the EEGs. In our experiments, we set $n = 50$.

In our model, we considered two zones of the piriform cortex (Figure 5.3). For each zone (subsystem) we analyzed the artificially generated EEGs, each of them being computed with 8 electrodes. The EEGs were recorded at 5000 samples/sec, for a duration of half a second.

connectivity	LLE *Zone1*	LLE *Zone2*
$p = 0.1$	0.757504	0.472464
$p = 0.2$	0.701987	0.475484
$p = 0.5$	0.675625	0.478652
$p = 1$	0.743389	0.610189
$p = 2$	0.591960	0.601312
$p = 10$	0.716974	0.592889

Table 5.3: The LLE for each of two zones, function of the level of connectivity between pyramidal cells.

We investigated the level of chaos and the synchronization between these two zones of the piriform cortex, when the efficiency of the pruning is higher or smaller than 50%. We decreased, and also increased the connectivity between the pyramidal cells. The level of connectivity was described by the maximum number of possible connections between the pyramidal neurons, where the possible values were $p = 0.1$, 0.2, 0.5, 1, 2, and 10. The case of the healthy brain, when the efficiency of pruning is 50 %, corresponds to $p = 1$.

The first experimental step was to compute the optimum embedding dimension for each zone, using the FNN Statistics. The second step was to estimate the LLE for each connectivity. The averages results of 20 experiments with the same model are shown in Table 5.3.

In order to evaluate the interdependence between two artificially generated EEGs, we used two measures, namely S and CC. For computing CC we used a lag between -150 and $+150$, and the absolute value is reported. The evolutions of the S and CC function of connectivity are presented in Table 5.4. We report, as above, the averages for 20 experiments with the same model.

5.3.2.3 Conclusions for this problem

The analysis of the two behaviors, namely of increasing and decreasing the connectivity level, reveals that both determine a decrease in the level of chaos in the system (see Figure 5.4). With regard to the degree of synchronization, represented by the non-linear interdependence S, only a decrease in connectivity leads to a consistent modification (see Figure 5.5). For a decrease in connectivity by 50% - one of the hypotheses explaining the occurrence of schizophrenia, S has a

connectivity	$S(X \mid Y)$	$S(Y \mid X)$	CC
$p = 0.1$	0.1385	0.1044	0.4932
$p = 0.2$	0.1354	0.1037	0.5563
$p = 0.5$	0.1555	0.1071	0.4866
$p = 1$	0.1129	0.1070	0.4168
$p = 2$	0.1115	0.1069	0.4590
$p = 10$	0.1222	0.0899	0.4527

Table 5.4: Nonlinear interdependence (S) and Cross correlation (CC) function of the level of connectivity between pyramidal cells.

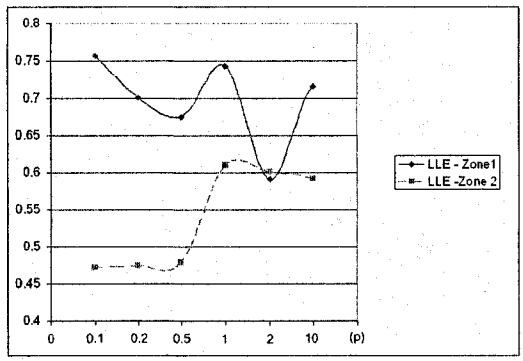

Figure 5.4: The evolution of LLE in *Zone1* and *Zone2* as a function of the level connectivity between the neurons (see Table 5.3).

maximum of more than 37% over the initial status value. The increase in communication between the two subsystems leads us to the conclusion that the *excessive* synaptic pruning hypothesis has a higher impact on the system dynamics than the insufficient pruning hypothesis.

The asymmetry of the model explains the differences between the $S(X|Y)$ and $S(Y|X)$ behaviors, the latter being less sensitive to the variance in connectivity.

Unlike S, the CC has a minimum value for $p = 1$, whereas the modification of the correlation, when $p = 0.5$ or $p = 2$, determines an increase of CC by 16.74% in the first case, and by 10.12% in the second case (see Figure 5.5).

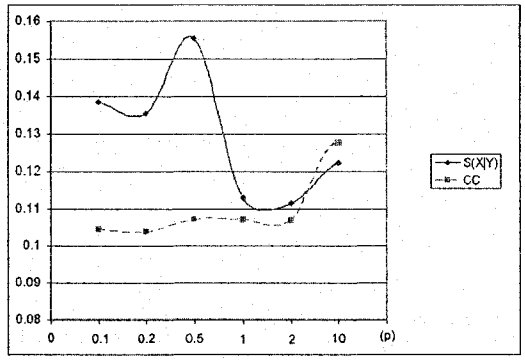

Figure 5.5: The evolution of $S(X|Y)$ and CC between *Zone1* and *Zone2* as a function of the level of connectivity between the neurons (see Table 5.4).

5.3.3 Problem of Stimulus Frequency

The problem of controlling the system using the stimulus frequency involves investigating the effect of the frequency of a stimulus applied in the bulb. More specifically, we analyzed the dependence of the level of chaos as a function of the frequency of a stimulus that is globally applied within the network. In addition, we studied the maximum nonlinear interdependence of two subsystems which are embedded in a larger system also quantified as a function of the frequency.

The medical rationale for this study is the following. During a partial epileptic seizure, the neurons from a small area become synchronized. In order to desynchronize them, we intended to find a method to increase the level of chaos. One possible solution is that a periodic stimulus is applied to a site *Zone1* located some distance from the epileptic focus *Zone2* which cannot be reached.

A particular form of synchronization is observed if a strong periodic force, denoted by $F(\omega)$, acts on two partially coupled chaotic systems. This force can suppress chaos and make the systems oscillate periodically with the period of the force. This regime can be interpreted as a *chaos-destroying synchronization.* In our study we intended to solve the inverse scenario: Can we apply a force so as to increase the chaos? To the best of our knowledge, such a solution is unavailable in the literature. The synchronization is used here to demonstrate the existence of a

functional relationship between the states of the two systems [5]. Pecora described this type of synchronization by using the term "dynamical interdependence" or "nonlinear interdependence" [125]. Strictly speaking, the phenomenon we detect is interaction, and not synchronization.

Our problem can redefined as follows: What kind of force should be applied and where should it be applied in order to obtain a greater level of chaos? In order to solve this, we did not use a precise mathematical model because such system interactions are not easily formulated mathematically. Rather, we chose to solve this problem using the earlier model of the piriform cortex.

For this model we hoped to find a periodic "force" applied in the bulb, $F(\omega)$, which generated chaos. We hoped to show *experimentally* that a particular frequency of this stimulus simultaneously produces a maximum nonlinear interdependence (larger than what is obtainable without such a stimulus) and also an increase in the level of chaos, described with the LLE.

The general aim of our research was to increase the level of chaos in one small part of the modelled piriform cortex. Thus, with regard to our epileptic model, we considered, within the piriform cortex, two zones (see Figure 5.3) where *Zone2* will be the epileptic focus. In order to solve our problem using this model, we opted to *not* insert a local stimulus in this subsystem, *Zone2*, but rather to insert a local stimulus in another subsystem *Zone1*, which is connected to the first one. This is a typical "Master-Slave" problem, where *Zone1* is the Master and *Zone2* is the Slave. The larger the nonlinear interdependence between these two subsystems ($S(1|2) > 0$), the greater the effect of insertion in *Zone1* will be to the signal in *Zone2*.

The main issue which must be addressed is the following : How can we increase the nonlinear interdependence between the two connected subsystems (*Zone1* and *Zone2*). We hoped to solve this problem by applying a stimulus $F(\omega)$ in the entire system, namely, a global stimulus inserted in the bulb. This insertion will be the preprocessing step. We hoped to show experimentally that a particular frequency of this stimulus produces the maximum nonlinear interdependence $S(1|2)$, which is larger than what is obtainable without any stimulus. In addition[8], we hoped to show that for this specific frequency, the LLE for the *Zone2* area of a brain which is susceptible to an epileptic seizure, is greater than what is obtainable without any stimulus.

[8]We add this second condition because we don't want our intervention to further decrease the LLE in the epileptic region *Zone2*. Out final aim is to increase the level of chaos in *Zone2* by applying an additional stimulus in *Zone1* after the preprocessing step of increasing the interactions between *Zone1* and *Zone2* is accomplished.

5.3.3.1 The Research Plan

As mentioned above, in our study, we considered two zones of the piriform cortex (Figure 5.3.2). For each zone (subsystem) we analyzed the artificially generated EEGs, each of them being computed with a fixed number of electrodes and computed at a suitable frequency.

Thereafter, we studied the frequency of the stimulus inserted in the bulb as a control parameter, and explored the relevant effect of modifying the frequency. To do this, we:

1. Computed the EEGs as a function of the number of electrodes for each subsystem.
2. Determined the optimum value for the embedding dimension for the phase space reconstruction using the FNN method *for the frequency of the stimulus.*
3. Computed the LLE and KY for EEGs generated by the subsystems, and the CC and S between the EEGs.

5.3.3.2 Results

As mentioned earlier, the general aim of our research was to increase the level of chaos in one small part of the modelled piriform cortex.

For each subsystem we analyzed the artificially generated EEGs, each of them being computed with 8 electrodes. The EEGs were recorded at 5000 samples/sec for a duration of half a second. The frequency of the input stimulus $F(\omega)$ had a set of values between 1 Hz and 500 Hz, namely 1, 3, 5, 10, 50, 80, 100, and 500 Hz. The amplitude of the signal had a continuous component of 0.2 mV, and an alternative component of 0.15 mV.

The first experimental step was to compute the optimum embedding dimension for each zone, using FNN Statistics. In the interest of brevity, we will not present the results here. After this step, we estimated the LLE and $DK-Y$ dimension, and then did 20 experiments with the same model. The averages of the results are shown in Table 5.5.

To evaluate the interdependence between the two artificially generated EEGs, we used two metrics, namely the S and CC[9]. The evolutions of the S and CC metrics as a function of

[9]For computing CC we used a lag between -150 and $+150$. The absolute value is reported.

Table 5.5: The LLE for each of the two zones, as function of the frequency of the stimulus. The lag is 1.

frequency	LLE *Zone1*	DK-Y1	LLE *Zone2*	DK-Y2
no stimulus	0.0834	3.38	0.0241	1.83
0 Hz	0.1047	4.02	0.0624	2.56
1 Hz	0.1354	4.28	0.0965	3.28
3 Hz	0.1202	4.14	0.0827	3.06
5 Hz	0.0854	3.16	0.0375	2.86
10 Hz	0.0847	3.39	0.0363	1.88
50 Hz	0.1110	3.39	0.0388	2.04
80 Hz	0.1224	3.88	0.0610	2.37
100 Hz	0.1245	4.02	0.0631	2.48
500 Hz	0.1008	3.63	0.0432	2.33

frequency of the input stimulus are presented in Table 5.6. We reported, as above, the averages for 20 experiments with the same model.

5.3.3.3 Conclusions for this problem

The following are the conclusions obtained as a result of our experiments.

1. $S(1|2)$ has a maximum very close to the maximum of the LLE for Zone 1. This happens at small frequencies of the stimulus, between $1-3$Hz. The fact that the neurons attain a maximum value of the LLE implies that they possess a larger freedom of movement. We have found that this maximum is close to the maximum of $S(1|2)$, when the neurons can "chat" more freely with each other. This result is not intuitive as one would expect a small LLE for a large $S(1|2)$. Indeed, if the EEGs are very close to being *synchronized* periodic oscillations (i.e., with a large S) they will have a small LLE implying that the EEGs are *stable* periodic oscillations - which is a regime which can be interpreted as *chaos-destroying synchronization.* On the contrary, we have found that the behavior portrayed by our model is different.

2. For a high frequency (100 Hz), we have discovered a local maximum for the LLE but, in this case, this is not a local maximum for $S(1|2)$. The neurons again have a large freedom

Table 5.6: Nonlinear interdependence (S) and the maximum Cross Correlation Coefficient($CCmax$) for each frequency of the stimulus inserted in bulb. The time lag is 1.

frequency	$S(1 \mid 2)$	$S(2 \mid 1)$	$CCmax$
no stimulus	0.1056	0.0040	0.0709
0 Hz	0.0947	0.0911	0.1362
1 Hz	0.1287	0.0687	0.1275
3 Hz	0.1406	0.0691	0.1803
5 Hz	0.1271	0.1083	0.2948
10 Hz	0.1178	0.1436	0.3414
50 Hz	0.1064	0.0953	0.1929
80 Hz	0.1059	0.0953	0.1843
100 Hz	0.1008	0.0840	0.1794
500 Hz	0.0541	0.0901	0.2172

of movement, but they don't "chat" anymore.

3. The evolution of $DK - Y$ for *Zone1* shows that the frequency which generated the maximum value for the LLE also generated the maximum value for the $DK - Y$. So, the increase in chaos seems to be consistent. When the LLE increases, the contribution of the positive Lyapunov exponents also increases and vice versa.

4. The CC for *Zone1* has a global maximum for 10 Hz. This measure of synchronization (the linear approach) has no relevance for our research. We infer that the model has a very powerful nonlinear behavior which cannot be described with a linear measure, since the linear component of the measures is very small.

5. We have found experimentally, using the S measures, that the connectivity between the two zones is bidirectional. The way that the model of the piriform cortex was built generated a difference between the $S(1|2)$ and $S(2|1)$, the former being the larger of the two. In this study we have only analyzed the behavior of $S(1|2)$.

6. By choosing this method of inserting a stimulus in the bulb we have also solved the problem of increasing the nonlinear interdependence between the two connected subsystems (*Zone1* and *Zone2*) and that of simultaneously increasing the level of chaos in *Zone1*.

In order to increase the the level of chaos in the epileptic focus (*Zone1*) we rendered this step to be the preprocessing step. After this step, we applied a periodic stimulus to a site (*Zone1*) located some distance from the epileptic focus (*Zone2*). Analyzing Table 5.5 we see that the preprocessing step itself yielded a contribution for increasing the level of chaos in *Zone2*. We can thus conclude that inserting a stimulus in the bulb can be a possible final solution (and not merely a preprocessing step) for increasing the level of chaos in the epileptic focus.

5.4 Conclusion

In this Chapter, we have described a large scale computational model for the piriform cortex, which can be used to explore the cause of the nonlinearity (and consequently, chaos) in the EEG computed from this part of the brain. We presented the limitations of a clinical exploration, and also the limitations of using a purely mathematical model. We then argued that the experimental approach was the only suitable strategy by which we could identify the effect of the control parameters on the level of chaos in the system.

We presented results for three problems that have been studied: (i) The problem of Density and Strength, (ii) The problem of Connectivity, and (iii) The problem of Stimulus frequency.

In the next Chapters, namely Chapter 6 and Chapter 7, we shall propose methods for controlling the chaos in *small* scale networks, leading to more mathematically-oriented approaches.

Chapter 6

Controlling Small Scale Models: Spike Annihilation in a Hodgkin-Huxley Neuron

The complexity of large scale networks, presented in the previous Chapter, demonstrated that it is not mathematically feasible to study problems of this nature. The present Chapter proposes some methods by which the behavior of *small* scale networks can be investigated. The underlying motivation is to consider the simplest neural modules capable of displaying chaotic behavior, and to use the knowledge gained from studying these systems to obtain a broader understanding of the possible relevance of chaotic dynamics to brain functioning.

Two models of neurons are investigated in this Chapter and in the following Chapter, namely, a classical Hodgkin-Huxley neuron, and a Bursting neuron. The results of the explorations of these models, and the control methods proposed are applied later to networks of neurons. The goal of this phase of the research is, as mentioned in Chapter 5, to develop methods for controlling the level of chaos, with the particular cases of desynchronizing the networks and of increasing the chaos. As opposed to the work proposed in the previous Chapter, small scale models lend themselves to a more mathematical analysis, inasmuch as the small size of the networks permits us to apply the mathematical tools related to computing steady states and Jacobian matrices.

6.1 Spike Annihilation for the Hodgkin-Huxley Neuron

The neural model investigated in this Chapter is the Hodgkin-Huxley (HH) neuron, which exhibits stable periodic solutions for a certain range of constant applied depolarizing currents. It is well known that, sometimes, networks of HH neurons can become synchronized. This synchronization can be an undesirable state (symptomatic of Parkinson's disease or epilepsy), and a method to annihilate this firing process can be useful.

In several neurological diseases, like essential tremor, the functions of the brain are severely impaired by synchronized processes, in which the neurons fire in a synchronized periodical manner at a frequency closely related to that of the tremor. Stimulation techniques have been developed to desynchronize these neuronal populations. One such technique is the electrical Deep Brain Stimulation (DBS) [102, 112], performed by administering a permanent high frequency periodic pulse train to the brain by means of so-called *depth* electrodes. The DBS method was developed empirically, and its mechanism has not yet been understood.

Another stimulation technique is the perturbation with brief stimuli. Clinical results for this technique (some of them are briefly presented in this thesis) prove that a carefully chosen brief pulse applied at a specific time, denoted by the term "vulnerable phase", can *annihilate* the firing behavior in the neuron. It is believed that by determining the vulnerable phase of a neuron, the result can be generalized to a population of neurons. Taking into consideration the latter generalization, a desynchronizing pulse would be effective only if it hits a cluster of neurons in a very precise *vulnerable phase.*

In this context, the first neural model analytically investigated in great detail was the Hodgkin-Huxley (HH) neuron, which exhibits stable periodic solutions for a certain range of constantly applied depolarizing currents.

The annihilation of the firing activity was predicted theoretically by Teorell (1971) [161] for a two-variable model of the HH neuron. He showed that the annihilation of the firing activity can be achieved by using a small brief test pulse injected into the refractory period, just prior to the neuron attaining to its firing level. Later, the annihilation of the spike train, by using a carefully chosen stimulus, was predicted by Rinzel, and also independently by Best (in 1979). Rinzel [134] calculated periodic solutions to the space-clamped HH equations when a depolarizing

current was constantly applied. The computational analysis of Best [16] stated that one could "shock" the HH neuron out of the repetitive mode by using a properly timed instantaneous current pulse. In addition, Guttman, Lewis, and Rinzel [68] confirmed experimentally that repetitive firing in a space-clamped squid axon, bathed in low Ca and merely stimulated by a suprathreshold step of current, can be annihilated by a brief depolarizing or hyperpolarizing pulse of the proper magnitude, applied at the proper phase[1]. In response to such perturbations, membrane potentials and ionic currents showed damped oscillations that converged towards a steady state. For the non-annihilating perturbations, the repetitive firing of the system resumed with an unaltered frequency, but with a modified phase.

We present now a few considerations about the dynamical properties of the HH neuron. This neural model can be in one of two states: A resting state and a state that fires in response to certain forms of stimulation. Usually, the neuron is considered to be in a equilibrium mode when it is in a resting state. However, this statement is not universal because there are two equilibrium states associated with this neuron, namely a fixed point and the limit cycle, both of which are stable. One problem to be considered here is the switching of the neuron from one equilibrium mode to the other, which is a phenomenon which can occur without modifying the number and the stability of the equilibria.

From a classical system theory point of view, the equilibrium point of a nonlinear dynamical system may disappear or may lose its stability if a control parameter is changed, depending on the type of bifurcation displayed by the system. In our research, the HH neuron is considered to be a dynamical nonlinear system whose equilibrium states are not to be radically changed with regard to its stability. We investigate the case when both equilibria, namely the fixed point and the limit cycle, co-exist and remain stable. In this particular situation, the system is bi-stable, and with a carefully chosen synaptic input, it is possible to switch the behavior from being resting to one which demonstrates spiking, or from being spiking to a resting (spike annihilation) mode. The goal of this research is to describe the properties of the stimulus that can achieve this switching.

[1]After the resting potential of the axon (whose central compartment was bathed in low Ca artificial seawater) had reached a steady state, the threshold for repetitive firing was established by a manually triggered stimulation with a step of current, 30 ms in duration, to avoid overstimulation of the axon. Thereafter, a slightly suprathreshold current step of approximately 30 ms duration, was used as a bias in order to initiate the repetitive firing. Upon being excited by this bias current, various magnitudes of brief 0.15 ms perturbations were added at various phases in the period of the response, to investigate the control of repetitive firing.

This above stimulus, chosen to be a brief pulse of current, is not a control parameter. Its behavior affects neither the existence of the equilibrium points, nor their stability. The control parameter is the strength of the constantly applied current and, during our investigation, it is set to be constant. We argue that injecting a constant current into the axon is not equivalent to injecting a brief pulse of current. In the former, the system can go through a bifurcation of the equilibrium by changing the existence of the equilibria or by affecting their stability. In the latter, however, the system can jump to an alternate location in the state space, which is achieved by the system resetting the initial condition. The neuron is driven to a state of "shock", and consequently, the membrane potential instantly switches to a new value. The fixed point, corresponding to the resting state, co-exists with the limit cycle, which corresponds to the spiking state, and the system continues to be bistable. This leads us to the goals of this research: (i) to prove analytically the existence of such stimuli, and (ii) to describe the characteristics of these brief depolarizing shock-stimuli that, when inserted at the appropriate time, can switch the neuron from the spiking to the resting state.

6.1.1 Our Contribution

In contrast to the previous pieces of work cited above, which validated experimentally or anticipated theoretically that annihilation is possible, we achieve the following:

1. We formally prove that the problem of spike annihilation has a well defined solution.
2. We formally derive the characteristics of the proposed solution.
3. We demonstrate experimentally the validity of the solution (i.e., by numerical simulations).

All of the results are novel, and to the best of our knowledge, unknown in the field. We thus believe that our analysis of the HH neuron has practical implications in clinical applications, especially in the case of the desynchronization of neuronal populations.

Section 6.1 presents an overview of the clinical research related to the problem of spike annihilation in HH neurons. Section 6.2 contains the dynamical formulation of the problem, namely the bistable neuron, the equations of the system, and its stable and unstable limit cycles. Section 6.3 investigates the problem of annihilation and presents a formal proof of the existence of the stimulus, and the suggested numerical approach for computing the bifurcation

point. Section 6.4 describes the experiments conducted for determining the properties of the annihilation stimulus, and Section 6.5 concludes the Chapter.

6.2 The Bistable HH Neuron

In this section we investigate the stability-related characteristics of the HH neuron. In the previous Section, we stated that the HH neuron can be perceived as a dynamical nonlinear system with two stable equilibria. This is formalized below.

Consider a two-dimensional dynamical system:

$$\frac{dV}{dt} = P(V, R), \tag{6.1}$$

$$\frac{dR}{dt} = Q(V, R), \tag{6.2}$$

where $P(V, R)$ and $Q(V, R)$ are polynomials of real variables V and R, and where the corresponding coefficients are real. The fundamental problem associated with the qualitative theory of such systems seems to be Hilbert's Sixteenth Problem [66], stated as follows:

> *Find the maximum number and the relative positions of the limit cycles of the system described by Equations (6.1) and (6.2).*

This problem remains unsolved.

It should be mentioned that there are many methods which yield *specific* results related to the study of limit cycles. However, the above general problem has not been solved, even for the simplest quadratic systems. Rather, we intend to explore, *numerically*, the less general system defined by Equations (6.3) and (6.4) proposed by Rinzel and Wilson [169], which, indeed, approximate the Hodgkin-Huxley neuron:

$$\frac{dV}{dt} = \frac{1}{\tau}[-(a_1 + b_1 V + c_1 V^2)(V - d_1) - e_1 R(V + f_1) + B + \sigma], \tag{6.3}$$

$$\frac{dR}{dt} = \frac{1}{\tau_R}(-R + a_2 V + b_2), \tag{6.4}$$

where $a_1, a_2, b_1, b_2, c_1, d_1, e_1, f_1, \tau$, and τ_R are constants[2], B is the background activity[3], and σ is an excitation stimulus. Apart from deriving certain specific analytic results, we propose to discover, *numerically*, the number and the positions of the limit cycles.

By introducing Hilbert's Sixteenth Problem as a motivation for the solutions of the system, we argue that the numerical approach to yield the number and the relative positions of the limit cycles of the system described by Equations (6.3) and (6.4), is the only reasonable strategy (instead of an analytical one) to tackle the problem.

It is true that there are some theoretical results [66], which can be postulated as theorems, that can be applied for two-dimensional nonlinear systems. But their contributions are only qualitative without being capable of describing the *complete* picture of the number and the relative positions of the limit cycles. Thus, in the interest of completeness we mention these formal results that can be used to prove that a system described by Equations (6.3) and (6.4) has a limit cycle and a bifurcation point.

6.2.1 Related Theoretical Foundation

The first useful Theorem, due to Poincare [169], states that a limit cycle must surround one or more equilibrium points.

Poincare Theorem:

> *If a limit cycle exists in an autonomous two-dimensional system, it must necessarily surround at least one equilibrium point. If it encloses exactly one equilibrium point, the latter must be a node, a spiral point, or a center, but can not be a saddle point.*

The Poincare Theorem is a necessary but not a sufficient condition for the existence of the limit cycle in systems described by Equations (6.3) and (6.4). In the general case of a two-dimensional

[2]In their experiments, Rinzel and Wilson [169] set the constants as: $a_1 = 17.81$, $b_1 = 47.71$, $c_1 = 32.63$, $d_1 = 0.55$, $e_1 = 0.55$, $f_1 = 0.92$, $a_2 = 1.35$, $b_2 = 1.03$, $\tau = 0.8$ ms and $\tau_R = 1.9$ ms. The stimulus σ was expressed in $\mu A/100$, and V was measured in deci-volts. All these settings were assigned values so as to mimic real-life brain phenomena.

[3]The background activity generates limit cycles in the system. Without this value, the system will converge through the stable spiral point.

nonlinear system, it is possible to find multiple steady states without limit cycles. Consequently, the applicability of the Poincare Theorem is limited, since by utilizing it, we will not be able to determine whether a system described by Equations (6.3) and (6.4) has a limit cycle.

On the other hand, we need a theorem that specifies the conditions under which a system is forced to have a limit cycle. In the literature [169], the *Poincare-Bendixon Theorem*[4] defines the conditions for the existence of a limit cycle. But more applicable to our scenario, is the *Hopf Bifurcation Theorem* [169], presented below, which defines the conditions for the existence of a stable or unstable limit cycle.

Hopf Bifurcation Theorem:

Consider a nonlinear dynamical system in $N \geq 2$ dimensions that depends on a parameter, β, as:

$$\frac{d\vec{X}}{dt} = \vec{F}(\vec{X}, \beta). \tag{6.5}$$

Let X_0 be an isolated equilibrium point of the system. Assume that there is a critical value of $\beta = \alpha$ with the following properties determined from the Jacobian, $J(\beta)$:

1. *X_0 is asymptotically stable for some finite range of values $\beta < \alpha$.*
2. *When $\beta = \alpha$ the system has at least one pair of pure imaginary eigenvalues $\lambda = \pm i\omega$, while all other eigenvalues have negative parts.*
3. *X_0 is unstable for some range of values $\beta > \alpha$.*

Then, the system defined by Equation (6.5) either possesses an asymptotically stable limit cycle over a range $\beta > \alpha$, or it possesses an unstable limit cycle over some range $\beta < \alpha$. Furthermore, in the neighborhood of $\beta = \alpha$, the frequency of the oscillation characterized by the limit cycle will be approximately $\frac{\omega}{2\pi}$, and this oscillation will emerge with infinitesimal amplitude sufficiently close to α. □

The *Hopf Bifurcation Theorem* indicates that *near* the critical value of $\beta = \alpha$ there is a limit cycle. It does not tell us whether this is an unstable limit cycle occurring when $\beta < \alpha$, or if

[4]The Poincare-Bendixon Theorem states the following: *Suppose that there is an annular region in an autonomous (i.e. constant coefficient) two-dimensional system that satisfies two conditions: (1) The annulus contains no equilibrium points, and (2) All trajectories that cross the boundaries of that annulus enter it. Then the annulus must contain at least one asymptotically stable limit cycle.*

it is an asymptotically stable limit cycle for $\beta > \alpha$. However, the theorem specifies where we can search in the parameter space, to locate a limit cycle behavior. Thus, although we are not able to provide the equation that describes the limit cycle, we can identify, by investigating the neighborhood of α, the qualitative description of the limit cycle.

To render our theoretical consideration meaningful, in the following, we shall derive:

1. The equilibrium states of the HH neuron by solving the system of equation described by the isoclines,
2. The Jacobian corresponding to the system described by Equations (6.3) and (6.4), at the equilibrium states,
3. The eigenvalues of the Jacobian, by solving the characteristic equation associated with the Jacobian, and
4. The requirements on the eigenvalues as specified by the *Hopf Bifurcation Theorem* for identifying the limit cycle.

6.2.2 Computing the equilibrium states

Consider a system described by Equations (6.3) and (6.4). We compute the the equilibrium states by solving the system of equations described by their isoclines. This is formalized in the following Lemma.

Lemma 6.1:

The equilibrium points of the HH neuron can be obtained by solving a cubic polynomial equation:

$$x_3V^3 + x_2V^2 + x_1V + x_0 = 0, \tag{6.6}$$

where:

$x_3 = -c_1,$
$x_2 = -(b_1 + a_2e_1 - c_1d_1),$

$$x_1 = -(a_1 - b_1 d_1 + a_2 e_1 f_1 + b_2 e_1),$$
$$x_0 = a_1 d_1 - b_2 e_1 f_1 + B.$$

Proof: From Equations (6.3) and (6.4), we see that the system has two isoclines, specified by the contours:

$$\frac{dV}{dt} = 0 \text{ and } \frac{dR}{dt} = 0,$$

which can be written as:

$$\frac{1}{\tau}[-(a_1 + b_1 V + c_1 V^2)(V - d_1) - e_1 R(V + f_1) + B] = 0, \tag{6.7}$$

and

$$\frac{1}{\tau_R}(-R + a_2 V + b_2) = 0. \tag{6.8}$$

The background activity B is the control parameter β specified in the *Hopf Bifurcation Theorem.*

The equilibrium states can be computed as solutions of Equations (6.7) and (6.8). By substituting R from Equation (6.8) as $R = a_2 V + b_2$, and utilizing this value in Equation (6.7), we obtain the equation:

$$x_3 V^3 + x_2 V^2 + x_1 V + x_0 = 0, \tag{6.9}$$

where the coefficients x_3, x_2, x_1, and x_0 are as defined in the Lemma statement. Hence the Lemma. □

Remarks:

1. The roots for the variable V in Equation (6.6) can be computed for specific values of B, the background stimulus, which is constantly applied to obtain a bistable neuron.

2. Using the settings of Rinzel and Wilson [169], assigned to mimic real-life brain phenomena, Equations (6.7) and (6.8) become:

$$\frac{1}{\tau}[-(17.81 + 47.71V + 32.63V^2)(V - 0.55) - 26R(V + 0.92) + B] = 0, \tag{6.10}$$

B	*Root1*	*Root2*	*Root3*
0	-0.6979	-0.6449 + 0.4856i	-0.6449 - 0.4856i
0.025	-0.6947	-0.6465 + 0.4854i	-0.6465 - 0.4854i
0.05	-0.6915	-0.6482 + 0.4852i	-0.6482 - 0.4852i
0.06	-0.6902	-0.6488 + 0.4852i	-0.6488 - 0.4852i
0.065	-0.6896	-0.6491 + 0.4852i	-0.6491 - 0.4852i
0.07	-0.6889	-0.6494 + 0.4851i	-0.6494 - 0.4851i
0.075	-0.6883	-0.6498 + 0.4851i	-0.6498 - 0.4851i
0.08	-0.6876	-0.6501 + 0.4851i	-0.6501 - 0.4851i
0.085	-0.6870	-0.6504 + 0.4851i	-0.6504 - 0.4851i
0.1	-0.6850	-0.6514 + 0.4850i	-0.6514 - 0.4850i
0.125	-0.6818	-0.6530 + 0.4849i	-0.6530 - 0.4849i
0.15	-0.6785	-0.6546 + 0.4848i	-0.6546 - 0.4848i
0.2	-0.6720	-0.6579 + 0.4847i	-0.6579 - 0.4847i
0.25	-0.6655	-0.6612 + 0.4846i	-0.6612 - 0.4846i

Table 6.1: The roots of the value V variable for the equilibrium equation of the HH neuron as a function of B, the background stimulus. The parameters of the neuron are as advocated in [169].

and

$$\frac{1}{\tau_R}(-R + 1.35V + 1.03) = 0. \tag{6.11}$$

The equilibrium states can thus be computed as solutions of Equations (6.10) and (6.11) leading to the resulting cubic polynomial equation:

$$-32.6304V^3 - 64.8632V^2 - 50.6416V + Bk - 14.8424 = 0. \tag{6.12}$$

The roots of the Equation (6.12) are computed for specific values of B, and tabulated in Table 6.1.

3. To consider the real-life settings, we have also computed the corresponding value of R for all the real values of the roots, V, namely for *Root*1 from Table 6.2. From this Table, we can deduce the range of values for R that are useful in simulating brain-like phenomena. These values will be used later in this Chapter.

B	*Root1*(V)	R=R(V)
0	-0.6979	0.0878
0.025	-0.6947	0.0922
0.05	-0.6915	0.0965
0.06	-0.6902	0.0982
0.065	-0.6896	0.09580
0.07	-0.6889	0.1000
0.075	-0.6883	0.1008
0.08	-0.6876	0.1017
0.085	-0.6870	0.1025
0.1	-0.6850	0.1052
0.125	-0.6818	0.1096
0.15	-0.6785	0.1046
0.2	-0.6720	0.1140
0.25	-0.6655	0.1228

Table 6.2: The value of R obtained for a real root of the equilibrium state as computed for a particular value of B. The parameters of the neuron are as advocated in [169].

6.2.3 Computing the Jacobian

We now consider a Jacobian-based analysis of the HH neuron, formalized in the following Lemma.

Lemma 6.2.

The Jacobian matrix of the system representing the HH neuron is given by:

$$J(V,R) = \begin{pmatrix} y_{12}V^2 + y_{11}V + y_{10} & y_{21}V + y_{20} \\ y_{30} & y_{40} \end{pmatrix},$$

where:

$y_{12} = -\frac{1}{\tau}3c_1$, $y_{11} = -\frac{1}{\tau}(2b_1 + 2c_1d_1 + a_2e_1)$, $y_{10} = -\frac{1}{\tau}(a_1 + b_1d_1 + e_1b_2)$,
$y_{21} = -\frac{1}{\tau}e_1$, $y_{20} = -\frac{1}{\tau}f_1$,
$y_{30} = \frac{1}{\tau_R}a_2$,
$y_{40} = -\frac{1}{\tau_R}$.

Proof: We know from the theory of dynamical systems that the Jacobian matrix of the system is :

$$J(V,R)=\begin{pmatrix} \frac{\partial V(V,R)}{\partial V} & \frac{\partial V(V,R)}{\partial R} \\ \frac{\partial R(V,R)}{\partial V} & \frac{\partial R(V,R)}{\partial R} \end{pmatrix}.$$

Evaluating each of these components yields:

$$\frac{\partial V(V,R)}{\partial V}=\frac{\partial[\frac{1}{\tau}[-(a_1+b_1V+c_1V^2)(V-d_1)-e_1R(V+f_1)+B]]}{\partial V}=\frac{1}{\tau}[-3c_1V^2-(2b_1+2c_1d_1)V-(a_1+b_1d_1)-e_1R],$$
$$\frac{\partial V(V,R)}{\partial R}=\frac{\partial[\frac{1}{\tau}[-(a_1+b_1V+c_1V^2)(V-d_1)-e_1R(V+f_1)+B]]}{\partial R}=-\frac{1}{\tau}e_1(V+f_1),$$
$$\frac{\partial R(V,R)}{\partial V}=\frac{\partial(\frac{1}{\tau_R}(-R+a_2V+b_2))}{\partial V}=\frac{1}{\tau_R}a_2,$$
$$\frac{\partial R(V,R)}{\partial R}=\frac{\partial(\frac{1}{\tau_R}(-R+a_2V+b_2))}{\partial V}=-\frac{1}{\tau_R}.$$

But Equation (6.8) can be used to eliminate R from the partial derivatives. By achieving this, and omitting the laborious algebraic steps, the result follows. □

Remarks:

1. Observe that the Jacobian J is not dependent on B. However, it is clear that J can be evaluated at each equilibrium point, which, in turn, is dependent on B.

2. Using the same settings of Rinzel and Wilson [169], the Jacobian matrix of the "real-life" HH neural system becomes:

$$J(V,R)=\begin{pmatrix} \frac{\partial V(V,R)}{\partial V} & \frac{\partial V(V,R)}{\partial R} \\ \frac{\partial R(V,R)}{\partial V} & \frac{\partial R(V,R)}{\partial R} \end{pmatrix},$$

where:

$\frac{\partial V(V,R)}{\partial V}=-122.36V^2-74.40V+10.55-32.5R;$
$\frac{\partial V(V,R)}{\partial R}=-32.5V-29.9;$
$\frac{\partial R(V,R)}{\partial V}=0.71053;$
$\frac{\partial R(V,R)}{\partial R}=-0.52632.$

As mentioned in the proof of the Lemma, Equation (6.11) can be used to eliminate R from the partial derivatives and thus, the Jacobian becomes:

B	$V_{equilib}$	λ_1	λ_2	stability
0	-0.6979	-0.2565 + 2.2485i	-0.2565 - 2.2485i	stable
0.025	-0.6947	-0.1731 + 2.2534i	-0.1731 - 2.2534i	stable
0.05	-0.6915	-0.0909 + 2.2554i	-0.0909 - 2.2554i	stable
0.06	-0.6902	-0.0579 + 2.2555i	-0.0579 - 2.2555i	stable
0.065	-0.6896	-0.0909 + 2.2554i	-0.0909 - 2.2554 i	stable
0.07	-0.6889	-0.0909 + 2.2554i	-0.0909 - 2.2554i	stable
0.075	-0.6883	-0.0100 + 2.2548i	-0.0100 - 2.2548i	stable
0.08	-0.6876	+0.0075 + 2.2543i	+0.0075 - 2.2543i	unstable
0.085	-0.6870	0.0225 + 2.2537i	0.0225 - 2.2537i	unstable
0.1	-0.6850	0.0721 + 2.2514i	0.0721 - 2.2514i	unstable
0.125	-0.6818	0.1504 + 2.2456i	0.1504 - 2.2456i	unstable
0.15	-0.6785	0.2299 + 2.2372i	0.2299 - 2.2372i	unstable
0.2	-0.6720	0.3825 + 2.2138i	0.3825 - 2.2138i	unstable
0.25	-0.6655	0.5300 + 2.1820i	0.5300 - 2.1820i	unstable

Table 6.3: Eigenvalues of the Jacobian computed from the real root of the equilibrium equation obtained with particular values of the background stimulus B.

$$J(V) = \begin{pmatrix} -122.36V^2 - 118.28V - 22.937 & -32.5V - 29.9 \\ 0.71053 & -0.52632 \end{pmatrix}.$$

6.2.4 Finding the bifurcation point

We shall now consider the problem of finding the neuron's bifurcation point by using the dynamical matrix of the system. This value of the bifurcation point is used to "set" the neuron so as to render it to be bi-stable.

Theorem 6.3.

A HH neuron obeying the Equations (6.3) and (6.4) has a bifurcation point if and only if a root of the equation
$\frac{1}{\tau}[-3c_1V^2 - (2b_1 + 2c_1d_1)V - (a_1 + b_1d_1) - e_1R] - \frac{1}{\tau_R} = 0$
satisfies the inequality:
$V > -f_1 - \frac{1}{e_1}\frac{\tau}{\tau_R}$.

Proof: It is well known that for the bifurcation point, the roots of the characteristic equation, computed from the Jacobian, are purely imaginary. It is also well known that a quadratic equation $x^2 - Sx + P = 0$ has imaginary roots if

Condition 1: $S = 0$,

Condition 2: $P > 0$,

where S and P are the sum and product of the roots, respectively.

Consider the Jacobian of the HH neuron as given by *Lemma 6.2.* Applying *Condition 1* to this Jacobian generates the equation:

$$\frac{1}{\tau}[-3c_1V^2 - (2b_1 + 2c_1d_1)V - (a_1 + b_1d_1) - e_1R] - \frac{1}{\tau_R} = 0. \tag{6.13}$$

This equation has two roots, say V_1 and V_2. The problem now is one of verifying whether V_1 and V_2 satisfy *Condition 2.* This in turn implies that for V_1 and V_2:

$$\frac{1}{\tau}\frac{1}{\tau_R}[-3c_1V^2 - (2b_1 + 2c_1d_1)V - (a_1 + b_1d_1) - e_1R] + \frac{1}{\tau_R}\frac{1}{\tau}e_1(V + f_1) > 0. \tag{6.14}$$

We can rewrite this inequality using the observation that V_1 and V_2 are solutions to the equation corresponding to *Condition 1*, namely:

$$\frac{1}{\tau}[-3c_1V^2 - (2b_1 + 2c_1d_1)V - (a_1 + b_1d_1) - e_1R] = \frac{1}{\tau_R}. \tag{6.15}$$

Using this relation, *Condition 2* becomes:

$$\tfrac{1}{\tau_R}\tfrac{1}{\tau_R} + \tfrac{1}{\tau_R}\tfrac{1}{\tau}e_1(V + f_1) > 0.$$

We know that τ_R and τ are time constants, being positive. We make a convention that e_1 is also a positive constant. With these considerations, *Condition 2* can be rewritten in a new form as:

$V > -f_1 - \tfrac{1}{e_1}\tfrac{\tau}{\tau_R}$.

The theorem follows since whenever these constraints are satisfied, we obtain purely imaginary roots. □

Remarks:

1. As before, using the same settings of Rinzel and Wilson [169], *Condition 1*, when applied to the Jacobian, generates the equation:

$$-122.36V^2 - 118.28V - 22.937 - 0.52632 = 0,$$

whose roots are -0.6879 and -0.2788.

It is easy to verify whether either of these roots satisfy the constraint specified by *Theorem 6.3.* Observe that the first root, $V = -0.6879$, satisfies the *Condition 2* that is equivalent to V > -0.9361, implying that the HH neuron has a bifurcation point.

2. From Equation (6.12), we can compute the value of B that corresponds to the root $V = -0.6879$. This value[5], of $B = 0.0777$, generates a bifurcation in the system.

3. The second root, -0.2788, does not have any biological significance, being distant from the resting potential of the neuron.

4. The values of the roots (and the corresponding stability consequences) are tabulated in Table 6.3 as a function of b. Examining Table 6.3, we can conclude (using the notation of the *Hopf Bifurcation Theorem*) that $\alpha = 0.0777$. Thus, if $B < 0.0777$ (namely, $\beta < \alpha$) the system has an stable spiral point. If $B > 0.0777$, the stable spiral point became unstable and the system has a stable limit cycle. The value $B = 0.0777$ is a subcritical or hard Hopf bifurcation point. The system has an unstable limit cycle for $B < 0.0777$, and this is a point that is not observable in the real world due to its instability. It is only possible to *detect* the *consequences* of its presence.

6.2.5 The Stable and Unstable Limit Cycles

If we consider B to be a control parameter, we can analytically compute the equilibrium point, which, for certain values of σ, leads to a *spiral stable point*, and which, for other values of σ, leads to an *unstable spiral point.* The behavior around a specific value, namely the change of the stability of the equilibrium point, induces the concept of a *subcritical (hard) Hopf bifurcation.*

[5]The more exact value is 0.07773267 and it is obtained for V=-0.687930 and R=0.101295. The Largest Lyapunov exponent for this Hopf bifurcation is 1.000287e-002. For his neural model, Cooley [36] found a value of 0.0765 ($7.65\mu A$) for the value of B. By increasing the stimulus further, he obtained finite trains of shortening duration, and finally, at higher intensities, claimed to obtain the annihilation.

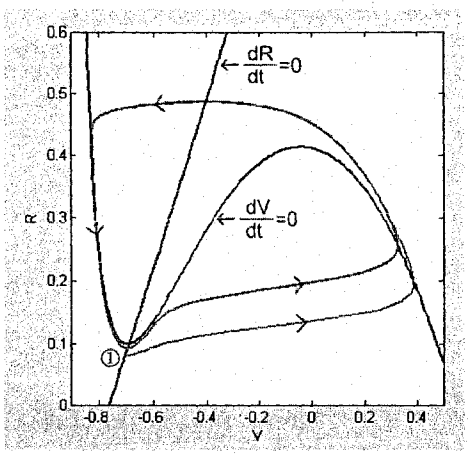

Figure 6.1: The phase space representing the *stable* limit cycle and the resulting isoclines ($\frac{dV}{dt} = 0$ and $\frac{dR}{dt} = 0$) obtained by using Rinzel and Wilson settings for the HH neuron. The starting point, (represented with '1') is $V_0 = -0.7$, and $R = 0.08$. In addition, $B = 0.08$.

Let us focus on the issue of the limit cycles themselves. By plotting the evolutions of the numerical solutions of the system (Equations (6.3) and (6.4)), we discover that for the settings of Rinzel and Wilson [169], there is a stable limit cycle to the right of the bifurcation point. To identify a hypothetical unstable limit cycle, we can modify the system's equations to make time run "backwards". The modification, which consists of rendering the sign of the two constants, τ and τ_R, to be negative, changes the unstable limit cycle to become asymptotically stable. In this way, by using a numerical method, we can identify the position of a second limit cycle, which happens to be unstable. The stable spiral point is surrounded by this unstable limit cycle which, in turn, acts as a *separatrix* defining a basin of attraction for the stable point.

In Figures 6.1 and 6.2 we present the stable and unstable limit cycles, together with the isoclines ($\frac{dV}{dt} = 0$ and $\frac{dR}{dt} = 0$). The trajectory starts at the point indicated by '1' and follows the arrowed curves. Observe that in the case of Figure 6.1, the trajectory of the HH neuron follows the stable limit cycle, and in Figure 6.2, the trajectory follows the unstable limit cycle. Figure 6.3 depicts the bifurcation diagram. When B is increased from the resting value, the steady state remains asymptotically stable and the spikes are generated only after the bifurcation point is reached, by increasing the value of B. In other words, the HH neuron indicates spiking at $B = 0.0777$, and the spiking process continues for all values of $B > 0.0777$.

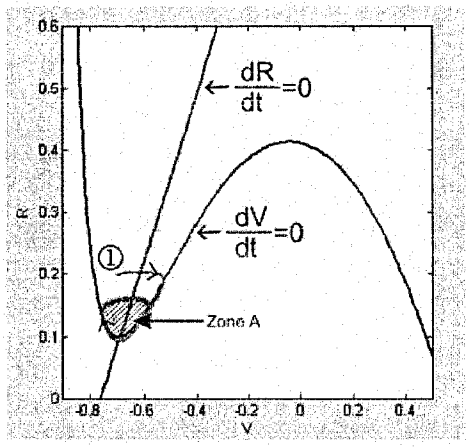

Figure 6.2: The phase space representing the *unstable* limit cycle and the isoclines ($\frac{dV}{dt} = 0$ and $\frac{dR}{dt} = 0$) for Rinzel and Wilson settings for the HH neuron. The starting point must be outside the zone called $Zone_A$, defined by the cycle. In this graph, the starting point (represented with '1') is $V_0 = -0.7$, and $R_0 = 0.2$. In addition, $B = 0.08$.

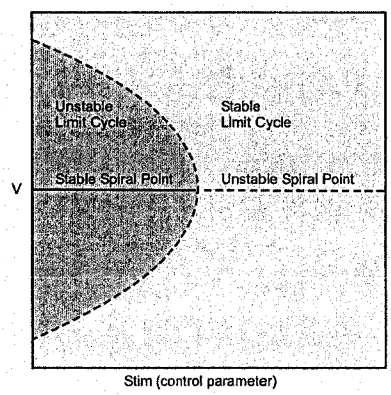

Figure 6.3: The bifurcation diagram for the system specified in Figures 6.1 and 6.2. The variable B is the control parameter. We consider B as a background stimulus that generates a bi-stable neuron.

6.3 The Problem of Annihilation

The problem of the annihilation of spikes for the HH neuron involves moving the state of the system, by using a pulse stimulus, from outside a particular zone (depicted as $Zone_A$) to being inside $Zone_A$, where $Zone_A$ is a basin of attraction of the stable spiral point which is described by an unstable limit cycle. For example, if the system is characterized by the settings specified by Rinzel and Wilson [169], $Zone_A$ is contained in the region given by $V \in [-0.6, -0.8]$ and $R \in [0.1, 0.15]$, as depicted in Figure 6.2. Figure 6.4 contains all the steady states of the system, including the stable spiral point, and the stable and unstable limit cycles.

The success of the annihilation process depends on four crucial issues:

1. What should be the initial point (V, R) for the system to exhibit annihilation ?
2. When should the pulse stimulus, σ, be applied to the system to annihilate it ?
3. What should the amplitude of the pulse stimulus be for the annihilation to be achieved ?
4. What should the duration of the pulse stimulus be for the annihilation to be achieved ?

The solution of the annihilation problem consists of determining a stimulus which adequately responds to all the above questions.

We now formally prove that the problem of spike annihilation is well-defined, and propose an algorithm for finding a solution to it. In addition, we also study the solution of annihilating the spikes by using multi-stimuli. Finally, we investigate the inverse problem, namely that of spike generation (see Figure 6.6).

The two problems are clarified in Figures 6.5 and 6.6. In Figure 6.5 we present the annihilation process. If the system starts in a carefully chosen configuration at State 1 on the stable limit cycle, the system can be driven to State 2 by applying a carefully chosen stimulus. From this state, it will then go to the stable fixed point. Similarly, in Figure 6.6, we depict the spike generation process. If the system starts in a stable fixed point or in State 1, in the close neighborhood of the stable fixed point, the system can be driven to State 2 by applying a specific stimulus, and, from this state, it will go further toward the stable fixed point.

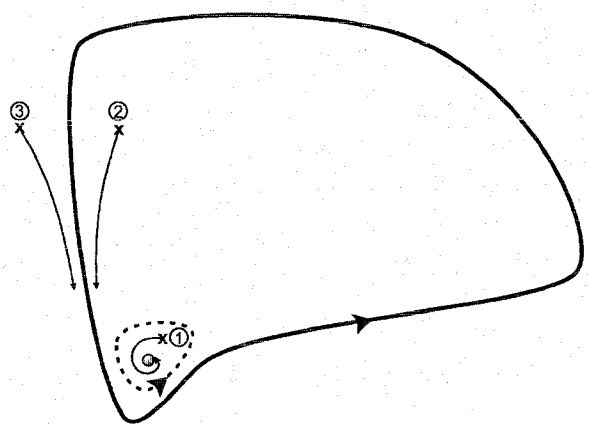

Figure 6.4: The stable fixed point, the stable limit cycle, and the unstable limit cycle (the *separatrix* given by the dashed line) are represented together. If the system starts in State 1, it will move towards to the stable fixed point. If it starts in State 2 or State 3, it will converge to the stable limit cycle.

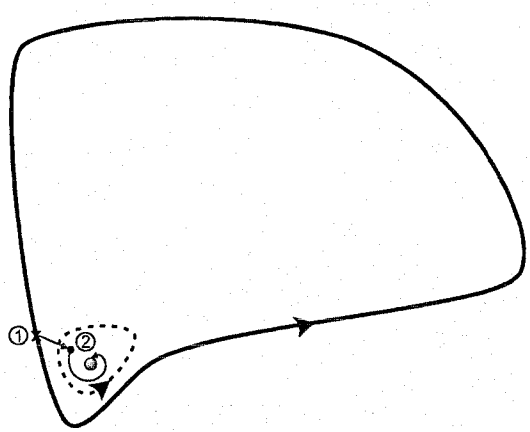

Figure 6.5: The annihilation process for the system specified in Figures 6.1 and 6.2. If the system starts in a carefully chosen configuration at State 1 on the stable limit cycle, the system can be driven to State 2 by applying a carefully chosen stimulus. From this state, it will then go to the stable fixed point.

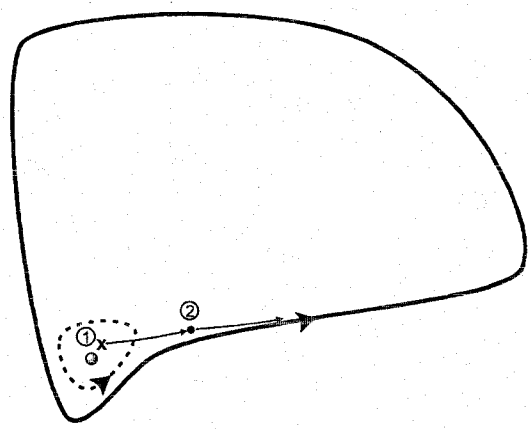

Figure 6.6: The spike generation process for the system specified in Figures 6.1 and 6.2. If the system starts in a stable fixed point or in the State 1, in the close neighborhood of the stable fixed point, the system can be driven to State 2, by applying a specific stimulus, and, from this state, it will go further toward the stable fixed point.

We propose to solve the problem of annihilation from two perspectives:

Problem 1: We plan to analytically demonstrate that the spike annihilation problem has a well-defined solution.

The strategy of solving *Problem 1* consists of:

(a) Computing the steady states.

(b) Analyzing the stability of the steady states.

(c) Computing the bifurcation points and the bifurcation diagram.

(d) Computing the stable and unstable limit cycles.

(e) Analyzing the existence of the stimulus that can annihilate the system.

Problem 2: We intend to numerically compute the characteristics of the stimulus that achieve annihilation, for the settings of Rinzel and Wilson [169].

The strategy of solving *Problem 2* consists of:

1. Proposing an algorithm for computing the moment of insertion, the magnitude, and the duration of the stimulus used to annihilate the system.

2. Analyzing the problem for the case when there are multiple stimuli.

6.3.1 The HH Neuron Annihilation Theorem

Since we are interested in annihilating the spikes, we shall demonstrate that this can be done by invoking a discretized[6] time model. To achieve this, first of all, we rewrite the dynamical system of equations for a bistable model of the HH neuron in a discrete-time manner as:

$$V[n+1] = V[n] + \frac{1}{\tau}[-(a_1 + b_1 V[n] + c_1 V^2[n])(V[n] - d_1) - e_1 R[n](V[n] + f_1) + Bk + \sigma], \quad (6.16)$$

$$R[n+1] = R[n] + \frac{1}{\tau_R}(-R[n] + a_2 V[n] + b_2). \quad (6.17)$$

The general **Theorem of Annihilation** is formally written below.

Theorem 6.4 (HH Neuron Annihilation)

Consider a system described by its discretized dynamical equations:

$$\begin{pmatrix} V[n+1] \\ R[n+1] \end{pmatrix} = \begin{pmatrix} V[n] \\ R[n] \end{pmatrix} + \begin{pmatrix} f_1(V[n], R[n]) \\ f_2(V[n], R[n]) \end{pmatrix} + \underline{S}[n], \text{ with } n = 0, 1, .. \quad (6.18)$$

where f_1 and f_2 specify the unexcited dynamics, and $\underline{S}[n]$ is the excitation applied to the system.

If the system has a stable limit cycle, a stable spiral point and an unstable limit cycle which separates the fixed point and the stable limit cycle, then, there exists

[6] A continuous-time approach cannot be invoked to prove this theorem, because, by virtue of its relation to Hilbert's Sixteenth Problem, it is not known how we can compute the explicit solutions for the system of equations.

an excitation function $\underline{S}[n]$, which equals 0 everywhere except at a specific point $(V[0], R[0])$ on the stable limit cycle, at which point $\underline{S}[0]$ has the value $[A, 0]^T$ for a duration of one iteration, and which when applied to the system, forces it from the stable limit cycle to the stable spiral point.

Proof: Consider the system defined by Equation (6.18), which has the excitation $\underline{S}[n]$.

Analyzing the Jacobian of the system, we observe that it has the same form[7] as the one corresponding to the continuous case. Thus, all the qualitative results obtained in the previous Section are also applicable for the discrete time approach, and thus, the system has a stable fixed point, a stable limit cycle and an unstable limit cycle (also known as a *separatrix*).

For the purpose of proof, we define, three distinct areas in the state space, as depicted by Figure 6.8:

1. We denote A_{In} as the region corresponding to the basin of attraction of the stable fixed point, bordered by the separatrix.
2. We observe two regions outside the separatrix, that can have as their boundaries the tangents in the maximum and minimum 'R' points on the separatrix, the stable limit cycle and the isoclines. We denote them as:
   (a) $A_{Out,1}$: The region where $V[n+1] > V[n]$ and $R[n+1] < R[n]$, and
   (b) $A_{Out,2}$: The region where $V[n+1] > V[n]$ and $R[n+1] > R[n]$.

Let us denote the intersection between the tangents in the maximum and minimum 'R' points on the separatrix, and the stable limit cycle (see Figure 6.8) as V_{A1},V_{A2}, V_{B1}, V_{B2}. The sequence of these points corresponds to the time evolution on the stable limit cycle.

Within the discrete-time model of computation, the problem of annihilation involves proving that there exists a stimulus A, which when applied between V_{A1} and V_{A2} or between V_{B1} and

[7]The Jacobian of the system is obtained by computing the partial derivative with respect to the state variables without involving time (continuous or discrete). If the system variable u is expanded infinitesimally around a quiescent point u_0 as $u = u_0 + \delta u$, the continuous system will lead to $\frac{du}{dt} = F(u)$ and the discrete system will lead to $u_{n+1} = F(u_n)$. By dropping the quadratic and higher order terms in δu, we can obtain for each of these two systems: $\frac{d\delta u}{dt} = DF(u_0)\delta u$ and $\delta u_{n+1} = DF(u_0)\delta u_n$, respectively. Observe that the Jacobian in both cases has the same form.

V_{B2} moves the system into the basin of attraction of the stable fixed point, namely within A_{In}. Observe that if the system is within this region, it is inside the separatrix, and it will thus converge to the fixed point. Indeed, it suffices to show that this input can be applied for a single time unit.

Consider the scenario in which the system is on an initial point $V[0]$ between V_{A1} and V_{A2}. Since the stable limit cycle and the separatrix are non-intersecting, there exists a positive "distance" d_0 between $V[0]$ and the separatrix. We intend to determine a value of A that moves the system from $(V[0], R[0])$ to an arbitrary point in A_{In}. Clearly, the magnitude A has to satisfy the condition :

$$(V[1] - V[0]) > d_0. \tag{6.19}$$

Computing V[1] as a function of V[0] we have:

$$V[1] = V[0] + f_1(V[0]) + A. \tag{6.20}$$

The condition (6.19) becomes:

$$(V[0] + f_1(V[0] + A - V[0]) > d_0 \implies (f_1(V[0] + A) > d_0 \implies A > d_0 - f_1(V[0]). \tag{6.21}$$

We now invoke the monotonic property of the function $V[n]$, that corresponds to the portion of the state space below the isocline, where $V[n+1] > V[n]$, namely in A_{In}. Here, the term $f_1(V[n]) = V[n+1] - V[n]$ is positive. We thus see that there exists a value of A, satisfying the condition (6.21), that moves the initial point of the system between V_{A1} and V_{A2}, to be in A_{In}. We have now to evaluate the sign of the expression $[d_0 - f_1(V[0])]$. Starting from $(V[0], R[0])$ on the stable limit cycle, with $V[0]$ between V_{A1} and V_{A2}, we know that, without adding the A stimulus, the next point $(V[1], R[1])$ will also be on the stable limit cycle. The difference between $V[1]$ and $V[0]$ is exactly $f_1(V[0])$. In this context, $f_1(V[0])$ will satisfy the condition $f_1(V[0]) < d_0$, because there is no intersection, between the limit cycle and the unstable limit cycle (described by the separatrix). We have now thus proved that $[d_0 - f_1(V[0])] > 0$. Thus, A is a positive value satisfying $A > d_0 - f_1(V[0])$.

The analogous rationale can be used if the initial point $V[0]$ is between V_{B1} and V_{B2}. In this case, there exists a distance d_1 (a positive value) between $V[0]$ and the separatrix. We intend

again to find a value of A that moves the system into region A_{In}. The magnitude that A has to satisfy, leads to the condition :

$$(V[0] - V[1]) > d_1. \tag{6.22}$$

Observe also that this part of the state space, (also below the isocline), corresponds to $V[n+1] > V[n]$, and, thus, the term $f_1(V[n]) = V[n+1] - V[n]$ is also positive.

Computing $V[1]$ and $R[1]$ as a function of $V[0]$ and $R[0]$ we have:

$$V[1] = V[0] + f_1(V[0]) + A. \tag{6.23}$$

The condition (6.22) thus becomes:

$$(V[0] - V[0] - f_1(V[0]) - A > d_1 \implies A < -d_1 - f_1(V[0]). \tag{6.24}$$

Observe that both d_1 and $f_1(V[0])$ are positive quantities, and thus the term $[-d_1 - f_1(V[1])]$ is a negative value. We have thus proved that there exists a value of A that moves the initial point of the system from being between V_{B1} and V_{B2}, to be within A_{In}.

Since both these cases are exhaustive, the theorem is proved. □

Comments:

1. For each interval $[V_{A1}, V_{A2}]$ or $[V_{B1}, V_{B2}]$ it is possible to chose a value $V[0]$, that corresponds to a particular time instant in the phase space. This time instant can be described as a percentage of the total period of time of the spike. For each chosen $V[0]$, there is a value d_0, and a corresponding magnitude A of a unit time stimulus, determined by the conditions (6.21) or (6.24).

2. The above proof shows that for any neuron described by Equation (6.18), there exists an unit time stimulus with the magnitude A satisfying the property that if it is applied in any place on the limit cycle between V_{A1} and V_{A2} or between V_{B1} and V_{B2} it will annihilate the spiking behavior. The problem of annihilation has also a solution for the case when the stimulus is longer then the unit of time. In this case, we need to define in the state space four regions inside the separatrix (see Figure 6.8), that can be bordered by the isoclines of the system, namely :

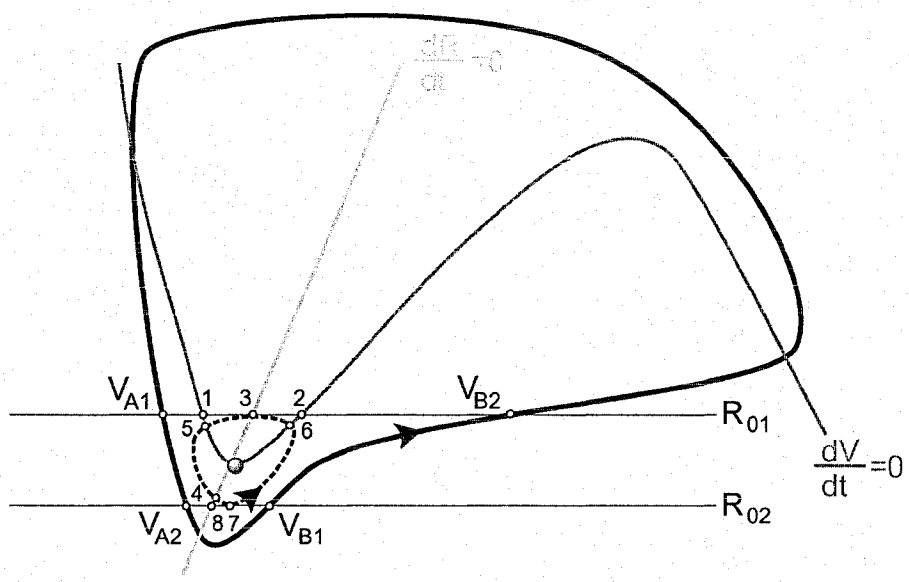

Figure 6.7: The stable spiral point, the stable and the unstable limit cycle for the bi-stable HH neuron.

(a) $A_{In,1}$ with the property $V[n+1] < V[n]$ and $R[n+1] < R[n]$,

(b) $A_{In,2}$ with the property $V[n+1] < V[n]$ and $R[n+1] > R[n]$,

(c) $A_{In,3}$ with the property $V[n+1] > V[n]$ and $R[n+1] > R[n]$,

(d) $A_{In,4}$ with the property $V[n+1] > V[n]$ and $R[n+1] < R[n]$.

The duration of the stimulus and its magnitude will determine if the system will move from the stable limit cycle, namely from a point in $[V_{A1},V_{A2}]$ to $A_{In,1}$ or to $A_{In,4}$, both of them *via* $A_{Out,1}$. The same determination has to be made if the system has to move from a point in $[V_{B1},V_{B2}]$ to $A_{In,2}$ or to $A_{In,3}$ *via* $A_{Out,2}$.

6.3.2 The numerical approach

In order to discover the properties of the stimulus which achieves the spikes annihilation, we have also opted to simulate this numerically. To do this, we have to work towards controlling the

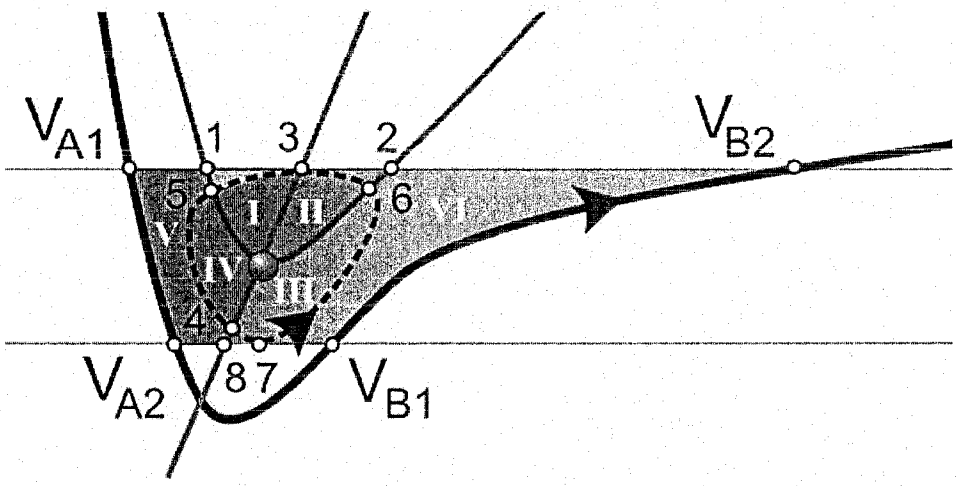

Figure 6.8: A zoom-in of the Figure (6.7), namely the phase space of the bi-stable HH neuron. The regions $A_{Out,1}$ and $A_{Out,2}$ correspond to *Area V* and *Area VI*, respectively. The regions $A_{In,1}$, $A_{In,2}$, $A_{In,3}$, and $A_{In,4}$ correspond to *Area I*, *Area II*, *Area III*, and *Area IV*, respectively.

model, namely, to move the system to a bi-stable state, in the neighborhood of the bifurcation point. All these steps will be discussed in the next Section.

6.4 Experiments

In this Section, the analytical results described in Section 6.3 are experimentally evaluated to verify their validity, and to explore the state space characteristics for each parameter of the annihilation stimulus. If a background stimulus B is applied to create a train of spikes, we demonstrate that it is possible to annihilate the limit cycle with an additional *brief* stimulus, and to move the system from a stable limit circle to an unstable spiral point.

The solution to this problem has to respond to the following questions:

1. What is the amplitude of the stimulus?
2. What is the suitable phase when the stimulus should be applied?

3. How long should the stimulus be?

4. Is it possible to apply two successive pulses instead of only a single one, in which the phase specification is not so precise? Would this pair of two successive pulses possess the property that they would together be able to annihilate the spikes if the first one, by itself, could not?

In order to analyze the effect of the stimulus, we have to choose initial values for V and R. We have studied this for various numerical settings, but present only one scenario here, in the interest of brevity. In Figure 6.9, we present an example of train spikes that we propose to annihilate with a stimulus. This train of spikes started from $V = -0.7043$ and $R = 0$, and was generated with $B = 0.08$. In addition, Figure 6.10 illustrates the corresponding Phase Space of the bi-stable neuron.

In Figure 6.11, we observe an example of annihilation, where the duration of the train of spikes is 40 ms. In Figure 6.12, we present the phase space for the bi-stable neuron, which is amplified in Figure 6.13 to illustrate a zoom-in of the Phase Space. In the next two figures, Figure 6.14 and 6.15, we present the same train of spikes with the same stimulus, depicted for 100 ms.

Figure 6.16 is an example of an unsuccessful annihilation observed using a stimulus $\sigma = 0.2$, applied at the time instant 3.4 ms from the beginning of the simulation.

From the bifurcation diagram, we chose the background stimuli B to be between 0.68 and 0.7. These stimuli generate a spike train. We here chose $V = -0.7043$ and $R = 0$ as initial values for the subsequent simulations.

For an additional stimulus σ, namely, a pulse of 0.1 ms duration[8], we identified its position of insertion and its amplitude. In Table 6.4, we present the range of values for σ (the minimum and the maximum values) for which we can annihilate the spikes. Each range is computed for different times of insertion of the stimulus (from 3.0 ms to 4.4 ms) and for different values of the quantity B. The neuron exhibited spikes only for a range of B, which spanned values from 0.68 to 0.70 $\mu A/100$. The results from Table 6.4 are depicted in Figure 6.17.

[8]We will analyze later the effect of the duration of the pulse.

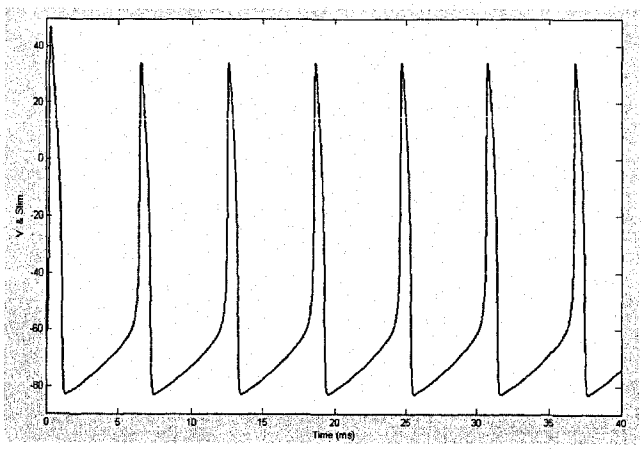

Figure 6.9: The train of the spikes generated with $B = 0.08$.

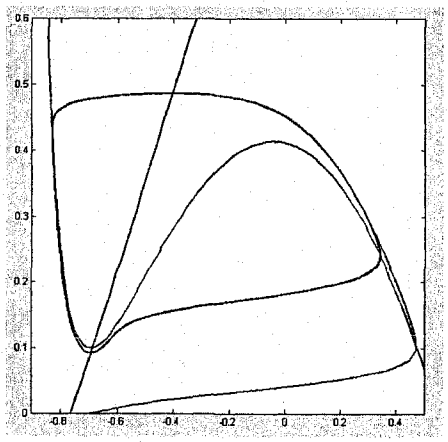

Figure 6.10: The phase space of the train of the spikes generated with $B = 0.08$.

	$B = 0.68$		$B = 0.69$		$B = 0.70$	
When	σ_{min}	σ_{max}	σ_{min}	σ_{max}	σ_{min}	σ_{max}
3.0ms	0.4	1.54				
3.1ms	0.14	1.57				
3.2ms	0.06	1.47	0.47	1.15		
3.3ms	0.028	1.34	0.19	1.23	0.50	0.97
3.4ms	0.014	1.21	0.09	1.17	0.21	1.08
3.5ms	0.008	1.09	0.05	1.06	0.11	1.02
3.6ms	0.005	0.97	0.03	0.95	0.062	0.93
3.7ms	0.003	0.85	0.018	0.84	0.03	0.83
3.8ms	0.002	0.74	0.016	0.73	0.027	0.72
3.9ms	0.002	0.63	0.01	0.63	0.02	0.62
4.0ms	0.002	0.53	0.008	0.53	0.016	0.52
4.1ms	0.002	0.45	0.007	0.44	0.015	0.43
4.2ms	0.002	0.35	0.007	0.34	0.015	0.33
4.3ms	0.002	0.25	0.008	0.25	0.017	0.25
4.4ms	0.002	0.16	0.011	0.15	0.024	0.14

Table 6.4: The amplitude and the moment of insertion of the stimulus σ in order to annihilate the spikes.

From this simulation we can conclude that :

1. The neuron spikes only for a specific range of values of B;
2. If the neuron generates spikes, these can be annihilated with particular stimuli found in the area plotted in Figure 6.17.

Consider now the problem of finding the vulnerable phase of the neuron, namely the duration of the period of the signal when the stimulus can be inserted in order to annihilate spikes.

For a value of $\sigma = 0.7$, we see from Figure 6.17 that the length of the vulnerable phase is between 3 ms to 4.4 ms, namely a width of 1.4 ms. Since the period is 6 ms, the neuron has an interval of 23.33% of its period where one can insert a proper stimulus to achieve this annihilation.

The reader can observe that for the experimental results reported, we conducted experiments with three different background stimuli in order to to generate a bi-stable neuron, namely with $B = 0.68$, $B = 0.69$ and $B = 0.70$. For all these values, we present in Figure 6.17 three

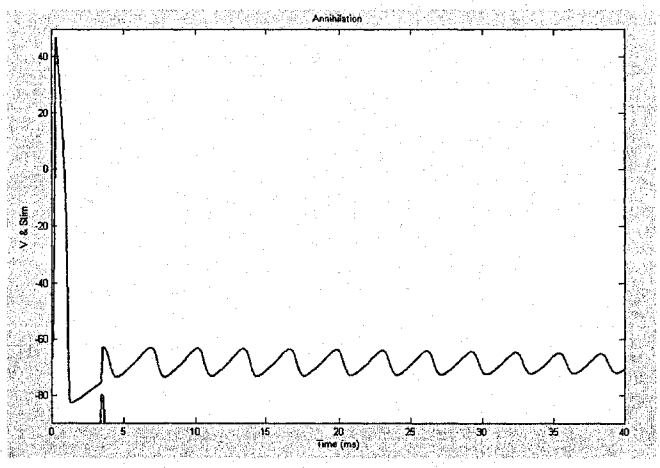

Figure 6.11: The annihilation of the train of spikes. The presentation is made for 40 ms.

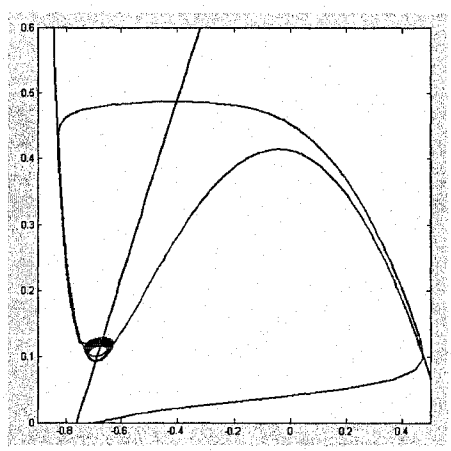

Figure 6.12: The phase space of a system with the train of spikes annihilated by a stimulus, σ. The presentation is made for 40 ms.

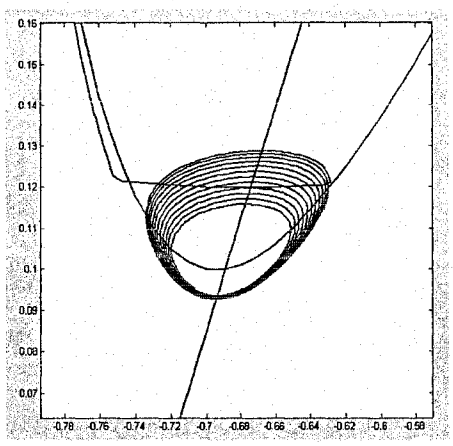

Figure 6.13: A zoom-in of the phase space of a system with the train of spikes being annihilated by a stimulus σ. The presentation is made for 40 ms.

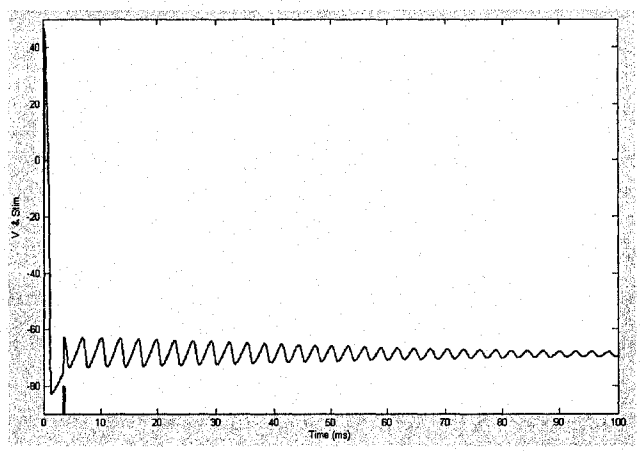

Figure 6.14: The annihilation of the train of spikes. The presentation is made for 100 ms.

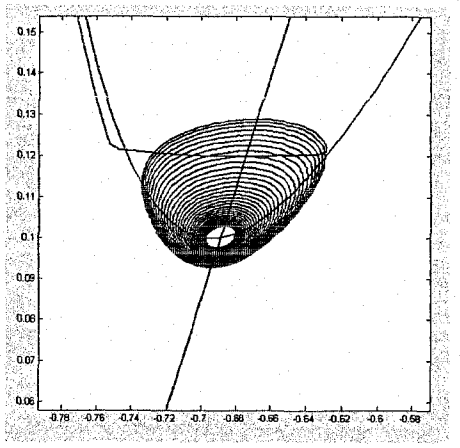

Figure 6.15: A zoom-in of the phase space of a system with the train of spikes being annihilated by a stimulus σ. The presentation was made for 100 ms.

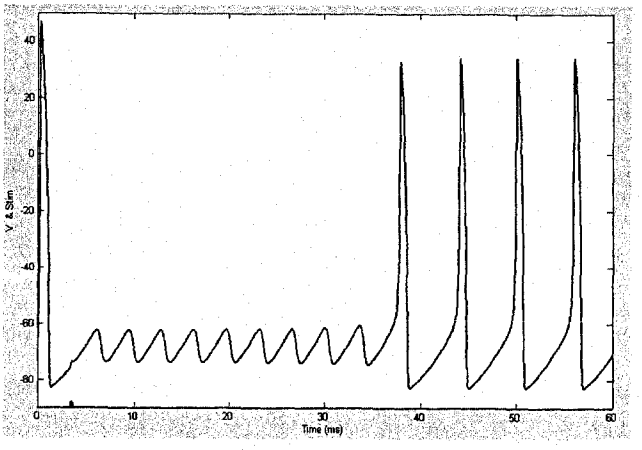

Figure 6.16: An example of an unsuccessful attempt to annihilate the spikes by using a stimulus σ applied at a time instant of 3.4 ms.

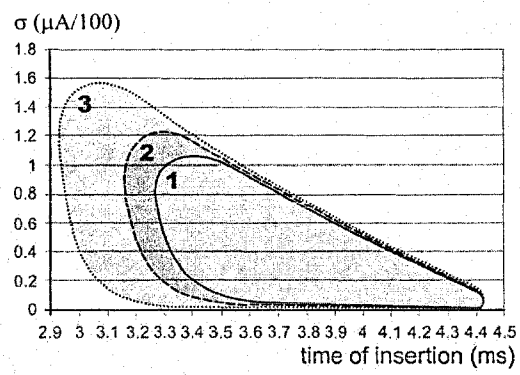

Figure 6.17: The three areas for the three different values for the background, B, namely 0.70 (*Area 1*), 0.69 (*Area 2*) and 0.68 (*Area 3*).

areas, namely those depicted by *Area 1*, *Area 2*, and *Area 3*. Fortunately, there seems to be an inclusion relationship between these three areas, namely *Area 1* is included in *Area 2* and *Area 3*. Consider now the scenario when a population of neurons from the brain receives a constant stimulus with the magnitude having minimum value of 0.68 for an interval of time. If the task is to annihilate this population, the imprecision of determining the background stimulus will not affect our selection of the annihilation stimulus. Choosing one with a magnitude corresponding to the minimum background is successful because such a stimulus is common for all background stimuli greater than this minimum one. For example, the area corresponding to a $B = 1$ includes the area corresponding to the minimum $B = 0.68$. This observation makes the choice of a successful annihilation stimulus easier and independent from the precision of determining B.

6.4.1 The Duration of the Stimulus

A brief analysis of the *duration* of the stimulus would be beneficial. Such a study would help the reader to decide on the best stimulus to be used to achieve the annihilation. To do this, we explore, numerically, the range of the duration for a stimulus with magnitude equal to unity. For example, if the time of insertion is set to be at 3.5 ms, the range of the duration of the stimulus can be between 0.0099 ms and 0.1095 ms, independent to the value of B whose value

lies between 0.68 and 0.7.

We mention that this numerical determination was made in a scenario with an *a priori* setting of the amplitude of the stimulus. In the general case, we want to apply a stimulus with the duration δ_1, smaller than the period of firing of the HH neuron, for example 6 ms. One possible approach to determine the magnitude of the stimulus is by using a heuristic search. An algorithm for computing a solution contains, first of all, the determination of the number of iterations corresponding to the duration of the stimulus, namely $k = \frac{\delta_1}{\delta_0}$, where δ_0 is the numerical time unit, typically chosen to be very small.

Next, we have to determine, by a heuristic search, the magnitude, A, of the stimulus, by estimating the pairs (V_0, R_0) and (V_{new}, R_{new}). This involves using k and the rule of computing the new initial point, proposed in Section 3.1, namely:

$$V_{new} = V_0 + f_1(V_k) + ... + f_1(V_0) + k * A,$$
$$R_{new} = R_0 + f_2(R_k) + ... + f_2(R_0).$$

The reader should observe that we have presented here the difficult scenario of achieving the spike annihilation with a pulse of duration "$k * \delta_0$". In a clinical application, the solution to the problem of annihilation can be reduced to the computation of the magnitude of a *brief* pulse, where it is sufficient to set $k = 1$.

6.4.2 How Many Stimuli?

In this Sub-section, we analyze the problem of using two successive stimuli to annihilate the spike train. This pair of successive pulses has the property that the first pulse is not able to annihilate the spike train by itself. However, in order to cumulate the effects of the stimuli, we have to apply a second pulse so as to have the distance in time between stimuli less than the period of firing of the HH neuron. Intuitively, if the distance between the stimuli is more than a period, the neuron does not memorize the effect of the first stimulus, which we can also verify.

To simulate this in a realistic setting, we assume that we don't know exactly the juncture in time where we can insert the single stimulus in order to annihilate the spikes, namely the range $[\theta_1, \theta_2]$. Thus, we intend to insert two stimuli, having the same amplitude and a temporary distance between them, δ_2.

Consider the general problem of inserting the first stimulus anywhere in the range of $[\theta_1 - \varepsilon, \theta_1 + \varepsilon]$. By proposing δ_2, the temporary distance between them, we intend to devise an algorithm for the heuristic search of the magnitude of the stimuli.

We set the initial magnitude to a small value. The proposed algorithm, then, has three phases:

- The first step consists of the computation of the pair (V^1_{new}, R^1_{new}), after the insertion of the first stimulus;
- The second step consists of the computation of the pair (V, R), knowing the pair (V^1_{new}, R^1_{new}) and the number of iterations required by dividing δ_2 by the integration time unit.
- The third step consists of the computation of the (V^2_{new}, R^2_{new}), after the insertion of the second stimulus.

If, after this computation, the new point, namely (V^2_{new}, R^2_{new}), is not a point inside the unstable limit cycle, we increase the initial magnitude with a quantity ΔA, and we repeat all the above three steps. Clearly, it is a straightforward "Hypothesize and Test" heuristic search scheme for the amplitude of the stimuli. The problem will lead to (or not lead to) a solution, depending on the values of ε and δ_2.

In this way, a pair of stimuli with a carefully chosen amplitude and a fixed temporal distance between them can annihilate a train of spikes by decreasing the accuracy of the place of insertion. The first stimulus is chosen with a random magnitude and is inserted into the neuron. At his juncture, we will not know if this stimulus is successful or not in annihilating the spikes. By taking into consideration *a posteriori* its magnitude and its moment of insertion, we want to be able to set the properties of the second stimulus so as to annihilate the neuron, if the first stimulus was not successful. In this way, we can extrapolate the problem of applying, in a range of time $[\theta_1 - \varepsilon_1, \theta_2 + \varepsilon_2]$, a pair of two stimuli with the same amplitude A, with a duration equal to unity and a temporary distance between them of δ_2. This leads us to a scheme for computing the properties of the second stimulus when the first stimulus is given. However, the problem of determining A, ε_1 and ε_2, having only δ_2, is still open.

By simulations, for the setting described in [169], we showed that, for a *Background* of 0.7,

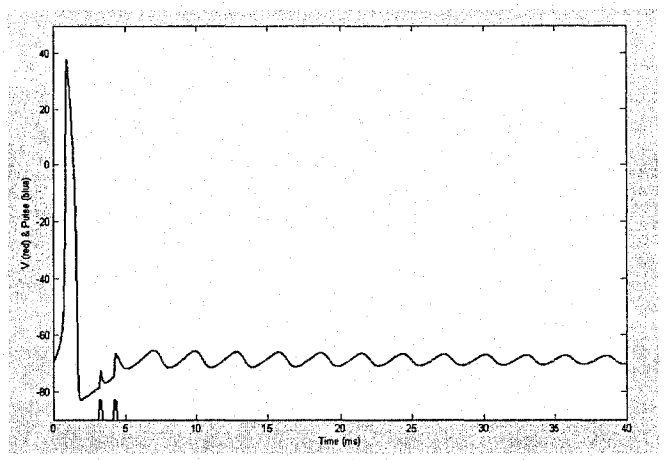

Figure 6.18: The annihilation using two stimuli with amplitude 0.7, the first applied at 3.2 ms and the second applied at 4.2 ms.

the range $[\theta_1, \theta_2]$ is 3.3 ms - 4.4 ms (see Table 6.4). We have tested the effect of a pair of two successive stimuli, the first being applied too early, at 3.2 ms, and the second one, at 4.2 ms. Both stimuli have the same amplitude, 0.7. From Table 6.4, we observe that the successful annihilation can be achieved with a stimulus having the amplitude between 0.015 and 0.33. In the scenario with the first stimulus being inserted too early, the second one was successful in annihilating the spikes at an amplitude of 0.7. Thus, the presence of the first stimulus in a zone outside of $Area1$ (see Figure 6.17) has a positive effect, allowing the second stimulus to achieve annihilation, also from a zone outside of $Area1$.

In Figure 6.18, we present an example of a successful annihilation by using two stimuli with amplitude of 0.7, the first one being applied at 3.2 ms, and the second one at 4.2 ms, where the neuron has a background stimulus, B, equal to 0.7.

6.4.3 Spike Generation

We present here, for sake of the completeness of the modelling approach, a particular case involving spike generation. In Section 2, we stated that the HH neuron has two equilibria, a fixed point and the limit cycle, both of them co-existing and being stable. Thus, the HH neuron

is bi-stable and, with a carefully chosen synaptic input, it is possible to switch its behavior from a resting state to a spiking (spike generation) state or from a spiking state to a resting state (which is the spike annihilation phenomenon). The spike annihilation problem was solved in Section 3. Here, we study the generation of the spiking behavior.

If the neuron is in the resting state, namely in the stable fixed point, there are no changes in time. Thus, there is no preference for the moment when one can insert a stimulus in order to move the point (V, R) to be outside of the unstable limit cycle. The stimulus will modify only the V component of the pair (V, R). Observe that in this case there are two limit values for this problem: A positive minimum value that moves the system to the left side of the fixed point and outside of the unstable limit cycle, and a negative maximum value that moves the system to the right side of the fixed point while being outside of the unstable limit cycle.

Again, to demonstrate that this can be achieved, we tested by simulations, the scenario when the system is in an equilibrium point ($V = 0.6889$, $R = 0.1$), for $B = 0.7$. In this situation, the system remains in this fixed point forever. If, however, at anytime we excited the system with a single pulse, for example one with the amplitude equal to unity, the system starts to oscillate *forever*. This phenomenon is portrayed in Figure 6.19. We observe here that, without any background activity, namely with $B = 0.0$, the system cannot oscillate, because it is not bi-stable.

6.5 Conclusions

This Chapter discussed the HH neuron and formally derived various properties of its stability. It also described the first (to the best of our knowledge) reported formal proof that the problem of spike annihilation has a well defined solution, and presented an algorithm for computing the properties of the stimulus. We elaborated, in Sections 6.3 and 6.4, all the details of this algorithm. We add that the method of perturbation with brief stimuli differs from the classical approach of modifying the control parameter and changing the Jacobian of the system. In our approach, we keep the system bi-stable all the time, and our task is to switch between these two states without modifying their stability.

To conclude, in this Chapter, we have analytically proved the existence of the brief current

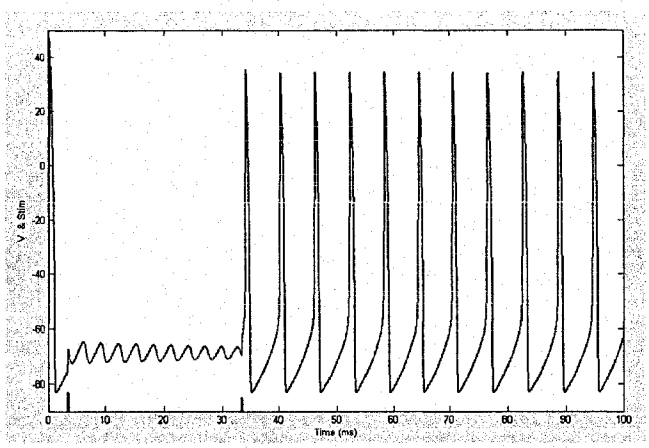

Figure 6.19: The annihilation and the generation of a new train of spikes. The first stimulus has an amplitude of 0.7 and is applied at 3.5 ms. The second stimulus has an amplitude of 0.5 and is applied at 33.5 ms. The value of B is 0.7.

pulse that annihilates the spikes of the HH neuron, when delivered to its repetitively firing state, and have also analyzed the properties of this pulse, namely, the range of time when it can be inserted, its magnitude, and its duration. In addition, we have also studied the solution of annihilating the spikes by using two successive stimuli, where the first one is unable to annihilate the spikes by itself. We have also briefly investigated the inverse problem to annihilation, namely, the spike generation problem, and proposed a straightforward numerical solution.

Chapter 7

Controlling Small Scale Models: Behavioral Synchronization in a Network of Bursting Neurons

7.1 Introduction

Bursting is a process in which a neuron alternates between a quiescent behavior (i.e., a salient non-spiking phase) and a rapidly varying spiking state where the latter is a fast repetitive spiking phase. A typical explanation for the bursting phenomenon is based on the dynamics of a system of nonlinear equations containing both fast and slow variables. The fast variables generate a firing activity and exhibit multistability between a resting state and the regular firing state. The slow variables, on the other hand, can be considered as control parameters for the fast variables.

Many mathematical complex models of busting neurons, inspired from the behavior of biological systems, have been developed. But these models are analytically intractable when the individual neurons are connected in networks [7, 40, 44, 95, 135, 152, 166].

The alternative strategy is to decrease the complexity to lead to the so-called phase oscillator neuron. Although the network built with *these* phase-oscillators allow accurate mathematical investigations [50, 63, 71, 94], the derived results are far from having biological significance.

7.1.1 Our Contribution

The contribution of this Chapter pertains to novel results related to the Bursting neural network as motivated by Rulkov's model [144]. Observe that, as mentioned earlier, such a model permits an explanation for the so-called bursting phenomenon in which a low frequency pulse output appears as an envelope of high frequency spikes. This Chapter includes the following results:

- It presents a stability analysis for *small* scale networks consisting of bursting neurons.
- It proves that if the inter-neuron coupling is arbitrarily small, (which is an accepted model that leads to bursting) the network exhibits chaos as demonstrated by a Lyapunov analysis.
- It shows that increasing the number of neurons in the network does not significantly increase the synchronization of the bursting. Indeed, we show that (with respect to the number of neurons) the network rapidly converges to a synchronized behavior. This is demonstrated by the inclusion and computation of two newly-proposed measures.
- Finally, it presents methods for controlling the slow variables in the network, leading to the goal of modifying the so-called *behavioral* synchronization[1].

All of these results are, to the best of our knowledge, novel, and of a pioneering sort.

In Section 7.2 we present an overview of the field, including a model of the bursting neuron. In Section 7.3 we investigate the conditions for triggering the burst in a network of coupled neurons. In Section 7.4 we describe a stability analysis of the system and present numerical results associated with this analysis. In Section 7.5 we investigate an asymptotic evolution of the proposed new measures used for describing the behavioral synchronization together with the cross-correlation. We also discuss a new hypothesis for the epileptogenesis. Section 7.6 includes new methods for controlling the fast and the slow variable in the network. Finally, Section 7.7 concludes the Chapter.

[1]The consequences of this to model the genesis of epileptic seizures, is also hypothesized.

7.2 Overview of the Field

The nervous system is perpetually active, creating its own dynamics, including periodic rhythms termed as beta (12-30 Hz) and gamma (30-80 Hz) patterns. These rhythms[2] are controversial, partly because they are technically difficult to induce and to spot. Some open questions remain:

- How does the brain use these rhythms and how are they generated ?
- What determines the frequency of the beta or gamma rhythms ?
- Why does the same collection of cells sometimes display a gamma rhythm and otherwise[3] a beta rhythm ?
- What causes the activity in some populations of neurons to be, at least temporarily, coherent?

Mathematics can play a central role in the part of neuroscience that has to do with these dynamics. The above questions are very difficult to solve because of the complexity of the underlying equations and the large number of interacting dynamic processes, each with their own respective time scales [93]. The objective of resorting to a formal mathematical model is that we can explain how the biophysics of the cells and synapses work together to create coherent synchronous rhythms.

The problem of describing the synchronization of nonlinear oscillators has been studied extensively. In particular, Winfree [175] and Kuramoto [94] have contributed with strong analytic results. Indeed, many kinds of synchronization (i.e., coordination[4] with respect to time) were reported including those described as Amplitude synchronization or Phase synchronization[5][128].

[2]The rhythms can appear for epochs under a second and require appropriate data filtering if they are to be observed.

[3]The same piece of tissue may be capable of multiple rhythms, with transitions between them. The hippocampal slice provides such an example, as shown by the 1997 work of Whittington and his collaborators [167]. If the slice is stimulated, provoking activity in both the excitatory and inhibitory cells, it displays a transient gamma rhythm. At a higher level of stimulation, the rhythms starts off as a gamma rhythm and then undergoes a period of 150-200 ms of incoherence, after which it switches to a slower beta frequency rhythm.

[4]The definition from the Merriam-Webster dictionary states that *to synchronize* is to cause *to happen at the same time.*

[5]Phase synchronization is the process by which two cyclic signals not only converge to a single common frequency, but also tend to oscillate with a *common* phase angle.

In this Chapter, we propose a new category of synchronization analyzed in a network of bursting neurons. Instead of describing this phenomenon in terms of two signals, we propose a synchronization that is based on behavior, which we call *"Behavioral Synchronization"*.

Consider two systems which are in their two functional modes called A and B, respectively. If both of them are in the same mode, either A or B, then they are said to be in a *synchronized behavioral* state, even though the outputs of the systems may be uncorrelated. In the model we proposed for investigation, the two output signals are chaotic and uncorrelated, and yet the systems can be behaviorally synchronized.

We investigate, here, a network of neurons that can generate the so-called bursting (firing) behavior. The individual neuron displays characteristic firing patterns determined by the number and kind of ion channels in their membranes. The firing process of any neuronal circuit depends on the interaction between the intrinsic properties of the individual neurons and the synaptic interactions that connect them into functional ensembles. One of the related neuroscience problems is to explain how the system's dynamics depend on the properties of the individual neurons, the synaptic architecture by which they are connected, and the strength and time duration of the synaptic connections.

7.2.1 The Model of Bursting Neuron

In this Section, we present a particular model of a Bursting neuron proposed by Rulkov [144], which is formally described by two dimensional maps as:

$$x(n+1) = \frac{\alpha}{[1+x(n)^2]} + y(n), \tag{7.1}$$

$$y(n+1) = y(n) - \sigma x(n) - \beta, \tag{7.2}$$

where $x(n)$ and $y(n)$ are the fast and slow dynamical variables of the "oscillator" neuron, respectively. The slow evolution of $y(n)$ is due to the small values of the positive parameters β and σ, which are of the order of 0.001 [144]. The value of the parameter α is selected to be in the region $\alpha > 4$, where the map produces chaotic oscillations in $x(n)$. Depending on the parameter α, the neuron demonstrates two qualitatively different regimes of chaotic behavior, namely, continuous

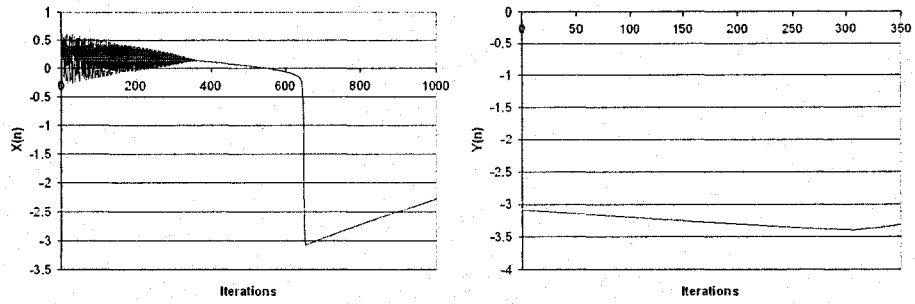

Figure 7.1: The variations of $x(n)$ (on the left) and $y(n)$ (on the right) for a Bursting neuron with $\alpha = 3.3$.

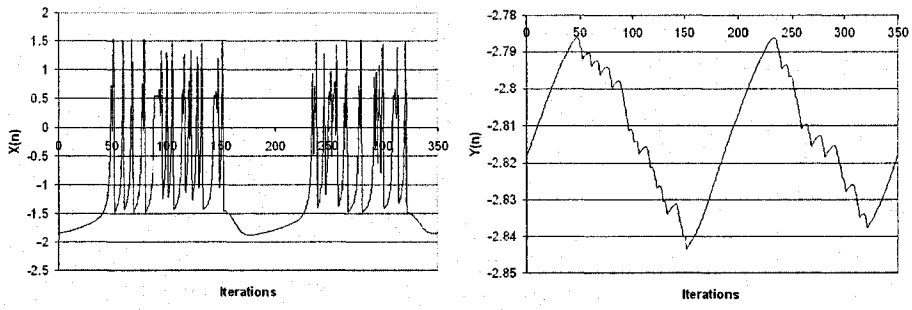

Figure 7.2: The variations of $x(n)$ (on the left) and $y(n)$ (on the right) for a Bursting neuron with $\alpha = 4.3$.

chaotic oscillations and chaotic bursts. This bursting dynamics was confirmed in experiments done with biological neurons [49].

Figures 7.1-7.3 depict the behavior of $x(n)$ and $y(n)$, as a function of time, when $\alpha = 3.3$, $\alpha = 4.3$, and $\alpha = 5.3$, respectively. Note that the variation of $x(n)$ and $y(n)$ for the Bursting neuron when $\alpha = 3.3$ in Figure 7.1, is void of bursting, the variation of $x(n)$ and $y(n)$ for the Bursting neuron when $\alpha = 4.3$ in Figure 7.2, where chaotic bursting is found, and for $\alpha = 5.3$ in Figure 7.3, where the system is continuously chaotic.

The slow evolution of $y(n)$ for the next m steps [144] is given by:

$$y(n+m) = y(n) - m(\beta + \sigma y^*(n,m)), \tag{7.3}$$

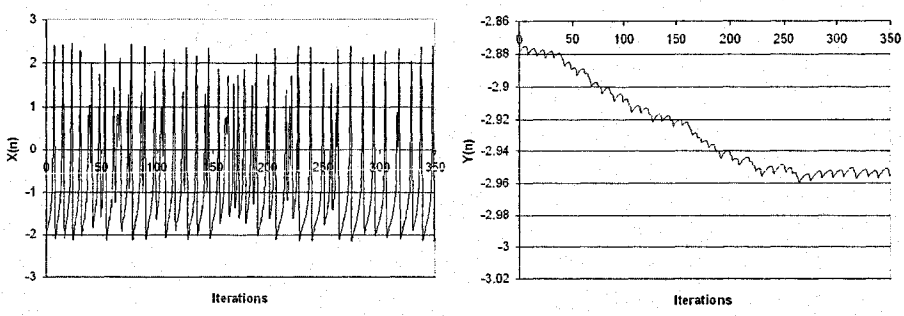

Figure 7.3: The variations of $x(n)$ (on the left) and $y(n)$ (on the right) for a Bursting neuron with $\alpha = 5.3$.

where $y^*(n,m) = \frac{1}{N}\sum_{j=n+1}^{n+m} x(j)$ is the mean value of $x(n)$ computed for m consecutive iterations.

From Equation (7.3), we see that the value $y(n)$ increases very slowly during the next m steps if $\sigma y^*(n,m) < -\beta$, and decreases very slowly if $\sigma y^*(n,m) > -\beta$. From this behavior, we can approximate $y(n)$ to be a constant of value γ. With this observation, Equation (7.1) becomes:

$$x(n+1) = \frac{\alpha}{[1+x(n)^2]} + \gamma. \tag{7.4}$$

For a specific value of γ, the system leads to a bifurcation which corresponds to the beginning of the burst in the system. The end of the chaotic burst is due to the external crisis of the chaotic attractor in the system. The duration of the chaotic burst is determined by the time interval that is required for the slow variable $y(n)$ to move from value γ_1 to γ_2. The complete mathematical explanation of these two bifurcations can be found in [144], and is omitted here as it is not required for the rest of this Thesis.

7.3 The Network of Neurons

Having now introduced individual Bursting neurons, we consider a network built with N such "oscillating" neurons [144], which are coupled electrically to each other through the variable $x(n)$. In this case, the variables[6] $X(n)$ and $Y(n)$ obey:

$$X_i(n+1) = \frac{\alpha}{[1+X_i(n)^2]} + Y_i(n) + \frac{\epsilon}{N}\sum_{j=1}^{N} X_j(n), \tag{7.5}$$

with

$$Y_i(n+1) = Y_i(n) - \sigma X_i(n) - \beta, \tag{7.6}$$

where $X_i(n)$ and $Y_i(n)$ are, respectively, the fast and slow dynamical variables of the i^{th} neuron and ϵ is the coefficient that describes the coupling between the neurons.

The coupling between neurons influences the fast dynamics of each neuron by adding the value $\Delta\gamma = \frac{\epsilon}{N}\sum_{j=1}^{N} X_j(n)$ to the almost constant term γ, in Equation (7.4). When the i^{th} neuron approaches the first bifurcation, its increased value of $\gamma+\Delta\gamma$ pushes the neuron over the bifurcation value and triggers the burst. The greater the value of N, the number of neurons which are involved, the greater $\Delta\gamma$ will be, and the triggering impact that is experienced by the remaining cell will be correspondingly larger. Such a switching phenomenon is also observed at the end of each burst. The condition for this is formalized below. The proof is essentially taken from [144], but we have filled in the missing details and modified the result for the scenario of a *network*.

Lemma 7.1.

Given a system of N neurons described by Equations (7.5-7.6). There exists a threshold , denoted $\Delta\gamma_{max}$, such that the system generates synchronized bursts if $\Delta\gamma > \Delta\gamma_{max}$.

[6] We mention here that the notation, which we used earlier, describes an individual neuron with state variables $x(n)$and $y(n)$. In the case of the *network* of Bursting neurons, the corresponding notation used for the i^{th} neuron is $X_i(n)$ and $Y_i(n)$, respectively.

Proof:

Consider the equation of the fast variable corresponding to *a single* neuron written as a uni-dimensional map [144]:

$$X(n+1) = F(X(n), \alpha, \gamma) = \frac{\alpha}{[1 + (X(n))^2]} + \gamma, \tag{7.7}$$

where the dynamics of the fast variable is considered independently of the second variable, and we assume that $\gamma = Y(n)$.

It has been shown in [144] that, in the γ-space, this map has three fixed points, referred to here as X_1^*, X_2^*, and X_3^*. However, if γ is larger than a threshold, denoted by γ^*, a bifurcation occurs and the fixed points X_1^* and X_2^* merge together and disappear, at which point, the neuron starts to burst.

If we now consider a *system* of neurons (in contrast to the above, where we performed an analysis for a *single* neuron), the uni-dimensional map corresponding to any arbitrary neuron can be written as:

$$X_i(n+1) = F(X_n, \alpha, \gamma) = \frac{\alpha}{[1 + (X_i(n))^2]} + \gamma + \Delta\gamma, \tag{7.8}$$

where, again, we have made the assumption that $\gamma = Y_i(n)$, and where we added an additional term $\Delta\gamma = \frac{\epsilon}{N} \sum_{j=1}^{N} X_j(n)$, which contains the contribution of the other participating neurons. Again, as in [144], the expression $\gamma + \Delta\gamma$ must be larger than the threshold in order to generate bursts. However, the variation on the term γ is small in comparison with the variation of $\Delta\gamma$, because $\Delta\gamma$ is a computational term derived from the fast variables.

From the above bifurcation argument, we see that if the term that corresponds to γ is increased till it crosses the threshold, the bursting phenomenon occurs. However, from the network's perspective, we now encounter two ways by which the γ-related components can be increased, namely, first of all, the γ term itself, as given in [144], and secondly, the $\Delta\gamma$ term, which is the contribution from the others neurons, and which is also of the same sign as γ.

Clearly, the combination of these two terms crosses the corresponding bursting threshold if the first term does, and so, the bursting neuron with $\Delta\gamma$ component will also demonstrate the

bursting phenomenon. But the $\Delta\gamma$ term is of a magnitude greater than the γ term, and so the combination of the terms will cause the threshold to be crossed earlier, and the bursting to occur at a faster rate. Hence the result. □

During this process of generating bursts, we observe that the bursts themselves get synchronized and that the fast chaotic oscillations corresponding to each neuron tend to become asynchronous. Thus, the oscillations are asynchronous and only the behavior of the neurons is the same. We shall refer to this process as "behavioral synchronization" which is defined below:

Definition 7.1.

Consider a bursting neuron that can be in one of the two states:
- A rapidly varying spiking state described by:
(i) $min(X_1(n)) > Threshold_1$ *for all* $t \in [N, N+\theta_1]$ *or*
- A quiescent state described by:
(ii) $max(X_1(n)) < Threshold_2$ *for all* $t \in [N+\theta_1, N+\theta_2]$,
where X_1 *is the fast variable, and* N *is the beginning of the rapidly varying spiking state.*
These two states are characterized by the time delays θ_1 *and* θ_2, *and two thresholds,* $Threshold_1$, *and* $Threshold_2$, *with the condition* $Threshold_2 < Threshold_1$.
Two neurons in the network are ***behaviorally synchronized*** *if there exist* δ_{11}, δ_{12}, *and* δ_{22} *which are small, for which the fast variable* X_2 *of the second bursting neuron satisfies one of the following conditions:*
(iii) $min(X_2(n)) > Threshold_1$ *for all* $t \in [N \pm \delta_{11}, N+\theta_1 \pm \delta_{12}]$ *or*
(iv) $max(X_2(n)) < Threshold_2$ *for* $t \in [N+\theta_1 \pm \delta_{12}, N+\theta_2 \pm \delta_{22}]$.

□

This definition shows that if the first neuron has started to burst, the second neuron will burst too, after a short delay of δ_{11}. In such a case the neurons exhibit *behavioral synchronization.* The bursting process will disappear after a time, and we permit a small delay δ_{12} between the end of bursting of the first neuron and the end of the bursting of the second. The quiescent state which comes after the bursting states also permits a time difference of δ_{22}.

An example of such a "behavioral synchronization" for a network of two coupled neurons is presented in Figure 7.4. The reader should compare this process with the behavior of the uncoupled network, as presented in Figure 7.5.

7.3.1 The Problems

In order to characterize the "behavioral synchronization" phenomenon, we propose two new measures that resemble frequencies:

a) High Pseudo-frequency measure : This measure, denoted by $F1$, is computed as the ratio between the average number of zero crossings and the length of the chaotic part of the signal.

b) Low Pseudo-frequency measure : This measure, denoted by $F2$, is computed as the average of the inverse of the time between the ends of two consecutive bursts.

The problems to be studied and the respective *modus operandi* of the solutions we propose are:

- We formally prove that the network of coupled bursting is unstable, and that it permits a chaotic behavior for a range of the control parameter, α. This problem is studied by resorting to the stability of the equilibrium points of the network.
- We explore the variation of these two new measures, namely $F1$ and $F2$, along with the cross correlation between each pair of neurons as a function of the size of the coupled network.
- Finally, we propose an algorithm to control the behavioral synchronization of the network.

7.4 The Stability Analysis

To fully appreciate the stability analysis, we shall consider the stability of a single bursting neuron, and then extend the results for the stability of a network of two neurons. The latter is

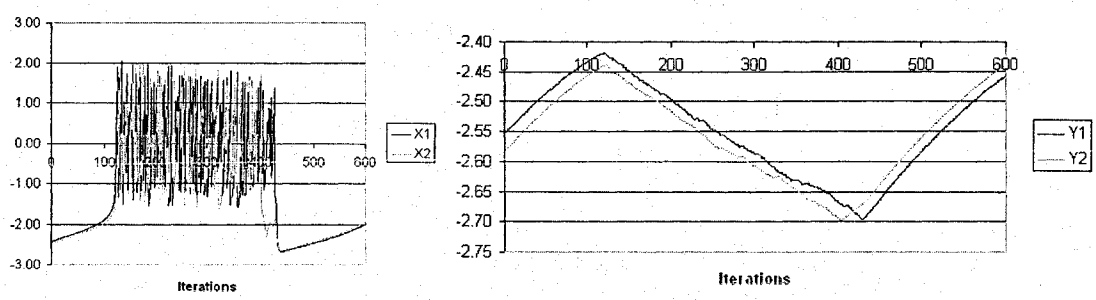

Figure 7.4: The variations of $X_1(n)$ and $X_2(n)$ (on the left) and $Y_1(n)$ and $Y_2(n)$ (on the right) for a network of two neurons which are coupled.

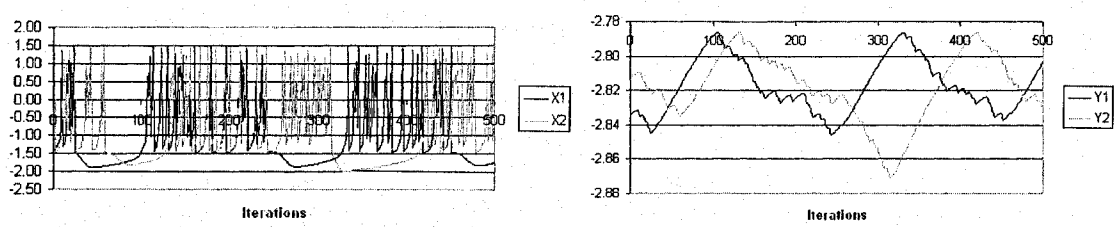

Figure 7.5: The variations of $X_1(n)$ and $X_2(n)$ (on the left) and $Y_1(n)$ and $Y_2(n)$ (on the right) for a network of two neurons which are not coupled.

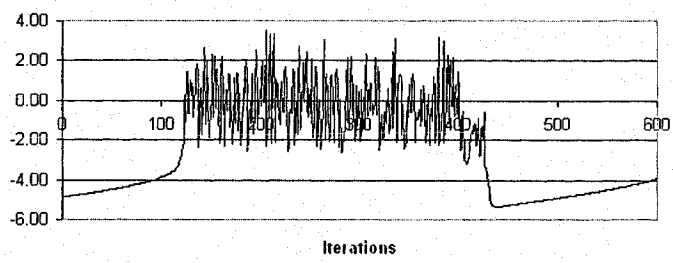

Figure 7.6: The amplitude of the summation of $X_1(n)$ and $X_2(n)$ for a network of two neurons which are coupled.

generalized with the help of some limiting approximations to yield the results for a network of N neurons.

7.4.1 The Stability of the Bursting Neuron

We first prove a theorem that describes the unstable/chaotic behavior of the bursting neuron.

Theorem 7.1.

Under the Jacobian analysis, the single unit Bursting neuron described by the Equations (7.1) and (7.2) has unstable solutions as $\sigma \rightarrow 0$.

Proof: The proof of the theorem is obtained by showing that the largest root of the characteristic equation corresponding to the Bursting neuron is positive.

Consider the bursting neuron, whose fixed point solution (x^*, y^*) is the solution to the system of equations:

$$x^* = \frac{\alpha}{[1 + x^{*2}]} + y^*, \tag{7.9}$$

$$y^* = y^* - \sigma x^* - \beta. \tag{7.10}$$

From Equation (7.10) we obtain

$$x^* = -\frac{\beta}{\sigma}. \tag{7.11}$$

With this solution, the y-coordinate, y^*, is obtained from Equation (7.9) as:

$$y^* = -\frac{\beta(\sigma^2 + \beta^2) + \alpha\sigma^3}{\sigma(\sigma^2 + \beta^2)}. \tag{7.12}$$

Computing the Jacobian of the system at *this* fixed point yields:

$$J(x^*, y^*) = \begin{pmatrix} -\frac{2\alpha x^*}{(1+x^{*2})^2} & 1 \\ -\sigma & 1 \end{pmatrix},$$

(7.13)

leading to the corresponding characteristic equation:

$$\lambda^2 + \left[\frac{2\alpha x^*}{(1+x^{*2})^2} - 1\right]\lambda + \left[\sigma - \frac{2\alpha x^*}{(1+x^{*2})^2}\right] = 0. \tag{7.14}$$

This equation has two roots as follows:

$$\lambda_{1,2} = \frac{1}{2}\left[-\left(\frac{2\alpha x^*}{(1+x^{*2})^2} - 1\right) \pm \sqrt{\left(\frac{2\alpha x^*}{(1+x^{*2})^2} - 1\right)^2 - 4\left(\sigma - \frac{2\alpha x^*}{(1+x^{*2})^2}\right)}\right]. \tag{7.15}$$

To render the notation simple, we denote $A = \frac{2\alpha x^*}{(1+x^{*2})^2} - 1$, leading to the formulation of $\lambda_{1,2}$ as:

$$\lambda_{1,2} = \frac{1}{2}(-A \pm \sqrt{A^2 - 4(\sigma - (A+1))}. \tag{7.16}$$

If the real part of the roots $\lambda_{1,2}$ is positive, the system is unstable. In our case, if σ is a very small quantity, (typically suggested to be $\sigma \approx 10^{-3}$), the largest root can be evaluated as:

$$\begin{aligned}\lambda_2 &= \tfrac{1}{2}(-A + \sqrt{A^2 - 4(\sigma - (A+1))}) > \tfrac{1}{2}(-A + \sqrt{A^2 - 4(-(A+1))} \\ &= \tfrac{1}{2}(-A + \sqrt{A^2 + 4A + 4}) = \tfrac{1}{2}(-A + (A+2)) = 1.\end{aligned}$$

Thus, the system is unstable and with a positive root that is greater than unity. □

Comments

1. The reader should observe that for arbitrarily small values of σ, the value of the positive root is not dependent on A. Only the constant σ can modify its magnitude.

2. We briefly investigate the maximum value of σ for which the largest root (above) is positive. Since $A = \frac{2\alpha x^*}{(1+x^{*2})^2} - 1$, this quantity evaluates to $A = -2\alpha\frac{\beta}{\sigma}\frac{1}{[1+(\frac{\beta}{\sigma})^2]^2} - 1$ at the fixed point $x^* = -\frac{\beta}{\sigma}$. Since all the constants in this expression are positive, A can be seen to be negative number. Furthermore, since $\lambda_2 = \frac{1}{2}(-A + \sqrt{A^2 - 4(\sigma - (A+1))})$, it is always positive. Indeed, the square root exists, whenever $A^2 - 4(\sigma - (A+1)) > 0$, which implies that $\sigma < \frac{(A+2)^2}{4}$. It should be observed that for the Bursting neuron, σ is usually set to be

σ	β	α	X^*	A	λ_1	λ_2
0.001	0.001	5	-1	2.5	2.4993	1.0007
0.001	0.001	4.5	-1	2.25	2.2492	1.0008
0.001	0.001	4	-1	2	1.9990	1.0010
0.001	0.001	1	-1	0.5	0.5020	0.9980
0.001	0.001	0.5	-1	0.25	0.2513	0.9987
0.002	0.001	4.5	-0.5	2.88	2.8789	1.0011
0.001	0.002	4.5	-2	0.72	0.7236	0.9964
0.004	0.001	4.5	-0.25	1.99	1.9859	1.0041
0.001	0.004	4.5	-4	0.12	0.1211	0.9989

Table 7.1: The roots of the characteristic equation for a single bursting neuron.

close to zero, and thus $\sigma < \frac{(A+2)^2}{4}$ is always satisfied. In conclusion, all allowable values of σ satisfy this inequality and generate a positive root for the characteristic equation.

3. For the sake of verification (and also to present a practical "feel" for the system dynamics) a tabulation of the roots for different typical values of the parameters is given in Table 7.1. Observe that we have set $\sigma \approx 10^{-3}$ (as is typical) and the other values are as given in the table.

7.4.2 The Stability of Network of Two Coupled Neurons

In this Section, we analyze the stability of a network of two coupled neurons. Although we have the results for the case of a single neuron, we investigate the case of coupling it with a second one, to verify if the simultaneous chaotic bursting behavior is affected by the coupling.

Theorem 7.2.

Under the Jacobian analysis, the network of two coupled Bursting neurons has unstable solutions as $\sigma \rightarrow 0$.

Proof: The proof of the theorem is obtained by showing that the largest root of the characteristic equation corresponding to the network of two coupled neurons is positive.

Consider the case of two coupled neurons, for which the set of equations are:

$$
\begin{aligned}
X_1(n+1) &= \tfrac{\alpha_1}{[1+X_1(n)^2]} + Y_1(n) + \tfrac{\epsilon}{2}(X_1(n) + X_2(n)),\\
Y_1(n+1) &= Y_1(n) - \sigma_1 X_1(n) - \beta_1,\\
X_2(n+1) &= \tfrac{\alpha_2}{[1+X_2(n)^2]} + Y_2(n) + \tfrac{\epsilon}{2}(X_1(n) + X_2(n)),\\
Y_2(n+1) &= Y_2(n) - \sigma_2 X_2(n) - \beta_2.
\end{aligned}
$$

In order to analyze the stability of the network, we first obtain the (vector) of fixed points $(X_1^*, Y_1^*, X_2^*, Y_2^*)$ by solving the system of equations:

$$
\begin{aligned}
X_1^* &= \tfrac{\alpha_1}{[1+X_1^{*2}]} + Y_1^* + \tfrac{\epsilon}{2}(X_1^* + X_2^*),\\
Y_1^* &= Y_1^* - \sigma_1 X_1^* - \beta_1,\\
X_2^* &= \tfrac{\alpha_2}{[1+X_2^{*2}]} + Y_2^* + \tfrac{\epsilon}{2}(X_1^* + X_2^*),\\
Y_2^* &= Y_2^* - \sigma_2 X_2^* - \beta_2.
\end{aligned}
$$

The solutions for this system are:

$$
\begin{aligned}
X_1^* &= -\tfrac{\beta_1}{\sigma_1},\\
Y_1^* &= \frac{[-\frac{\beta_1}{\sigma_1}(1-\frac{\epsilon}{2}) + \frac{\beta_2}{\sigma_2}\frac{\epsilon}{2})](1+\frac{\beta_1^2}{\sigma_1^2}) - \alpha_1}{1+\frac{\beta_1^2}{\sigma_1^2}},\\
X_2^* &= -\tfrac{\beta_2}{\sigma_2},\\
Y_2^* &= \frac{[-\frac{\beta_2}{\sigma_2}(1-\frac{\epsilon}{2}) + \frac{\beta_1}{\sigma_1}\frac{\epsilon}{2})](1+\frac{\beta_2^2}{\sigma_2^2}) - \alpha_2}{1+\frac{\beta_2^2}{\sigma_2^2}}.
\end{aligned}
$$

We compute the Jacobian of the system around this point to be:

$$
J(X_1^*, Y_1^*, X_2^*, Y_2^*) = \begin{pmatrix}
-\frac{2\alpha_1 X_1^*}{(1+X_1^{*2})^2} + \frac{\epsilon}{2} & 1 & \frac{\epsilon}{2} & 0\\
-\sigma_1 & 1 & 0 & 0\\
\frac{\epsilon}{2} & 0 & -\frac{2\alpha_2 X_2}{(1+X_2^{*2})^2} + \frac{\epsilon}{2} & 1\\
0 & 0 & -\sigma_2 & 1
\end{pmatrix}. \tag{7.17}
$$

As before, to render the notation simple, we denote $A = -\frac{2\alpha_1 X_1}{(1+X_1^2)^2} + \frac{\epsilon}{2}$ and $B = -\frac{2\alpha_1 X_1}{(1+X_1^2)^2} + \frac{\epsilon}{2}$, whence the eigenvalues are obtained by solving the characteristic equation of the system:

$$\begin{vmatrix} A-\lambda & 1 & \frac{\epsilon}{2} & 0 \\ -\sigma_1 & 1-\lambda & 0 & 0 \\ \frac{\epsilon}{2} & 0 & B-\lambda & 1 \\ 0 & 0 & -\sigma_2 & 1-\lambda \end{vmatrix} = 0, \text{ or}$$

$$(A-\lambda)[(1-\lambda)[(1-\lambda)(B-\lambda)+\sigma_2(1-\lambda)]-[-\sigma_1(B-\lambda)(1-\lambda)-\sigma_1\sigma_2]+\tfrac{\epsilon}{2}[-(1-\lambda)^2\tfrac{\epsilon}{2}]=0.$$

This reduces to a quartic equation:

$$\lambda^4 + C_3\lambda^3 + C_2\lambda^2 + C_1\lambda + C_0 = 0$$

where:

$C_3 = -A - B - 2,$

$C_2 = AB + 2A + 2B + 1 + \sigma_1 + \sigma_2 - (\frac{\epsilon}{2})^2,$

$C_1 = -A - B - 2AB - \sigma_1 B - \sigma_2 A - \sigma_1 - \sigma_2 + 2(\frac{\epsilon}{2})^2,$ and

$C_0 = AB + \sigma_1\sigma_2 - (\frac{\epsilon}{2})^2 + A\sigma_2 + B\sigma_1.$

Consider now the case when ϵ is set to zero. In such a case, the quartic equation can be factored to be two quadratics as:

$$(\lambda^2 + C_{11}\lambda + C_{10})(\lambda^2 + C_{21}\lambda + C_{20}) = 0$$

where:

$C_{11} = -A - 1,$

$C_{10} = \sigma_1 + A,$

$C_{21} = -B - 1,$ and

$C_{20} = \sigma_2 + B.$

Thus the roots of polynomial are seen to be:

$\lambda_{1,2} = \frac{1}{2}(-A \pm \sqrt{A^2 - 4(\sigma_1 - (A+1))},$

$\lambda_{3,4} = \frac{1}{2}(-B \pm \sqrt{B^2 - 4(\sigma_2 - (B+1))},$

and since these are all positive, the result follows for $\epsilon = 0$.

The result demonstrating the positive roots for any arbitrarily small ϵ is shown by observing that if the characteristic equation is written as f, a function of λ *and* ϵ, the partial derivative of $\frac{\partial f}{\partial \epsilon}$ around $\epsilon = 0$ is:

$\frac{\partial f}{\partial \epsilon} = -\frac{\epsilon}{2}(\lambda - 1)^2.$

α_1=α_2	λ_1	λ_2	λ_3	λ_4
4	2.0991	1.9990	1.0010	1.0009
4.5	2.3493	2.2492	1.0008	1.0007
5	2.5994	2.4993	1.0007	1.0006

Table 7.2: The roots of the characteristic equation for a network of two coupled bursting neurons.

Since the latter expression is both continuous and *bounded*, a small perturbation in ϵ leads to a correspondingly small perturbation in f, implying that the root will be positive if ϵ is correspondingly small. The formal "$\epsilon - \delta$" arguments are omitted and can be easily filled in. Thus, in conclusion, the positive roots of the characteristic equation demonstrate the instability of the system. □

Comment:

As in the case of the stability analysis of a single neuron, for the sake of verification, a tabulation of the roots for different typical values of the parameters is given in Table 7.2. Observe that we have set (as is typical), $\sigma_1 = \sigma_2 = \beta_1 = \beta_2 = 0.001$, $\epsilon = 0.1$, and the other values are as given in the table.

7.4.3 The General Case of N Neurons

In this subsection, we analyze the stability of a network of N coupled neurons. Our aim is to verify that the chaotic bursting behavior of a single neuron is not affected by coupling it to $N - 1$ other neurons.

Theorem 7.3.

Under a Jacobian analysis, the network of N coupled Bursting neurons has unstable solutions as $\sigma \rightarrow 0$ and $\epsilon \rightarrow 0$.

Proof: The proof of the theorem is obtained by showing that the largest root of the characteristic equation corresponding to the network of N coupled neurons is positive.

Consider the case of N coupled bursting neurons. The characteristic equation created from the Jacobian of the system is:

$$J(X_1^*, Y_1^*, \ldots, X_N^*, Y_N^*) = \begin{vmatrix} A_1 - \lambda & 1 & \frac{\epsilon}{2} & 0 & \cdots & \frac{\epsilon}{2} & 0 \\ -\sigma_1 & 1-\lambda & 0 & 0 & \ldots & 0 & 0 \\ \frac{\epsilon}{2} & 0 & A_2 - \lambda & 1 & \cdots & \frac{\epsilon}{2} & 0 \\ 0 & 0 & -\sigma_2 & 1-\lambda & \cdots & 0 & 0 \\ \vdots & \vdots & \vdots & \vdots & \vdots & \vdots & \vdots \\ \frac{\epsilon}{2} & 0 & \frac{\epsilon}{2} & 0 & \cdots & A_N - \lambda & 1 \\ 0 & 0 & 0 & 0 & \ldots & -\sigma_N & 1-\lambda \end{vmatrix} = 0, \tag{7.18}$$

where $A_i = -\frac{2\alpha_i X_i^*}{(1+X_i^{*2})^2} + \frac{\epsilon}{2}$ for all $i = 1 \ldots N$, and X_i^* and Y_i^* determine the fixed points of the system.

It is well known that *the determinant of a block diagonal matrix is the product of the determinant of the individual blocks.* In our setting, we see that, if the coupling coefficient ϵ is very small, the Jacobian becomes block diagonal. Thus, in the limits as $\epsilon \longrightarrow 0$, the solutions of the characteristic equation, namely of Equation (7.18), tends towards the solutions of the characteristic equations of each of the 2×2 block.

As is the previous case dealing with the stability of a network of two coupled neurons, the characteristic equation can be factored to be N quadratics as:
$(\lambda^2 + C_{11}\lambda + C_{10})(\lambda^2 + C_{21}\lambda + C_{20})...(\lambda^2 + C_{N1}\lambda + C_{N0}) = 0$, where:

$C_{11} = A_1$; $C_{10} = \sigma_1 - (A_1 - 1)$,

$C_{21} = A_2$; $C_{20} = \sigma_2 - (A_2 - 1)$,

...

$C_{N1} = A_N$; $C_{N0} = \sigma_N - (A_N - 1)$.

Thus the roots of polynomial are seen to be:

$\lambda_{1,2} = \frac{1}{2}(-A_1 \pm \sqrt{A_1^2 - 4(\sigma_1 - (A_1 + 1))}$,

$\lambda_{3,4} = \frac{1}{2}(-A_2 \pm \sqrt{A_2^2 - 4(\sigma_2 - (A_2 + 1))}$,

...

$\lambda_{2N-1,2N} = \frac{1}{2}(-A_N \pm \sqrt{A_N^2 - 4(\sigma_N - (A_N + 1))}$,

$\alpha_{1,2}$	λ_1	λ_2	λ_3	λ_4	λ_5
	λ_6	λ_7	λ_8	λ_9	λ_{10}
4	2.2492	1.9990	1.0010	1.0008	1.0010
	1.9990	1.9990	1.9990	1.0010	1.0010
4.5	2.4993	2.2492	1.0007	1.0008	1.0008
	2.2492	2.2492	2.2492	1.0008	1.0008
5	2.4993	2.7494	1.0007	1.0006	1.0007
	2.4993	2.4993	2.4993	1.0007	1.0007

Table 7.3: The roots of the characteristic equation for a network of 5 coupled bursting neurons.

and since these are all positive, the result follows for $\epsilon = 0$.

Thus, each neuron has two positive roots for *its* characteristic equation. In conclusion, the Equation (7.18) has $2N$ positive roots, and thus the networks is unstable, independent of the size of N, the number of coupled neuron. Hence the result. □

Comment:

1. As in the previous case, it is easily seen that f is a polynomial of ϵ of degree N. Since the partial derivative of $\frac{\partial f}{\partial \epsilon}$ around $\epsilon = 0$ is both continuous and *bounded* (since ϵ does not appear in any denominator), a small perturbation in ϵ leads to a correspondingly small perturbation in f. Thus, we believe that the above result is also true in the neighborhood of $\epsilon = 0$.

2. As in the previous stability analysis scenarios, for the sake of verification, a tabulation of the roots for different typical values of the parameters for a network with 5 neurons is given in Table 7.3. Observe that we have set, as is typical, $\sigma_i = \beta_i = 0.001$ $(\forall\ i)$, $\epsilon = 0.1$, and the other values as stated in the Table.

7.5 Simulations Results for Computing New Measures

In Sections 7.2-7.3, we showed the chaotic properties of an individual bursting neuron, and of a network of such neurons. We now address the question whether a coupled network results in synchronization. In other words, if we are given a network with thousands of neurons would it be possible to describe the synchronization by computing the earlier mentioned measures, namely the pseudo-frequencies $F1$ and $F2$, and the Cross Correlation Coefficient (CC).

The problem we face is of a computational sort. Indeed, computing these measures when the number of neurons is large is almost prohibitively expensive. But it turns out that the $F1$, $F2$ and CC tend to converge (and that, rather quickly) with the number of neurons. In other words, it happens that the synchronization behavior for relatively small N (say 4 or 5) actually approximates the behavior for large values of N with a negligible error. To demonstrate this we numerically compute these indices for networks of various sizes.

We numerically analyze the bursting model of the neuron for a few cases, namely for networks in which $N = 2$ (when the pair is coupled/uncoupled) and when $N = 3, 4$. Of course, these experiments were done for an ensemble of parameter settings[7], but in the interest of brevity we merely mention a single case when the parameters were set as is typical in a real-life setting. Thus, for all the experiments reported here, we have set the parameters to be as realistic as possible, as below:

$\alpha = 4.3$,
$\sigma = 0.001$,
$\beta = 0.001$.

The coupling coefficient for the experiments with networks involving coupled neurons was $\epsilon = 0.1$.

The notation we use is:

E_p = The iteration index of the termination of the previous burst (i.e, the "Previous End"),
S = The iteration index of the start of the Bursting period,
E = The iteration index of the end of the Bursting period,
Z = The number of zero crossings during the length of the burst.

[7]We mention that these parameters will also be the same as the number of neurons is increased.

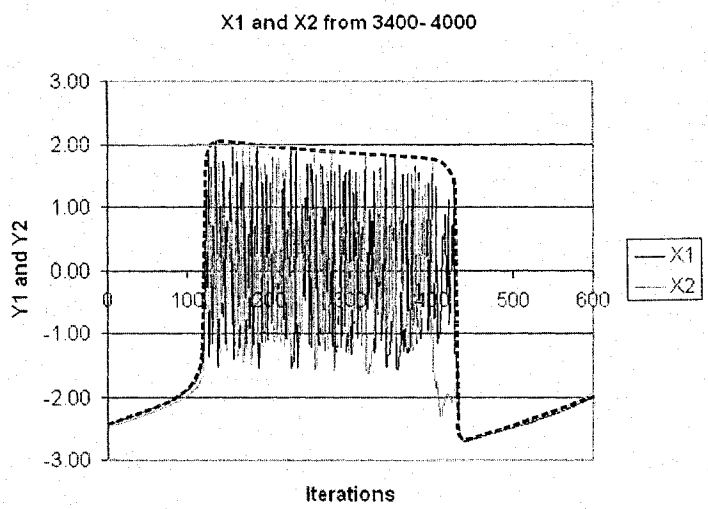

Figure 7.7: The envelope of the X_1 and X_2 signals for a network of two neurons with coupling, is represented with dotted line.

Note that as a result of these terms, the length of the burst is $E - S$, and the length of the "periodic signal" is the difference $E - E_p$.

7.5.1 A Network with Two Neurons

Consider the case of a network with two neurons (characterized by their fast and slow variable, namely $(X_1(n), Y_1(n))$ and $(X_2(n), Y_2(n))$. The behavior of the coupled neurons is presented in Figure 7.4. The behavior of the uncoupled neurons is presented in Figure 7.5.

For the case of the coupled neurons, we compute LLE (see Section 2.6) for each signal, by evaluating it for the firsts 5 bursts of each signals. We find that:

1. For the first neuron, the LLEs are $\{0.43011, 0.3612, 0.2298, 0.2251, 0.3053\}$ and the average LLE is 0.3103.

2. For the second neuron, the LLEs are $\{0.3242, 0.3484, 0.2089, 0.2860, 0.2962\}$ and the

average LLE is 0.2927.

In all the situations, the positive values for the LLE correspond to a chaotic behavior.

Observe also the appearance of behavioral synchronization. From Tables 7.4 and 7.5 , we see that for the network without coupling, the S iteration indices[8] for the X_1 and X_2 values are:

$X_1 = 3201$ vs. $X_2 = 3211$ for a specific burst, and

$X_1 = 3606$ vs. $X_2 = 3633$ for the following burst.

As opposed to this, from Tables 7.6 and 7.7, the difference between the corresponding S indices *after* coupling is:

$X_1 = 1631$ vs. $X_2 = 1632$ for a specific burst and

$X_1 = 2136$ vs. $X_2 = 2137$ for the following burst,

which represents a difference of only a single iteration unit.

It is thus clear that, in the case of coupled neurons, the beginning of the bursting behavior is almost synchronized.

The reader should observe from Tables 7.4 and 7.5 that the values of $F1$ are approximately equal for both the neurons. The same observation is also true for $F2$. When a coupling occurs, $F1$, the high pseudo-frequency that describes the chaotic oscillations, is larger, and $F2$, the low pseudo-frequency that describes the overall signal, is smaller (see Tables 7.6 and 7.7). The variation of $F2$ also seen as an envelope of signals X_1 and X_2, is shown with a dotted line in Figure 7.7. The synchronization, in this case too, is clear.

To further illustrate the synchronic behavior, we also compute the cross correlation between the two signals. In Table 7.8, we present the values for the CC for the case of the uncoupled and coupled signals, respectively. The average values for CC are 0.2528 and 0.2015 for these cases. It is thus clear that although the behavior is the *same*, namely that, both are of a bursting nature, the signals themselves are *marginally correlated*, and that the coupling doesn't increase the relationship between them.

[8]All the interpretations are made using only the phenomenon displayed by the fast variable. The behavior of the slow variable mimics the former.

E_p	S	E	$E-S$	$E-E_p$	Z	$Z/(E-S)$
2849	2932	3094	162	245	62	0.3827
3094	3201	3325	124	231	41	0.3306
3325	3404	3523	119	198	47	0.3949
3523	3606	3742	136	219	41	0.3014
3742	3832	3951	119	209	35	0.2941
		Averages	132	220.4	45.2	0.34074

Table 7.4: The values of the pertinent indices E_p, S, E, and Z etc. (see Section 7.5.1) for the *first* signal involving two *uncoupled* neurons. In this case $F1 = 0.34074$, and $F2 = 0.0045$

E_p	S	E	$E-S$	$E-E_p$	Z	$Z/(E-S)$
2734	2821	2957	136	223	34	0.25
2957	3033	3124	91	167	38	0.4175
3124	3211	3371	160	247	46	0.2875
3371	3460	3557	97	186	32	0.3298
3557	3633	3813	180	256	60	0.3333
		Averages	132.8	215.8	42	0.32362

Table 7.5: The values of the pertinent indices E_p, S, E, and Z etc. (see Section 7.5.1) for the *second* signal involving two *uncoupled* neurons. In this case $F1 = 0.3236$ and $F2 = 0.0046$

E_p	S	E	$E-S$	$E-E_p$	Z	$Z/(E-S)$
1478	1632	1915	283	437	145	0.5123
1915	2136	2472	336	557	160	0.4567
2472	2704	2940	236	468	98	0.4025
2940	3112	3331	219	391	115	0.5159
3331	3522	3826	304	495	143	0.4703
		Averages	275.4	469.6	132.2	0.4801

Table 7.6: The values of the pertinent indices E_p, S, E, and Z etc. (see Section 7.5.1) for the *first* signal involving two *coupled* neurons with $\epsilon = 0.1$. In this case $F1 = 0.4801$ and $F2 = 0.0021$

E_p	S	E	$E-S$	$E-E_p$	Z	$Z/(E-S)$
1447	1631	1927	296	480	150	0.5067
1927	2137	2453	316	526	155	0.4905
2453	2701	2945	244	492	127	0.5204
2945	3112	3347	235	402	122	0.5191
3347	3524	3801	277	454	130	0.4693
		Averages	273.6	470.8	136.8	0.5012

Table 7.7: The values of the pertinent indices E_p, S, E, and Z etc. (see Section 7.5.1) for the *second* signal involving two *coupled* neurons with $\epsilon = 0.1$. In this case $F1 = 0.5012$ and $F2 = 0.0021$

$S(1)$	$E(1)$	$S(2)$	$E(2)$	CC
2932	3068	2821	2957	0.2432
3201	3292	3033	3124	0.2481
3404	3523	3211	3430	0.2849
3606	3703	3460	3557	0.2093
3832	3951	3633	3752	0.2789
			Averages	0.2528

$S(1)$	$E(1)$	$S(2)$	$E(2)$	CC
1632	1915	1632	1915	0.2384
2137	2453	2137	2453	0.1557
2704	2940	2704	2940	0.2504
3112	3331	3112	3331	0.1725
3524	3801	3524	3801	0.1906
			Averages	0.2015

Table 7.8: The Cross Correlations between the pairs of signals: *without coupling* (left table) and *with coupling* (right table).

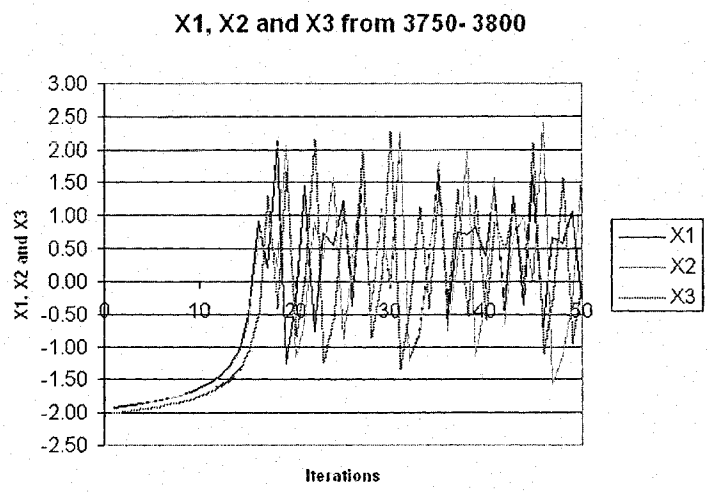

Figure 7.8: The X_1,X_2 and X_3 for a network with three *coupled* neurons.

7.5.2 A Network with Three Neurons

Consider the case of a network with three neurons (characterized by their fast and slow variables, namely $(X_1(n), Y_1(n))$, $(X_2(n), Y_2(n))$, and $(X_3(n), Y_3(n))$. The behavior of the coupled neurons is presented in Figure 7.8.

Observe also, as in the case of the network built with two coupled neurons, the appearance of behavioral synchronization. As stated before, the larger the number, N, of neurons which are involved, the greater the value of $\Delta\gamma$, and the larger the triggering impact that is experienced by the remaining cell. In Tables 7.9, 7.10, and 7.11, we see that[9], in certain cases, there are no differences between the indices corresponding to the beginning of the bursts, as from the figures below:

$$X_1 = X_2 = 3765 \text{ (from Tables 7.9 and 7.10)},$$
$$X_1 = X_3 = 2592 \text{ (from Tables 7.9 and 7.11)},$$
$$X_1 = X_3 = 3154 \text{(from Tables 7.9, and 7.11), and}$$
$$X_2 = X_3 = 1936 \text{ (from Tables 7.10 and 7.11)}.$$

[9]The Parameters can be seen in the introduction of Section 7.5.

E_p	S	E	$E-S$	$E-E_p$	Z	$Z/(E-S)$
1121	1407	1705	298	584	162	0.5436
1705	1937	2329	392	624	227	0.5790
2329	2592	2909	317	580	169	0.5331
2909	3154	3517	363	608	206	0.5674
3517	3765	4100	335	583	206	0.6149
		Averages	341	595.8	194	0.5616

Table 7.9: The values of the pertinent indices E_p, S, E, and Z etc. (see Section 7.5.1) for the *first* signal involving three *coupled* neurons with $\epsilon = 0.1$. In this case $F1 = 0.5689$ and $F2 = 0.0016$.

E_p	S	E	$E-S$	$E-E_p$	Z	$Z/(E-S)$
1145	1406	1706	300	561	166	0.5533
1706	1936	2329	393	623	221	0.5623
2329	2591	2931	340	602	185	0.5441
2931	3155	3518	363	587	193	0.5316
3518	3765	4113	348	595	195	0.5603
		Averages	348.8	593.6	192	0.5503

Table 7.10: The values of the pertinent indices E_p, S, E, and Z etc.(see Section 7.5.1) for the *second* signal involving three *coupled* neurons with $\epsilon = 0.1$. In this case $F1 = 0.5504$ and $F2 = 0.0016$.

It is thus clear that the beginning of the bursting behavior is exactly synchronized in some cases, and almost exactly synchronized in the others.

Tables 7.9, 7.10, and 7.11 also contain the corresponding values of $F1$ and $F2$.

As in the previous case, we also compute the cross correlation between the pairs of signals. In Table 7.12, we present the values for the CC for three pairs of signals, $(1,2)$, $(2,3)$ and $(1,3)$. The average value for CC are 0.1829, 0.165 and 0.1807, which are all smaller than the value for the network of two *coupled* neurons, namely 0.2015, and also smaller than the value for the network of the two *uncoupled* neurons, namely 0.2528. The results presented here are typical for an ensemble of parameters settings. We can conclude that the greater the value of N, the number of neurons in the network, the smaller is the cross correlation between the bursting neurons.

E_p	S	E	$E-S$	$E-E_p$	Z	$Z/(E-S)$
1175	1405	1713	308	538	184	0.5974
1713	1936	2333	397	620	223	0.5617
2333	2592	2913	321	580	192	0.5981
2913	3154	3521	367	608	211	0.5749
3521	3766	4106	340	585	196	0.5764
		Averages	346.6	586.2	201.2	0.5817

Table 7.11: The values of the pertinent indices E_p, S, E, and Z etc.(see Section 7.5.1) for the *third* signal involving three *coupled* neurons with $\epsilon = 0.1$. In this case $F1 = 0.5804$ and $F2 = 0.0017$.

S	E	$CC(1,3)$	$CC(2,3)$	$CC(1,3)$
1407	1705	0.1761	0.1874	0.1692
1937	2329	0.2034	0.1612	0.1651
2592	2909	0.2003	0.166	0.182
3155	3517	0.1794	0.1383	0.1588
3766	4100	0.1555	0.1721	0.2286
	Averages	0.1829	0.165	0.1807

Table 7.12: Cross correlations between the pairs of signals measured between the corresponding S and E time instants.

E_p	S	E	$E-S$	$E-E_p$	Z	$Z/(E-S)$
1494	1732	2069	337	575	183	0.5430
2069	2307	2676	369	607	203	0.5501
2676	2955	3343	388	667	221	0.5695
3343	3617	3936	319	593	186	0.4793
3936	4164	4550	386	614	218	0.5647
		Averages	359.8	611.2	202.2	0.5413

Table 7.13: The values of the pertinent indices E_p, S, E, and Z etc. (see Section 7.5.1) for the *first* signal involving four *coupled* neurons with $\epsilon = 0.1$. In this case $F1 = 0.5413$ and $F2 = 0.0016$.

7.5.3 A Network with Four Neurons

Consider the case of a network with four neurons[10] (characterized by their fast and slow variable, namely $(X_1(n), Y_1(n))$, $((X_2(n), Y_2(n))$, $(X_3(n), Y_3(n))$ and $(X_4(n), Y_4(n))$. Observe, as in the previous cases, the appearance of behavioral synchronization. Our conclusion here is that, the greater the number N of neurons involved, the greater is $\Delta\gamma$, and thus the triggering impact experienced by the remaining cell is larger. From Tables 7.13-7.16 we see that, in certain cases, there are no differences between the indices corresponding to the beginning of the burst:

$$X_1 = X_2 = 1732 \text{ (from Tables 7.13 and 7.14)},$$
$$X_1 = X_2 = X_3 = 2955 \text{ (from Tables 7.13-7.15), and}$$
$$X_1 = X_2 = X_3 = X_4 = 4164 \text{ (from Tables 7.13-7.16)}.$$

Again, the beginning of the bursting behavior is exactly synchronized in some cases and almost exactly synchronized in rest. The values of the pseudo-frequencies $F1$ and $F2$ are also included in the tables. The reader can observe that the values of $F1$ for all four signals are almost the same. The same comment can also be made for $F2$.

As in the previous cases, we have also computed the cross correlation CC between the various (six) pairs of signals, and these are given in Table 7.17.

The average values for CC are $\{0.1618, 0.1735, 0.1682, 0.1558, 0.1808, 0.1681\}$, which are *comparable* to the average values of CC computed in the case of three coupled neurons $\{0.1829, 0.165, 0.1807\}$.

[10]The Parameters can be seen in the introduction of Section 7.5.

E_p	S	E	$E-S$	$E-E_p$	Z	$Z/(E-S)$
1510	1732	2052	320	542	190	0.5937
2052	2306	2688	382	636	211	0.5523
2688	2955	3354	399	666	218	0.5463
3354	3617	3932	315	578	185	0.5873
3932	4164	4542	378	610	200	0.5291
		Averages	358.8	606.4	200.8	0.5617

Table 7.14: The values of the pertinent indices E_p, S, E, and Z etc. (see Section 7.5.1) for the *second* signal involving four *coupled* neurons with $\epsilon = 0.1$. In this case $F1 = 0.5617$ and $F2 = 0.0016$.

E_p	S	E	$E-S$	$E-E_p$	Z	$Z/(E-S)$
1494	1729	2055	326	561	193	0.5920
2055	2305	2697	392	642	231	0.5892
2697	2955	3361	406	664	219	0.5394
3361	3618	3933	315	572	174	0.5523
3933	4164	4549	385	616	214	0.5558
		Averages	364.8	611	206.2	0.5657

Table 7.15: The values of the pertinent indices E_p, S, E, and Z etc. (see Section 7.5.1) for the *third* signal involving four *coupled* neurons with $\epsilon = 0.1$. In this case $F1 = 0.56574$ and $F2 = 0.0016$.

E_p	S	E	$E-S$	$E-E_p$	Z	$Z/(E-S)$
1512	1730	2061	331	549	187	0.5649
2061	2306	2679	373	618	233	0.6246
2679	2956	3351	395	672	220	0.5569
3351	3618	3935	317	584	181	0.5709
3935	4164	4547	383	612	213	0.5561
		Averages	359.8	607	206.8	0.5746

Table 7.16: The values of the pertinent indices E_p, S, E, and Z etc. (see Section 7.5.1) for the *fourth* signal involving four *coupled* neurons with $\epsilon = 0.1$. In this case $F1 = 0.5746$ and $F2 = 0.0016$.

S	E	$CC(1,2)$	S	E	$CC(1,3)$	S	E	$CC(1,4)$
1732	2052	0.2125	1729	2055	0.1630	17320	2061	0.2321
2306	2676	0.1584	2305	2676	0.1434	2307	2676	0.1366
2955	3343	0.1457	2955	3343	0.2286	2956	3343	0.1220
3617	3932	0.1728	3617	3933	0.1523	3618	3935	0.1695
4164	4550	0.1200	4164	4549	0.1803	4164	4547	0.1809
	Averages	0.1618			0.1735			0.1682
S	E	$CC(2,3)$	S	E	$CC(2,4)$	S	E	$CC(3,4)$
1732	2052	0.1600	1732	2052	0.2129	1730	2055	0.1523
2305	2688	0.1440	2306	2679	0.1472	2306	2679	0.1644
2955	3354	0.1870	2956	3351	0.2391	2956	3351	0.2043
3618	3832	0.1422	3618	3932	0.1626	3618	3933	0.1806
4164	4542	0.1460	4164	4542	0.1422	4164	4547	0.1393
	Averages	0.1558			0.1808			0.1681

Table 7.17: Cross correlations between the pairs of signals measured between the corresponding S and E time instants.

7.5.4 The Epileptic Seizure: A New Explanation

The literature contains many hypotheses for the generation of epileptic seizures[11] caused by aberrant synaptic networks [102]. Registered EEGs from epileptic patients during seizures have led to the conclusion that the seizures are caused by large populations of neurons being synchronized. There are two primary characteristics for the EEGs generated by epileptic seizures. The first is that the amplitude of EEG's during seizures is several times greater than those recorded under normal conditions. The second is that the primary frequency found on EEGs decreases during the seizure to about 3 Hz. These two observations have generated various models using which one can investigate the behavior of a single common phase and phenomenon for *all* the neurons. One of these models, which is based on synchronization derived from firefly populations, has yielded a few rigorous mathematical concepts [175]. A resulting control solution in the study of such nonlinear oscillators is the so-called "phase resetting" solution by the insertion of a stimulus in Equation (7.5). Apart from phase resetting, it is also possible to modify the

[11] One particular definition of epileptic seizures was proposed by Jackson and reformulated by Penfield and Jasper, as being "state(s) produced by an abnormal excessive neuronal discharge within the central nervous system" (taken from Steriade [157]). This definition does not mention a specific cause, thus permitting the assumption that the neurological disease can be produced by a variety of factors.

dynamics of the coupled Hodgkin-Huxley neurons by spike annihilation, if the corresponding stimulus is carefully inserted at a specific chosen time. This is being addressed in the first part of this Chapter.

By using the bursting neural network model, we propose a new hypothesis which can explain the generation of epileptic seizures. When the coupling between the neurons is large enough to generate a value $\Delta\gamma$ greater that the threshold $\Delta\gamma_{max}$, we have shown that the system generates synchronized bursts such as those described above. Using this model, we believe that it is not mandatory for each neuron to be synchronized with *all* the other neurons in order to generate the behavior analogous to an epileptic seizure. Rather, we believe that is sufficient that they are synchronized in bursts, thus leading to the so-called *behavior synchronization* that we have demonstrated. By performing a summation of the signals obtained from the network of two coupled neurons, one can observe (as in Figure 7.6) an increase in the amplitude of the resulting signal which has a value greater than that of the individual neurons, and which has a frequency that is "low" as determined by the slow variable.

For the parameters reported, we see that the resulting signal has a maximum value of 3.5371, while the maximum individual amplitudes are 2.7621 and 2.5114 for the first and the second signal, respectively. For the network built with three coupled neurons, the maximum amplitude obtained by the summation of all three neurons is 5.3491.

The pseudo-frequencies $F2$ have a value of 0.0045 and 0.0046 in the case of a network of two uncoupled neurons, a smaller value of 0.0021 when we encounter a network of two *coupled* neurons, and a much smaller value of 0.0016 for the case of a network of three coupled neurons. This behavior can be compared with what happens in the human brain. During epileptic seizures, the frequency slows down from approximately $40 - 50$ Hz to approximately $3 - 5$ Hz.

We present in Figure 7.9 the evolutions of $F1$, $F2$ and CC. The graph represents the relative variations (in percentages) of the measures for the case of having 2, 3 and 4 coupled neurons, as opposed to the scenarios of having uncoupled neurons. The computed relative variation is compared to the measures obtained for two uncoupled neurons.

To conclude this section we can state from Table 7.18 that if one increases the size of the network N, the measures $F1$, $F2$ and CC will have an asymptotic behavior as depicted in Figure 7.9.

Signals	2 Uncoupled	2 Coupled	3 Coupled	4 Coupled
1st signal	F1=0.34074	F1=0.2015	F1=0.5689	F1=0.5413
	F2=0.0045	F2=0.0021	F2=0.0016	F2=0.0016
2nd signal	F1=0.3236	F1=0.5012	F1=0.5504	F1=0.5617
	F2=0.0046	F2=0.0021	F2=0.0016	F2=0.0016
3rd signal			F1=0.5804	F1=0.5657
			F2=0.0017	F2=0.0016
4th signal				F1=0.5746
				F2=0.0016
	CC(1,2)=0.2528	CC(1,2)=0.2015	CC(1,2)=0.1829	CC(1,2)=0.1618
			CC(2,3)=0.165	CC(2,3)=0.1558
			CC(1,3)=0.1807	CC(1,3)=0.1618
				CC(1,4)=0.1682
				CC(2,4)=0.1808
				CC(3,4)=0.1558
Averages	F1=0.3236	F1=0.5012	F1=0.5654	F1=0.5608
	F2=0.0046	F2=0.0021	F2=0.0016	F2=0.0016
	CC=0.2528	CC=0.2015	CC=0.1762	CC=0.1680

Table 7.18: The averages for $F1$, $F2$ and CC for the network of 2 uncoupled neurons and the networks of 2, 3, and 4 coupled neurons.

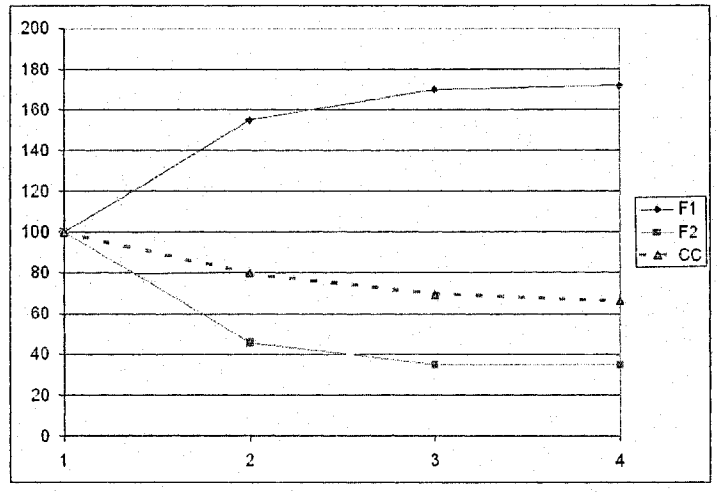

Figure 7.9: The relative variations (in percents) for F1, F2 and CC, for the case of 2 coupled neurons (point 2) , 3 coupled neurons (point 3) and 4 coupled neurons (point 4) compared with the case of two uncoupled neurons (point 1).

7.6 Controlling the Synchronization

Consider the Equations (7.5-7.6) which describe the network of oscillating neurons. As mentioned earlier, such a model, permits an explanation for the so-called bursting phenomenon in which a low frequency pulse output appears as an envelope of high frequency spikes, and exhibits a form of synchronization. In this Section, we intend to control such a system, i.e., "manipulating" the duration of the bursting phenomenon, by using the classical family of pulse-stimuli.

There are two almost contradictory tasks that come into the scene when we want to control a network of Bursting neurons. The first problem involves *excluding* the network from its bursting behavior for a reasonable duration. The second, and opposing constraint problem, involves forcing the network to remain in a bursting phase for a reasonable duration. In the network of Hodgkin-Huxley neurons, we had demonstrated in Chapter 6 that by inserting a stimulus $Stim$ in the equation which describes the fast variable $V(t)$, (the one analogous to our present variable, $X_i(n)$) such a control could be affected. The novelty of our present contribution consists of a process in which we insert the pulse-stimulus in the updating equation which describes $Y_i(n)$, the

slow variable, instead of incorporating the excitation in the updating equation that describes the fast variable. Indeed, both of the above tasks can be solved by inserting a stimulus in the second equation, namely in Equation (7.6). We shall show that the sign of the stimulus determines which task is solved, and thus, a negative stimulus will maintain a quiescent behavior (i.e., a salient non-spiking phase), while a positive stimulus will drive the network into its fast repetitive spiking phase.

The formal analysis below is followed by the experimental verification.

We start the formal analysis with some well-established mathematically considerations. We know from the theory of differential equations [160] that the solution to a system of differential equations contain two components:

- The complementary function which is obtained by setting the forcing function to be zero, and
- The particular integral whose form is completely determined by the explicit form of the forcing function.

In particular, if the forcing function is a constant, the particular integral will lead to a mere perturbation in the state-variable domain. In addition, if the forcing function is only for a short duration, it will again have no effect other than perturbing the solution in the state space. Observe that such a perturbation neither effects the final form of the solution nor the stability. Both of these issues are determined by the dynamics of the system, as dictated by the dynamical equation themselves, and not by the (constant) forcing function.

We now consider the issue of controlling the quiescent behavior, and later that of controlling the bursting behavior. The simulated results verifying these phenomena follow thereafter.

7.6.1 Maintaining the Quiescent Behavior

In the case of maintaining the quiescent behavior, the stimulus generates a process known as phase resetting. The place in time where the stimulus is inserted is determined as a function of the frequency of the variable $Y_i(n)$ *before* the point where the burst is generated. The value

of the stimulus is chosen to be *negative*, in order to decrease $Y_i(n)$. The result, which describes this phenomenon, is formalized below.

Theorem 7.4.:

Consider a system of N neurons described by Equations (7.5-7.6). The system will maintain the quiescent non-bursting behavior if a vector pulse S, applied to neuron i, has its first component value to be zero (i.e., $X_i(n)$ is always unexcited), and the second component is zero everywhere (i.e., $Y_i(n)$ is unexcited) except in a very short temporal interval δ_1, during the quiescent non-bursting behavior, where $Y_i(n)$ is excited with an input whose value is $A < O$.

Proof: Since any *constant* forcing function has the effect of merely changing the particular integral to a perturbed starting point (and not the stability), our task is to formulate the perturbation due to the excitation.

We know from *Lemma 7.1.*(Section 7.3) that when $\Delta\gamma$ is greater than $\Delta\gamma_{max}$, the system generates synchronized bursts. In order to delay the appearance of the bursting process, we have to decrease $\Delta\gamma$. Thus, we have to merely prove that the excitation $A < 0$ for the second variable of an arbitrary neuron i will decrease the value of $\Delta\gamma$, and that this will delay the generation of the apparition of the synchronized burst.

Consequently, we have to prove that:

$$\Delta\gamma(X_j^*(n+1), \forall j = 1..N) < \Delta\gamma(X_j(n+1), \forall j = 1..N),$$

where $\{X_j^*(n+1)\}$ is the first state variable of neuron j after the insertion of the stimulus at iteration n, and $\{X_j(n+1)\}$ is the corresponding state variable if there was no such stimulus.

Consider the system prior to the insertion. We have, for all $j = 1..N$,

$X_j(n) = \frac{\alpha}{[1+(X_j(n-1))^2]} + Y_j(n-1) + \frac{\epsilon}{N}\sum_{k=1}^{N} X_k(n-1)$, and

$Y_j(n) = Y_j(n-1) - \sigma X_j(n-1) - \beta$.

At the iteration n a stimulus with the value A is inserted to excite the (second) variable $Y_i(n)$. Thus the new system states, denoted by $\{X_j^*(n+1), Y_j^*(n+1)\}$ become:

$$X_j^*(n) = \frac{\alpha}{[1+(X_j(n-1))^2]} + Y_j(n-1) + \frac{\epsilon}{N}\sum_{k=1}^{N} X_k(n-1), \text{ for all } j = 1..N,$$

and
$Y_j^*(n) = Y_j(n-1) - \sigma X_j(n-1) - \beta$, for $j \neq i$, and
$Y_j^*(n) = Y_j(n-1) + A - \sigma X_j(n-1) - \beta$, for $j = i$.

Observe that $X_j^*(n) = X_j(n)$, for all $j = 1..N$. For the second state variable, however, observe that, with the lone exception of Y_i^* (when $Y_i^*(n) = Y_i(n) + A$), all the state variables have the same *previous* values, i.e., $Y_j^*(n) = Y_j(n)$, for all $j = 1..N$, $j \neq i$, which, in turn, effects the $\{X_j(n)\}$ by virtue of the state dynamics.

Consequently, by introducing the effect of the state dynamics at the time n, we get:

$$X_j^*(n+1) = \frac{\alpha}{[1+(X_j^*(n))^2]} + Y_j^*(n) + \frac{\epsilon}{N}\sum_{k=1}^{N} X_k^*(n) = X_j(n+1), \text{ for all } j = 1..N,\ j \neq i,$$
$$X_j^*(n+1) = \frac{\alpha}{[1+(X_j^*(n))^2]} + Y_j^*(n) + \frac{\epsilon}{N}\sum_{k=1}^{N} X_k^*(n) = X_j(n+1) + A, \text{ for } j = i.$$

Since $\Delta\gamma\Big(X_j(n+1), \forall j = 1..N\Big) = \frac{\epsilon}{N}\sum_{k=1}^{N} X_k(n+1)$, we compute
$\Delta\gamma\Big(X_j^*(n+1), \forall j = 1..N\Big) = \frac{\epsilon}{N}\sum_{k=1}^{N} X_k^*(n+1)$,
which differs from $\Delta\gamma\Big(X_j(n+1), \forall j = 1..N\Big)$ only due to X_i^*, the contribution of neuron i. Thus,
$$\Delta\gamma\Big(X_j^*(n+1), \forall j = 1..N\Big) = \Delta\gamma\Big(X_j(n+1), \forall j = 1..N\Big) + \epsilon\frac{A}{N},$$
and, since $A < 0$,
$$\Delta\gamma\Big(X_j^*(n+1), \forall j = 1..N\Big) < \Delta\gamma\Big(X_j(n+1), \forall j = 1..N\Big).$$

This implies that the output will not exceed the required bursting threshold as quickly as in the absence of the stimulus, and thus such an excitation will force the system to remain in the quiescent state. Hence the result ! □

7.6.1.1 Numerical verification

A simple simulation intended to prove the controlling of the quiescent behavior is included in the context of completeness. The case we present involves a model consisting of two neurons[12] in which the first neuron receives a stimulus with the value -0.1 at the iteration index $4,100$, chosen randomly during the quiescent behavior. The second neuron receives a stimulus with the value -0.2 at the iteration index $4,110$, also chosen randomly during the quiescent behavior. The results of executing this controlling operation are portrayed in Figure 7.10. Note that in

[12]The Parameters used are exactly the same as those mentioned in the introduction of Section 7.5.

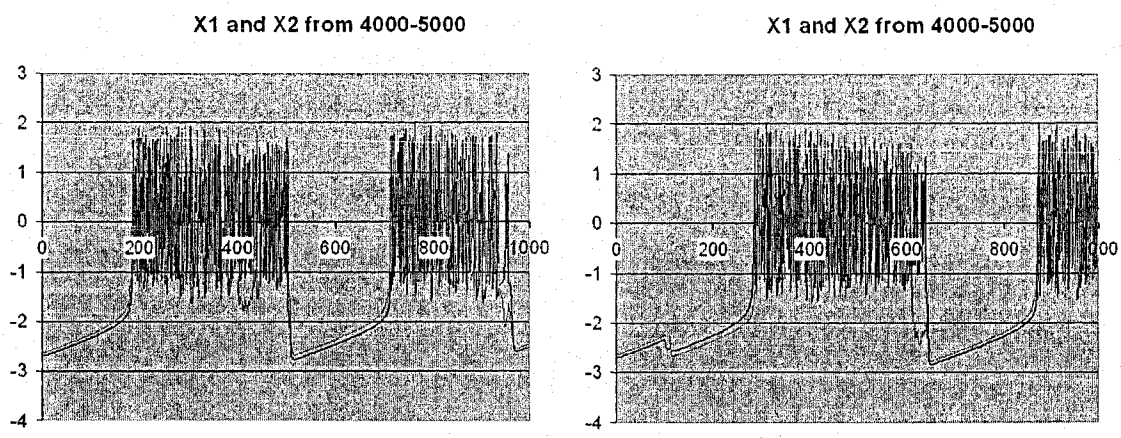

Figure 7.10: Graph displaying the maintenance of the quiescent behavior. In the graph on the left we represent the fast variables X_1 and X_2 for the case when no stimulus is inserted in the network. The graph on the right shows the scenario when the stimuli are added to the slow variables Y_1 and Y_2 for maintaining the quiescent behavior. The x-axis represents the value of the time index *after* the iteration 4,000.

the graph on the left we represented the fast variable X_1 and X_2 in the case when no stimulus is inserted in the network. The graph on the right shows the scenario when the stimuli are added to the slow variables Y_1 and Y_2, with the magnitudes mentioned above. The effect of the insertion consists of the generation of a delay in the appearance of the burst. Thus, when no stimuli are inserted, the bursting phenomenon occurs near iteration index 4,186 and if the stimuli are inserted, the bursting is delayed to the index 4,283.

Similar results are available for a variety of networks and with an ensemble of network parameters. However, these results cannot be easily displayed if the number of neurons is greater than two, and hence we omit their inclusion.

7.6.2 Maintaining the Bursting Behavior

In the case of maintaining the bursting behavior, the place in time where the stimulus is inserted is determined as a function of the frequency of the variable $Y_i(n)$ *after* the point where the burst

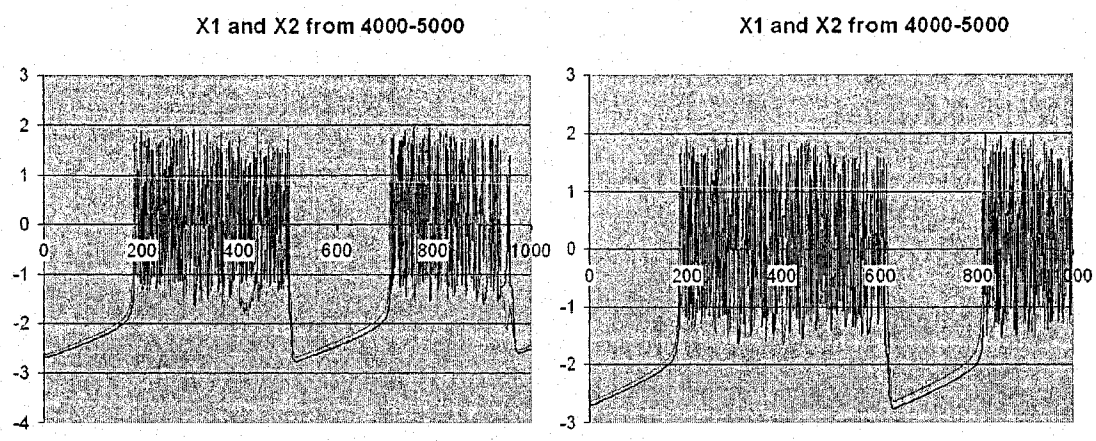

Figure 7.11: Graph displaying the delay of the burst by stimulating Y_1 and Y_2. In the graph on the left we represent the fast variables X_1 and X_2 for the case when no stimulus is inserted in the network. The graph on the right shows the scenario when the stimuli are added to the slow variables Y_1 and Y_2 for maintaining the bursting behavior. The x-axis represents the value of the time index *after* the iteration 4,000.

is generated. In contrast with the previous controlling method, the value of the stimulus is chosen to be *positive*, in order to increase $Y_i(n)$. This is formalized below.

Theorem 7.5.:

Consider a system of N neurons described by Equations (7.5-7.6). The system maintains the bursting behavior if a vector pulse S, applied to neuron i, has its first component value to be zero (i.e., $X_i(n)$ is always unexcited), and the second component is zero everywhere (i.e., $Y_i(n)$ is unexcited) except in a very short temporal interval δ_1, during the busting behavior, *where $Y_i(n)$ is excited with an input whose value is $A > O$.*

Proof: We again know from *Lemma 7.1* (Section 7.3) that when $\Delta\gamma$ is greater than $\Delta\gamma_{max}$, the system generates synchronized bursts. In order to maintain the bursting behavior, we have to increase $\Delta\gamma$. Thus, we have to merely prove that the excitation $A > 0$ for the second variable of an arbitrary neuron i will increase the value of $\Delta\gamma$, and that this will delay the termination of the bursting phenomenon.

The same arguments as the ones presented in the proof of the *Theorem 7.4* can be applied here for computing the $\Delta\gamma$ after the insertion of the stimulus. Using the same notation that $\{X_j^*(n+1)\}$ is the first state variable of neuron j after the insertion of the stimulus at iteration n, and that $\{X_j(n+1)\}$ is the corresponding state variable if there was no such stimulus, we compute[13], as in the proof of *Theorem 7.4*:

$$\Delta\gamma\Big(X_j^*(n+1), \forall j = 1..N\Big) = \frac{\epsilon}{N} \sum_{k=1}^{N} X_k^*(n+1),$$

which differs from $\Delta\gamma\Big(X_j(n+1), \forall j = 1..N\Big)$ only due to X_i^*, the contribution of neuron i. Thus,

$$\Delta\gamma\Big(X_j^*(n+1), \forall j = 1..N\Big) = \Delta\gamma\Big(X_j(n+1), \forall j = 1..N\Big) + \epsilon\frac{A}{N},$$

and, since $A > 0$,

$$\Delta\gamma\Big(X_j^*(n+1), \forall j = 1..N\Big) > \Delta\gamma\Big(X_j(n+1), \forall j = 1..N\Big).$$

This implies that the output will not go below the required bursting threshold more rapidly, and thus, such an excitation will force the system to remain in the bursting state. Hence the result! □

[13]The details are identical to the earlier computations, and omitted to avoid repetition.

7.6.2.1 Numerical verification

To prove the controlling effect of the bursting behavior, we now present a single simulation result. Here too, our model involves two neurons[14] in which the first neuron receives a stimulus with the value 0.1 at the iteration index 4,400, chosen randomly during the bursting behavior, and second neuron receives a stimulus with the value 0.2 at the iteration index 4,410, also chosen randomly during the bursting behavior. The results of the stimulation using these values are given in Figure 7.11. Again, the graph on the left displays the fast variables X_1 and X_2 when no stimulus is inserted, and the graph on the right shows the scenario when the stimuli are added to the slow variables Y_1 and Y_2, inserted as above. The effect of the stimulus consists of delaying the termination of the bursting phenomenon which occurs, for the unexcited case, near iteration index 4,502, and if the stimuli are inserted, the latter delays it to the index 4,607.

Again, similar results are available for a variety of networks and for other network and stimulation parameters, and are not included in the interest of readability.

7.6.3 Generating the Bursting Behavior

A corollary of the above case is when we want to create (as opposed to extend) a bursting phase from a quasi-stable quiescent phase. In this case, it is easy to see, using arguments similar to those given in Section 7.6.1, that this can be achieved if a stimulus is inserted in the fast variable $X_i(n)$, with a positive value, anywhere during the quiescent behavior. The "proof" or justification of this can be seen as follows: We saw in *Lemma 7.1* (Section 7.3) that when the coupling between the neurons is large enough to generate a value $\Delta\gamma$ greater that $\Delta\gamma_{max}$, the system generated synchronized bursts. Now, we extend those principles to show that instead of waiting for the value of $\Delta\gamma$ to be $\Delta\gamma_{max}$, we can *enforce* it to trigger by including a positive excitation for any neuron, and anywhere in time during the quiescent behavior. This positive stimulus must have the value greater than $\Delta\gamma_{max}$.

[14]The Parameters used are exactly the same as those mentioned in the introduction of Section 7.5

7.7 Conclusion

The bursting neuron, originally proposed by Rulkov [144], permits an explanation for the so-called *bursting* phenomenon in which a low frequency pulse output serves as an envelope of high frequency spikes. Rulkov's model is both analytically tractable and experimentally meaningful. In this paper, we presented a stability analysis for *small* scale networks consisting of bursting neurons. We proved that if the coupling is arbitrarily small, (which is the accepted model that leads to bursting) the network exhibits chaos, as demonstrated by the positive roots of the characteristic equation associated with the dynamical system. We then showed that the network rapidly converges to a synchronized behavior implying that increasing the number of neurons does not contribute significantly to the synchronization of the individual bursting neurons. The consequences of such a deduction lead to a phenomenon which we called *behavioral synchronization*, and the implications of this phenomenon have been examined by proposing a new hypothesis for the genesis of epileptic seizures. Finally, we have developed methods for controlling the behavioral synchronization of the network, namely those that can be invoked to maintain the quiescent or the bursting behaviors.

Chapter 8

Summary, Conclusions and Future Research

The main aim of this research was to investigate and propose methods and algorithms for controlling models related to the brain so as to recognize and modify their level of chaos. We believe that this process of controlling chaos will be a step forward in the area of medical research, for example, for desynchronizing an epileptic brain.

This chapter summarizes the work done so far and suggests future direction in this research area. They are catalogued below on a topic-by-topic basis.

- **Chaotic Pattern Recognition**
  We presented an original and novel algorithm for Pattern Recognition (PR) using Chaotic Neural Networks. The algorithm is based on a formal hypothesis proposed by Freeman [56] who developed a model for an olfactory system. Freeman conjectured that the brain is essentially a chaotic system in the absence of a stimulus (pattern) that it is supposed to recognize. During perception, when the attention is focussed on any sensory stimuli, the brain activity become periodic. We designed a PR system, namely a Chaotic Neural Network, which demonstrated such a phenomenon. The conclusions related to this area of research are: (i) The Adachi Neural Network (AdNN) is not chaotic. (ii) In order to obtain a chaotic network, it is possible to modify the AdNN to yield the Modified Adachi Neural

Network (M-AdNN) where we have only a pair of non-zero eigenvalues in the corresponding Jacobian. (iii) The M-AdNN has PR capabilities. The question of why the M-AdNN yield cycles of finite periodicity remains open. The research presented here has been published in [32], [33] and [30].

- **Modelling Inaccurate Perception**
  We proposed a new approach for modelling a PR system which loses its ability to recognize, even though the *quality* of the stimulus is "perfect" (i.e., noiseless). By using a Chaotic Neural Network, we provided a chaotic rationale for both perception and the lack thereof, even in cases when the stimulus is "error-free". In this area of research the conclusions are: (i) The M-AdNN can be generalized to obtain the Modified for Blurring Adachi Neural Network (Mb-AdNN), a network with a control parameter m, namely the number of non-zero eigenvalues in the corresponding Jacobian. (ii) By increasing m, the Mb-AdNN gradually loses its PR capabilities. This process could explain, using the principles of chaos, the generation of blurring and illusions. The research presented here has been published in [31] and [29].

- **Controlling Chaotic Behavior Using Large Scale Models**
  In this area, our goal was to discover methods by which we could increase the level of chaos in *almost* synchronized large scale networks, as in the epileptic brain. We investigated, in the piriform cortex (modelled as a large scale network), the dependence of the level of chaos as a function of a few variables (or parameters).

  To be more specific, we examined the following problems:

  - **Problem of Density and Strength:** We investigated the dependence of the level of chaos as a function of the density of the neurons in the network, and the strength of the connections between then.
  - **Problem of Connectivity** In this case we analyzed the dependence of the level of chaos as a function of the density of the connectivity of the synapses.
  - **Problem of Stimulus Frequency**: In this case we studied the dependence of the level of chaos as a function of the frequency of a stimulus that is globally applied within the network.

We conclude that: (i) It is possible to control the level of chaos in the EEG obtained from a model of the piriform cortex. (ii) The nonlinear measures of the EEG depend strongly on the architecture of the model (including the parameters such as the number of neurons, their connections, their level of inhibition or excitation). (iii) The LLE and the nonlinear interdependence corresponding to two zones in the piriform cortex can be modified (i.e., increased or decreased) by inserting a stimulus with a specific frequency in the olfactory bulb.

- **Controlling Chaotic Behavior Using Small Scale Models: Spike Annihilation in a Hodgkin-Huxley Neuron**
  We proposed some methods by which the behavior of *small* scale networks can be investigated. To achieve this, we used a classical model of Hodgkin-Huxley neuron. We analytically proved the existence of a brief current pulse, which, when delivered to the HH neuron during its repetitively firing state, annihilates its spikes. We also formally derived the characteristics of this brief current pulse. We then proceeded to explore experimentally, by numerical simulations, the properties of this pulse, namely the range of time when it could be inserted, its magnitude, and its duration. To conclude, each HH neuron under a spiking mode can be annihilated with a short time pulse with a specific amplitude and a specific time of insertion.

- **Controlling Chaotic Behavior Using Small Scale Models: Behavioral Synchronization in a Network of Bursting Neurons**
  We presented, a stability analysis for small scale networks consisting of bursting neurons. We then showed that the network rapidly converges to a synchronized behavior implying that increasing the number of neurons does not contribute significantly to the synchronization of the individual bursting neurons. Finally, we developed methods for controlling the behavioral synchronization of the network. The conclusions of this area of research are: (i) The network of coupled busting neurons is always unstable. (ii) When the number of coupled bursting neurons is increased, each of the two pseudo frequencies that describe behavioral synchronization will converge to a constant value. (iii) It is possible to control the behavioral synchronization in a network of coupled bursting neurons by exciting it appropriately.

8.1 Future Research

This section presents, in some detail, one particular area of future research that can yet be pursued in the area of *large* scale chaotic neural networks. We propose, in the future, to investigate the antiepileptic effect of new "patterned stimuli", (determined by our results presented in Chapters 6 and 7), versus low frequency brain stimulation for kindled seizures in rats.

The various therapies that are currently available for epileptic patients leave many without effective treatment. Indeed, up to 40% of those with temporal lobe epilepsy must endure the specter of intractability. In addition, for those who initially find some refuge in current treatments, many ultimately suffer from significant side effects, particularly in the face of long-term treatment. Thus, a significant need remains for effective treatments which have no side effects. Focal brain stimulation has the potential to be such a treatment, as indicated recently by both laboratory and clinical findings. Several animal studies have explored the possibility of using electrical stimulations to stop seizures once they have begun. Typically, these have involved in delivery of high frequency patterns to core brain structures like the thalamus, brainstem or basal ganglia. Additional studies have employed brain slices studied in a dish. Few, however, have involved novel brain stimulation configurations based on theoretical considerations, and/or low frequency stimulus (LFS) patterns, which we have observed to be amazingly effective against amygdala kindled seizures. The hypotheses of this future work (in rats) are:

1. Stimuli that will reinstate a "chaotic" pattern of behavior in the *in vivo* seizure network will prove to be effectively antiepileptic by disrupting the normal ease of triggering a kindled seizure.

2. The more extensively the network is exposed to the stimulus pattern, the greater the likelihood that behavioral and/or electrographic seizures are reduced.

We propose that these experiments be conducted in the piriform cortex (adjacent to the amygdala), as this is one of the most seizure-sensitive areas of the brain to kindling. We believe that we can modulate its activity either directly at the kindled focus, or through its primary input, the olfactory bulb. Previous results [113], using 90 sec of exposure to a LFS sinusoidal wave at the kindled focus elevated the seizure threshold in the amygdala by more than 200-400%. This elevation was not immediate (i.e., for example, minutes later), but appeared almost

a day later and, incredibly, lasted for several days before returning to the baseline level. The elevated threshold effect occurred in rats that were previously selectively bred to be either seizure-prone or seizure-resistant to amygdala kindling. We believe that good efficacy of the LFS in both categories indicates a broad-based action that is not dependent upon the animal's genetic background.

The details about how such a research endeavor can be undertaken are yet to be determined.

Bibliography

[1] H. D. I. Abarbanel, R. Brown, and J. B. Kadtke. Prediction in chaotic nonlinear systems: Methods for time-series with broad-band Fourier spectra. *Physical Review A*, 41:1782–1807, 1990.

[2] M. Adachi and K. Aihara. Associative dynamics in a chaotic neural network. *Neural Networks*, 10(1):83–98, 1997.

[3] D. J. Albers, J. C. Sprott, and W. D. Dechert. Routes to chaos in neural networks with random weights. *International Journal of Bifurcation and Chaos*, 8(7):1463–1478, 1998.

[4] D. M. Alexander and G. G. Globus. Edges of chaos dynamics in recursively organized neural systems. *Fractals of Brain, Fractal of Mind: In Search of a Symmetry Bond. (Edited by E. MacCormac and M. I. Stamenov), John Benjamins Publishing Co. Amsterdam/Philadelphia*, 1996.

[5] J. Arnold, P. Grassberger, K. Lehnertz, and C. E. Elger. A robust method for detecting interdependences: application to intracranially recorded EEG. *Physica D*, 134:419–430, 1999.

[6] V. Athitsos and S. Sclaroff. An appearance-based framework for 3D hand shape classification and camera viewpoint estimation. In *Proceedings of IEEE International Conference on Automatic Face and Gesture Recognition, (FG2002)*, volume 5, pages 45–50, Washington, D.C., May 2002.

[7] E. Av-Ron, H. Parnas, and L. A. Segel. A basic biophysical model for bursting neurons. *Biological Cybernetics*, 69:87–95, 1993.

[8] A. Babloyantz. *Evidence of chaotic dynamics during sleep cycle. In Dimensions and entropies in chaotic system, (eds:G.Mayer-Kress).* Springer-Verlag, Berlin, 1998.

[9] P. F. Baldi, M. C. Vanier, and J. M. Bower. On the use of Bayesian methods for evaluation compartmental neural model. *Journal of Computational Neuroscience*, 5:285–314, 1998.

[10] C. A. Barnes, M. S. Shuster, J. Shen, and B. L. McNaughton. Multistability of cognitive maps in the hippocampus of old rats. *Nature*, 388:272–275, 1997.

[11] P. M. Battelino, C. Grebogy, E. Ott, and J. A. Yorke. Chaotic attractors on a three-torus and torus break-up. *Physica D*, 39:299–314, 1989.

[12] J. Belair, U. an der Heiden, L. Glass, and J. Milton (eds.). *Dynamical Diseases: Mathematical Analysis of Human Illness.* American Institute of Physics, Woodbury, N.Y., 1995.

[13] G. Benettin, L. Galgani, A. Giorgilli, and J. M. Strelcyn. Tous les nombres characteristiques de Lyapunov sont effectivement calculables. *Compte Rendues Acad. Sc. Paris*, 286:431–433, 1978.

[14] G. Benettin, L. Galgani, A. Giorgilli, and J. M. Strelcyn. Lyapunov characteristic exponents for hamiltonian systems; a method for computing all of them, part i and part ii. *Meccanica*, 15:9–30, 1980.

[15] E. Bessar. *Biophysical and physiological systems analysis.* Addison-Wesley, London, 1960.

[16] E. N. Best. Null space in the Hodgkin-Huxley equations: a critical test. *Biophysical Journal*, 27:105–116, 1979.

[17] U. S. Bhalla and J. M. Bower. Exploring parameter space in detailed single neuron models: Simulations of the mitral and granule cells of the olfactory bulb. *Journal of Neurophysiology*, 69:1948–1965, 1993.

[18] U. S. Bhalla and J. M. Bower. Multiday recordings from olfactory bulb neurons in awake freely moving rats: spatially and temporally organized variability in odorant response properties. *Journal of Computational Neuroscience*, 4:221–256, 1997.

[19] I. Biederman. Recognition by components: A theory of human image understanding. *Psychological Review*, 94:115–147, 1987.

[20] A. Bjorck. Numerics of Gram-Schmidt orthogonalization. *Linear Algebra and its applications*, 197:297–316, 1994.

[21] V. E. Bondarenko. Epilepsy-like phenomena in chaotic neural networks. In *Proceedings of IEEE International Conference on Neural Networks*, volume 2, pages 774–777, Washington, D.C., June 2005.

[22] V. Booth and J. Rinzel. A minimal compartmental model for a dendritic origin of bistability of motoneuron firing patterns. *Journal of Computational Neuroscience*, 2:299–312, 1995.

[23] J. M. Bower. Reverse engineering the nervous system: An in vivo, in vitro, and in computo approach to understand the mammalian olfactory system. In *An Introduction to Neural and Electronic Networks, second edition (S.F. Zornetzer, J.L. Davis and C. Lau (eds))*, pages 3–28, Academic Press, New York, 1995.

[24] J. M. Bower and D. Beeman. *The Book of GENESIS.* Springer TELOS, 1998.

[25] E. Bradley. *Time-series analysis. Intelligent data analysis: An introduction (Eds: M. Berthold and D. Hand).* Springer-Verlag, Berlin, 1999.

[26] M. Breakspear and J.R. Terry. Topographic orientation of nonlinear interdependence in multichanel human EEG. *Neuroimage*, 16:822–835, 2002.

[27] W. Buskist and D. W. Gerbing. *Psychology: Boundaries and Frontiers.* Harper Collins, New York, 1990.

[28] D. Calitoiu, D. Nussbaum, and B. J. Oommen. Investigating schizophrenia using local connectivity considerations within the piriform cortex. In *Proceedings of CCECE05, The 18th Annual Canadian Conference on Electrical and Computer Engineering*, pages 1652–1656, Saskatoon, Canada, May 2005.

[29] D. Calitoiu, B. J. Oommen, and D. Nussbaum. Desynchronizing a chaotic pattern recognition neural network to model inaccurate perception. *To appear in IEEE Transactions on Systems, Man and Cybernetics.*

[30] D. Calitoiu, B. J. Oommen, and D. Nussbaum. Periodicity and stability issues of a novel chaotic pattern recognition neural network. *To appear in Pattern Analysis and Applications Journal.*

[31] D. Calitoiu, B. J. Oommen, and D. Nussbaum. Modeling inaccurate perception: Desynchronization issues of a chaotic pattern recognition neural network. In *Proceedings of the 14th Scandinavian Conference in Image Analysis*, volume 821-830, pages 3–16, Joensuu, Finland, June 2005.

[32] D. Calitoiu, B. J. Oommen, and D. Nussbaum. Neural network-based *chaotic* pattern recognition : Part 1 - stability and periodicity issues. In *Proceedings of PRIP'2005, the 2005 Conference on Pattern Recognition and Information Processing*, pages 252–259, Minsk, Belarus, May 2005. *This talk was a Plenary talk of the Conference.*

[33] D. Calitoiu, B. J. Oommen, and D. Nussbaum. Neural network-based *chaotic* pattern recognition- part 2: Stability and algorithmic issues. In *Proceedings of CORES'2005, the 2005 Conference on Computer Recognition Systems*, Wroclaw, Poland, May 2005. Springer. *This talk was a Plenary talk of the Conference.*

[34] C. C. Canavier, D. A. Baxter, J. W. Clark, and J. H. Byrne. Nonlinear dynamics in a model neuron provide a novel mechanism for transient synaptic inputs to produce long-term alterations of postsynaptic activity. *Journal of Neurophysiology*, 69:2252–2257, 1993.

[35] C. C. Canavier, D. A. Baxter J. W. Clark, and J. H. Byrne. Multiple modes of activity in a model neuron suggest a novel mechanism for the effect of neuromodulators. *Journal of Neurophysiology*, 729:872–881, 1994.

[36] J. Cooley. Digital computer solutions for excitable membrane models. *Journal of Cellular and Comparative Physiology*, 66:99–108, 1965.

[37] A. Das, P. Das, and A. B. Roy. Applicability of lyapunov exponent in eeg data analysis. *Complexity International*, 9:1–8, 2002.

[38] A. Destexhe, A. Babloyantz, and T. J. Sejnowski. Ionic mechanisms for intrinsic slow oscillations in thalamic relay neurons. *Biophysical Journal*, 65:1538–1552, 1993.

[39] R. L. Devaney. *A first course in chaotic dynamical systems: theory and experiments.* Addison Wesley, Reading (MA), 1992.

[40] G. deVries. Multiples bifurcations in a polynomial model of bursting oscillations. *Journal of Nonlinear Science*, 8:281–316, 1998.

[41] D. D'Humieres, M. R. Beasley, B. Huberman, and A. Libchaber. Chaotic states and routes to chaos in the forced pendulum. *Physical Review A*, 26:3483–3496, 1982.

[42] W. L. Ditto, S. N. Rauseo, and M. L. Spano. Experimental control of chaos. *Physical Review Letters*, 65:3211–3214, 1990.

[43] M. M. Dodson and S. Kristensen. Hausdorff dimension and diophantine approximation. *Fractal geometry and applications: a jubilee of Benoit Mandelbrot. Part 1, Proc. Sympos. Pure Math., Amer. Math. Soc., Providence, RI*, 72:305–347, 2004.

[44] B. Doiron, C. R. Laing, A. Longtin, and L. Maler. Ghostbursting: a novel bursting mechanism in pyramidal cells. *Journal of Computational Neuroscience*, 12:5–25, 2002.

[45] U. Dressler and G. Nitsche. Controlling chaos using time delay coordinates. *Physical Review Letters*, 68:1–4, 1992.

[46] R. Duda, P. Hart, , and D. Stork. *Pattern Classification (2nd edition).* John Wiley and Sons, Inc. New York, 2000.

[47] W. Duke, W. S. Pritchard, and K. K. Krieble. Dimensional analysis of resting human EEG II: Surrogate data testing indicates nonlinearity but not low-dimensional chaos. *Psychophysiology*, 32:486–491, 1995.

[48] J. P. Eckmann and D. Ruelle. Ergodic theory of chaos and strange attractors. *Review of Modern Physics*, 57:617–659, 1985.

[49] R. C. Elson, A. I. Selverston, R. Huerta, N. F. Rulkov, M. I. Rabinovich, and H. D. I. Abarbanel. Synchronous behavior of two coupled biological neurons. *Physical Review Letters*, 81(25):5692–5695, 1998.

[50] G. B. Ermentrout and N. Koppel. Multiple pulse interactions and averaging in systems of coupled neural oscillators. *Journal of Mathematical Biology*, 29:195–217, 1991.

[51] K. Falconer. *Fractal Geometry.* John Wiley and Sons, Inc. New York, 2004.

[52] L. Fausett. *Fundamentals of Neural Networks.* Prentice Hall, Englewood Cliffs, NY, 1994.

[53] A. Fell. The disorder mind. *UC Davis Magazine*, 19:1–7, 2001.

[54] R. FitzHugh. Mathematical models of excitation and propagation in nerve. *Biological Engineering (ed. H.P.Schwan)*, pages 1–85, 1969.

[55] R. H. Forgus and L. E. Melamed. *Perception : A cognitive-Stage Approach (2nd edition).* McGraw-Hill, New York, 1976.

[56] W. J. Freeman. Tutorial in neurobiology: From single neurons to brain chaos. *International Journal of Bifurcation and Chaos*, 2:451–482, 1992.

[57] W. J. Freeman. Brain dynamics: Brain chaos and intentionality. *Integrative Neuroscience, E. Gordon(ed.), Harwood Academic Publishers, Sydney, Australia*, pages 163–171, 2000.

[58] M. Friedman and A. Kandel. *Introduction to Pattern Recognition, statistical, structural, neural and fuzzy logic approaches.* World Scientific, Singapore, 1999.

[59] K. Fukunaga. *Introduction to Statistical Pattern Recognition.* Academic Press Professional Inc., San Diego, CA, 1990.

[60] J. Glanz. Mastering the nonlinear brain. *Science*, 277:1758–1760, 1997.

[61] L. Glass. Chaos focus issue on nonlinear dynamics of physiological function and control. *Chaos*, 1:247–334, 1991.

[62] I. Goldhirsch, P. L. Sulem, and S. A. Orszag. Stability and Lyapunov stability of dynamics systems: A differential approach and anumerical method. *Physica D*, 27:311–319, 1987.

[63] E. R. Grannan, D. Kleinfeld, and H. Sompolinsky. Stimulus-dependent synchronization of neural assemblies. *Neural Computation*, 4:550–569, 1980.

[64] P. Grassberger and I. Procaccia. Characterization of strange attractors. *Physical Review Letters*, 50:346–349, 1983.

[65] P. Grassberger and I. Procaccia. Measuring the strangeness of strange attractors. *Physica D*, 9:189–202, 1983.

[66] J. J. Gray. *The Hilbert Challenge.* Oxford University Press, 2000.

[67] C. Grebogi, E. Ott, and J. A. Yorke. Unstable periodic orbits and the dimensions of multifractal chaotic attractor. *Physical Review A*, 37:335–348, 1988.

[68] R. Guttman, S. Lewis, and J. Rinzel. Control of repetitive firing in squid axon membrane as a model for a neuron oscillator. *Journal Physiology*, 305:377–385, 1980.

[69] L. B. Haberly. Neuronal circuitry in olfactory cortex: Anatomy and functional applications. *Chemical Senses*, 10:219–238, 1985.

[70] L. B. Haberly and J. M. Bower. Olfactory cortex - model circuit for study of associative memory. *Trends Neuroscience*, 12:258–264, 1985.

[71] D. Hansel, G. Mato, and C. Meunier. Phase dynamics of weakly coupled Hodgkin-Huxley neurons. *Europhysics Letter*, 23:337–350, 1960.

[72] M. E. Hasselmo and J. M. Bower. Acetylcholine and memory. *Trends Neuroscience*, 16:218–222, 1993.

[73] G. He, Z. Cao, P. Zhu, and H. Ogura. Controlling chaos in a chaotic neural network. *Neural Networks*, 16(8):1195–1200, 2003.

[74] A. D. Heilman and J. Quattrochi. Computational models of epileptiform activity in single neurons. *BioSystems*, 78:1–21, 2004.

[75] M. Henon. A two-dimensional mapping with a strange attractor. *Communication in Mathematical Physics*, 50:69–77, 1976.

[76] B. Henry, N. Lovell, and F. Camacho. Nolinear dynamics time series analysis. *Nonlinear Biomedical Sygnal Processing - M. Akay (ed.) Willey IEEE Press*, 2:1–27, 2000.

[77] H. G. E. Hentschel and I. Procaccia. The infinite number of generalized dimensions of fractals and strange attractors. *Physica D*, 8:435–444, 1983.

[78] R. C. Hilborn. *Chaos and Nonlinear Dynamics.* Oxford University Press, 1994.

[79] A.V. Holden. *Chaos - Nonlinear Science: Theory and Applications.* Manchester University Press, 1986.

[80] J. J. Hopfield. Neural networks and physical systems with emergent collective computational properties. *Proceedings of the National Academy of Science USA*, 79:2254–2558, 1982.

[81] J. J. Hopfield. Neural networks with graded responses have collective computational properties like those of two-state neurons. *Proceedings of the National Academy of Science USA*, 81:3088–3092, 1984.

[82] J. Hounsgaard, H. Hultborn, B. Jesperson, and O. Kiehn. Bistability of α-motoneurons in the decerebrate cat and in the acute spinal cat after intravenous 5-hydroxytryptophan. *Journal of Physiology*, 405:345–367, 1988.

[83] K. Ikeda. Multiple-valued stationary state and its instability of the transmitted light by a ring cavity system. *Optics Communications*, 30:257–261, 1979.

[84] V. In, S. E. Mahan, W. L. Ditto, and M. L. Spano. Experimental maintenance of chaos. *Physical Review Letters*, 74(22):4420–4423, 1995.

[85] V. In, M. L. Spano, and M. Ding. Maintaining chaos in high dimensions. *Physical Review Letters*, 80(4):700–703, 1998.

[86] M. Inoue and A. Nagayoshi. A chaos neuro-computer. *Physica Letters A*, 158:373–376, 1991.

[87] K. Kaneko and I. Tsuda. *Complex Systems: Chaos and Beyond.* Springer, New York, 2000.

[88] T. Kapitaniak. *Controlling Chaos Theoretical and Practical Methods in Non-linear Dynamics.* Academic Press Limited, New York, 1996.

[89] J. Kaplan and J. A. Yorke. Functional differential equations and approximations of fix points. *Springer Lecture Notes in Mathematics*, (730):204–227, 1979.

[90] J. A. S. Kelso, S. L. Bressler, S. Buchanan, G. C. DeGuzman, M. Ding, A. Fuchs, and T. Holroyd. A phase transition in human brain and behavior. *Physical Letter A*, 169:134–144, 1992.

[91] M. B. Kennel, R. Brown, and H. D. I. Abarbanel. Determining embedding dimension for phase-space reconstruction using a geometrical construction. *Physical Review A*, 45(6):3403–3411, 1992.

[92] T. Kohonen. *Self-Organizing Maps.* Springer, Berlin, 1997.

[93] N. Koppel. We got rhythm: dynamical systems of the nervous system. *Notices of the AMS*, 47:6–16, 2000.

[94] Y. Kuramoto. *Chemical oscillations, waves and turbulence.* Springer Verlag, New York, USA, 1984.

[95] C. R. Laing and A. Logtin. A two-variable model of somatic-dentritic interactions in a bursting neuron. *Bulletin of Mathematical Biology*, pages 1–32, 2002.

[96] J. Lamberts, P. L. C. Van den Broek, J. Van Egmond, R. Dirksen, and A. M. L. Cohen. Correlation dimension of the human electroencephalogram corresponding to cognitive load. *Neuropsychobiology*, 41(3):149–153, 2000.

[97] D. P. Lathrop and E. J. Kostelich. Characterization of an experimental strange attractor by periodic orbits. *Physical Review A*, 40(7):4028–4031, 1989.

[98] H. A. Lechner, D. A. Baxter, J. W. Clark, and J. H. Byrne. Bistability and its regulation by serotonim in the endogenously bursting neuron R 15 in Aplysia. *Journal of Neurophysiology*, 75:957–962, 1996.

[99] R. G. Levin and M. Segal. The effects of serotonin depletion and Raphe grafts on hippocampal electrophysiology and behavior. *Journal of Neuroscience*, 11:1585–1596, 1991.

[100] E. N. Lorentz. Deterministic nonperiodic flow. *Journal of Atmospheric Sciences*, 26:130–141, 1963.

[101] E. N. Lorentz. *The essence of chaos.* University of Washington Press, Seatle, WA, 1993.

[102] H. Luders. *Deep brain stimulation and epilepsy.* Martin Dunitz, Taylor and Francisc Group, London and New York, 2003.

[103] M. C. Mackey and U. der Heiden. The dynamics of recurrent inhibition. *Journal of Mathematical Biology*, 19:211–225, 1984.

[104] M. C. Mackey and L. Glass. Oscillation and chaos in physiological control systems. *Science*, 197:287–289, 1977.

[105] M. Makishima and T. Shimizu. Wandering motion and co-operative phenomena in a chaotic neural network. *International Journal of Bifurcation and Chaos*, 8(5):891–898, 1998.

[106] B. B. Mandelbrot. *The fractal geometry of nature.* Freeman, San Francisco, 1982.

[107] R. Manuca, M. Casdagli, and R. Savit. Nonstationarity in epileptic EEG and implications for neural dynamics. *Mathematical Bioscience*, 147:1–22, 1998.

[108] D. Marr. *Minds, Brains and Computers- An anthology.* Blackwell Publishers, Malden, MA, 2000.

[109] M. Martelli. *Introduction to discrete dynamical systems and chaos.* Wiley-Interscience series in discrete mathematics and optimization, 1999.

[110] M. W. Matlin. *Perception.* Allyn and Bacon, Needham Heights, MA, 1983.

[111] R. M. May. Simple mathematical models with very complicated dynamics. *Nature*, 261:459–467, 1976.

[112] H. S. Mayberg, A. M. Lozano, V. Voon, H. E. McNeely, D. Seminowicz, and S. H. Kennedy C Hamani, J. M. Schwalb. Deep brain stimulation for treatment-resistant depression. *Neuron*, 45:651–660, 2005.

[113] D. C. McIntyre, K. L. Gilby, and C. A. Carrington. *Effect of low frequency stimulation on amygdala kindled afterdischarge thresholds and seizure profile in Fast and Slow kindling rat strains.* American Epilepsy Society Abstracts, 2002.

[114] J. Milnor. On the concept of attractor. *Communications in Mathematical Physics*, 99:177–195, 1985.

[115] J. G. Milton and D. Black. Dynamic diseases in neurology and psychiatry. *Chaos*, 5:8–13, 1995.

[116] J. G. Milton, P. H. Chu, and J. D. Cowan. Spiral waves in integrate-and-fie neural networks. *Advances in Neural Information Processing Systems*, 5:1001–1007, 1993.

[117] J. G. Milton, J. Gotman, G. M. Remillard, and F. Andermann. Timing of seizure recurrence in adult epileptic patients: a statistical analysis. *Epilepsia*, 28:471–478, 1987.

[118] K. Natarajah, R.U. Acharya, F. Alias, T. Tiboleng, and S. K. Puthusserypady. Nonlinear analysis of EEG signals at different mental states. *BioMedical Engineering Online*, 7:31–39, 2004.

[119] S. Newhouse, D. Ruelle, and F. Takens. Occurrence of strange AxiomA attractor near quasiperiodic flows on t^m ($m \geq 3$). *Communications in Mathematical Physics*, 64:35–40, 1978.

[120] H. Nozawa. A neural network model as a globally coupled map and its applications. *Technical Report of IEICE*, pages 11–18, 1992.

[121] K. Ogata. *Modern Control Engineering- second edition.* Prentice Hall, Englewood Cliffs, 1990.

[122] E. Ott, C. Grebogy, and J. A. Yorke. Controlling chaos. *Physical Review Letters*, 64:1196–1199, 1990.

[123] E. Ott, T. Sauer, and J. Yorke. *Coping with Chaos.* John Wiley and Sons, Inc., New York, 1994.

[124] N. H. Packard, J. P. Crutchfield, J. D. Farmer, and R. S. Shaw. Geometry from a time series. *Physical Review Letter*, 45:7712–716, 1980.

[125] L. M. Pecora. Synchronization conditions and desynchronizating patterns in coupled limited-cycle and chaotic systems. *Physical Review E*, 58:347–360, 1998.

[126] P. Penev and J. Atick. Local feature analysis: A general statistical theory for object representation. *Network: Computation in Neural Systems*, 7(3):477–500, 1996.

[127] J. Piaget. *The mechanism of perception.* Harper-Collins, New York, 1969.

[128] A. S. Pikovsky, M. Rosemblum, and J. Kurths. *Synchronization: A Universal Concept in Nonlinear Sciences.* Cambridge University Press, Cambridge, UK, 2001.

[129] Y. Pomeau and P. Manneville. Intermittent transition to turbulence in dissipative dynamical systems. *Communications in Mathematical Physics*, 74:189–197, 1980.

[130] H. A. Posch and W. G. Hoover. Lyapunov instability of dense Lennard-Jones fluids. *Physical Review A*, 38:473–482, 1988.

[131] R. Q. Quiroga, J. Arnold, and P. Grassberger. Learning driver-response relationships from synchronization patterns. *Physical Review E*, 61:5142–5148, 2000.

[132] P. E. Rapp. Chaos in the neuroscience: cautionary tales from the frontier. *Biologist*, 40:89–94, 1993.

[133] P. E. Rapp, T. Bashore, J. Martinerie, A. Albano, I. Zimmerman, and A. Mess. Dynamics of brain electrical activity. *Brain Topography*, 2:99–118, 1989.

[134] J. Rinzel. Numerical calculation of stable and unstable periodic solutions to the Hodgkin-Huxley equations. *Mathematical Biosciences*, 49:27–59, 1980.

[135] J. Rinzel and G.B. Ermentrout. *Analysis of neural excitability and oscillations, In Methods in Neuronal Modeling: From Ions to Networks. C.Koch and I Segev (Eds).* MIT Press, Cambridge, MA, 1998.

[136] B. Ripley. *Dynamical Systems: Stability, Dynamics, and Chaos.* CRC Press, Boca Raton, 1994.

[137] B. Ripley. *Pattern Recognition and Neural Networks.* Cambridge University Press, Cambridge, England, 1996.

[138] F. J. Romeiras, C. Grebogi, E. Ott, and W. P. Dayawansa. Controlling chaotic dynamical systems. *Physica D*, 58:165–192, 1992.

[139] S. Rose. *From Brains to Consciousness?* Princeton University Press, Princeton, NY, 1998.

[140] M. T. Rosenstein, J. J. Collins, and C. J. De Luca. A practical method for calculating largest Lyapunov exponents from small data sets. *Physica D*, 65:117–134, 1993.

[141] M. T. Rosenstein, J. J. Collins, and C. J. De Luca. Reconstruction expansion as a geometry-based framework for choosing proper delay times. *Physica D*, 73:82–98, 1994.

[142] O. E. Rossler. An equation for continuous chaos. *Physics Letters A*, 57:397–398, 1976.

[143] D. Ruelle and F. Takens. On the nature of turbulence. *Communications in Mathematical Physics*, 20:167–192, 1971.

[144] N. F. Rulkov. Regularization of synchronized bursts. *Physical Review Letters*, 86(1):183–186, 2001.

[145] E. R. Sanabria, H. Su, and Y. Yaari. Initiation of network bursts by Ca dependent intrinsic bursting in rat pilocarpine model of temporal lobe epilepsy. *Journal of Physiology*, 532:205–216, 2001.

[146] S. F. Schiff, K. Jerger, D. H. Duong, T. Chay, M. L. Spano, and W. L. Ditto. Controlling chaos in the brain. *Nature*, 370:615–620, 1994.

[147] S. F. Schiff, P. So, and T. Chang. Detecting dynamical interdependence and generalized synchrony through mutual prediction in a neural ensemble. *Physical Review E*, 54:6708–6724, 1996.

[148] J. Schurmann. *Pattern classification, a unified view of statistical and neural approaches.* John Wiley and Sons, New York, 1996.

[149] I. Shimada and T. Nagashima. A numerical approach to ergodic problem of dissipative dynamical systems. *Prog. Theor. Physics*, 61:1605–1616, 1979.

[150] J. W. Shuai, Z. X. Chen, R. T. Liu, and B. X. Wu. Maximum hyperchaos in chaotic nonmonotonic neuronal networks. *Physical Review E*, 56:890–893, 1997.

[151] S. Sinha. Controlled transition from chaos to periodic oscillations in a neural network model. *Physica A*, 224:433–446, 1996.

[152] E. Sivan, L. Segel, and H. Parnas. Modulated excitability: a new way to obtain bursting neurons. *Biological Cybernetics*, 72:455–461, 1995.

[153] C. A. Skarda and W. J. Freeman. How brains make chaos to make sense of the world. *Behavioral and Brain Science*, 10:161–165, 1987.

[154] M. Small. *Applied Nonlinear Time Series Analysis: Applicatins in Physics, Physiology and Finance.* World Scientific Publishing Company, 2005.

[155] J. C. Sprott. *Chaos and Time-Series Analysis.* Oxford University Press, Oxford, England, 2003.

[156] C. J. Stam. Nonlinear dynamical analysis of EEG and MEG. review of an emerging field. *Clinical Neurophysiology*, 116:2266–2301, 2005.

[157] M. Steriade. *Neuronal Substrate of Sleep and Epilepsy.* Cambridge University Press, 2003.

[158] S. Strogatz. *Sync: the emerging science of spontaneous order.* Hyperion, New York, 2003.

[159] F. Takens. Detecting strange attractors in turbulence. *Dynamical Systems and Turbulence (D. Rand and L. S. Young -eds) Lecture Notes in Mathematics*, 898:366–381, 1981.

[160] M. Tenenbaum and H. Pollard. *Ordinary differential equations; an elementary textbook for students of mathematics, engineering, and the sciences.* Harper and Row, New York, 1963.

[161] T. Teorell. A biophysical analysis of mechano-electrical transduction. *in Handbook of Sensory Physiology, vol 1, W.R.Loeswenstein ed, Springer Verlag, Berlin*, pages 291–339, 1971.

[162] J. Theiler. Spurious dimensions from correlation algorithms applied to limited time series data. *Physical Review A*, 34:2427–2432, 1986.

[163] J. Theiler. On the evidence for low-dimensional chaos in an epileptic electroencephalogram. *Physics Letters A*, 196:335–341, 1995.

[164] J. Theiler, S. Eubank, A. Longtin, B. Galdrikan, and Farmer J.D. Testing for nonlinearity in time series: the method of surrogate data. *Physica D*, 58:77–94, 1992.

[165] S. Theodoridis and K. Koutroumbas. *Pattern recognition.* Academic Press, New York, 1999.

[166] X. J. Wang. Genesis of bursting oscillations in the Hindmarsh-Rose model and homoclinicity to a chaotic saddle. *Physica D*, 62:263–274, 1993.

[167] M. A. Whittington, I. M. Stanford, S. B. Collin, J. G. R. Jeffreys, and R. D. Traub. Spatiotemporal patterns of gamma frequency oscillations tetanically induced in the rat hippocampal slice. *The Journal of Physiology*, 502:591–607, 1997.

[168] S. Wiggins. *Global Dynamics, Phase Space Transport, Orbits Homoclinic to Resonances, and Applications.* AMS, Providence, RI, 1993.

[169] H. Wilson. *Spikes decisions and actions: Dynamical foundations of neuroscience.* Oxford University Press, 1999.

[170] H. R. Wilson and J. D. Cowan. Excitatory and inhibitory interactions in localized populations. *Biophysical Journal*, 12:1–23, 1972.

[171] H. R. Wilson and J. D. Cowan. A mathematical theory of the functional dynamics of cortical and thalamic nervous tissue. *Kybernetik*, 13:55–80, 1973.

[172] M. Wilson. *CIT Thesis, Ph.D. Thesis.* California Institute of Technology, Pasadena, 1990.

[173] M. Wilson and J. M. Bower. A computer simulation of olfactory cortex with functional implications for storage and retrieval of olfactory information. *Neural Information Processing Systems (D. Anderson -ed.) American Institute of Physics, New York*, pages 114–126, 1988.

[174] M. Wilson and J. M. Bower. The simulation of large-scale neural networks. *Methods in Neuronal Modelling: From Synapses to Networks, edited by C.Koch and I.Segev Cambridge, MA: MIT Press*, pages 291–334, 1989.

[175] A. Winfree. *The geometry of biological time.* Springer-Verlag, New York, 1982.

[176] L. Wittgenstein. *Philosophical Investigations (3rd edition).* Prentice Hall, Englewood Cliffs, NY, 1999.

[177] A. Wolf, J. B. Swift, H. L Swinney, J. A. Vastano, J. Kaplan Rlitz, and J. A. Yorke. Determining Lyapunov exponents from a time series. *Physica D*, 16:285–317, 1985.

[178] J. J. Wright and D. T. J. Liley. Dynamics of the brain at global and microscopic scales. Neural networks and the EEG. *Behavioral and Brain Sciences*, 19:285–320, 1996.

[179] W. Yang and M. Ding. Preserving chaos: Control strategies to preserve complex dynamics with potential relevance to biological disorders. *Physical Review E*, 51:102–110, 1995.

[180] D. Zipser, B. Kehoe, G. Littleworth, and J. Fuster. A spiking network model of short-term memory. *Journal of Neuroscience*, 13:3406–3420, 1993.

Appendix A

Dynamical Systems Definitions

This Appendix presents formal definitions of some relevant concepts in the filed of dynamical systems theory. This review is necessarily brief. We refer the reader to various book and references [109, 136, 168] for more details.

Definition A.1: **A discrete-time dynamical system** can be represented as the iteration $f : R^n \longrightarrow R^n$ of a differentiable function:

$$x_{t+1} = f(x_t),\ t \in N, x \in R^n,$$

where N denotes the set of natural numbers and R^n denotes the n-dimensional space of real numbers. Note that, in general, the function f can be non-linear.

Definition A.2: For each $x \in R^n$, the iteration of f generates a sequence of distinct points which define a trajectory of f. Given an initial state x_0 , the evolution of the system starting from x_0 is determined by the sequence of states: $\{x_0, x_1 = f(x_0), x_2 = f(x_1) = f^2(x_0), \ldots\}$. The sequence is called the **trajectory** of the system starting from x_0 . The sequence can also be defined as the set $\{f^m(x_0)|m > 0\}$, where $f^m(x)$ is the composition of f with itself m times.

Definition A.3: A point x' is called a **fixed point** of f if $f^m(x') = x'$, for all $m \in N$.

Definition A.4: A fixed point x' is called an **attracting fixed point** of f if there exists a neighborhood around x' , $O(x')$, such that $\lim_{m\to\infty} f^m(x') = x'$, for all $x \in O(x')$.

Definition A.5: A fixed point x' is called a **repelling fixed point** of f if there exists a

neighborhood around x' , $O(x')$, such that $\lim_{m\to-\infty} f^m(x') = x'$, for all $x \in O(x')$. In other words, a repelling fixed point is an attracting fixed point in the reverse sequence.

Definition A.6: A fixed point x' is called a **Periodic-2 fixed point** of f if $f^2(x') = x'$. Note that a function may have a fixed point of any period.

Definition A.7: **A system of equations** is a set of functions $F = \{f_i\} : R^n \longrightarrow R^n, i = 1, 2, ..m$. All the above definitions of fixed points also hold for systems of equations. For a non-linear system, F is denoted using a matrix, and the set X of x_i can be written vectorially as $X_{t+1} = F \cdot X_t$.

Definition A.8: An **eigenvalue** is a scalar λ , and an **eigenvector** is a vector v, such that $F * v = \lambda * v$. For a linear system of n equations, the eigenvalues give the rate of contraction or expansion, and the eigenvectors give the axis along which the system contracts or expands. The eigenvalues, λ_i, $i = 1, 2, ..., n$, at the fixed points determine the behavior of the system as follows:
a) if for all i, $\lambda_i \in (-1, 1)$, the system is **stable** and **contracting**, and the fixed point is an **attracting fixed point**,
b) if for all i, $\lambda_i \in (-\infty, -1)$ and $\lambda_i \in (1, \infty)$, the system is **expanding**, and the fixed point is a **repelling fixed point**,
c) if $\lambda_j \in (-\infty, -1)$ or $\lambda_j \in (1, \infty)$, for some integer(s) j, and if $\lambda_i \in (-1, 1)$ for $i = 1, 2, ..., j - 1, j + 1, ..., n$, then the system is **unstable** and **expanding** in the direction of the eigenvector(s) that corresponds to λ_j , and is **contracting** in all other corresponding eigenvector directions. The fixed point is also a **repelling point**, specifically referred to as a **saddle point**. (The case of an eigenvalue that is equal to unity, it is defined to be non-hyperbolic and requires other methods to analyze the system around the fixed point.)

Definition A.9: For a non-linear system of equations, F, let J be the matrix of partial derivatives matrix, Jacobian, computed at the quiescent point, X^*. The linearized approximation for the nonlinear model is given by the linear equation $X(n + 1) = J(X^*) \cdot X(n)$. In particular, around a fixed point, the eigenvalues of the linearized system govern whether or not the non-linear system is contracting or expanding in its neighborhood.

Definition A.10: Analogous to the eigenvectors of the linear system, the non-linear system are characterized by invariant sets, called **stable** or **unstable manifolds**. A **saddle point** is

characterized by both a stable manifold and an unstable manifold.

For a two-dimensional system, the stable and unstable manifolds, specified by WS and WU are curves tangential to the stable and unstable eigenvectors at the saddle point X', satisfying:
a) Stable Manifold $WS = \{X | F(X) \in WS$, and $\lim_{m\to\infty} F^m(X) = X'\}$,
b) Unstable Manifold $WU = \{x | F(X) \in WU$, and $\lim_{m\to\infty} F^m(X) = X'\}$.

Appendix B

The Pole Placement Technique

In this Appendix, we explain how the pole placement technique for a control system works.

Consider a control system defined by $X' = AX + B$ where A is an $n \times n$ matrix, and B is a n-dimensional column vector. The *pole placement problem* determines a matrix K in such a way that the eigenvalues of the matrix $A - BK^T$ have specified (complex) values $\{\mu_1, ..., \mu_m\}$. The eigenvalues of the matrix $A - BK^T$ are called the "regulator poles" of the system, and the problem of placing these poles at the desired locations by choosing K is our primary concerns [138].

The necessary and sufficient condition for a unique solution of the pole placement problem is stated in the following results:

Result B.1 The pole placement problem has a unique solution if and only if the $n \times n$ matrix[1] $C = (B|AB|A^2B|...|A^{n-1}B)$ is of the rank n.

Result B.2 The solution of the pole placement problem is

$$K^T = (\alpha_n - a_n, ..., \alpha_1 - a_1)T^{-1},$$

where $T = CW$, and

[1] C is called the controllability matrix.

$$W = \begin{pmatrix} a_{n-1} & a_{n-2} & \dots & a_1 & 1 \\ a_{n-2} & a_{n-3} & \dots & 1 & 0 \\ \vdots & \vdots & \vdots & \vdots & \vdots \\ a_1 & 1 & \dots & 0 & 0 \\ 1 & 0 & \dots & 0 & 0 \end{pmatrix}.$$

If we denote $\{a_1, ..., a_n\}$ as the coefficients of the characteristic polynomial of A,

$$|sI - A| = s^n + a_1 s^{n-1} + ... + a_n,$$

and if $\{\alpha_1, ..., \alpha_n\}$ are the coefficients of the characteristic polynomial of $A - BK^T$, it can be shown that the roots of $|sI - A|$ are $\{\mu_j\}$ which satisfy:

$$\prod_{j=1}^{n}(s - \mu_j) = s^n + \alpha_1 s^{n-1} + ... + \alpha_n.$$

Appendix C

Bifurcations and Crises

In this Appendix, we shall describe the classifications of bifurcations and crises.

An important problem in nonlinear dynamics is the modification of the orbits of the system if parameters of the system are changed.

Same possible changes [123] which involve chaotic orbits are listed below. As the system parameter changes, the following could occur:

1. A chaotic attractor appears.
2. A chaotic transient is created from a situation where there were only nonchaotic orbits.
3. A formerly nonfractal basin boundary becomes fractal.
4. A scattering problem changes from being nonchaotic to chaotic.
5. Finally, a chaotic set experiences stepwise changes in its magnitude in the phase space. These may or may not be attractors and thus, for example, any one could lead to the boundary of a fractal basin.

We shall now consider some of these above scenarios in greater detail.

C.1: Bifurcations

A **bifurcation** is a quantitative change in the dynamical behaviour of a system or the topological structure of its phase portrait as one or more parameters pass through a critical value. Any point in parameter space where the dynamical system is structurally unstable is called a **bifurcation point**, and the set of all such points is a **bifurcation set** [155]. If the eigenvalue of a dynamical system becomes stable or unstable, the system has a **continuous** (or **subtle** or **supercritical**) **bifurcation**. However, if the eigenvalue of the system appears or vanishes, the system has a **discontinuous bifurcation** which is also called a **catastrophic** or **subcritical** bifurcation.

C.2: Intermittency Transitions to a Chaotic Attractor

Consider a nonlinear system with a control parameter p. If $p < p_T$, where p_T is a critical transition value, the attractor of the system is a periodic orbit. For p slightly larger than p_T there are long durations of the time ("laminar phases") during which the orbit appears to be periodic and closely resembles the orbit for $p < p_T$. However, this regular (approximatively periodic) behaviour is intermittently interrupted by a finite duration "burst" in which the orbit behaves in a decidedly different manner. These bursts occur at seemingly random times, but one can define a mean time T(p) between the bursts. As p approaches p_T from above, the mean time between bursts approaches infinity, and the orbit of the attractor becomes always "laminar" so that the motion is truly periodic. As p increases substantially above p_T, the burst becomes so frequent that the regular oscillation (laminar phase) can no longer be distinguished.

In the intermittency transition, one has a simple periodic orbit which is replaced by chaos as p passes though p_T. This necessarily implies that the stable attracting periodic orbit either becomes unstable, or is destroyed as p increases through p_T. When the first scenario occurs, the stable orbit is not replaced by another stable periodic orbit in its vicinity, as, for example, in the forward period doubling bifurcation. During the bursts, the orbit diverges from the vicinity of the original periodic orbit.

There are three types of generic bifurcations which meet these requirements [123]:

- The saddle-node bifurcation (which are those whose stable and unstable orbits coalesce and obliterate each other.
- The inverse period doubling bifurcation, in which an unstable periodic orbit collapses

onto a stable periodic orbit of one half its period, and other orbits are replaced by unstable periodic orbits of the lower period.

- The system possesses subcritical bifurcations of the periodic orbit.

Pomeau and Manneville [129] distinguish three types of intermittency transitions corresponding to the three types of generic bifurcations mentioned above:

1. Type I : Those which possess the so-called **saddle-node**. In this case the system loses stability through saddle-node bifurcations, and we can assume that the system contains both stable and unstable fixed points which collide as the control parameter reaches its critical value.

2. Type II: Those which of the so-called **Hopf** type. Here, the system loses its stability through Hopf bifurcations, that occurs when a steady state solution loses its stability as some control parameter is varied, leading to a pair of complex eigenvalues, and, thus, an oscillatory output.

3. Type III: Those which possess the **inverse period doubling** phenomena. In this scenario, the system loses its stability through period-doubling, pitchfork bifurcations. Here, we assume that the system undergoes a cascade of such period-doublings in such a way that at the accumulation point one will observe an aperiodic behaviour.

C.3: Crises

When a chaotic attractor collides with an unstable periodic orbit or its basin of attraction, it leads to a **crisis** phenomenon. There are three types of crises:

1. A **boundary crisis** is one in which the attractor touches its basin boundary. In this case, the basin of attraction separates the attractor from another coexistent attractor. After the crisis, the attractor is destroyed.

2. An **interior crisis** is one in which the attractor touches an unstable periodic orbit or limit cycle within its basin of attraction. When the collision occurs, the attractor suddenly expands in size but remains bounded.

3. An **attractor merging crisis** is one in which two or more attractors simultaneously touch a periodic orbit on the basin boundary that separates them. The attractors merge to form a single chaotic attractor. This type of crisis occurs in systems with symmetries.

Following a boundary crisis, the nonlinear dynamical system can have chaotic transients. As opposed to this, subsequent to an interior crisis or an attractor merging crisis, the system can display a variety of temporal behaviours such as the so-called "crisis-induced intermittency".

As this level of detail is sufficient for the Thesis, we close this section by remarking that more details of these crises can be found in [129].

Appendix D

Gram-Schmidt Reorthonormalization

In this Appendix, we describe the Gram-Schmidt Reorthonormalization[1], modified from a more general presentation given in [20].

Given a set of n independent vectors $(v_1, v_2, ..., v_n)$, the Gram-Schmidt reorthonormalization (GSR) constructs a set of orthogonal unit vectors $(v_1', v_2', ..., v_n')$ which spans the same space as the original set of vectors.

The first vector is computed by merely normalizing its previous version:

$$v_1' = \frac{v_1}{||v_1||}. \tag{D.1}$$

To compute the second vector, the GSR procedure "removes" the part of v_2 which is aligned with v_1', and then normalizes as:

$$v_2' = \frac{v_2 - \langle v_2, v_1' \rangle v_1'}{||v_2 - \langle v_2, v_1' \rangle v_1'||}. \tag{D.2}$$

As a result of this, v_2' is now orthogonal to v_1', and these two vectors span the same two-dimensional subspace as v_1 and v_2.

For any arbitrary k^{th} vector, the GSR procedure will generate:

$$v_k' = \frac{v_k - \sum_{i=1}^{k-1} \langle v_k, v_i' \rangle v_i'}{||v_k - \sum_{i=1}^{k-1} \langle v_k, v_i' \rangle v_i'||}. \tag{D.3}$$

[1]This Appendix was included as per the request of the External Examiner.

The new computed orthogonal set of vectors $(v_1', v_2', ..., v_k')$ spans the same $k - dimensional$ subspace as the set $(v_1, v_2, ..., v_k)$ for any k up to and including $k = n$.

Appendix E

Definitions describing distances

In this Appendix, we present some of the basic definitions used for describing distances and measures. There are essentially taken from [51].

The basic notions from set theory and point set topology involve the concept of an *n-dimensional Euclidian space*, R^n, whence it is is possible to define the *Euclidian distance* or *metric*. If X and Y are points of R^n, the distance between them is $|X-Y| = (\sum_{i=1}^{n} |x_i - y_i|)^{1/2}$.

An infinite set, A, is *countable* if its elements can be listed in the form $X_1, X_2, X_3, ...$, as a result of which the element of A can be mapped onto the set of integers. The sets Z and Q are countable, but R is uncountable.

A subset A of R^n is *open* if for all points X in A, there is some ball $B(X,r)$, centered at X and of positive radius r, that is contained in A. A set is closed if, whenever $\{X_K\}$ is a sequence of points of A converging to a point X of R^n, then X is in A.

The class of Borel sets is the smallest collection of subsets of R^n with the following properties:

(a) Every open set and every closed set is a Borel set.

(b) The union of every finite or countable collection of Borel sets is a Borel set, and the intersection of every finite or countable collection of Borel sets is a Borel set.

Informally speaking, a measure is a concept for attributing a numerical "size" to sets, such that if a set is decomposed into a finite or countable number of pieces in a reasonable way, then the size of the whole is the sum of the sizes of the pieces.

We define μ as a measure on R^n if μ assigns a non-negative number, possibly ∞, to each subset of R^n such that:

(a) $\mu(\emptyset) = 0$.

(b) $\mu(A) \leq \mu(B)$ if $A \subset B$.

(c) If $A_1, A_2, \ldots$ is a countable (or finite) sequence of sets then:

$$\mu\Big(\bigcup_{i=1}^{\infty} A_i\Big) \leq \sum_{i=1}^{\infty} \mu(A_i), \tag{E.1}$$

where the equality condition in the above relation, i. e.

$$\mu\Big(\bigcup_{i=1}^{\infty} A_i\Big) = \sum_{i=1}^{\infty} \mu(A_i), \tag{E.2}$$

is satisfied if the sets A_i are disjoint Borel sets.